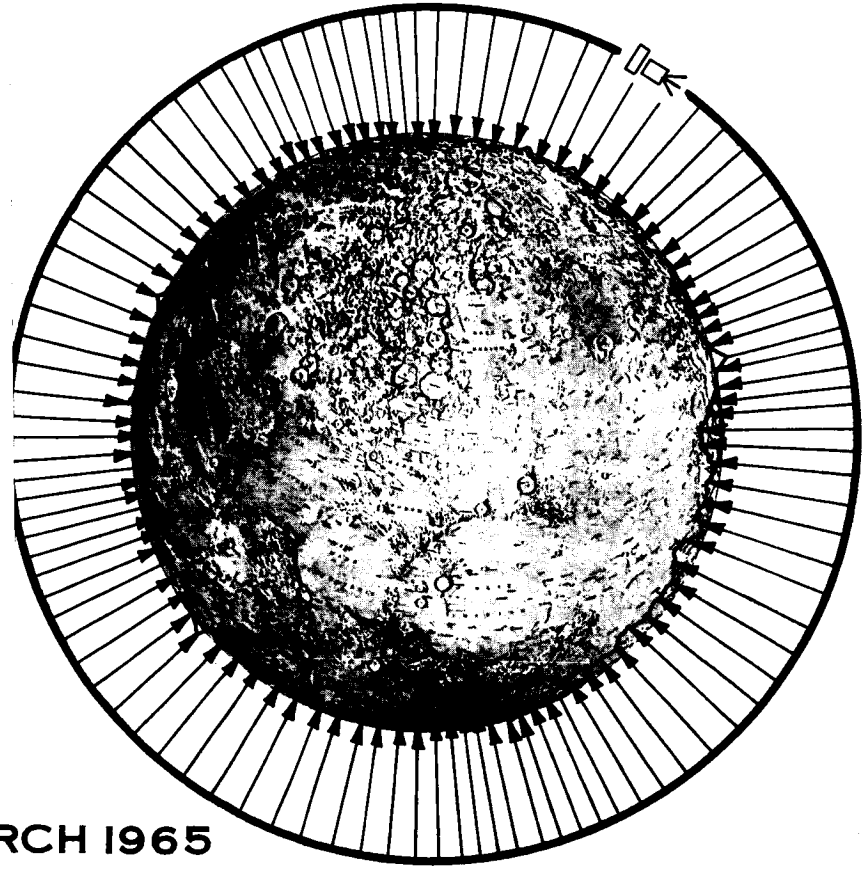


NASA-CR-65001

LUNAR CONTOUR MAPPING SYSTEM LUCOM

FINAL REPORT - CONTRACT NO.
NAS 9-3269

GPO PRICE \$ _____
OTS PRICE(S) \$ _____
Hard copy (HC) \$ 11.00
Microfiche (MF) \$ 1.75



MARCH 1965

RADAR SENSOR SYSTEM FOR THE ACQUISITION OF LUNAR SURFACE DATA

N65-23291 (ACCESSION NUMBER)	_____ (THRU)
<u>354</u> (PAGES)	_____ (CODE)
<u>CR-65001</u> (NASA CR OR TMX OR AD NUMBER)	<u>14</u> (CATEGORY)

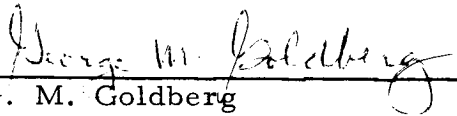
FACILITY FORM 602

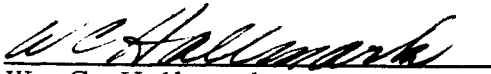
LTV MILITARY ELECTRONICS DIVISION
LING-TEMCO-VOUGHT, INC.
P. O. BOX 6118,
DALLAS, TEXAS 75222

LUNAR CONTOUR MAPPING SYSTEM (LUCOM)

FINAL REPORT

Submitted under terms of
Contract No. NAS 9-3269
to
NASA Manned Spacecraft Center
Advanced Spacecraft Technology Division
Lunar Surface Technology Branch/ET33
2101 Webster - Seabrook Road
Houston, Texas 77058


G. M. Goldberg
LUCOM Project Manager


W. C. Hallmark
Manager - Advanced Guidance
Systems


R. H. Myers
Product Line Director
Guidance & Controls

Ling-Temco-Vought, Inc.
LTV Military Electronics Division
P. O. Box 6118
Dallas, Texas 75222

TABLE OF CONTENTS

	Page	
1.0	INTRODUCTION	1
1.1	LUCOM CONCEPT	1
1.1.1	<u>LUCOM TASKS</u>	3
1.1.2	<u>LUCOM FUNCTIONS</u>	5
1.2	CONCEPTUAL SYSTEM DESIGN	5
1.2.1	<u>LUCOM ANTENNA</u>	7
1.2.2	<u>LUCOM SENSOR</u>	7
1.2.3	<u>DATA PROCESSOR</u>	7
1.2.4	<u>TELEMETRY CONDITIONER AND ENCODER</u>	7
1.2.5	<u>TAPE RECORDER</u>	7
1.2.6	<u>SEQUENCE CONTROL UNIT</u>	8
1.2.7	<u>TELEMETRY TRANSMITTER</u>	8
1.2.8	<u>JUNCTION CONTROLLER</u>	8
1.2.9	<u>POWER SUPPLY</u>	8
1.3	STUDY OBJECTIVES	8
1.4	STUDY ASSUMPTIONS	10
1.5	LUCOM SYSTEM ACCURACY	11
2.0	TECHNICAL STUDY APPROACH	15
2.1	DISCUSSION OF THE PROBLEM	17
2.1.1	<u>FRAME OF REFERENCE</u>	17
2.1.2	<u>CURRENT SELENOGRAPHY</u>	18
2.1.3	<u>DATA ACQUISITION</u>	20
2.1.4	<u>DATA TRANSMISSION</u>	24
2.1.5	<u>DATA HANDLING</u>	25
2.2	APOLLO INSTRUMENTATION	26
2.2.1	<u>GUIDANCE EQUIPMENT</u>	26
2.2.2	<u>CAMERAS</u>	27
2.3	SYSTEM DESIGN APPROACH	29
2.3.1	<u>DESIGN OBJECTIVES</u>	29
2.3.2	<u>DESIGN CONSTRAINTS</u>	30
2.3.3	<u>ANALYTICAL TECHNIQUES</u>	31
2.3.4	<u>LUCOM SIMULATION ROUTINE</u>	35
2.3.5	<u>INVESTIGATIONS</u>	36
2.3.6	<u>CRITICAL PROBLEM AREAS</u>	37
3.0	ORBIT AND VEHICLE DYNAMICS	39
3.1	COORDINATE SYSTEMS	39
3.1.1	<u>THE "SELENOCENTRIC COORDINATE SYSTEM" GROUP</u>	39
3.1.2	<u>VEHICLE ATTITUDE COORDINATE SYSTEMS</u>	43

TABLE OF CONTENTS (Cont'd.)

	Page	
3.2	DEFINITION OF ORBIT PARAMETERS AND ORBIT ELEMENTS	47
3.2.1	<u>DEFINITION OF GROUND TRACK</u>	50
4.0	SENSOR STUDIES	53
4.1	LASER INVESTIGATION	53
4.1.1	<u>LASER ALTIMETER - FUNCTIONAL BLOCK DIAGRAM</u>	53
4.1.2	<u>TRANSMITTING AND RECEIVING MODES</u>	55
4.1.3	<u>INDUSTRY SURVEY</u>	55
4.1.4	<u>EFFECT OF LASER PULSE RATES ON THE DERIVED PROFILE</u>	58
4.1.5	<u>RANGING ACCURACY REQUIREMENTS OF THE LASER</u>	60
4.1.6	<u>RELIABILITY CONSIDERATIONS</u>	60
4.1.7	<u>LASER ALTIMETER TRADE-OFF CHARACTERISTICS</u>	60
4.1.8	<u>SUMMARY OF THE LASER INVESTIGATION</u>	62
4.2	LUCOM RADAR SENSOR INVESTIGATION	62
4.2.1	<u>RADAR RETURN SIGNAL INTERPRETATION</u>	63
4.2.2	<u>SURFACE SCATTERING MODEL</u>	66
4.2.3	<u>RETURN SIGNAL AND SURFACE CHARACTER- ISTICS RELATIONSHIP</u>	67
4.2.4	<u>RADAR PROFILE PARAMETRIC ANALYSIS</u>	70
4.3	RADAR SENSOR DESIGN	88
4.3.1	<u>EVALUATION OF TECHNIQUES</u>	90
4.3.2	<u>SYSTEM DESIGN DISCUSSION</u>	91
4.3.3	<u>TRADE-OFFS AND ERROR ANALYSIS</u>	94
4.3.4	<u>SELECTION OF COMPONENTS</u>	103
5.0	DATA HANDLING	117
5.1	TELEMETRY STUDY	117
5.1.1	<u>CONSTRAINTS</u>	117
5.1.2	<u>DATA STORAGE</u>	118
5.1.3	<u>VEHICLE DATA LINK</u>	118
5.1.4	<u>PCM FRAME FORMAT</u>	133
5.1.5	<u>R. F. LINK ANALYSIS</u>	134
5.1.6	<u>DATA LINK ERRORS</u>	134
5.1.7	<u>EQUIPMENT PERFORMANCE CHARACTERISTICS</u>	138
5.1.8	<u>TRADE-OFF ANALYSES</u>	138
6.0	DATA UTILIZATION	145
6.1	DETERMINATION OF THE LUNAR FIGURE	145

TABLE OF CONTENTS (Cont'd.)

	Page
6.1.1	<u>IMPROVEMENT OF THE APOLLO ORBIT</u> 145
6.1.2	<u>GROUND TRACK ERROR AS A FUNCTION</u> <u>OF ORBIT ELEMENTS</u> 149
6.1.3	<u>FOURIER SERIES TECHNIQUE</u> 152
6.1.4	<u>LEAST SQUARES FIT METHOD</u> 155
6.2	<u>VERTICAL CONTROL FOR PHOTOGRAPHS</u> 161
6.3	<u>DETERMINATION OF SLOPES AND SURFACE</u> <u>RELIEF</u> 163
6.4	<u>INTERIM SELENODETTIC CONTROL</u> 164
6.5	<u>COMPUTER PROGRAMS</u> 166
6.5.1	<u>ILLUMINATED AREA ROUTINE</u> 166
6.5.2	<u>RADAR SIMULATOR ROUTINE</u> 168
6.5.3	<u>LEAST SQUARES ROUTINE</u> 170
6.5.4	<u>FOURIER COEFFICIENTS ROUTINE</u> 170
6.5.5	<u>CONTOUR AND SURFACE FITTING AND</u> <u>PLOTTING ROUTINE</u> 171
6.5.6	<u>BENCH MARK RECOGNITION PROGRAM</u> 171
7.0	<u>CONCLUSION AND RECOMMENDATIONS</u> 173
8.0	<u>LUCOM PHASE II STATEMENT OF WORK</u> 175
8.1	<u>INTRODUCTION</u> 175
8.2	<u>OBJECTIVES AND SCOPE</u> 175
8.2.1	<u>OBJECTIVES</u> 175
8.2.2	<u>SCOPE</u> 176
8.3	<u>TASKS</u> 176
8.3.1	<u>LUNAR SURFACE RELIEF MODEL</u> 176
8.3.2	<u>SYSTEM SIMULATION</u> 177
8.3.3	<u>STATISTICAL SENSOR DESIGN</u> 177
8.3.4	<u>TRADE-OFF STUDIES</u> 178
8.3.5	<u>ANTENNA STUDY</u> 178
8.3.6	<u>DATA-LINK TECHNOLOGY</u> 178
8.3.7	<u>DATA USEABILITY TECHNIQUES</u> 179
8.4	<u>TECHNICAL CONSULTANTS</u> 180
8.5	<u>SUMMARY DISCUSSION</u> 181

APPENDICES

4.1-A	<u>LASER MATHEMATICAL MODEL</u> 183
4.2-A	<u>AN INTRODUCTION TO SPECIAL CALCULATIONS</u> <u>FROM DIGITAL RECORDS</u> 199

TABLE OF CONTENTS (Cont'd.)

	Page
4.3-A	
through	
4.3-H RADAR SENSOR ANALYTICAL DEVIATIONS	219
5-A TELEMETRY TABLES (AI through AXV)	290
5-BI SEQUENCE CONTROL UNIT - STATE DIAGRAM DEFINITIONS	331
5-BII LOGIC EQUATIONS FOR SEQUENCE CONTROL UNIT	334
5-C BIT ERROR PROBABILITY	337

LIST OF ILLUSTRATIONS

Figure		Page
1. 1-1	LUCOM CONCEPT	4
1. 2-1	LUCOM FUNCTIONAL-BLOCK DIAGRAM FOR COMMAND SERVICE MODULE	6
1. 1. 2-1	DATA UTILIZATION - FLOW DIAGRAM	13
2. 0-1	LUCOM SENSOR TRADE-OFF ANALYSIS FLOW DIAGRAM	16
2. 1. 1-1	LUCOM COORDINATE SYSTEMS	18
2. 2. 2-1	FIRST RETURN GEOMETRY	38
3. 1. 1. 1-1	SELENOCENTRIC SYSTEMS	40
3. 1. 2-1	VEHICLE ATTITUDE COORDINATE SYSTEMS	45
3. 1. 2-2	COORDINATE TRANSFORMATION SEQUENCE	46
3. 2-1	RELATION OF ORBIT PARAMETERS TO VEHICLE POSITION COORDINATE SYSTEM	47
3. 2. 1-2	SUB-ORBITAL TRACK CROSSING	49
4. 1. 1-1	LASER ALTIMETER BLOCK DIAGRAM	54
4. 1. 2-1	LASER ALTIMETER TRANSMITTING AND RECEIVING MODES OF OPERATION	56
4. 1. 4-1	LASER GEOMETRY USED FOR EXAMINING EFFECT OF LINE-OF-SIGHT DEVIATIONS FROM THE VERTICAL	58
4. 1. 4-2	EFFECT OF TERRAIN SLOPE ON RANGE MEASUREMENTS	60
4. 1. 4. 3	SIMULATED LASER RANGE MEASUREMENTS COMPARED AGAINST THE ACTUAL PROFILE	61
4. 2. 1-1	RELATIONSHIP OF RETURN POWER, AREA EXCITED AND RANGE	64
4. 2. 3-1	AREA GROWTH FOR FINITE PULSE	68
4. 2. 3-2	UNWEIGHTED AREA GROWTH FROM RANDOM SURFACE	69
4. 2. 4. 3. 1-1	AUTO-COVARIANCE FUNCTION	73
4. 2. 4. 3. 1-2	POWER SPECTRAL DENSITY	73
4. 2. 4. 3. 2-1	WEIGHTING FUNCTION DESCRIPTION	75
4. 2. 4. 3. 2-2	DIGITAL ANTENNA PATTERN	75
4. 2. 4. 3. 2-3	27X27 ANTENNA MASK	76
4. 2. 4. 3. 3-1	AREA DEPTH RELATIONSHIP (TYPICAL)	78
4. 2. 4. 4. 1-1	QUANTIZED BUILD-UP VS AREA	80
4. 2. 4. 4. 1-2	QUANTIZED BUILD-UP VS AREA	82
4. 2. 4. 4. 1-3	QUANTIZED BUILD-UP VS AREA	83
4. 2. 4. 4. 1-4	QUANTIZED BUILD-UP VS AREA	84

LIST OF ILLUSTRATIONS (Cont'd.)

Figure		Page
4.2.4.4.2-1	GROUND TRACK (S. M.)	86
4.2.4.4.2-2	A/D TRANSFORMATION VS THRESHOLD AREA	87
4.2.4.4.2-3	A/D TRANSFORMATION OF 1° BEAMWIDTH AND VIDEO BUILD-UP	89
4.3.2.2-1	PRELIMINARY LUCOM RADAR SENSOR	93
4.3.3.1-1	PEAK OUTPUT POWER	96
4.3.3.1-2	SENSOR & ANTENNA WEIGHT & VOLUME	98
4.3.3.1-3	PRIME POWER	100
4.3.3.2-1	RMS ERROR	102
4.3.4.2-1	PRELIMINARY LUCOM DATA PROCESSOR	106
4.3.4.2-2	MICROELECTRONIC DATA PROCESSOR	108
4.3.4.3-1	APERTURE SIZE VS FREQUENCY	110
4.3.4.3-2	ANTENNA GAINS	113
4.3.4.3-3	ANTENNA WEIGHTS	114
4.3.4.3-4	SLOT ARRAY ANTENNA	116
5.1.3.1-1	DATA LINK BLOCK DIAGRAM MODEL NO. 1	121
5.1.3.2-1	DATA LINK BLOCK DIAGRAM MODEL NO. 2	123
5.1.3.3.2-1	MULTIPLEXER - ENCODER BLOCK DIAGRAM	125
5.1.3.3.5-1	TYPICAL BIT SYNCHRONIZER AND DATA DETECTOR	127
5.1.3.3.5-2	VCO AND DATA REGENERATOR	129
5.1.3.3.5-3	PHASE DIAGRAM	130
5.1.3.3.6-1	INPUT - OUTPUT SIGNALS	131
5.1.3.3.6-2	SEQUENCE CONTROL UNIT LOGIC DIAGRAM	132
5.1.6-1	PEAK SIGNAL/RMS NOISE (db)	136
5.1.8-1	VHF DATA LINK	140
5.1.8-2	S-BAND DATA LINK	141
5.1.8-3	TRANSMITTER POWER (WATTS)	142
5.1.8-4	DATA LINK MODEL NO. 1 ALT. ERROR RATE	143
5.1.8-5	DATA LINK MODEL NO. 2 ALT. ERROR RATE	144
6.1.1-1	SPACE CRAFT OCCULTATIONS	146
6.1.1-2	ORBIT PATHS	147
6.1.4-1	LEAST SQUARES FIT PROBLEM	156
6.3-1	ORBIT CROSSING GEOMETRY	163
6.4-1	NUMERICAL SURFACE TECHNIQUES	165
4.1-A.1.1-1	SUN SPECTRUM OUTSIDE EARTH'S ATMOSPHERE VS. 6000°K BLACK BODY (FROM REF. 1)	184
4.1-A.1.2	ISOTROPIC REFLECTION GEOMETRY	185
4.1.A.3-1	FREQUENCY SPECTRUM	191

LIST OF ILLUSTRATIONS (Cont'd.)

Figure		Page
4.1-A.3-2	INTENSITY OF A LASER SPOT	192
4.1-A.3-3	NUMBER OF RECEIVED SIGNAL PHOTOELECTRONS	194
4.1-A.4-1	GEOMETRY OF LASER RANGING AGAINST A SLOPING TERRAIN	195
4.1-A.4-2	RECEIVED PULSE WIDTH NORMALIZED TO TRANSMIT PULSE WIDTH AS A FUNCTION OF TERRAIN SLOPE	197
4.3-B-1	NOISE SAMPLES	224
4.3-B-2	VIDEO RETURN	224
4.3-B-3	FREQUENCY SPECTRUM	224
4.3-D-1	THRESHOLD DETECTION	236
4.3-D-2	DETECTION PROBABILITY (P_d)	236
4.3-D-3	LOCK-ON PROBABILITY	240
4.3-D-4	THRESHOLD-TO-NOISE VS FALSE ALARM PROBABILITIES	242
4.3-E-1	4 PPS - 5° BEAMWIDTH	246
4.3-E-2	100 PPS - 5° BEAMWIDTH	247
4.3-E-3	1000 PPS - 5° BEAMWIDTH	248
4.3-E-4	4 PPS - 3° BEAMWIDTH	249
4.3-E-5	100 PPS - 3° BEAMWIDTH	250
4.3-E-6	1000 PPS - 3° BEAMWIDTH	251
4.3-E-7	4 PPS - 1° BEAMWIDTH	252
4.3-E-8	100 PPS - 1° BEAMWIDTH	253
4.3-E-9	1000 PPS - 1° BEAMWIDTH	254
4.3-E-10	PROFILE ANALYSIS VS THEORETICAL THRESHOLD AREAS	255
4.3-F-1	C-BAND MAGNETRONS	258
4.3-F-2	X-BAND MAGNETRONS	259
4.3-F-3	KU BAND MAGNETRONS	260
4.3-F-4	MODULATORS	261
4.3-F-5	SENSOR WEIGHT	263
4.3-F-6	SENSOR VOLUME	264
4.3-F-7	SENSOR-ANTENNA WEIGHT-VOLUME 5° BEAMWIDTH	266
4.3-F-8	SENSOR-ANTENNA WEIGHT-VOLUME 3° BEAMWIDTH	267
4.3-F-9	SENSOR-ANTENNA WEIGHT-VOLUME 1° BEAMWIDTH	268

LIST OF ILLUSTRATIONS (Cont'd.)

Figure		Page
4. 3-H. 1-1	FLOW DIAGRAM FOR SIGNAL SIMULATION	275
4. 3-H. 1-2	EXAMPLES OF SIGNAL BUILDUP	276
4. 3-H. 1-3	MEAN DELAY VS NOISE AND THRESHOLD	278
4. 3-H. 1-4	RMS ERROR VS NOISE AND THRESHOLD	279
4. 3-H. 1-5	MEAN DELAY VS BANDWIDTH	280
4. 3-H. 1-6	RMS ERROR VS BANDWIDTH	281
4. 3-H. 3-2	VERTICALITY THRESHOLD ERROR	284
5-B1-1	SEQUENCE CONTROL UNIT STATE DIAGRAM	333

LIST OF TABLES

Table		Page
1. 5-1	LUCOM SYSTEM ACCURACY	12
4. 3. 4. 3-1	ANTENNA DEPTH (FEET)	111
6. 1. 4-1	LUCOM ORBIT CALCULATION	160
4. 1-A. 1-1	BACKGROUND NOISE PHOTOELECTRONS	187
4. 1-A. 2-1	PHOTOMULTIPLIER CHARACTERISTICS AT 25°C	188
4. 3-B-1	BANDWIDTH COMPARISON	226
4. 3-B-2	NOISE FIGURE (db)	227
4. 3-C-1	MINIMUM RANGE - GATE WIDTH (t_{rg})	231
4. 3-D-1	THRESHOLD-TO-NOISE (db)	238
4. 3-D-2	SIGNAL-PLUS-NOISE-TO-NOISE (db)	238
4. 3-E-1	PEAK POWER REQUIREMENTS (KW)	256
4. 3-F-1	MAGNETRON TRADE-OFF REGULATIONS	257
4. 3-F-2	SENSOR & ANTENNA WEIGHTS (lbs)	265
4. 3-F-3	SENSOR & ANTENNA VOLUMES (IN ³)	265
4. 3-G-1	PRIME POWER REQUIREMENT (WATTS)	272
4. 3-H. 8-1	ERROR STATEMENT	288
5-AI		290
through 5-AXV	TELEMETRY TABLES	through 329

FORWARD

This Final Report documents the technical investigation of LUCOM System feasibility performed by Ling-Temco-Vought, Inc., during the period 5 August 1964 through 18 March 1965 under Contract No. NASA 9-3269. The contract has been administered under the technical direction of Mr. J. G. Garcia representing Mr. John Dornbach, Chief, Lunar Surface Technology Branch, Space Environment, Advanced Spacecraft and Technology Division, NASA, Manned Spacecraft Center.

Six monthly reports were submitted during the contract period to provide a periodic indication of progress. Those LUCOM team members who contributed to the monthly progress reports and this final document include: W. O. Allen, Jr., R. L. Bently, R. E. Davis, George M. Goldberg, J. C. Laswell, D. F. Sellers, D. C. Taulman, J. T. Wakefield, W. F. Webber, R. W. Wilson, A. D. Gondran and R. M. Woolheater.

The work was performed at the Military Electronics Division facilities located on Jupiter Road, Garland, Texas.

This document, and the information contained therein, is unclassified.

ABSTRACT

LUCOM SYSTEM CONCEPT

The LUnar COntour Mapping (LUCOM) System is conceived as a lunar survey package in the Apollo module, consisting of a specially designed radar terrain sensor, a data processor, a telemetry signal conditioner and encoder, two tape recorders, a sequence control unit, a junction controller, and a telemetry transmitter. This equipment is designed to acquire three-dimensional lunar surface data in a continuous pulsed mode, and transmit these data in digital form back to a ground station for processing and use in improving selenographic knowledge of the moon. Specifically, LUCOM will aid in (1) recomputing the size and shape of the moon, (2) providing vertical control for Apollo photography, (3) mapping surface relief features on the dark side of the moon, and (4) establishing a selenodetic control network for updating locations of known features.

PROGRAM OBJECTIVES

This six month study had, as its major objective, the technical determination of the LUCOM System conceptual feasibility. Specific goals included; (1) Definition of sensor, telemetry, storage and interface performance requirements, (2) Establishment of functional and physical characteristics of all system components, (3) Integration of orbital parameters with the system requirements, (4) Definition of automated techniques to reduce the LUCOM data, and (5) Analysis of component error sources.

PROGRAM RESULTS

It is concluded that the LUCOM System design goals are feasible, and that such a subsystem can be fabricated within the physical and functional design limitations of the Apollo System. It is further concluded (based on available estimates of the assumed Apollo orbital error of 100 meters),

that LUCOM can determine the lunar radius from any point in orbit to within \pm 419 feet. Additional conclusions are as follows: (1) A pulse-type radar sensor with the following characteristics, will provide optimum performance for the LUCOM prototype system: Frequency - X band; PRF - 100 pps; Antenna beamwidth - 3° ; Antenna aperture - 2.6 feet; Transmitted pulsewidth - 1.5 microseconds; Peak output power - 11.5 kw; Prime power - 117 watts; Sensor weight & volume - 42 lbs., 557 in.³; Antenna weight & volume - 24.5 lbs., 2000 in.³; (2) A pulse code modulation (PCM) technique has been selected and analyzed as optimum for LUCOM Data Link, and all components (with the possible exception of the tape recorder) are state-of-the-art; (3) Total volume, weight and power for the entire telemetry subsystem - 1065.3 in.³, 38.8 lbs., 92.2 watts; (4) Computer techniques have been evolved to recreate lunar profiles and perform other selenographic tasks, and (5) LUCOM can be readily adapted to other earth-orbiting or planetary missions, to perform vital sensing functions.

1.0 INTRODUCTION

Ling-Temco-Vought, Inc. recognized the need for an altimeter as an essential requirement for the Apollo mission early in 1962. As the Apollo program grew in scope, more and more consideration was given to the specific potential uses of such a ranging device, even though the orbital altitudes were so excessive as to challenge the radar sensor technology. Gradually, however, high altitude radar terrain sensors became an accepted fact as advanced systems went from conceptual design to installation and flight testing.

Finally, in 1964, the concept of a radar mapping system for Apollo attained maturity and was presented to NASA, MSC for consideration. In August 1964, work began under contract to define the system in more detail, analyze its components, and determine its basic credibility.

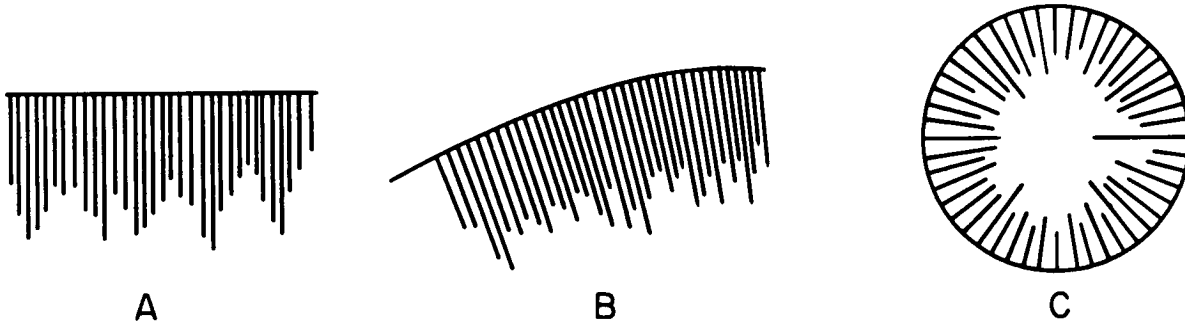
1.1 LUCOM CONCEPT

The LUnar COntour Mapping (LUCOM) System for Apollo is conceived as a lunar survey package consisting of a specially designed radar terrain sensor, a data processor, a telemetry signal conditioner and encoder, two tape recorders, a sequence control unit, a junction controller, and a telemetry transmitter. This equipment is designed to acquire tri-dimensional lunar surface data in a continuous pulsed mode, and transmit this data back to a ground station for processing and use in improving selenographic knowledge of the moon.

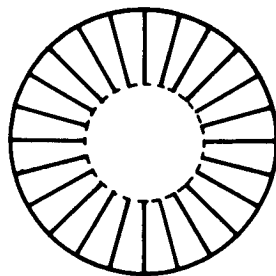
When Apollo orbits the moon, LUCOM will acquire tens of thousands of vertical measurements from the surface to the vehicle in orbit. These distances, by themselves, have little relative meaning unless at least one end of the loop is closed. If each range measurement is conceived as a matchstick of varying lengths, they could be stacked (in sequence) in unlimited arrangements, as pictured on the next page.



Since each matchstick represents a radar measurement from the orbiting vehicle to the unknown surface of the moon, one end of the stick can represent the vehicle. If the vehicle path is known, then the sticks would line up, (on one end at least) along that line of flight, as demonstrated below.



The LUCOM concept assumes that the Apollo orbit can be computed and plotted, somewhat similar to the shape drawn in sketch C, above. Using the same sketch, therefore, to illustrate one of the goals of the System as simply as possible, it is apparent that by connecting the remaining open end of matches with a dotted line, as shown below, a spherical shape is created based on actual measurements.



This concept is described in more applicable terms in Figure 1.1-1. Once the orbit is calculated and refined, the Center-of-mass can be calculated based on Kepler's Law. Each altimetry reading, measured in Time, can then be plotted along a vector to the Center-of-mass. By subtracting the value of the altimetry measurement from the total length of the radius (from the orbit to the Center-of-mass), the length of the radius from the Center-of-mass to the lunar surface will remain. When all the radii are plotted and the surface points connected, a new size and shape of the moon emerges as the end product of LUCOM.

1.1.1 LUCOM TASKS

In broad terms, the LUCOM System concept involves the acquisition of a number of accurate, equally spaced altimetry readings from the lunar surface for each orbit made by the Apollo vehicle. These readings, converted to digital form and transmitted to earth, would be used to perform the following tasks:

- (a) Using the orbit as a base reference datum, and the calculated center-of-mass as a radial point of departure, establish a series of radii to the lunar surface for the improved computation of the size and shape of the moon.
- (b) Using the ranging measurements timed to coincide with the mapping camera exposures and correlated with time and attitude information and orbital parameters, provide a common datum for all photo elevations.
- (c) Using systematic techniques and computer programs, automatically reduce the digital ranging measurements to plots of slopes, relief anomalies, the density and distribution of relief features, and selenographic relief contours of the back side of the moon.
- (d) Using the revised figure of the moon, orbital parameters, guidance data, and tracking data, establish a preliminary selenodic control network for the ultimate correction of coordinates for all known points.

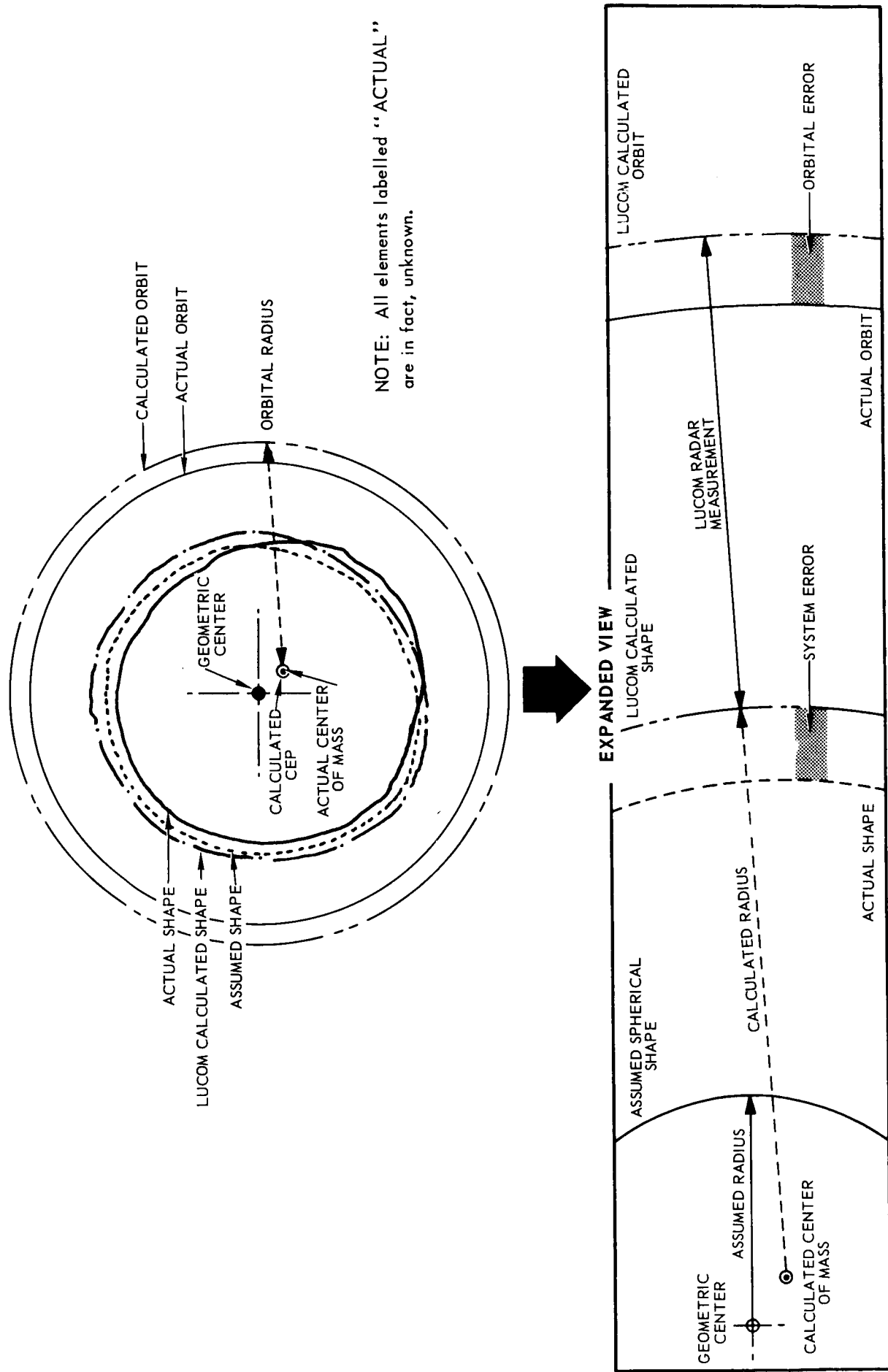


FIGURE 1.1-1

1.1.2

LUCOM FUNCTIONS

The basic ingredient of the LUCOM concept, the ranging measurement from the vehicle in orbit to the surface of the moon, is the most complex in terms of accuracy, resolution and interpretation. The most practical instrument available to perform this function is some type of radar altimeter. On the other hand, a laser ranging device may provide (in the 1967-1970 time period) even greater potential for accurate reconstruction of a surface profile. Regardless of the type ultimately selected for Apollo, the sensor characteristics will directly influence the anticipated value of the acquired signal, and the systems ability to reconstruct the ground profile. In addition to its ranging function, the sensor must convert the return signal to digital form for subsequent transmission to earth, and the pulse rate must be timed and correlated with the Apollo guidance and the optical instrumentation.

These functions are related to the "Data Acquisition" phase of operation. Additional "Data Handling" functions are performed by the data-link (or telemetry) equipment, which converts the data to PCM format and transmits the code to ground receiving stations. The third group of functions, "Data Reduction", takes place at a central location by means of banks of computers and specialized programs devised for practical utilization of the data. The term "Data Utilization" is used instead of "Data Reduction" throughout this document because it provides a more precise connotation of the process for achieving the LUCOM objectives. The conceptual methods for accomplishing these goals are illustrated in the form of a

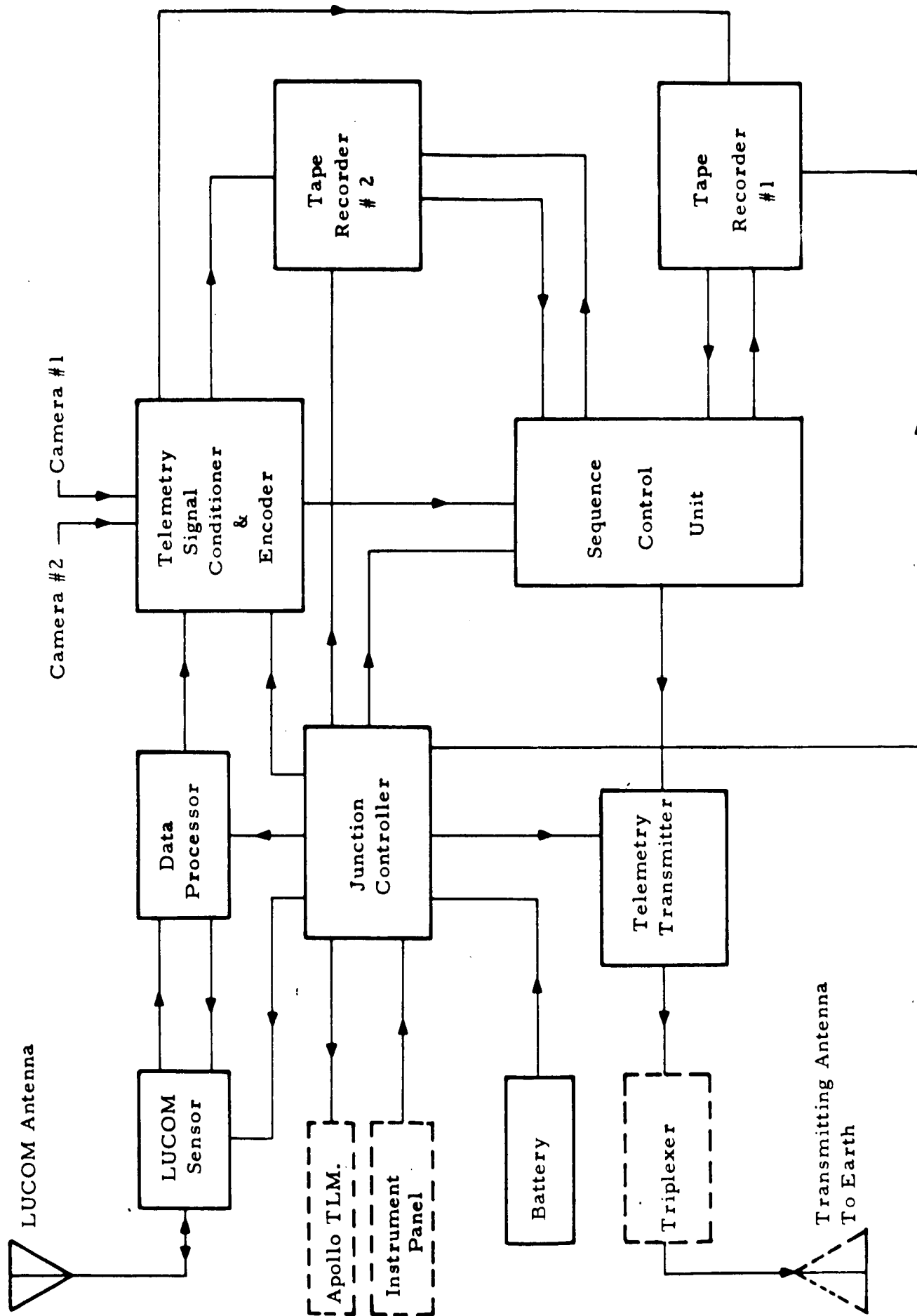
- * Flow Diagram in Figure 1.1.2-1. External Apollo and orbital inputs are correlated with the sensed lunar profile data, and by means of data utilization techniques, improvements in orbit datum reference, size and shape, coordinates, and control network, are obtained in a logical sequence.

1.2

CONCEPTUAL SYSTEM DESIGN

The primary components of the conceptual LUCOM System are shown in the functional diagram of Figure 1.2-1. Blocks enclosed by a dashed line represent interface with Apollo equipment. The block including Apollo Telemetry is a signal from the LUCOM Telemetry indicating that the LUCOM System is operating. The block labeled "Instrumentation Panel" represents the command signal for the LUCOM System "ON" command, which could be a switch on the instrument panel or a signal from other Apollo electronic equipment. The block labeled Triplexer could be a diplexer depending on the Apollo on-board equipment which regulates transmission from two or more sources. The transmitting antenna is the Apollo

* See page 13



LUCOM FUNCTIONAL-BLOCK DIAGRAM FOR COMMAND SERVICE MODULE
 FIGURE 1.2-1

transmission antenna to the earth Deep Space Instrumentation Facility (DSIF) stations. The components shown in Figure 1.2-1 which are enclosed by solid lines are the primary components of the LUCOM System. They are briefly described in the following paragraphs.

1.2.1 LUCOM ANTENNA

This is the combined transmitter-receiver antenna for the radar terrain sensor. The electrical design will probably be a phased array.

1.2.2 LUCOM SENSOR

The radar sensor consists of a transmitter-receiver which obtains an altimeter type profile of the lunar terrain. This data is in the form of a pulse. The output of the Sensor is presented to the Data Processor.

1.2.3 DATA PROCESSOR

The Data Processor is a digital ranging package. It senses the time of the peak of the transmitted pulse and through a timing clock opens the range gate for the received signal. Using the range gates and a clock oscillator, the range to the Lunar Surface is determined. The range information is transmitted from the Data Processor to the Telemetry Signal Conditioner and Encoder components.

1.2.4 TELEMETRY CONDITIONER AND ENCODER

The inputs to the Telemetry Conditioner and Encoder are: the range signal and short focal length camera time (camera #1). The inputs are synchronized by a telemetry clock and transmitted to the tape Recorders or to the Sequence Control Unit. The most probable telemetry format will be a PCM type.

1.2.5 TAPE RECORDER

The two tape recorders will most probably be a magnetic recording type. The information obtained during the time that the CSM and Earth are not in line-of-sight will be stored on one recorder; upon regaining line-of-sight, the other recorder will be utilized to store information while the first recorder transmits. The output of the recorders will be presented to the Sequence Control Unit.

1.2.6 SEQUENCE CONTROL UNIT

Basically this unit determines the sequence of transmitting the information from either recorder or the direct output of the Telemetry Conditioner and Encoder. The output of this unit is presented to the Telemetry Transmitter.

1.2.7 TELEMETRY TRANSMITTER

This component transmits the data obtained by the other components of the LUCOM System.

1.2.8 JUNCTION CONTROLLER

The distribution of various power requirements and common grounding for the LUCOM System is the basic function of the Junction Controller components.

1.2.9 POWER SUPPLY

The operational power will be provided by the LUCOM system battery.

1.3 STUDY OBJECTIVES

This six month study had, as its major objective, the determination of the LUCOM System conceptual feasibility. The technical information presented in this document confirms not only that the system design goals are credible, but that even a crude prototype may provide sufficient profile information to recompute the size and shape of the moon to within a few hundred feet of its actual figure. Specific goals of the program (in condensed form) include:

- (1) System Definition
 - (a) Define the system in functional form.
 - (b) Define sensor, telemetry and storage performance requirements.
 - (c) Establish elements of a computer program for plotting sub-orbital tracks for LUCOM data.

- (d) Determine feasibility of establishing photo control network and vertical datum.
- (e) Devise computer programs to derive slopes, relief histograms, etc. from LUCOM data.
- (f) Provide integrated system performance specifications.
- (g) Provide integrated block diagram.

(2) Sensor Design Studies

- (a) Establish design perspective.
- (b) Perform detailed parametric analysis of optimum type radar.
- (c) Document trade-off analyses of sensor parameters.
- (d) Provide detailed sensor performance specification.
- (f) Perform general sensor error analysis.
- (g) Define components for sensor and layout for antenna.
- (h) Define physical parametric trade-offs.

(3) Telemetry Subsystem Design

- (a) Define data-link requirements.
- (b) Establish functional and physical characteristics of data-link components.
- (c) Establish preliminary description of operational sequence.
- (d) Provide block diagram of telemetry subsystem.

- (4) Laser Investigation
 - (a) Define requirements for optical ranging sensor.
 - (b) Compare various laser devices and define performance trade-offs.
 - (c) Define technological problems in meeting LUCOM requirements.
 - (d) Perform quantitative study for estimate of laser performance.
 - (e) Provide block diagram of theoretical device.

All of these goals were attained. As in most conceptual studies, many assumptions were made prior to the investigation of LUCOM as a system, in order to provide a suitable background environment for its operation. During some phases of study, however, the depth of investigation was limited by inadequate knowledge of the Apollo environment.

1.4 STUDY ASSUMPTIONS

The following assumptions were based on the best and most practicable reasoning possible at the time of study, and on certain information provided by NASA, MSC:

- (1) Eighty mile circular orbit.
- (2) Apollo attitude stabilization $\pm 0.5^\circ$ - Rates 1.2 min/sec.
- (3) No attitude program (except pitch to accommodate IMU)
- (4) LUCOM antenna flush mounted - no structural penalty trade-off.
- (5) Radar and camera boresighted to within accuracy of 5 minutes of arc - no parallax.
- (6) Lunar $\delta = 25$ db (or 0.31% coefficient of reflectivity/unit area).

- (7) Gemini recorder (RCA type) with potential of 138 altitude readings per second, will be operational.
- (8) Continuous line-of-sight between CSM and auxiliary module will be maintained.
- (9) All LUCOM Data will be transmitted to earth (from CSM).
- (10) Cameras similar to ORBITER Payload.

These and other assumptions were used as limiting factors in the study with the premise that changes in the instrumentation or mission profile may or may not affect the ultimate system design. No specific physical limitations were used in developing the system other than the design goal of minimum size, weight and power requirements.

1.5 LUCOM SYSTEM ACCURACY

Due to the lack of firm Apollo information and other factors, it was not possible to perform a complete system error analysis in the LUCOM Study. A tentative summary of assumed and computed errors is shown in Table 1.5-1. The Apollo orbit error figure was taken from data published last fall (1964). The numbers for vertical determination are shown to indicate that as long as this figure is small relative to one half beamwidth, no geometrical error is produced. However, a verticality error is included in the radar sensor error analysis. This is based on an assumption of $1/2^\circ$ Apollo stabilization accuracy.

The terrain histogram error is the σ of the reconstructed A/D transformed profiles compared to the LAC chart profiles from which they were taken.

In combining these numbers into a total error figure, it was not known whether the Apollo estimated error was a 1σ or a 3σ number. A total is shown for each number as indicated by the notations. Time did not permit completion of the profile analysis for the 5° data and, consequently, there is no terrain histogram error figure for that summation. It will be noted that the radar error is almost insignificant compared to the Apollo orbit error and the error resulting from the reconstructed terrain histogram. The 1° and 3° terrain histogram errors, as discussed in section 4.2, can be improved by further study and selection of proper radar parameters, i. e., beamwidth and tracking area.

LUCOM SYSTEM ACCURACY

LUNAR RADIUS DETERMINATION

ANNENNA BEAMWIDTH	5° σ^2	3° σ^2	1° σ^2
APOLLO ORBIT ERROR - 333 FEET			
3 = 333 = 111 FEET	12.3 X 10 ³	12.3 X 10 ³	12.3 X 10 ³
1 = 333	111. X 10 ³	111. X 10 ³	111. X 10 ³
VERTICAL DETERMINATION			
INERTIAL PLATFORM GYRO COMPASS ~.05°			
STAR TRACKER ~.003°			
HORIZON SCANNER ~.05°			
ALIGNMENT ERRORS .15°			
RMS .17°	0	0	0
LUCOM RADAR SENSOR	9.0 X 10 ³	0.97 X 10 ³	0.04 X 10 ³
TERRAIN HISTOGRAM OF A/D TRANSFORMED PROFILES		162. X 10 ³	43.1 X 10 ³
Σ^*		175.3 X 10 ³	55.4 X 10 ³
RSS		419 FEET	235 FEET
$\Sigma^\#$		274 X 10 ³	154 X 10 ³
RSS		573 FEET	393 FEET

TABLE 1.5-1

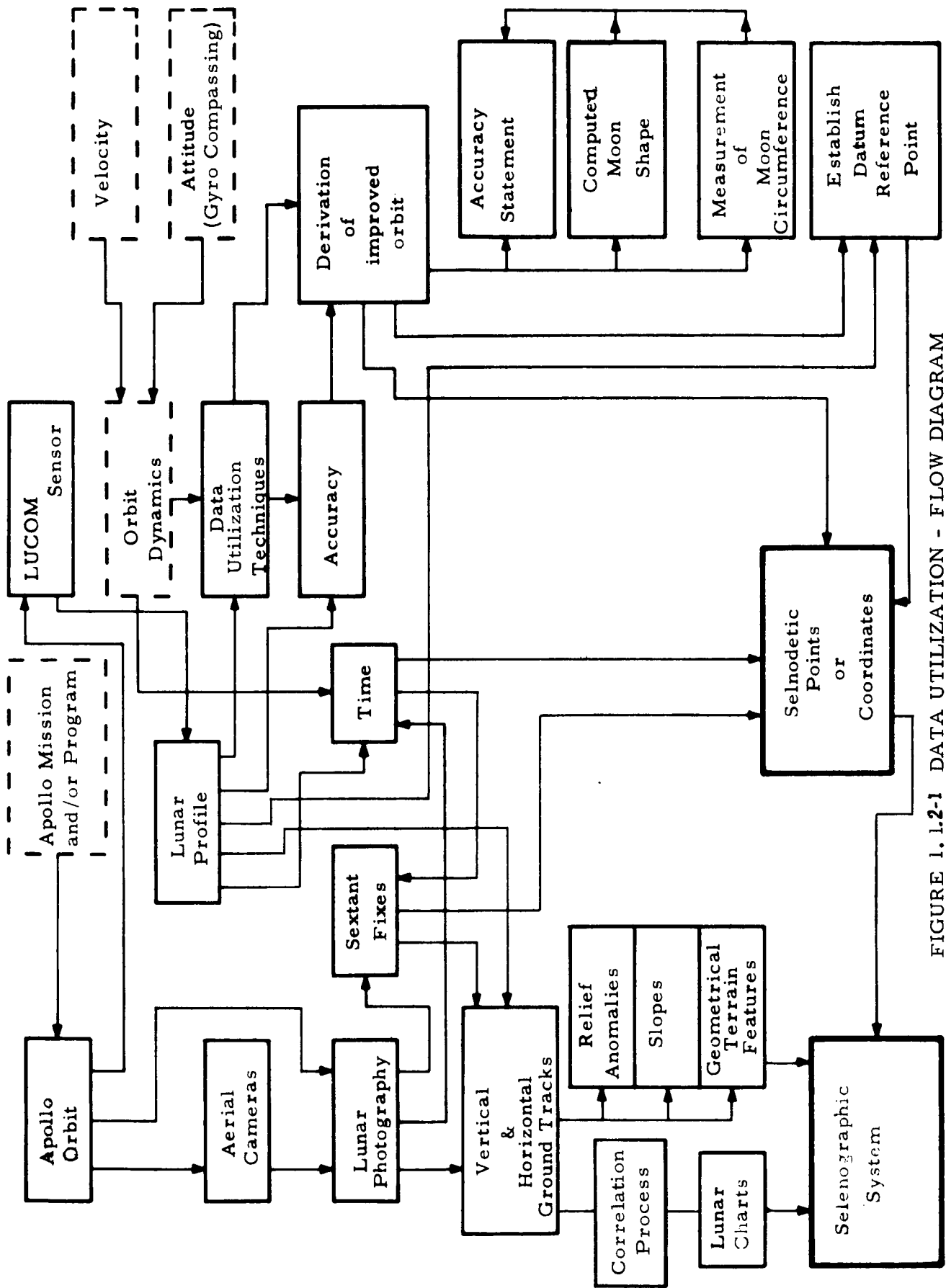


FIGURE 1.1.2-1 DATA UTILIZATION - FLOW DIAGRAM

2.0 TECHNICAL STUDY APPROACH

The development of a system from its initial concept to ultimate operational use involves a complex chain of events. Normally, it is not enough to know what the system will do or how it will perform; the designer must be aware of the conditions under which it will perform, and the effects of this environment on the system characteristics and performance. LTV was aware at the start of this study program, that only limited Apollo data would be made available during the course of investigation. As in any advanced design objective, therefore, it was decided to concentrate on the general requirements for the LUCOM system and on the functional characteristics of the various components which make up the system. Primary emphasis was placed on performing quantitative analyses of the sensor and telemetry components, so that various parameters could be presented in the form of operational trade-offs. The term "trade-off" is used to indicate that when one element or characteristic of a component is weighed against any other element to measure efficiency, accuracy, response, or cost, the selection of either of the elements is evaluated in terms of optimum gain for the entire system. Sometimes this means that one system component is compromised in order to gain overall system improvement, but not always. Trade-off analyses performed early in a program are considered preliminary because the analysis is based on inconclusive data. As environmental and mission data solidifies, however, the trade-offs assume a more meaningful form and provide a solid basis for system final design. As an example of the type of trade-offs considered for LUCOM, a simple flow diagram, Figure 2.0-1, illustrates the procedure used in analyzing the primary sensor parameters. The blocks are keyed to indicate the flow of inputs and/or component characteristics into the various phases of analyses, the techniques used, and the result of these analyses. Although this method worked very well for the system components, different approaches were necessary for other areas of study. One of the unique features of the LUCOM concept, for example, involves an operation almost entirely divorced from the physical aspects of the system - data utilization. The LUCOM hardware represents only that portion of the total system which senses, acquires and transmits profile data in real time. The remaining aspect involves reduction of the data,

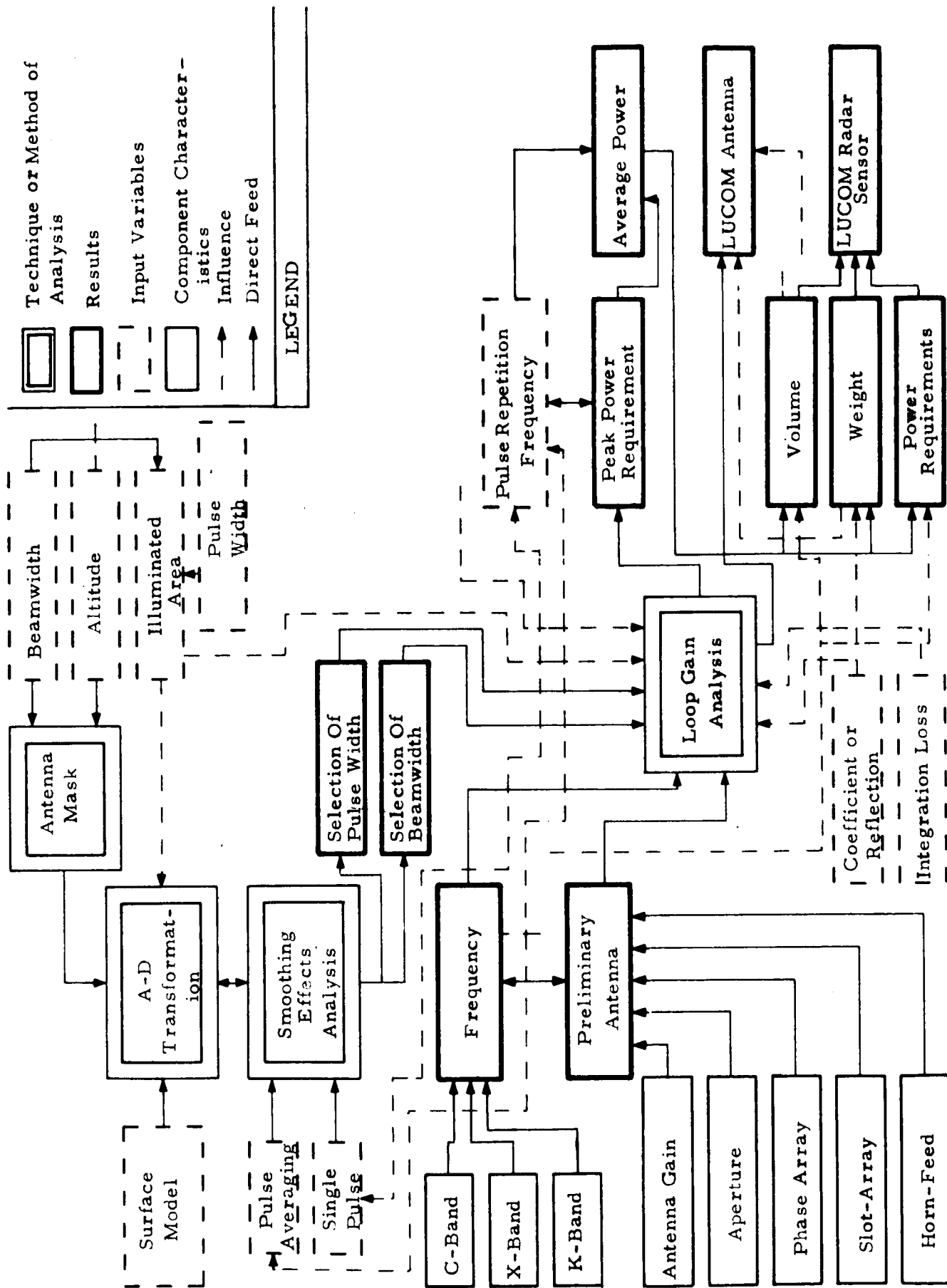


FIGURE 2.0-1. LUCOM SENSOR TRADE-OFF ANALYSIS FLOW DIAGRAM

and utilization of computer techniques to convert it to meaningful scientific information. For this part of the system, various techniques for data conversion were investigated, and numerous computer programs either revised or studied with a view towards practical application to the specific LUCOM objectives.

2.1 DISCUSSION OF THE PROBLEM

The determination of a more accurate figure of the moon is one of the main objectives of the LUCOM system. This requirement which is common to all the program objectives, provides a coherent function which unifies the system concept.

2.1.1 FRAME OF REFERENCE

In the LUCOM concept the Apollo orbit is the base reference from which measurements are made to the lunar surface. The LUCOM accuracy is dependent, to a great extent, on the computation of the Apollo orbit and the capability of deriving the position of the space craft at any given time with the greatest possible precision. When the elements of the orbit, and the coordinates of a frame of reference at the moon to which this orbit can be referenced, are known, the position of the space craft can be determined within the accuracy of the instrumentation relative to a chosen reference point. Due to the great length of the lunar geocentric orbit radius, and the large position errors at the moon associated with small angular errors at the earth, it is imperative to reference the orbit to lunar local geometry. This may be done to ultimate accuracy only by means of the "local" instrumentation; i. e., the Apollo navigation system. The lunar coordinate system universally used was axes x , y and z with $+x$ directed toward the earth, $+z$ (the rotational axis) directed positively toward the north pole (in the same direction as the earth's north pole), and $+y$ orthogonal to x and z directed eastward, toward the direction of motion of the moon in the sky and the earth's eastern horizon. A discussion of this coordinate system and the coordinates of the satellite orbit are included in section 3.0 of this report. The selenocentric reference for this system has its origin at the center of the visible disc and on the line from the hypothetical observer at the moon's center to the earth. This point is defined as the intersection of the lunar meridian through the earth's center and the plane of the lunar equator at the point where the moon's mean longitude equals the longitude of the ascending node. Ideally, the point of reference for a selenocentric system would be one which has been so located and which is consequently adaptable to analytic study.

A difficulty which arises, however, is identification by remote means of that point on the lunar surface. This requires determinations on all three axes of the selenocentric coordinate system. The ultimate result of this process would be complete definition of a spheroidal surface at some radius R from the lunar center of mass. Given the Apollo orbit, one of the coordinates would be directly available by altimetry from the Apollo. The surface coordinates are not directly available from a space craft in orbit, but may be computed from altimetry determinations and central angles. Figure 2.1.1-1 shows these relationships:

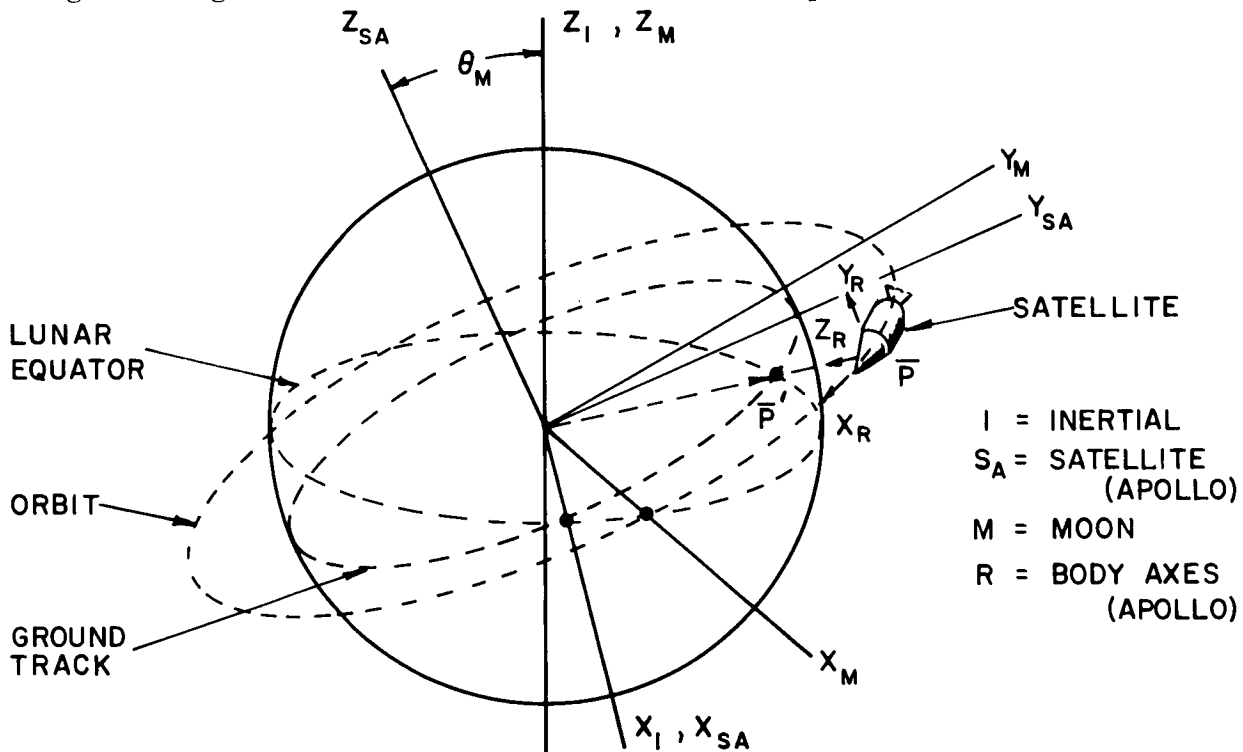


FIGURE 2.1.1-1 LUCOM COORDINATE SYSTEMS

2.1.2 CURRENT SELENOGRAPHY

To propose the implementation of a system such as LUCOM to the problems outlined in the preceding paragraph, it is necessary to have knowledge of the present state of selenodetic data. A comprehensive analysis of selenodetic accuracy has not been found in the available literature. Errors in knowledge of lunar cartography have a number of complex sources. The most prominent of these are probably:

- (a) Errors in mean apparent (geocentric) longitude and latitude

- (b) Uncertainty of applying practical engine divided coordinate system to lunar surface (reference point)
- (c) Error in observation of optical librations
- (d) Resolution of lunar detail from earth
- (e) Uncertainty of radius of selenoid with resulting horizontal errors

The reference system used by the earliest true lunar topographer, Tobias Mayer (1723-1762), had as its reference the central peak of the crater Manilius, however, modern astronomers have chosen the small crater Mosting A (Long. $-5^{\circ} 10' 19'' \pm 8''$; Lat. $-3^{\circ} 11' 24'' \pm 5''$, Franz 1889, 1901) near the central meridian as the reference for surface coordinates. Using this crater as an initial point, selenocentric control systems provide the capability for locating objects on the lunar surface to ± 506 meters CEP at the center of the apparent lunar disk.

Methods have been devised for locating these features three dimensionally, but since these methods relate to the limb of the moon or to the neighboring star fields, their uncertainty increases as the center of the disk is approached.

Shadow techniques have been used by several investigators. This work has been based on the rationale that since variations in elevation on the lunar surface are only local anomalies on some mean spheroid, then relative altitudes may be derived by observational methods from the vantage point of the earth. Dr. R. B. Baldwin (Measure of the Moon - 1963) and others have used the method of observing the progressive changes of shadow length to compute altitudes as well as observing the differential rate of motion of shadows on the surface to indicate slope of the surface itself. All these efforts are still hampered, however, by lack of an absolute datum by which to scale the reference spheroid.

The determination of an absolute spherical datum has been attempted by Baldwin and others from shadow analyses, with results comparable to the uncertainties in horizontal determinations. A recent project of selenocentric control adjustment claimed to be the most extensive ever obtained from astronomical data has been completed by AMS, with a computed uncertainty of $+1094$ meters horizontally and ± 858 meters vertically. A similar selenocentric system is being completed by ACIC, using different methods and source data.

It is interesting to note that the reduction at JPL of data from the successful Ranger VII photographic shot, results in an unaccountable residual in time of 1.5 second. An evaluation of timing accuracy in the mission showed an uncertainty of only .03 second. The discrepancy of 1.5 second in impact time could be explained by a displacement of the moon's center of mass 3.0 km closer to the earth than previously thought. Displacement of the lunar center of mass to the east or west of the geometrical center of the moon's figure would have long since been detected as an asymmetry in the librational motions, but a displacement of the center of mass toward or away from the earth on the moon's orbital radius vector could not be detected observationally, because of the uniformity of the moon's rotation and synchronism with its orbital period. The difference in these two periods was determined by Banachiewicz in 1955 to be ± 0.1 second, about 1 part in 23.6 million. Therefore, since the location of the moon's center of mass relative to the geometrical figure may be measured directly from an altimeter instrument in orbit around the moon, it is apparent that the LUCOM system can make a heretofore unavailable scientific determination, aside from considerations of the precision of the measurement.

2.1.3 DATA ACQUISITION

The data required by the LUCOM System is in the form of altitude measurements taken from the orbiting space craft, so that by subtracting these readings from the orbit radius, the surface of the moon can be described. This requires a sensor of the altimeter type, adapted to the LUCOM requirements and environment.

Requirements for the sensor are generated by the LUCOM program operational objectives. These relate specifically to:

- (a) Range
- (b) Target characteristics (lunar surface)
- (c) Resolution required
- (d) Data rate
- (e) Available field of view
- (f) Power availability

- (g) Weight availability
- (h) Space availability
- (i) Environment.

2. 1. 3. 1 Range

Range is a function of orbit altitude and was derived from the orbit and vehicle dynamics study. The range at which the sensor must operate reflects requirements on the sensor with respect to peak power, antenna beamwidth and gain, and sensor size and weight. All these parameters were analyzed relative to range and other requirements in the trade-off parameters discussed in section 4. 0.

2. 1. 3. 2 Lunar Surface Characteristics

Characteristics of the lunar surface are of great importance from several standpoints. The albedo of the surface in the spectral region of the sensor determines the signal power return from the surface to the sensor, and is one of the parameters in the loop gain equation of the sensor.

The surface texture, or detail structure of the surface, is the characteristic reproduced by the sensor in digital form as the result of continuous pulsed ranging measurements. Because these data will undergo a "smoothing" effect, it is necessary to predict the resolution of slopes, differential altitudes, etc.

The character of the lunar surface as determined by previous studies gives a clue to this requirement. Work done by Baldwin and others has been studied, as well as a review of the basic factors which affect resolution of detail on the lunar surface. Lunar slopes over long distances are more convex than those on earth. This results partly from the fact that the lunar radius is one-fourth that of the earth, as well as the apparent lack of processes of sedimentation on the moon which produce leveling effects on earth.

The variety of lunar slopes and details which the sensor will be required to resolve, will range from small craters and rubble on a surface which will have a long slope ranging from 0. 1% to slopes of 30⁰ - 40⁰ in some

large craters. In areas of the mare, the slopes have low gradients and appear to change very little over long distances. The lunar maria on the visible side are by far the most conspicuous relief features, covering the greatest percentage of area, and having the lowest slope gradients. The photographs (however indistinct) taken by Russia's LUNIK III, show an even greater number of maria on the dark side. The advantages inherent in acquiring a more accurate surface profile over these large, relatively flat areas with the LUCOM radar sensor, are significant. Only in the rugged mountain areas (as shown on the LAC profiles used for the Radar Parametric Profile Analysis) will the ranging accuracy decrease due to the tracking threshold used.

2. 1. 3. 3 Resolution

The problem of resolution in a sensor is primarily related to the range of operational requirements. Obviously, the best possible resolution is desired. The problem, therefore, was to determine what resolution could be attained within the practical constraints of the state-of-the-art and within the limitations placed on power, space and weight available on the Apollo CSM or LSM.

2. 1. 3. 4 Physical and Environmental

Trade-off studies were necessary to determine the most economical and effective selection of parameters, since the problems of a radar used in an orbiting vehicle are related to the physical environment as well as the functional requirements.

The radar consists typically of two elements, a receiver-transmitter and antenna. The receiver-transmitter generates the radio frequency signal, detects the return signal and measures the elapsed time as a function of range to and from the target area.

The antenna configuration determines the shape of the radiant energy pattern, and the orientation of the antenna determines the direction to the illuminated area. The antenna aperture is immutably related to operating wave length and frequency by the relationship:

$$A = k \lambda = \frac{k}{f}$$

That is, for a specified beamwidth, the antenna aperture is directly proportional to wavelength and inversely proportional to frequency. This relationship requires larger and larger antenna aperture for smaller beamwidth and improved angular resolution. This is the most restrictive physical requirement imposed by the radar on the vehicle in which it is mounted. Typical apertures for 5°, 3°, and 1° beams in c, x and K_a bands are:

Parabolic Antennas

<u>Band</u>	<u>Aperture (Inches)</u>		
	5°	3°	1°
C (5 KMC)	37	62	180
X (10 KMC)	19	31	86
K (30 KMC)	6	10	31

Regardless of other factors to be discussed later, angular resolution of detail on the surface improves as the antenna beamwidth is narrowed. It is apparent that K_a band would yield the smallest antenna in the table above, but this end of the spectrum is straining at the state-of-the-art. There is a limitation in the transmitted power level possible in K band components. This requires a trade-off analysis relative to availability of components in the time period of the projected operation. Parameters which enter the trade-offs are:

- (a) Antenna beamwidth
- (b) Transmitted pulse width
- (c) Tracking area (detection threshold)
- (d) Transmitted power
- (e) Receiver noise figure
- (f) Coefficient of reflection of target surface.

These trade-offs have been made and are discussed in the investigative description of the laser and radar sensor work (section 4.0).

2.1.3.5 Laser

Problems relative to application of a laser altimeter to the LUCOM program are similar to those for the radar in several respects. Relationships of beamwidth, pulsewidth, transmitted power and receiver noise are the same in principle. The problem of attitude and stabilization of the vehicle, however, becomes much more critical for the laser. The extremely narrow beamwidth of the laser does remove uncertainty as to the identity of the illuminated area on the surface, as long as platform stability is maintained. At the present time, however, lasers are inefficient, pulse rates are low, and average power requirements are too high for this application.

2.1.4 DATA TRANSMISSION

The Apollo mission has been considered as having two possible configurations, viz., consisting of (1) the Apollo CSM with separately manned survey module (LSM), and (2) the Apollo CSM only.

In the first example, the LUCOM System would be installed in the LSM, thus requiring additional storage and telemetry instrumentation in order to transmit acquired data to the CSM.

If a minimum energy orbit (8 - 80 NM) were to be considered, the most critical problem is that imposed by loss of line of sight between the CSM and the LSM. Line of sight distance between the two vehicles is

$$D_{(LOS)} = d_{(CSM)} + d_{(LSM)}$$

where d = lunar horizon distance from vehicle

$$D_{(LOS)} = \sqrt{2Rh_{(CSM)} + h_{(CSM)}^2} + \sqrt{2Rh_{(LSM)} + h_{(LSM)}^2}$$

$$R = 939 \text{ NM}$$

$$h_{(CSM)} = 80 \text{ NM}$$

$$h_{(LSM)} = 8 \text{ NM}$$

$$D_{(LOS)} = 396 + 123 = 519 \text{ nautical miles}$$

The difference in period between the 80 nautical mile orbit and the 8 to 80 nautical mile orbit is about 100 seconds. Thus, in about 5 orbits, line of sight contact will be lost between the vehicles and will not be regained for about 58 orbits or 116 hours, when the Apollo will be overtaken by the LSM. Obviously this arrangement cannot be proposed for a 48 hour total mission since the two craft could not rendezvous within that time limit.

The equal time orbit requires more energy than the 8 - 80 nautical mile minimum energy orbit. The energy required to go from the 80 nautical mile orbit to the 8 - 80 nautical mile orbit is $\Delta V = 160$ ft/sec whereas the energy required to go to the equi-period orbit is $\Delta V = 337$ ft/sec. The altitude of the orbit with low point at 8 nautical miles and period equal to the 80 nautical mile orbit, is 152 nautical miles.

Although this would be a practical arrangement from the standpoint of communication between the CSM and LSM, it would require maximum fuel load, and impose a severe range requirement on the altitude sensor in going from 8 to 152 nautical miles altitude.

In the present study primary emphasis has been placed on the requirements of the 80 nautical mile circular orbit.

2.1.5 DATA HANDLING

Data handling consists of all instrumental functions which operate on or transmit the sensed data within the space craft, or between the Apollo CMS and LSM and between the Apollo CSM and earth.

The major requirements of this element of the LUCOM System are generated by:

- (a) Total orbit period
- (b) Orbital phasing of vehicles
- (c) Range separation between vehicles and between moon and earth
- (d) Data rate
- (e) Storage-playback real time philosophy

The format of the data from the LUCOM System is dictated almost entirely by the S band telemetry system used with the Deep Space Instrumentation Facility (D. S. I. F.) with which it must be compatible.

A discussion is included in section 5.0 on the analysis of data handling between the CSM and an LSM vehicle, however, the main emphasis has been on a system contained entirely within the CSM. This simplifies the data handling problem in the system by eliminating a data link between the LSM and CSM, and at the same time, simplifies problems of storage in the CSM. It also simplifies the selection of frequencies and alleviates problems of interference between the LSM-CSM data link and the CSM-earth link.

The basic requirement for all data handling operations in LUCOM originates with the desired data rate of the sensor information. The maximum non-ambiguous pulse repetition frequency for the sensor is slightly less than 1000 per second when operating at 80 nautical miles altitude. This, plus the required accuracy, establishes the maximum number of good pulses necessary to be transmitted in a given time interval. This rate is probably excessive for a radar sensor since at 1000 per second an altitude reading would be obtained every 5.5 feet. This is well below the resolution of the radar so would not yield discrete data at this same rate. Data rate for a laser sensor could probably approach this figure because of the extremely narrow beamwidth.

No particular problems are anticipated in intrasystem data flow because this rate is well within state-of-the-art rates for telemetry and PCM systems.

2.2 APOLLO INSTRUMENTATION

In the absence of up to date information regarding characteristics of the Apollo instrumentation, assumptions and figures of typical instruments of the same type have been used.

2.2.1 GUIDANCE EQUIPMENT

It is assumed that the Apollo guidance equipment will include the following items:

- (a) Inertial platform

(b) Star tracker

(c) Horizon scanner

With these instruments, the following sequence of functions can be used to give local vertical.

Gyro compassing, in which the horizon scanner coerces the platform around with the rotation of the radius vector, would place the platform in the orbital plane within a few minutes of arc or better. This platform attitude would then be referenced to the celestial sphere to give orbit inclination relative to the body of the moon. The platform mounted star trackers would be used for this. By measuring the angle from the orbit plane to known stars, the orbit plane angle relative to inertial space would be known. This would be transposed to selenocentric coordinates in a further step.

Position in the plane would depend on the horizon scanner. These instruments are good to 0.1° or better with smoothing. By using the star trackers to given an angle to local vertical in the orbital plane, the sub-orbital point on the surface can be found. This would then depend on several measurements:

(a) Gyro compassing accuracy = $.050^\circ$

(b) Star tracking accuracy = $.003^\circ$

(c) Horizon scanner local vertical accuracy = $.050^\circ$

(d) Alignment errors = .15

The RMS of these errors is $.17^\circ$. This does not yield a significant radar error since it is much less than half the radar antenna beamwidths considered in this study. The Apollo vehicle attitude program and stabilization limit cycle will be controlling factors in establishing verticality errors. Until these are known, it is not possible to realistically evaluate the operational program in all details.

2.2.2 CAMERAS

The cameras to be used in the LUCOM mission have not been defined sufficiently for analysis, however, certain assumptions can be made for

the purpose of discussing methods of utilizing LUCOM to perform the objectives of the mission. The cameras to be used in the orbiter payload have been publicized, and it has been assumed that the Apollo cameras will be similar. These cameras are the two-lens Kodak system giving a 24 inch focal length with a 1 meter resolution from 46 KM. This is approximately equivalent to a resolution of 3.2 meters from 80 nautical miles. The lower resolution lens would yield approximately 25 meters.

The areas covered on 60 x 219 mm film and 60 x 60 mm film by the high and low resolution lenses respectively are about 14.5 x 52.8 KM and 116 x 116 KM. These are 7.16 x 26.2 n.m. and 57.3 x 57.3 n.m. The ground intercepts of the radar beamwidths from 80 n.m. are: (to -3 db points)

<u>Beamwidth</u>	<u>Ground Intercept (n. m.)</u>
1°	1.4
3°	4.3
5°	7.0

Assuming that the stabilization of the Apollo stays within the limit cycle of the control system and vertical accuracy is the same, the displacement of the nadir point of the photograph will be about 0.7 mile on the surface.

Under these conditions, the radar first return will be from a point in the suborbital path if the surface is flat. If the surface has some predominant slope, it will be self revealing by simple geometry and can be accounted for in finding the correlation between altimetry information and photographs. The slopes will be determined by computer routines, and taking into account the vehicle attitude at the point of reference, the origin of the first radar return can be calculated. This geometry is shown in Figure 2.2.2-1, on page 38.

This determination is subject to all the statistical errors encountered in dealing with real terrain, but in that respect is not different from other determinations of the altimeter and will have comparable accuracy.

Computations of this nature will permit the elevation of the photograph nadir point, or any other point encompassed by the sensor data, to be determined. This will be increasingly practicable as the data reduction is carried toward the high latitude region of the inclined orbit where the sub-orbit tracks lie virtually on top of one another for great distances, and interpolation transversely between orbits is comparable in quality to longitudinal information.

In a continuation of these studies, current information would be necessary to permit realistic appraisal of the contribution of the Apollo instrumentation to the LUCOM System. The characteristics of the Apollo vehicle attitude program are an essential input to any theoretical simulation of LUCOM performance. Some of the characteristics of individual components may be assumed, but realism provides more factual results.

2.3 SYSTEM DESIGN APPROACH

In order to identify the technical areas involved in the LUCOM study effort, an analysis of the over-all objectives was made to evolve a system design approach.

2.3.1 DESIGN OBJECTIVES

The design objectives of the study may be placed in two main categories, those directed toward the operational objectives of the program, and the design objectives concerned with developing the concept of the LUCOM System instrumentation.

The operational objectives are:

- (a) Determination of the lunar figure
- (b) Vertical control of photographs
- (c) Definition of lunar slopes and details
- (d) Establishment of interim selenodetic control system.

In all these objectives, the central task is measurement of the shape and size of the moon, since the accuracy achievements of all of the remaining goals are dependent, to some extent, upon the accuracy of this determination. Out of these objectives come the requirements and constraints on the LUCOM System concept and instrumentation.

The primary tasks for achieving the system design concept included the study and development of:

- (a) Altitude sensor concept
- (b) Data handling concept including data link and telemetry

- (c) Data utilization techniques
- (d) Trade-off studies to develop trends in effectiveness, power, weight and size, between system components.

2.3.2 DESIGN CONSTRAINTS

The proposed mode of operation for the LUCOM System consists of the acquisition of lunar surface profile data by use of a sensor aboard the Apollo CSM and recording of attitude, position and time data necessary to correlate the profile data with the apparent moon. This requires the basic functions of an altitude sensor of some kind, together with data handling equipment. The occulting nature of the near equatorial orbit, and the requirement for data acquisition on the back side of the moon, in turn generate the requirement for data storage for at least a half orbit period. Further, the practical problem of telemetering the data taken on the back side while continuing to acquire data on the front side, generates the requirement for dual recording and playback capability in the storage equipment.

Design constraints imposed by operation in the mode described here may be listed as:

- (a) Weight - 80 pounds returnable weight (cameras included in this). Total system weight was not specified, but minimum weight is imperative.
- (b) Power - primary power limitation was not specified but minimum power demand is desirable.
- (c) Size - minimum allowable size was not specified but minimum size is desirable.
- (d) The system must operate in lunar environment and survive all operational phases of boosting, etc.
- (e) The system must operate from orbit altitude of 80 nautical miles.
- (f) The system must take continuous data around 24 orbits and by storing and retransmitting the data, relay all the data back to earth (taking into account the periods of almost half of each orbit when the

vehicle is behind the moon at which time communication to earth is not possible).

- (g) The system must be compatible with the S band telemetry system of the earth D. S. I. F.
- (h) The system must interface compatibly with the Apollo systems.
- (i) System data and data utilization techniques must permit maximum fidelity in reconstructing the lunar figure and surface details.

The above listed items are the major constraints imposed on the system. Many other more detailed but no less significant constraints naturally occur in the system design development. These "design limitations" are discussed in detail in the individual sections of section 5 devoted to the system elements.

2. 3. 3 ANALYTICAL TECHNIQUES

The broad spectrum of studies necessary to explore all the technical areas of the LUCOM Program required identification of critical problem areas in order to concentrate effort in these areas, and retain continuity towards the final program goals.

The studies which were made in the specific areas of technology are:

- (a) Apollo orbit analysis
- (b) Vehicle Coordinate System Study
- (c) Lunar surface analysis
- (d) Data utilization techniques
- (e) Computer Program Design
- (f) Data acquisition (Sensor Studies)
- (g) Data Handling
- (h) System Integration

These areas of study, discussed in detail in later portions of the report, are introduced briefly in this section.

2.3.3.1 Apollo Orbit Analysis

Since the Apollo orbit is the base line for the LUCOM altimeter measurements, it is essential that there be a thorough understanding of the orbital elements so the equations can be mechanized in the computer programs. First the equations were derived for computing the orbit elements. These equations were then written into a computer program which is shown in a later section. This routine computes the coordinates of a point in orbit.

2.3.3.2 Vehicle Coordinates System Study

The next step in this sequence of work was derivation of a set of coordinates for the vehicle body axes. This was done to facilitate handling body attitude angles and resolution of the direction coordinates of the radar and camera pointing vectors. Having done this, it was then possible to take Apollo attitude information at any point in the orbit and mathematically derive the true directions in which the radar and camera pointed, thus relating an area on the lunar surface to the space craft axes.

The next step in this study phase was derivation of a least squares fitting method by which the altimeter data could be processed to yield the most probable shape of the moon. The math for this method was formulated and written into a computer program.

At this point, it would be possible to simulate the physical situation of the space craft in lunar orbit and to make coordinate transformations from the axes of the cameras and radar in orbit, to the lunar surface.

2.3.3.3 Lunar Surface Analysis

Altimeter performance analysis depends strongly on knowledge of the surface characteristics and the altimeter representation of the surface. Consequently a study was made for the purpose of deriving an analytical basis for interpretation of the sensor performance. This method, a form of simulation, related especially to a radar altimeter, and incorporates an area - depth (A/D) transformation computer routine.

The Radar Profile Parametric Analysis was accomplished by selecting a typical rough area of lunar topography on the LAC charts, drawing simulated sub-orbital tracks, and reading elevation profiles along these tracks. Data was then inserted into the prepared computer routine. The computer routine first examined the differences of the altitude readings relative to horizontal distance to evaluate roughness. This was in the form of a power spectral density determination computed at various horizontal sampling intervals. The interval spacing which gave the highest equivalent density was chosen as the grid interval to be used in a subsequent process in which the rate of build up of power in a radar return pulse versus time was examined relative to variations of certain important radar parameters. These parameters, pulse width, beamwidth and radar detection threshold illuminated area, were then used in radar trade-off analyses. These processes are described more fully in Section 4.0 of this report.

2.3.3.4 Data Utilization Techniques

In order to mechanize the use, application and analysis of the LUCOM data, it was apparent that computer routines were necessary and should be used to the fullest possible extent. It was with this in view that the orbit computation routines were devised. In addition, a computer program, with sub-routines as needed, was generated to form a complete simulation of the LUCOM operational mission at least in a static sense. By "static" is meant that the program would make point-to-point computations based on input data which is compatible to some sampling time interval, but not continuous in the sense of a "flyable" analog flight simulator which handles continuously variable inputs.

Although a "simulator" routine was written and tested, lack of Apollo data and program time prevented its actual implementation during the LUCOM study period. This is discussed more fully in Sections 2.3.4 and 7.5.

Through the use of computer routines described in Section 7.5, the LUCOM data utilization can be completely automated. This includes:

- (a) Determination of orbit parameters
- (b) Coordinate transformation to describe lunar surface in terms of LUCOM altimeter data.
- (c) Best fit least squares determination of most probable lunar shape.

- (d) Automatic determination of slopes and relief details.
- (e) Determination of relationship of photographic nadir point to most probable radar measurement point.
- (f) Determination of relationship of photographic nadir point to vehicle location in orbit and in turn to lunar coordinates.
- (g) Automatic plotting of lunar surface slopes and features.
- (h) Automatic interpolation of LUCOM determined surface elevations to selenodetic coordinate system.
- (i) Improvement of Apollo orbit parameters by use of LUCOM data used as orbital period determinations.

2. 3. 3. 5 Computer Programs

The computer programs mentioned in paragraph 2. 3. 3. 4, are those which would be used in the LUCOM technique and operational program. However, during the study, computer programs were used as an analytical tool. For example, the A/D (area depth) transformation was used as an aid in analyzing radar representation of the surface and to furnish an analytical process against which to make trade-off analyses.

In the beginning of the study a computer routine which was the basic framework for the computer simulator routine, was used to give a preliminary computation of radar parameters. This is discussed more fully in section 7. 5. The systems and analysis areas of LTV have an ASI-210 high speed digital computer which has been used for most of these computations. The IBM 7090 in the Arlington Electronics Division of LTV was used for the A/D transformation process.

2. 3. 3. 6 Data Acquisition - (Sensor Studies)

In the sensor design studies, the analyses were based primarily on assumed and computed characteristics of the surface of the moon used in computation of power required to operate at the altitude of the orbit and at the orbital velocity of Apollo. The power required and duty cycle capabilities were studied relative to the data rate which was considered

reasonable or limiting. For radar, the altitude limited the maximum pulse repetition frequency to 1000 or less to avoid ambiguity. This then set a limit on duty cycle for an assumed pulse width. The A/D transformation process in the profile parametric analysis gave a trade-off of pulse width, beamwidth and illuminated area which helped establish these important parameters independently of consideration of power, size and weight. When a nominal pulse width, beamwidth and tracking area were decided on, antenna gain was automatically defined, since antenna gain and beamwidth are synonymous when frequency is held constant. The radar design analysis then consisted of varying these parameters against probability of detection, I. F. bandwidth, noise figure and other radar parameters as discussed in Section 4. 0.

Much the same kind of analysis was used in the Laser study. In that case, however, the efficiency of the laser is so low that duty cycle was dictated not by minimum data rate on the one hand against range ambiguity on the other, but by power input to the laser (as will be seen in the discussions in Section 4. 0).

2. 3. 3. 7 Data Handling

As in the studies of the sensors, the principal methods of approach to the problem of telemetry consisted in: (1) establishing criteria based on the data rate from the sensor (this assumed to be 1000 per second or less); (2) the requirements for storage; and (3) transmission range between vehicles, etc. It was then possible to establish criteria for trade-offs of efficiency, weight, space, and power requirements.

2. 3. 4 LUCOM SIMULATION ROUTINE

The central element of the LUCOM study computer programs is the simulation routine. This computer program comprises all the elements of the LUCOM functional program having the following elements:

- (a) Three axis coordinate systems.
- (b) Range to surface.
- (c) Antenna pattern illumination function.
- (d) Antenna gain function.
- (e) Coefficient of reflection of surface.

The configuration of this program is designed to solve the basic radar range equation

$$P_r = \frac{P_t G^2 \lambda^2 A \sigma}{h^4}$$

where

P_r = Power received at receiving antenna.

G = Antenna two-way gain.

λ = Transmitting wavelength.

A = Illuminated area on the surface.

σ = Coefficient of reflection of the surface.

h = Range to target area.

In the program, given the orbit altitude and the orientation of the vehicle body axes, as provided by the Apollo instrumentation and the other constants, it computes h , A , and the ratio of P_r/P_t .

By the addition of sub-routines consisting of the orbit computation routine described in Section 7.5., and the least squares fitting program, the entire LUCOM problem can be run. As yet, these programs have not been integrated, but they have been run separately. Combining them should be a routine task. Computer storage capacity will be a limiting factor on the ASI-210 and may necessitate going to the IBM 7090 to run the entire program.

2.3.5 INVESTIGATIONS

Some areas of the study were not investigated extensively, i. e., the coefficient of reflection of the lunar surface, σ . Based on information from previous investigators, a number of -25 db was used in the first computer runs. A study was begun on this to justify adoption of a number to be used in the radar design studies. It was learned that the number -25 db was being used at NASA, for the X and K band radars, and that it was considered a conservative number which might be adopted for LUCOM.

The major problem areas in system integration are:

- (a) LUCOM internal interfaces

- (b) External interfaces (Apollo-LUCOM)
- (c) Electromagnetic Interference (EMI)
- (d) Physical accommodations - mounting, cooling, heating, etc.

LUCOM internal interfaces (i. e., consistency of signal data requirements and accommodation of data rate, timing, phasing, etc.), have been carefully considered in the design studies of the major system elements. These were used as system criteria in each of the areas to insure compatibility of the sensor to the data handling equipment, etc. The interface with Apollo instrumentation and vehicle has not been fully explored because that information was not available. However, the systematic study of interface problems is routine in programs of this kind, and will be handled as a matter of course when the program warrants.

2. 3. 6 CRITICAL PROBLEM AREAS

The following are considered to be problem areas:

- (a) Radar Antenna.
- (b) Laser efficiency.
- (c) Apollo stabilization.
- (d) Apollo orbit determination.

The radar studies and profile parametric analyses indicate that resolution increased toward narrower beamwidths, but that the standard antennas to achieve the narrow beamwidths severely penalized the radar, becoming the largest and heaviest element in the system. Study is needed in the area of lighter antenna configurations (such as inflatable types), and techniques for improving efficiency of operation at shorter wavelengths.

The laser (at this time) is relatively inefficient and at a pulse repetition frequency of one per second, the average input power requirement is 50 to 100 watts.

Apollo stabilization and the Apollo attitude program are unknown at present, but it is anticipated that errors caused by inaccuracy of Apollo

stabilization will be one of the large error sources in operation of the laser sensor or a very narrow beamwidth radar.

Apollo orbit accuracy is of course an area of speculation at present, but as shown in the summary of accuracies in Section 1.0, the assumed orbit error of 100 meters is one of the largest errors to be reckoned with. Better information on the predicted accuracy for Apollo orbit is required.

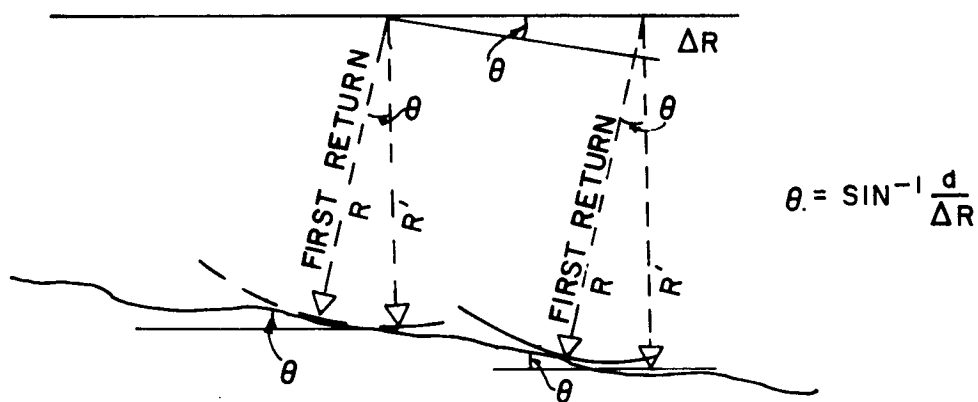


FIGURE 2.2.2-1

3.0 ORBIT AND VEHICLE DYNAMICS

Because the orbit is the baseline reference for the LUCOM measurements, the precise geometry of the orbit and the orientation of the orbit with respect to inertial space and the lunar body must be known or computed. This section defines the orbit elements traditionally used to describe the general case of an elliptic orbit. With these orbit elements in mind, the basic orbital equations are determined according to the mechanics of a two body system. These equations and the coordinate systems necessary to relate the vehicle position to inertial space and the lunar surface, are presented in the following paragraphs.

3.1 COORDINATE SYSTEMS

Two groups of coordinate systems have been developed, a "selenocentric" group and a "vehicle attitude" group. The "selenocentric" group provides the basic framework necessary for relating the orbit parameters, the vehicle position, and the vehicle ground track to a common lunar body reference coordinate system. The "vehicle attitude" group provides the means for reflecting the deviation in attitude of the vehicle (yaw, pitch and roll) into the lunar body reference coordinate system.

3.1.1 THE "SELENOCENTRIC COORDINATE SYSTEM" GROUP

3.1.1.1 The Lunar Body Reference Coordinate System

The lunar body reference coordinate system is represented by the $X_m Y_m Z_m$ coordinate system in Figure 3.1.1.1-1. The origin of this coordinate system coincides with the center of the moon. This coordinate system is fixed in the moon and rotates about the Z_m axis with a period of 27.321 days. The X_m - Y_m plane determines the lunar equator. The X_m axis is located at the center of the lunar disk when the moon is located simultaneously on the line of apsides and at the node of its orbit.

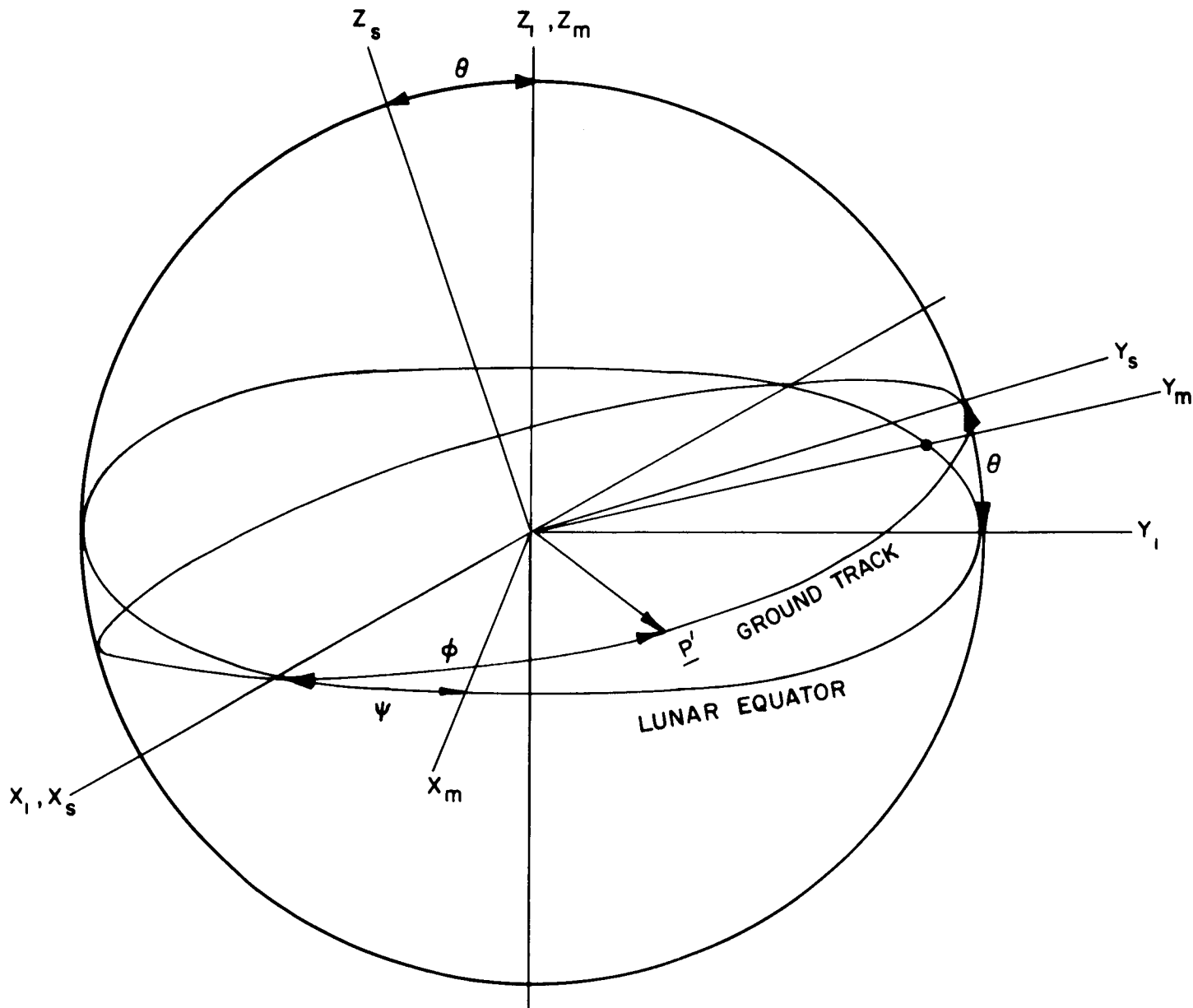


FIGURE 3.1.1.0 SELENOCENTRIC SYSTEMS

3. 1. 1. 2 Vehicle Position Coordinates

When terrestrial observations are made, the center of mass of the moon must be deduced indirectly from heliometer measurements which must be adjusted for taking into account the physical librations of the moon. In the case of a satellite in orbit, the center of mass of the orbited body is, in a manner of speaking, the first thing that is known, and all elements of the orbit are referenced to the center of mass of the body. Consequently, the origin of the coordinate system defining the position of the lunar space craft, $X_S Y_S Z_S$, is located at the center of mass of the moon. Referring to Figure 3. 1. 1. 1-1, the X_S - Y_S plane defines the plane of the orbit while the Z_S axis is the axis of rotation of the orbit. The X_S axis is defined by the intersection of the plane of the orbit and the plane of the lunar equator. The $X_S Y_S Z_S$ coordinate system moves along with the moon in space, but it does not rotate with respect to inertial space.

3. 1. 1. 3 Reference Inertial Coordinates

It is not possible to relate the space craft position to the lunar body reference coordinates from the information and definitions given thus far. One can introduce a reference inertial coordinate system, $X_i Y_i Z_i$, and define independent relations directly between $X_i Y_i Z_i$ and $X_M Y_M Z_M$ and directly between $X_i Y_i Z_i$ and $X_S Y_S Z_S$. Then, since independent relationships between $X_M Y_M Z_M$ and $X_i Y_i Z_i$ and $X_S Y_S Z_S$ and $X_i Y_i Z_i$ are defined, one can indirectly relate $X_M Y_M Z_M$ and $X_S Y_S Z_S$ to each other. Referring again to Figure 3. 1. 1. 1-1, the $X_i Y_i Z_i$ coordinate system is a mutually perpendicular system with the Z_i axis coincident with the Z_M axis and the X_i axis coincident with the X_S axis; the coincidence of the two axes with the axes of the previously defined coordinate systems provide part of the information necessary to relate the space craft to the lunar body reference coordinates. The X_i - Y_i plane lies in the plane of the lunar equator, thus it is coplanar with the X_M - Y_M plane. The $X_i Y_i Z_i$ coordinate system, whose origin is at the center of mass of the moon, moves along with the moon; but it does not rotate with respect to inertial space.

3. 1. 1. 4 Inter-relations of the Selenocentric Coordinate Systems

The position relations between the $X_i Y_i Z_i$ system and the $X_M Y_M Z_M$ and $X_S Y_S Z_S$ systems should be visualized easily from the following description. Referring again to Figure 3. 1. 1-1-1, assume the $X_i Y_i Z_i$ system and an imaginary XYZ system totally coincident initially; then rotate the XYZ

system about the still coincident Z_i - Z axes by an angle, ψ . This rotated position of the XYZ system is adopted as the $Z_m Y_m Z_m$ system. The Z_m and Z_i axes are then coincident while the X_m , Y_m , X_i , and Y_i axes are all coplanar. Assume now the $X_i Y_i Z_i$ system and a second imaginary XYZ system totally coincident; then rotate the XYZ system about the still coincident X_i - X axes by an angle, θ . This rotated position of the second XYZ system is adopted as the $X_s Y_s Z_s$ system. The X_s and X_i axes are then coincident while the Y_s , Z_s , Y_i and Z_i axes are all coplanar.

The angle, θ , between the Z_i and Z_m axes is called the inclination of the plane of the orbit. The angle, ψ , between the X_s and X_m axes locates the descending node of the space craft orbit.

The descriptions and conditions given above meet the criteria necessary to describe mathematically the inter-relations of the coordinate systems of the selenocentric group. Those necessary mathematic definitions are that Z_i - Z_m are coincident, X_i - X_s are coincident, and that the angles, θ and ψ , are defined as angular displacements of particular axes.

Obtaining the relations between the coordinate systems involves a transformation of axes. This is most conveniently expressed in matrix notation. To this end let

$$\bar{1}X_S, \bar{1}Y_S, \bar{1}Z_S, \bar{1}X_M, \text{ etc.}$$

be unit vectors along the axes indicated by the subscripts. In this notation a bar placed under a symbol denotes a vector quantity. The three coordinate systems, then, are related by the expressions

$$\begin{bmatrix} \bar{1}X_I \\ \bar{1}Y_I \\ \bar{1}Z_I \end{bmatrix} = \begin{bmatrix} A \end{bmatrix} \begin{bmatrix} \bar{1}X_S \\ \bar{1}Y_S \\ \bar{1}Z_S \end{bmatrix} \quad \text{and} \quad \begin{bmatrix} \bar{1}X_I \\ \bar{1}Y_I \\ \bar{1}Z_I \end{bmatrix} = \begin{bmatrix} B \end{bmatrix} \begin{bmatrix} \bar{1}X_M \\ \bar{1}Y_M \\ \bar{1}Z_M \end{bmatrix}$$

where

$$\begin{bmatrix} A \end{bmatrix} = \begin{bmatrix} 1 & 0 & 0 \\ 0 & \cos \theta & -\sin \theta \\ 0 & \sin \theta & \cos \theta \end{bmatrix} \quad \text{and} \quad \begin{bmatrix} B \end{bmatrix} = \begin{bmatrix} \cos \psi & -\sin \psi & 0 \\ \sin \psi & \cos \psi & 0 \\ 0 & 0 & 1 \end{bmatrix}$$

These two matrix expressions relate the $X_S Y_S Z_S$ and $X_M Y_M Z_M$ systems directly to the $X_i Y_i Z_i$ systems. The relation of $X_S Y_S Z_S$ to $X_M Y_M Z_M$ is obtained indirectly then by the expression,

$$\begin{bmatrix} \underline{1} X_S \\ \underline{1} Y_S \\ \underline{1} Z_S \end{bmatrix} = \begin{bmatrix} A \end{bmatrix}^{-1} \begin{bmatrix} B \end{bmatrix} \begin{bmatrix} \underline{1} X_M \\ \underline{1} Y_M \\ \underline{1} Z_M \end{bmatrix}$$

3.1.2 VEHICLE ATTITUDE COORDINATE SYSTEMS

The attitude of the space craft is defined by relating the orientation of the space craft with respect to a "fixed" coordinate system whose origin is coincident with the terminus of the position vector from the center of mass of the moon to the center of mass of the space craft. For the LUCOM mission it is convenient for this "fixed" coordinate system, $X_p Y_p Z_p$, to be fixed with respect to the position vector and the orbital tangential velocity vector of the space craft. The mutually perpendicular coordinate system, $X_p Y_p Z_p$, as shown in Figure 3.1.2-1 is defined in the following manner. The Z_p axis, or yaw axis, is coincident with, but opposite in direction to, the space craft position vector, \underline{P} . The X_p axis, or roll axis, lies in the orbital plane of the space craft and points the direction of the tangential velocity component in the orbital plane of the space craft. The Y_p axis, or pitch axis, is perpendicular to the $X_p Z_p$ plane. This axis system then rotates with an angular velocity equal to the angular velocity of the space craft position vector, \underline{P} . It is assumed that as the LUCOM mission progresses, instrumentation information (such as horizon scanner output) and some mode of control will maintain the attitude of the vehicle such that the vehicle body axes are always closely aligned to the $X_p Y_p Z_p$ axes.

The relationship between the $X_p Y_p Z_p$ system and the vehicle body axes, $X_v Y_v Z_v$, is most conveniently determined by introducing two intermediate axis systems. The immediate axes systems are generated by a rotation method similar to the method of generation of the $X_M Y_M Z_M$ and the $X_S Y_S Z_S$ systems from the $X_i Y_i Z_i$ system which is described in Paragraph 3.1.1.4. The sequence of rotation used to relate the vehicle body coordinates to the "fixed" coordinate system is called the Eulerian sequence. Figure 3.1.2-2 illustrates the transformation sequence of $X_p Y_p Z_p$ to $X_v Y_v Z_v$. The definition illustrated in Figure 3.1.2-2 of the two intermediate

axes systems, $X_1Y_1Z_1$ and $X_2Y_2Z_2$, and the angles generated, alpha, beta, and gamma, allows the mathematical relation between $X_pY_pZ_p$ and $X_vY_vZ_v$ to be written.

Starting with the $X_pY_pZ_p$ system and moving toward the $X_vY_vZ_v$ system, and using the unit vector rotation previously introduced in Paragraph 3.1.1.4, the mathematical relations between the coordinate systems are written in matrix notation. The relation between $X_pY_pZ_p$ and $X_1Y_1Z_1$ is written as

$$\begin{bmatrix} \underline{1X_1} \\ \underline{1Y_1} \\ \underline{1Z_1} \end{bmatrix} = \begin{bmatrix} \\ \\ \end{bmatrix} \begin{bmatrix} \underline{1X_p} \\ \underline{1Y_p} \\ \underline{1Z_p} \end{bmatrix}, \text{ where } C = \begin{bmatrix} \cos \alpha & \sin \alpha & 0 \\ -\sin \alpha & \cos \alpha & 0 \\ 0 & 0 & 1 \end{bmatrix}$$

The relation between $X_1Y_1Z_1$ and $X_2Y_2Z_2$ is written as

$$\begin{bmatrix} \underline{1X_2} \\ \underline{1Y_2} \\ \underline{1Z_2} \end{bmatrix} = \begin{bmatrix} \\ \\ \end{bmatrix} \begin{bmatrix} \underline{1X_1} \\ \underline{1Y_1} \\ \underline{1Z_1} \end{bmatrix}, \text{ where } D = \begin{bmatrix} \cos \beta & 0 & -\sin \beta \\ 0 & 1 & 0 \\ \sin \beta & 0 & \cos \beta \end{bmatrix}$$

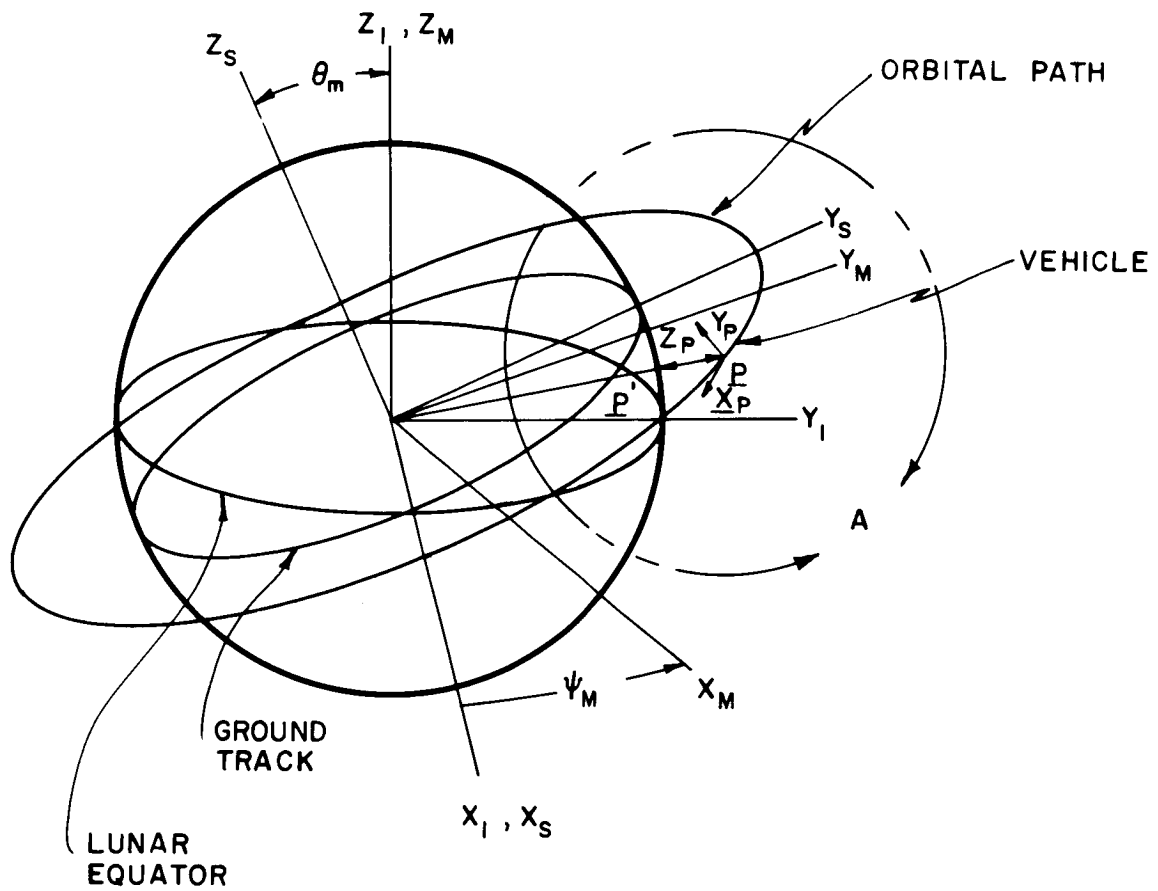
The relation between $X_2Y_2Z_2$ and $X_vY_vZ_v$ is written as

$$\begin{bmatrix} \underline{1X_v} \\ \underline{1Y_v} \\ \underline{1Z_v} \end{bmatrix} = \begin{bmatrix} \\ \\ \end{bmatrix} \begin{bmatrix} \underline{1X_2} \\ \underline{1Y_2} \\ \underline{1Z_2} \end{bmatrix}, \text{ where } E = \begin{bmatrix} 1 & 0 & 0 \\ 0 & \cos \vartheta & \sin \vartheta \\ 0 & -\sin \vartheta & \cos \vartheta \end{bmatrix}$$

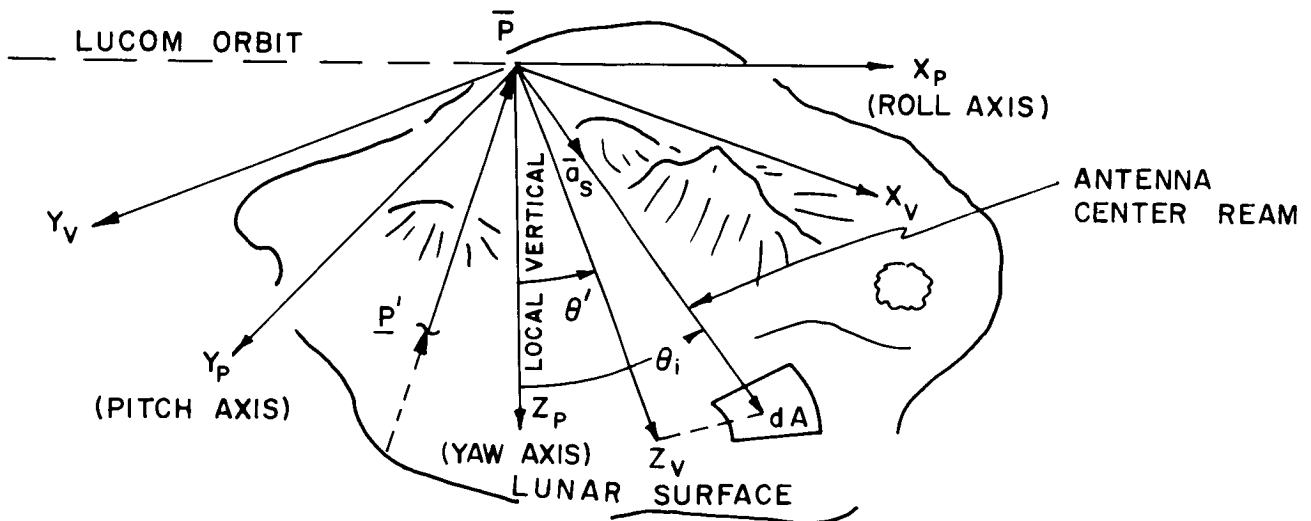
The body axes of the space craft, X_v , Y_v , Z_v are chosen to be the principal axes, that is, axes chosen such that all products of inertia are zero. Applying the relations obtained above, the expression for the orientation of the body axis with respect to the fixed axes is:

$$\begin{bmatrix} \underline{1X_v} \\ \underline{1Y_v} \\ \underline{1Z_v} \end{bmatrix} = \begin{bmatrix} \\ \\ \end{bmatrix} \begin{bmatrix} \\ \\ \end{bmatrix} \begin{bmatrix} \\ \\ \end{bmatrix} \begin{bmatrix} \underline{1X_p} \\ \underline{1Y_p} \\ \underline{1Z_p} \end{bmatrix}$$

Since the space craft orientation with respect to the "fixed" coordinate system is now defined mathematically, and since the "fixed" system is

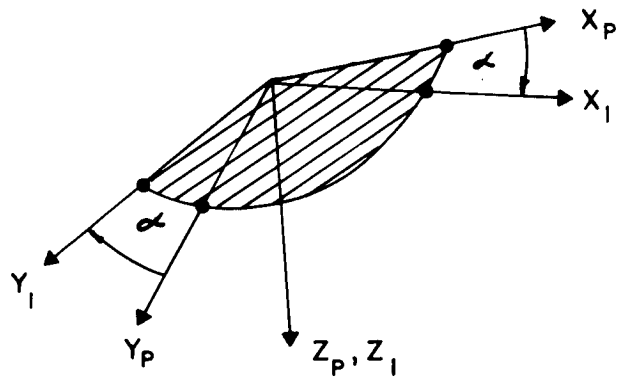


a.

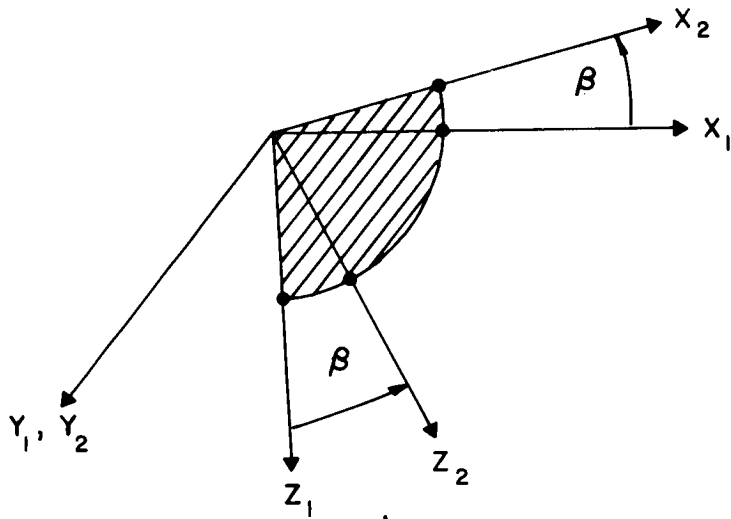


b.

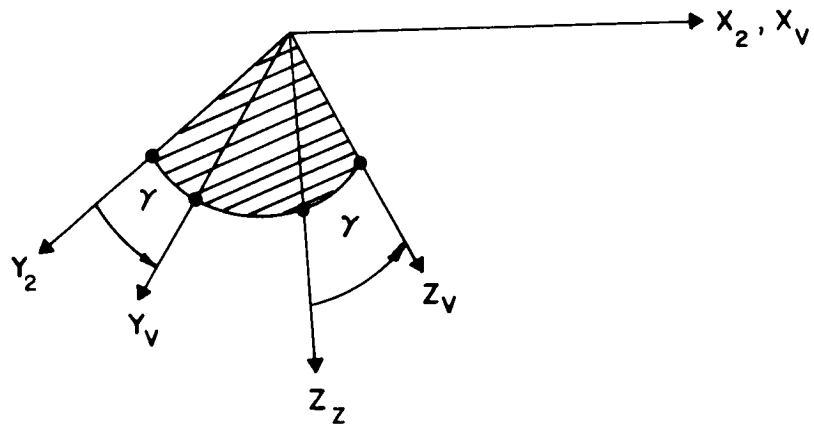
FIGURE 3.1.2-1 VEHICLE ATTITUDE COORDINATE SYSTEMS



a.



b.



c.

defined by a known vector and a previously defined orbit, the effect of yaw, pitch, and roll can be imposed to accurately compute the location of the antenna center beam upon the lunar surface.

3.2 DEFINITION OF ORBIT PARAMETERS AND ORBIT ELEMENTS

The definition of the $X_S Y_S Z_S$ system in Paragraph 3.1.1.2 defined the plane of the orbit of the space craft. Three more parameters are required to establish the orbital path of the space craft in that plane. The three parameters are illustrated in Figure 3.2-1 which shows the path of the space craft in the $X_S Y_S$ plane.

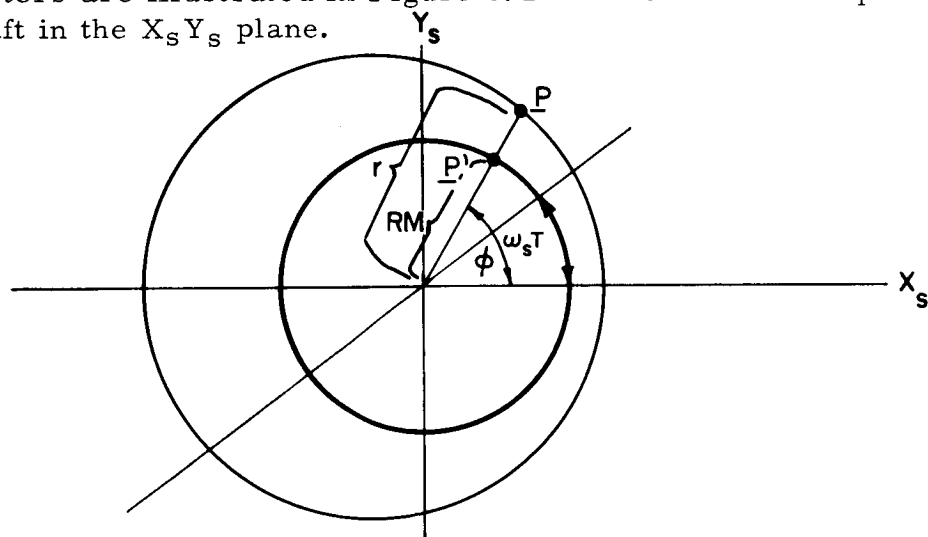


FIGURE 3.2-1 RELATION OF ORBIT PARAMETERS TO VEHICLE POSITION COORDINATE SYSTEM

The parameters are: ϕ , the true anomaly, r , the distance from the center of mass of the moon to the center of mass of the space craft, T , the time of passage of periselenium, and ω_s , the average angular velocity of the space craft radius vector. In the development to follow, the orbit is assumed to be circular. A circular orbit is a special case for an elliptical orbit, and therefore, $\omega_s T$, displacement from periselenium, becomes indeterminate and is taken to be zero. The position of the space craft can then be expressed by the position vector

$$\underline{P} = r \cos \phi \underline{1X}_s + r \sin \phi \underline{1Y}_s.$$

This vector can be expressed in the lunar body reference coordinate system by applying a previously derived transformation; that is, \underline{P} may be written as

$$\underline{P} = \begin{bmatrix} r \cos \phi & r \sin \phi & 0 \end{bmatrix} \begin{bmatrix} A \end{bmatrix}^{-1} \begin{bmatrix} B \end{bmatrix} \begin{bmatrix} \underline{1X}_m \\ \underline{1Y}_m \\ \underline{1Z}_m \end{bmatrix}$$

Carrying out the indicated operation, the result is

$$\begin{aligned} \underline{P} &= r (\cos \theta \cos \phi + \sin \phi \sin \psi \cos \theta) \underline{1X}_m \\ &+ r (\sin \phi \cos \psi \cos \theta - \sin \psi \cos \theta) \underline{1Y}_m \quad (3.2.1.0) \\ &+ r (\sin \phi \sin \theta) \underline{1Z}_m \end{aligned}$$

In this expression, theta is constant with respect to time, while psi, phi, and r vary with respect to time. Time, t, is equal to zero when phi is equal to zero. Psi is defined as

$$\psi = \psi_0 + \omega_m T$$

where ψ_0 (ψ_0) is the longitude of the node at time, t, equal to zero and

$$\omega_m = \frac{2}{27.321} \frac{\text{rad}}{\text{day}} .$$

The orbit parameters, phi and r, are related to the orbit elements by infinite series expressions. The first few terms are

$$\begin{aligned} r &= A \left[1 + \frac{E^2}{2} - E \cos M - \frac{E^2}{2} \cos 2M - \dots \right] \\ \phi &= M + 2E \sin M + 1.25 \sin 2M + \dots \end{aligned}$$

where A = semi-major axis

E = eccentricity

M = mean anomaly.

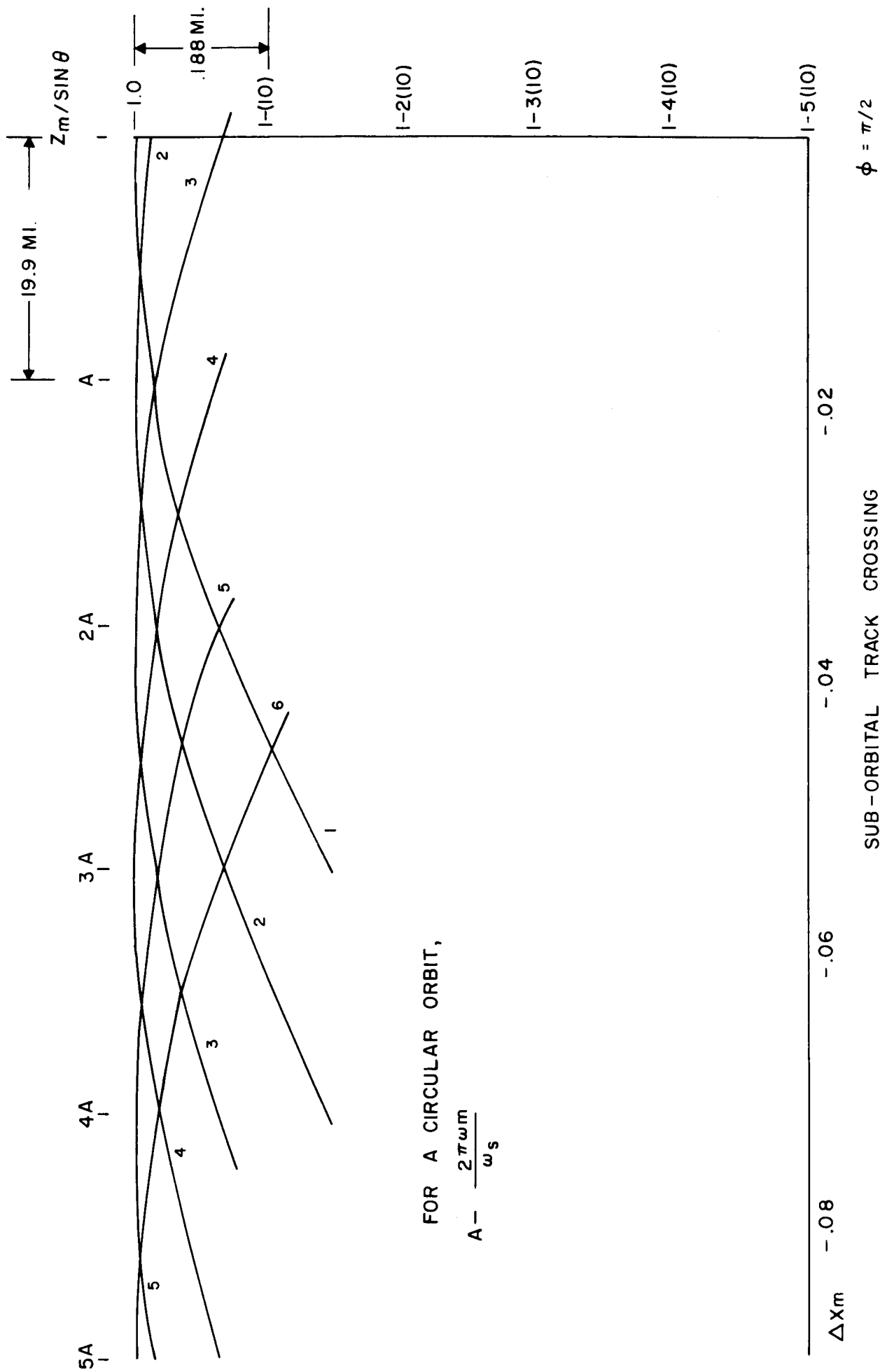
M is further related by the expression

$$M = W_s (t - T)$$

where t = time

ω_s = average angular velocity of space craft radius vector

T = time of passage of periselenium.



SUB-ORBITAL TRACK CROSSING

FIGURE 3.2.1-2

These relations will be used in the task of reducing LUCOM data in order to determine the selenoid.

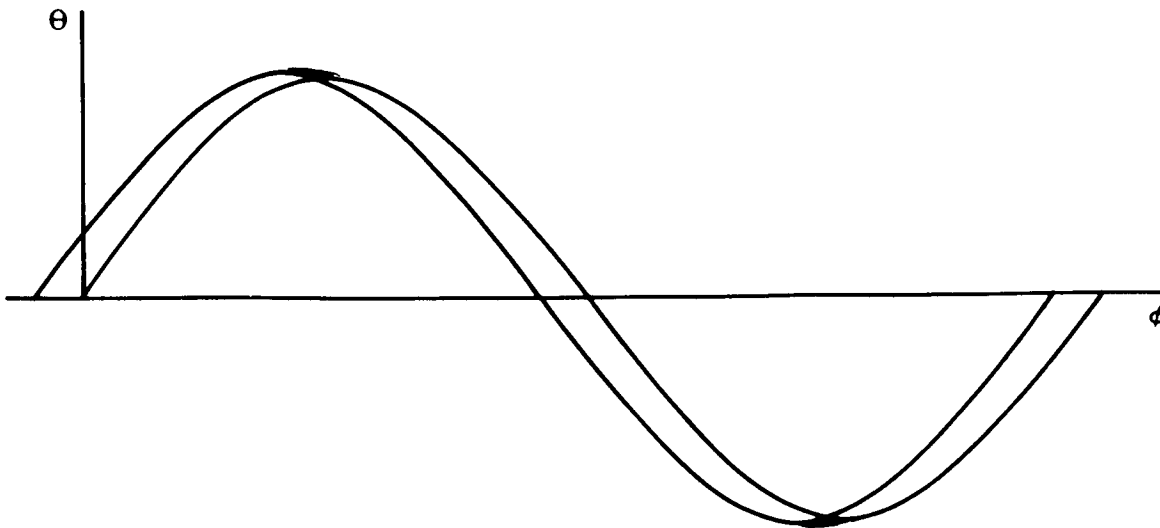
3.2.1 DEFINITION OF GROUND TRACK

The lunar ground track may be defined as the intersection of the space craft radius vector and the lunar surface. At any instant a vector, \underline{P}' , to the lunar surface directly beneath the space craft may be expressed in the lunar body reference coordinate system, $X_m Y_m Z_m$, shown in Figure 3.1.1.1-1, by the equation:

$$\begin{aligned} \underline{P}' = & R_m (\cos\theta \cos\psi + \sin\theta \sin\psi \cos\theta) \underline{1X}_m \\ & + R_m (\sin\theta \cos\psi \cos\theta - \sin\psi \cos\theta) \underline{1Y}_m \quad (3.2.1.1) \\ & + R_m (\sin\theta \sin\theta) \underline{1Z}_m \end{aligned}$$

The definition of \underline{P}' is merely an extension of equation 3.2.1.0 derived in paragraph 3.2. Notice that the equations are identical except, r , the radius of the orbit has been replaced by R_m , the distance from the center of mass of the moon to the surface of the moon.

If the moon did not rotate, the ground track would be simply a closed path of the intersection of the plane of the orbit and the moon. However, due to the rotation of the moon, the ground track does not meet itself after one period of the orbit. The general character of the ground track is shown in Figure 3.2.1-1 below. In the shaded area the successive tracks intersect each other.



For orbits of small inclination, the cosine of the angle of inclination, theta, is approximately equal to one. Under this condition, equation 3.2.1.1 may be simplified to

$$\begin{aligned} \underline{P}' &= R_m \cos(\theta - \psi) \underline{1X}_m \\ &+ R_m \sin(\theta - \psi) \underline{1Y}_m \\ &+ R_m \sin\theta \sin\psi \underline{1Z}_m \end{aligned} \quad (3.2.1.2)$$

Letting A equal distance along the lunar equator, the ground track can be expressed by the pair of parametric equations:

$$\begin{aligned} Z_m &= R_m \sin\theta \sin\psi \\ A/R_m &= (\theta - \psi). \end{aligned} \quad (3.2.1.3)$$

The expression for the ground track for an orbit of small inclination is simplified even further provided that the orbit is a circular, or zero-eccentricity, orbit. For a circular orbit equation 3.2.1.3 becomes

$$\begin{aligned} Z_m &= R_m \sin\theta \sin\omega_s t \\ A/R_m &= (\omega_s - \omega_m) t - \psi_0 \end{aligned}$$

or

$$Z_m = R_m \sin\theta \sin \left[\frac{\omega_s}{\omega_s - \omega_m} (A/R_m + \psi_0) \right] \quad (3.2.1.4)$$

Intersections, or ground track crossings, will occur when

$$A/R_m = \psi_0 = \pi/2 - \frac{\omega_m}{\omega_s} \left[\pi/2 + (n + m) \right]$$

where n is the nth orbit and m is the mth orbit. Figure 3.2.1-2 shows several ground track crossings. Notice the difference in the scales of the ordinate and the abscissa. For this plot the inclination of the orbit is taken to be ten degrees. In the region of crossing, the ground tracks of the successive orbits are almost parallel lines. This fact will be used to improve the accuracy of the determination of the selenoid.

4.0 SENSOR STUDIES

Two general types of ranging sensors were examined for application to the LUCOM mission: laser and radar sensors. A laser feasibility study was performed in which the various devices were analyzed in terms of meeting LUCOM requirements. Although the reliability of a single cavity system is low, high ranging accuracy is obtained. Also included in the following sections are analyses on mapping the lunar surface with pulsed RF energy, lunar surface scattering models, and radar parameter trade-offs.

From these studies, an optimum radar sensor design based on specific characteristics, was derived.

4.1 LASER INVESTIGATION

For laser ranging (or altimetry), only a few devices have been developed which presently possess the potential for meeting the LUCOM System requirements. All of these devices are solid state, Q-switched lasers, differing only in the materials used. Two of the potential lasers would utilize neodymium doped calcium tungstate and the other would use ruby_o as the lasing material. One neodymium laser would operate at 10,600 Å, and the other would generate a signal at this wavelength which would be passed through a non-linear medium creating second_o-harmonic generation at 5300 Å. The ruby system would operate at 6943 Å. To date, only ruby laser systems have been extensively used in ranging applications. Airborne altimeters of this type have been developed and system feasibility has been shown for several applications.

4.1.1 LASER ALTIMETER - FUNCTIONAL BLOCK DIAGRAM

The basic altimeter system is shown in Figure 4.1.1-1. The laser transmitted will be composed of a laser cavity, a cavity Q control device (such as a Kerr cell, a Pockel cell, or a rotating prism,) a primary power

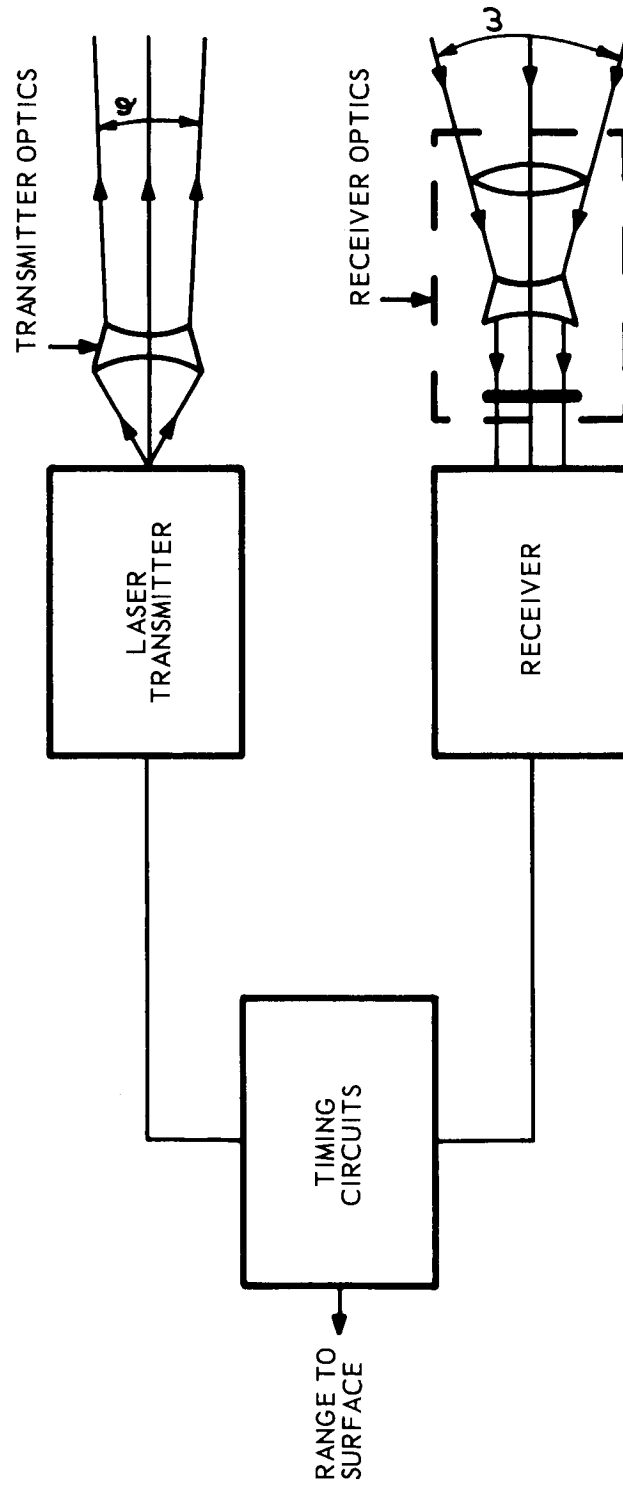


FIGURE 4.1.1-1. LASER ALTIMETER BLOCK DIAGRAM

supply, flash tubes, trigger circuits, and cooling equipment. There probably would be secondary power supplies also associated with the transmitter. The receiver would have a photomultiplier tube, a photomultiplier power supply, and a receiver amplifier as the major elements. Cooling equipment might also be required for the receiver. The timing circuitry would be composed of a high speed counter and various electronic and delay circuitry. The total altimeter system would also include receiver and transmitter optics, an optical filter, and associated interface electronics.

4.1.2 TRANSMITTING AND RECEIVING MODES

Figure 4.1.2-1 depicts both the transmitting and receiving modes of operation. In the transmitting phase, the laser generates a pulse of light that passes through a set of optics which reduces the transmitted beamwidth to some angle φ . The transmitted pulse starts a counter which runs until the return pulse is detected in the receiver. The receiver optics has a small field of view, ω , which is large enough to insure that the area on the ground which the signal pulse illuminated lies within the field of view. A filter is used to reduce the optical bandwidth the detector sees to only that narrow region within which the laser operates. The optical bandwidth may be as narrow as 10 \AA .

4.1.3 INDUSTRY SURVEY

During the initial portion of the program, Mr. C. R. Kline, Manager of Optical Radar Systems Development of the Westinghouse Aerospace Division, produced some calculations describing the requirements for a laser ranging system off the moon's surface. The system considered uses a 3 milliradian beam with a 10 nanosecond pulse. The receiver has a 12 inch aperture. The hypotheses used to calculate the number of detected electrons were: (a) False alarm time of 10^3 seconds, and (b) Probability of detection of 90%. The calculations to determine the output power requirements (both peak power and average power) were based on the following assumptions:

- (a) A ranging distance of 100 nautical miles.
- (b) A quantum efficiency of 15%.
- (c) An optical efficiency of 50%.
- (d) Reflectivity off the lunar surface of 10%.

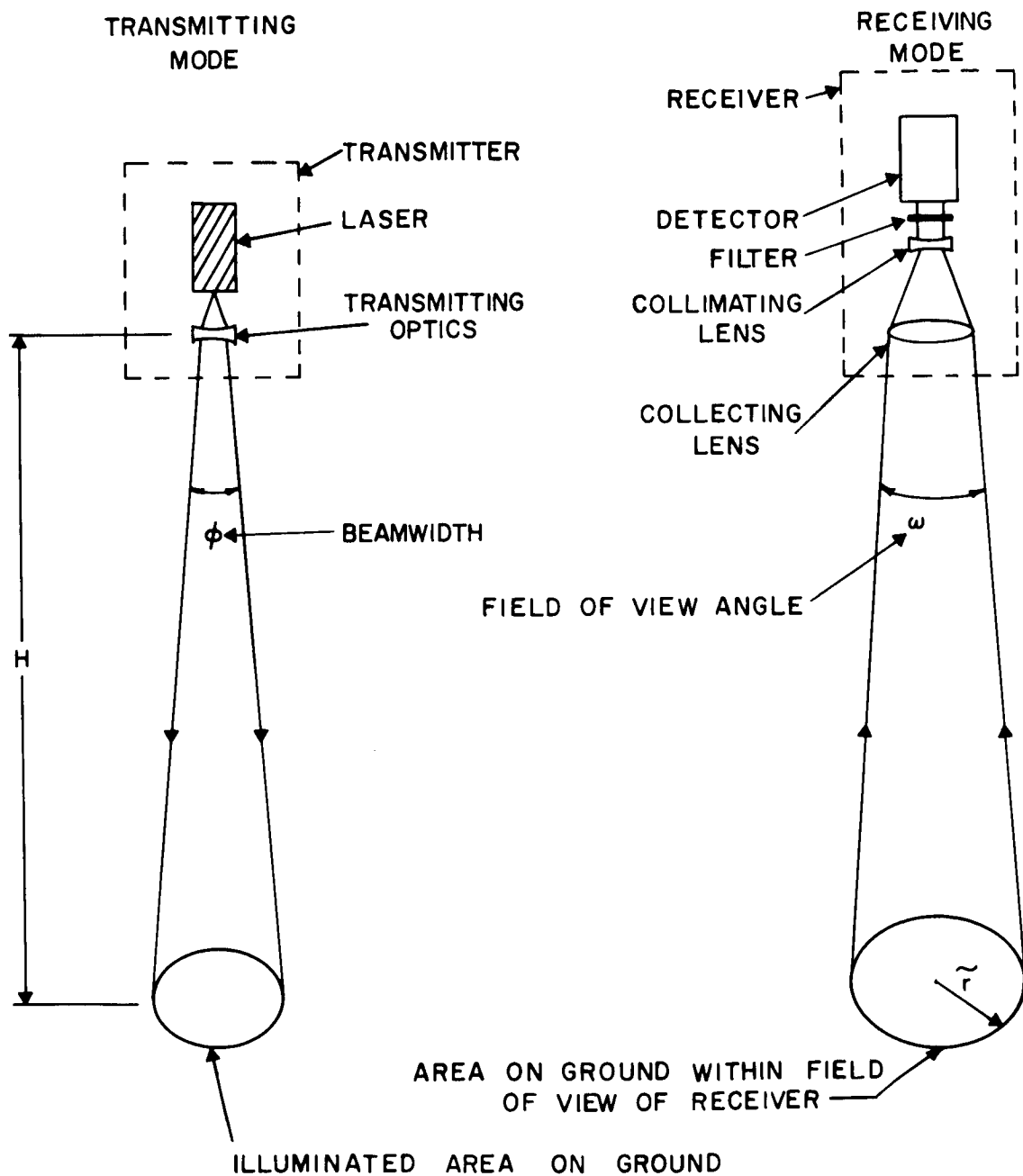


FIGURE 4.1.2-1. LASER ALTIMETER TRANSMITTING AND RECEIVING MODES OF OPERATION

The peak input power required for ruby was calculated to be 1 kilowatt at 10 pulses per second (pps). For calcium tungstate the input power requirement was found to be 300 watts at 10 pps. From this analysis it appeared (because of lower threshold requirements allowing the use of a lower input power) that calcium tungstate is preferable to ruby in this application. After system requirements had been more firmly determined, Mr. Manuel Hunter of the Light Military Electronics Department, Defense Electronics Division, General Electric Company provided LTV with an analysis of the system they would currently propose for the LUCOM application. The requirements supplied them by LTV were:

- (a) A 3 meter ranging accuracy
- (b) 80 nm range
- (c) 48 hour continuous operating life
- (d) 50 lb. maximum weight

The parameters of the system they proposed are as follows:

Receiver Aperture	A_o	= 182 cm ² or app. 6" aperture
Receiver Bandwidth	B_r	= 10 A ^o
Optical Eff. of Xmtr.	η_r	= .9
Optical Eff. of Rcvr.	η	= .5
Signal Photo Electrons req'd	N_s	= 25
Probability of Detection	P_D	= .9
Probability of False Alarm	P_{FA}	= 10 ⁻⁸ (Bright Side)
Reflectivity	η_m	= 0.1
Xmtr. Field	φ	= .1 milliradian
Peak Power	P_t	= 1 megawatt
Xmtr. Energy	U_t	= 30 x 10 ⁻³ joule
Pulse Width	t_p	= 30 ns

Range Accuracy	$\Delta R = \pm 15 \text{ ft.}$
PRF	= 1 pps
Weight, including cooling	= 50 lb

4.1.4 EFFECT OF LASER PULSE RATES ON THE DERIVED PROFILE

The best source material now available describing the topography of the lunar surface has horizontal resolution not much greater than 3000 feet. Interpolation of data derived from these source materials cannot reasonably be performed to any less than the 1600 ft. spacing of the matrix now being used in the area-depth transformation studies. The area on the ground illuminated by a laser with a nominal beam width of 0.5 milliradian would have a diameter of only 245 feet at 490,000 feet altitude. Therefore, the effect of the beamwidth of the laser on determining the terrain profile cannot be taken into account using source material now available. This means that it is not necessary to utilize an area-depth analysis of the laser return. The derived profile will be sensitive to deviations of the laser line-of-sight from the local vertical. A first order approximation of the errors caused by these deviations can be determined by assuming that the laser beam will fall on a plane as shown in Figure 4.1.4-1, with ϕ

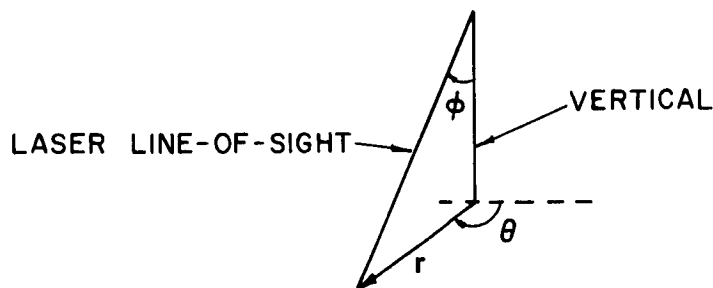


Figure 4.1.4-1 Laser Geometry used for Examining Effect of Line-of-Sight Deviations from the Vertical.

being distributed uniformly between 0 and 2π radians, and with r having the Rayleigh distribution,

$$p(r) = r/\sigma^2 e^{-r^2/2\sigma^2}$$

This approximation assumes that $\tan \phi$ is approximately linear in the range expected, that H is constant, and that the pitch and roll rates of the vehicle are equal. Although this approximation will not duplicate the phases of frequencies in the errors, the order of magnitude of the errors should be determinable.

The (r, θ) coordinate system can be readily transformed into a (x, y) coordinate system by the set of transformation equations:

$$x = r \cos \theta, \quad y = r \sin \theta.$$

Both x and y will be random variables with the same associated Gaussian distribution:

$$p(x) = \frac{1}{\sqrt{2\pi}\sigma} e^{-x^2/2\sigma^2}$$

$$p(y) = \frac{1}{\sqrt{2\pi}\sigma} e^{-y^2/2\sigma^2}$$

A computer routine was used to supply sets of normally distributed random numbers. The 3σ value was assumed to correspond to a ϕ of 0.5° , i. e., at 490,000 feet the 3σ value for x and y is:

$$3\sigma = (490,000 \text{ feet}) \tan 0.5^\circ = 4270 \text{ feet.}$$

The corresponding standard deviation, σ , in both x and y is:

$$\sigma = 1420 \text{ feet,}$$

for the set of random numbers produced by the computer. These numbers were used to provide deviations of the x and y coordinate for each point of a selected profile. The elevation of the matrix point nearest to the displaced coordinate was used as the laser reading. The argument for using this number follows from noting Figure 4.1.4-2 that the range measure-

ment will be $\left[\frac{H}{\cos \phi} + \frac{\Delta H}{\cos \phi} \right]$, which for the ϕ angles of interest, will be

to an approximation just $H + \Delta H$, independent of ϕ . The resulting profile line, using this simulation is shown in Figure 4.1.4-3. The pulse rate used here was one pulse per second.

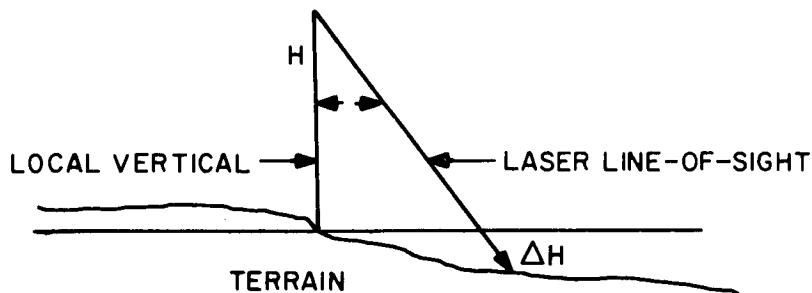


Figure 4.1.4-2. Effect of Terrain Slope on Range Measurements.

4.1.5 RANGING ACCURACY REQUIREMENTS FOR THE LASER

Sensitivity studies of ranging accuracy requirements for the case in which this information is used for determining vertical and horizontal scale factors of lunar photography, indicate that ranging accuracy no greater than 50 feet is required for any camera focal length at 490,000 foot altitude.

4.1.6 RELIABILITY CONSIDERATIONS

At present the reliability of a pulsed laser system is determined primarily by the reliability of the flash tube. One conservative recommendation has been to replace currently available flash tubes in field use after 4000 cycles. Laser cavities also deteriorate after pulsing for long periods. A system designed for LUCOM might, therefore, be designed to replace its own cavity and flash tube (which could be a single unit) on a periodic basis in order to achieve maximum reliability.

4.1.7 LASER ALTIMETER TRADE-OFF CHARACTERISTICS

The total energy requirements, P , for a laser system is given by:

$$P = N \left(E_q + \frac{E_T}{\eta_q} \right)$$

where N is the number of pulses per second, E_T is the energy of each transmitted pulse, E_q is the threshold energy required for the laser and η_q is the efficiency of the laser. A representative value for laser efficiency is at present about 0.5% (i.e., $\eta_q = 5 \times 10^{-3}$.) It is possible

X INDICATES RETURN FROM LASER ASSUMING THAT 99% OF THE TIME THE LASER BEAM DOES NOT DEVIATE FROM THE LOCAL VERTICAL BY MORE THAN 0.5 DEGREES

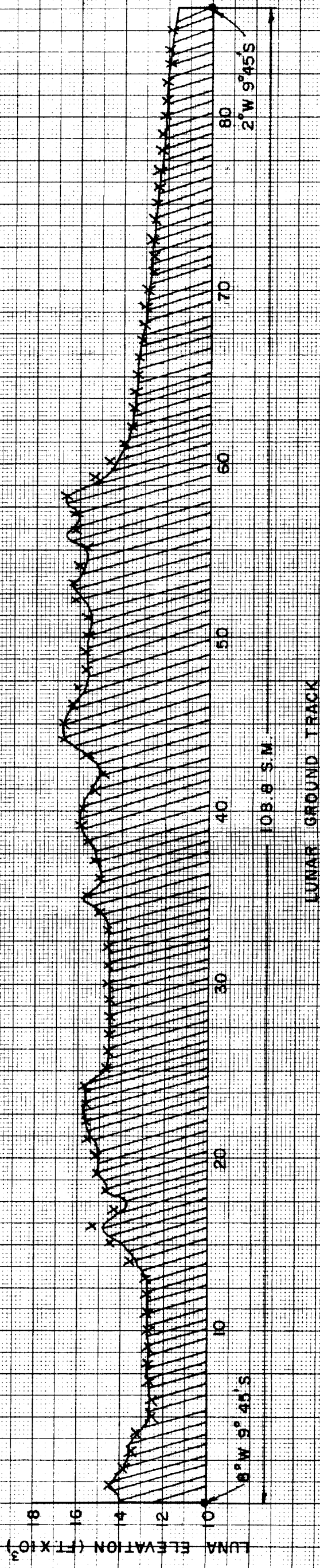


FIGURE 4.1.4.3. SIMULATED LASER RANGE MEASUREMENTS COMPARED AGAINST THE ACTUAL PROFILE

that a laser using ruby ($\lambda = 6943\text{\AA}$) could be used with a threshold energy, E_p , as low as 50 joules. At one pulse per second ($N + 1$),

$$P = \left[50 + \frac{7.7 \times 10^{-3}}{5 \times 10^{-3}} \right] \text{ watts}$$
$$= 51.5 \text{ watts,}$$

where $E_T = 7.7 \times 10^{-3}$ joules (assuming 25 signal photoelectrons needed). This calculation assumed that a multiple bounce detector was used. With a conventional photomultiplier with one-fourth the quantum efficiency,

$$E_T = 30 \times 10^{-3} \text{ joule and}$$

$$P_T = 56 \text{ watts}$$

Higher pulse rates using ruby would probably severely increase the cooling requirements of the system, thereby increasing the weight of the system a great amount. It should be noted that the General Electric analysis quoted a 50 pound weight for a very similar system operating at one pulse per second. The detector used in this system has a quantum efficiency one-fourth that assumed in the calculations of this report. These quantum efficiencies were based on a Westinghouse report that an efficiency improvement by a factor of four can be expected using multiple reflection techniques.

4.1.8 SUMMARY OF THE LASER INVESTIGATION

A conservative model for a laser altimeter was developed for the LUCOM application. This model was used to determine energy requirements and possible data rates. It was determined that a solid state calcium tungstate laser utilizing second-harmonic generation has the greatest potential. However, to date only ruby lasers have been extensively used in ranging and altimetry applications. It was found that a ruby laser operating at a pulse repetition frequency of one pulse per second would require approximately 50 watts input power. The information derived by the laser altimeter could be used either to reconstruct the terrain profile along the ground track of the vehicle or as a control for stereo photography. See Appendix 4.1-A for a description of the mathematical model.

4.2 LUCOM RADAR SENSOR INVESTIGATION

The radar sensor investigation involved several related areas of study: Signal Return Study, Profile Parametric Analysis, Statistical Sensor Design, Error Analysis, and Functional Design.

Although only a limited approach towards establishing the structural relationship between the surface and the return signal was undertaken, major effort was expended in simulating the various radar parameters over a "worst case" lunar profile.

The Radar Profile Parametric Analysis served the vital function of providing an analytical basis for making radar parametric trade-offs. It did this by narrowing the field of values for each of the parameters which make up the functional characteristics of a radar sensor which must be defined prior to realistic design for a specific use. As a result of this work, the broad spectrum of radar variables was effectively analyzed and evaluated in terms of simulated operation over a realistic portion of the lunar surface.

Subsequent statistical trade-off evaluation was based on this preliminary analysis. Block diagrams of an optimum sensor were completed, and functional characteristics defined in detail. Physical characteristics were ultimately established based on the quantitative analyses and on the environmental limitations.

4.2.1 RADAR RETURN SIGNAL INTERPRETATION

Given sufficient data describing the characteristics of a surface, it is possible to predict the radar return signal wave shape from a large area scattering surface. For LUCOM, the inverse is desired. That is, given a return signal, it is desired to reconstruct the character of the reflecting surface. Neither existing instrumentation nor analysis techniques can reconstruct an exact duplicate of scattering surface physical characteristics except for a few simplified structures. Although a given surface will produce a unique return signal, a given return signal does not always correspond to a unique surface. Appropriate analysis of the return signal, however, can yield a significant inference of the required statistical characteristics. Figure 4.2.1-1 illustrates the mechanics by which the radar return signal is generated. Conceptually, the process occurs in the following serial steps:

- (a) An energy pulse is generated at the transmitting antenna.
- (b) The energy pulse advances toward the surface in the form of an expanding spherical shell whose outer surface is the leading edge of the energy pulse, and whose inner surface is the trailing edge of the energy pulse.

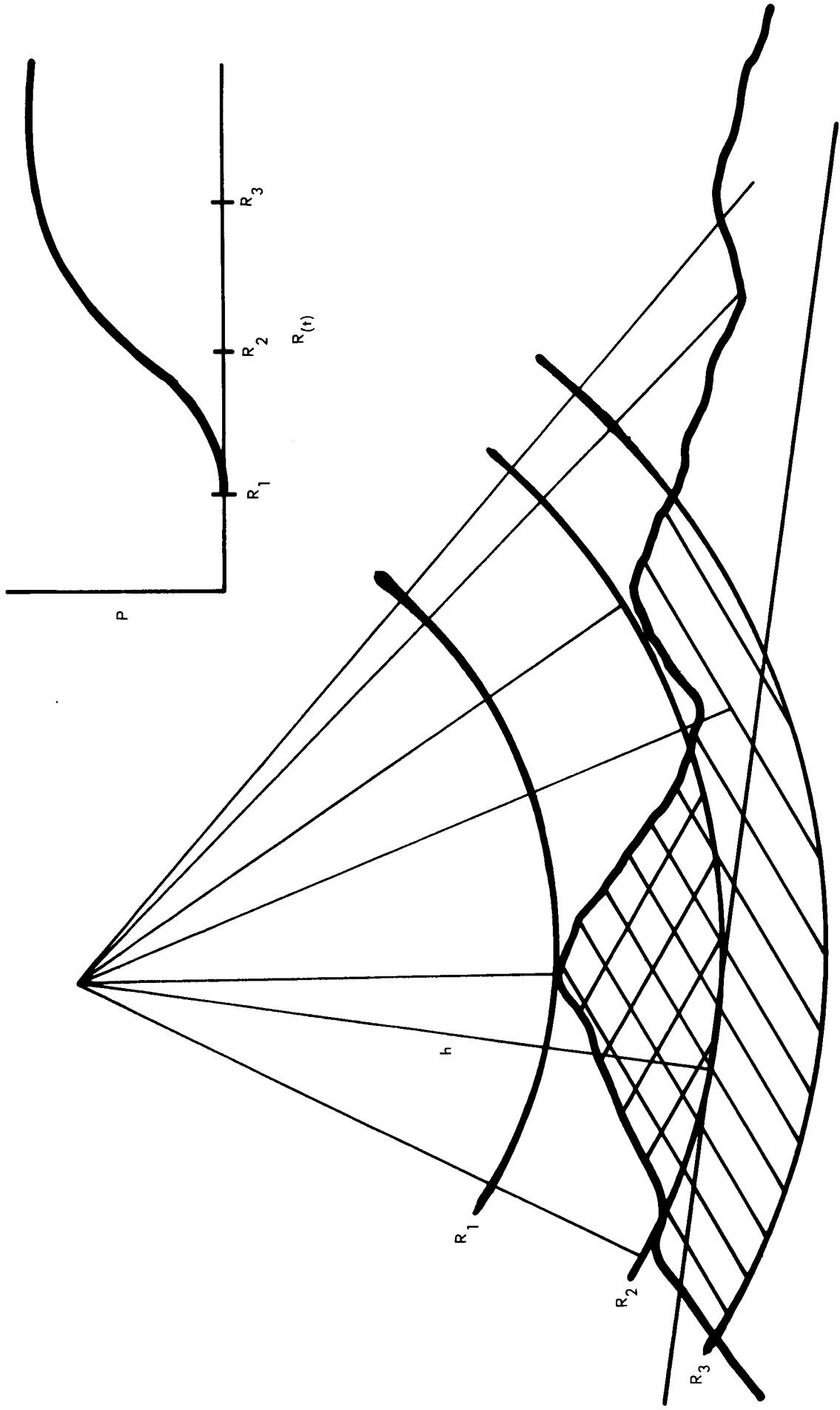


FIGURE 4.2.1-1 RELATIONSHIP OF RETURN POWER, AREA EXCITED AND RANGE

- (c) At a time, $t = R/C$, where C is the electromagnetic propagation constant, the energy pulse is incident on the surface. The surface then reacts to the incident energy according to the laws of physics to reflect some portion of the energy at the boundary, passing some portion of the incident energy to the interior where the reduced energy pulse propagates (subject to such absorption and/or re-radiation as the characteristics of the media may govern), or a portion of the energy may excite the surface material (microscopic effect) which in turn re-radiates a portion of the energy as a multipole transmitter.
- (d) The return energy propagates back to the receiving antenna where it is detected.
- (e) That part of the incident energy which penetrates the surface encounters a similar effect at each substrata boundary.

The characteristics of the first boundary and the medium it encloses are by far the determining factors governing the return signal structure and its strength. Subsurface effects, in general, may be completely submerged by the first surface return. However, if the physical character of the medium enclosed by the first surface is not appreciably different from that of free space, that surface and its enclosed medium will not appreciably interact with the incident energy to produce an effect on return signal structure. It is quite possible that the major contributor to the return signal structure will be a substratum surface. It is also likely that the return signal may be composed of several components, each of which represents a stratified layer. Although no work at defining a system capable of resolving multiple signal components was undertaken during this study, such a system can be defined and implemented. For purposes of this study, the lunar surface was assumed to enclose a homogeneous medium, and the primary mechanism for generating a return signal was assumed to occur at the first boundary. The reflected energy at a boundary depends on the wavelength and angle of incidence of the incident energy pulse and the electrical properties of the media separated by the boundary. If the boundary is not planar, but irregular with either periodic or random variations in height measured from some datum level, the exact law governing the return energy is not known.

Most theories of rough surface scattering use one or more of the following assumptions:

- (a) The dimensions of the scattering elements are taken as either much smaller or much greater than the wavelength of the incident radiation.
- (b) The radius of curvature of the scattering element is taken to be much greater than the wavelength of the incident radiation.
- (c) Shadowing effects are neglected.
- (d) Only the far field is included in the analysis.
- (e) Multiple scattering is neglected.
- (f) The density of irregularities is not considered.
- (g) The treatment is restricted to a particular model of surface roughness.

The model which seems to be the most applicable to the LUCOM System consists of a rough surface given by the two-dimensional distribution of its height above a certain mean level. The analysis of signal structure for such a model requires a fair amount of sophistication and computer assistance. Because the effort required was well beyond the scope of this study, only a limited approach toward establishing the structural relationship between the surface and the return signal was undertaken. Equation 4.2.3, which illustrates the relationship between return signal power and range as a function of statistically distributed scatterers, was developed under the following assumptions:

- (a) The scattering coefficient is homogeneous across the area.
- (b) The detail scattering mechanism at the surface results in a diffuse but isotropic field.
- (c) The variations in elevation about the datum are normal.

- (d) The datum was taken to be the mean of all elevations contained in the antenna pattern.
- (e) The antenna is isotropic to the half angle beam limit where the gain falls sharply to zero.

In itself, equation 4.2.3 is not of any great significance. However, by predicting return signal structure based on equation 4.2.3 it is possible to show the relationship between surface statistics and signal structure, thereby gaining insight into applicable techniques and signal analysis schemes to be implemented for LUCOM.

$$P_R = \frac{K}{2} \sin^2 \varphi_o \frac{\Delta R}{R(R-\Delta R)} + \frac{2K}{\sqrt{\pi}} \sum_{n=0}^{\infty} \left[\frac{(-1)^n}{n!(2n+1)} \left\{ h^{2n+1} (\cos^2 \varphi_o - 1) \frac{\Delta R}{2R(R-\Delta R)} + (2n+1) h^{2n} (1 - \cos^3 \varphi_o) (\ln R - \ln (R-\Delta R)) \right\} \right] - \frac{2K}{\sqrt{\pi}} \sum_{n=0}^{\infty} \frac{(-1)^n}{n!(2n+1)} \sum_{p=0}^{m-2} \frac{(-1)^{p+2} (\cos^{p+4} \varphi_o - 1)}{(p+2)!(m-p-2)!(p+4)(p+1)} \sum_{j=0}^P \frac{(-1)^{j+1} (p+1)! R^{p-j} \Delta R^{j+1}}{(j+1)!(p-j)!},$$

$$(m = 2n+1),$$

where φ_o = antenna 1/2 beamwidth
(including effects of range weighting and finite pulsewidth).

EQUATION 4.2.3

4.2.3 RETURN SIGNAL AND SURFACE CHARACTERISTICS RELATIONSHIP

The relationship between return signal and surface characteristics may be better shown through qualitative consideration of elevation statistics and return signal build-up. Referring to Figures 4.2.3-1 and 4.2.3-2, as the leading edge advances, more and more scatterers are included in the excitation region. The instantaneous return from those scatterers is, then,



FIGURE 4.2.3. -1 AREA GROWTH FOR FINITE PULSE

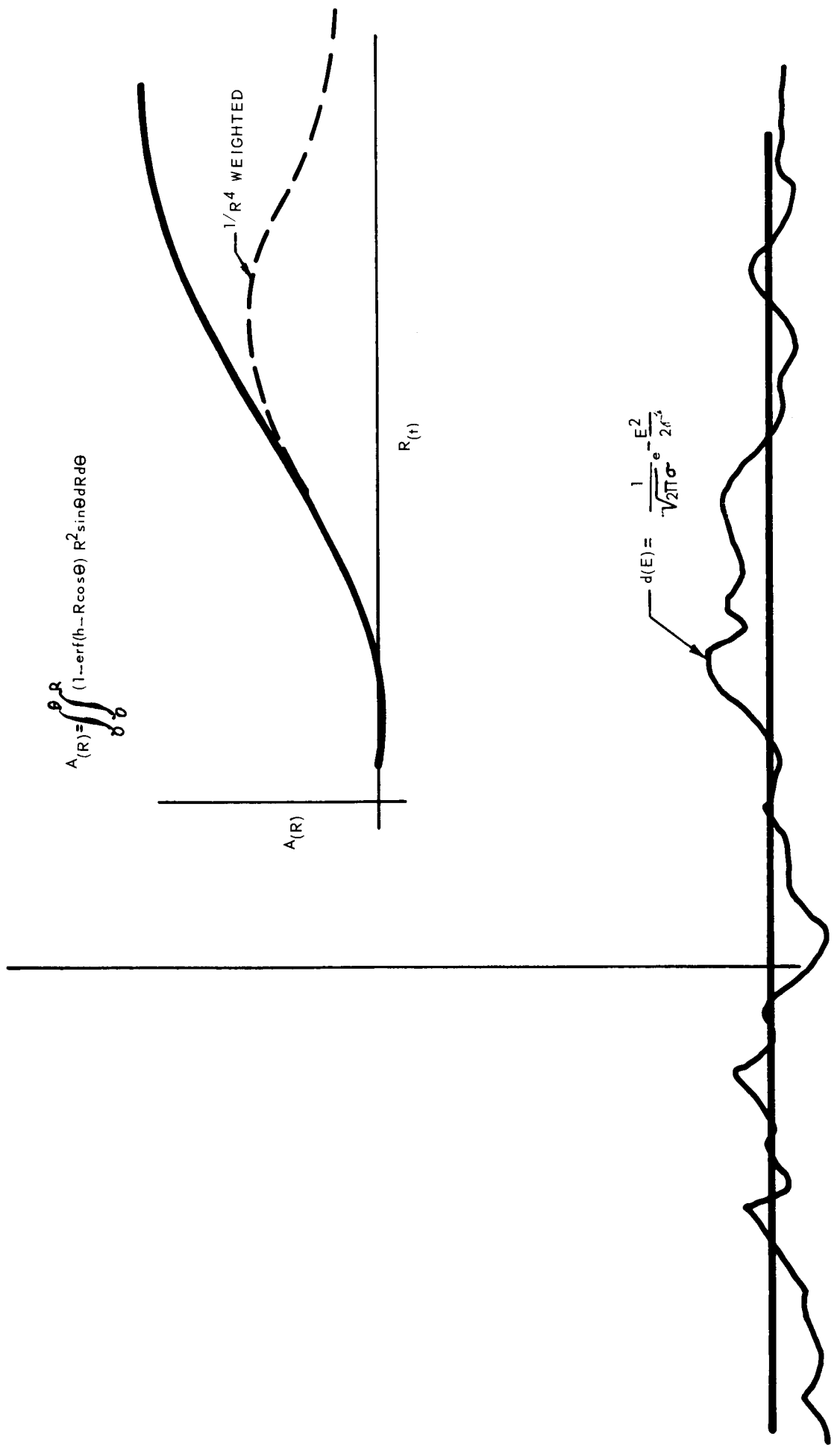


FIGURE 4.2.3-2 UNWEIGHTED AREA GROWTH FROM RANDOM SURFACE

a measure of the relative number of scatterers in the beam pattern greater than some fixed elevation. The signal build-up follows a form equivalent to an accumulation function, at least until the trailing edge begins to have an effect. By analyzing the shape of the leading edge through pulse height spectra and video sampling, it appears that a significant inference can be made as to the relative frequency of occurrence of elevations in the lunar surface. Before definitive results can become available, it will be necessary to complete a thorough feasibility study of the entire process and to test the validity of all simplifying assumptions against such data as is either now available or can be made available during the LUCOM development cycle.

4.2.4 RADAR PROFILE PARAMETRIC ANALYSIS

This section describes a quantitative radar sensor parametric analysis which was accomplished to provide a basis for the preliminary selection of LUCOM radar parameters. The approach used in this analysis is considered unique and quantitatively accurate. The data is presented in four sections: a documentation of the conditions considered in the analysis, the procedural methods used in the analysis, the results of the analysis, and conclusions which were derived from these results.

4.2.4.1 Surface Model

The initial step in performing radar profile analysis for the LUCOM System was the selection of a "target" model, representative of the lunar surface. Specifically, profile data was derived from Lunar Aeronautical Chart (LAC) 77, bound by coordinates, $8^{\circ} 00' W$, $9^{\circ} 40' S$ to $2^{\circ} 00' W$, $9^{\circ} 40' S$ and $8^{\circ} 00' W$, $10^{\circ} 20' S$ to $2^{\circ} 00' W$, $10^{\circ} 20' S$. A lunar surface model (representing a rugged mountainous area) was selected in an attempt to provide a realistic approach for the determination of the LUCOM System parameters, such as:

- (a) Pulse width
- (b) Beamwidth
- (c) Tracking area

The profiles derived from these charts, regardless of the accuracy of their source, can be considered a "worst" case.

4.2.4.2 Parameters

The primary parameters which were investigated in this analysis are:

- (a) Beamwidth - The requirements for the antenna beamwidth must be established as a function of altitude (orbit) and the lunar surface model. Antenna beamwidth affects system performance in terms of its effect on the sensitivity coefficient of the system to antenna orientation errors, and two-way gain characteristics.
- (b) Pulsewidth - Previous experience and current work have indicated that reproduction of profiles may vary considerably in form as the transmitted pulse width is varied. The present study has included an investigation of the effects of various pulse widths, and has resulted in the specification of suitable values for this parameter.
- (c) Tracking Area - The effective illuminated area upon which the radar sensor bases its detection threshold affects the LUCOM System performance through the smoothing effect of large tracking areas. The tracking area is an important parameter in terms of the radar sensor design, in that the transmitter power is a direct function of the tracking area and illuminated area.

The limitations and variations of the above parameters which were analyzed are as follows:

Beamwidths	1°, 3°, 5°
Pulse Widths	.1, .5, 1.0, 1.5 and 2.0 microseconds
Tracking Areas	2.7, 10.5, 15.7, 24.3, and 35.1 million square feet
Vehicle Altitude (Assumed)	480,000 feet (80 nautical miles)
Vehicle Dynamics (Assumed)	Stabilized vertically

4.2.4.3 Analysis Procedure

This section describes the procedural techniques involved in the Lunar Surface Model Analysis. Procedural data flow is: grid analysis, antenna mask construction, and area/depth transformation.

4.2.4.3.1 Surface Grid Analysis

The selection of the lunar surface model was followed by the preparation of a surface matrix. This was accomplished by determining the elevations of the surface at regularly spaced intervals at the intersection of the rows and columns of an orthogonal grid applied to the surface area being investigated. The first consideration for construction of the grid matrix is to determine the length and width of the grid. This is accomplished by sampling the surface model (reading approximately 80 points on a single row of a test grid). Applying the least squares fit operation, the distance varying trends are removed from the test profile. By the use of the autocovariance function:

$$C(\tau) = \frac{\sum_{i=0}^N X_i \cdot X_{i+\tau}}{\frac{1}{N} \sum_{i=0}^N X_i \cdot X_i}$$

where $\frac{1}{N} \sum_{i=0}^N X_i \cdot X_i$ is normalized to maximum value, the autocovariance

curve is derived (Figure 4.2.4.3.1-1). From the autocovariance function¹, the power spectral density (Figure 4.2.4.3.1-2) is computed by the discrete cosine transformation. The above computations are accomplished by company developed computer programs. The explanation presented above merely describes the mechanics of the various computer programs.

The power spectral density curve (Figure 4.2.4.3.1-2) is used to obtain the maximum grid interval for the lunar surface model. The maximum grid interval (GIm) is derived as:

$$GIm = \frac{1}{2 \times fc}$$

and $RHO(f) = .01$, due to small power content of the frequency. From Figure 4.2.4.3.1-1 $RHO(f)$ corresponds to a frequency content of 1×10^{-4}

¹ Reference Appendix 4.2.4-A.

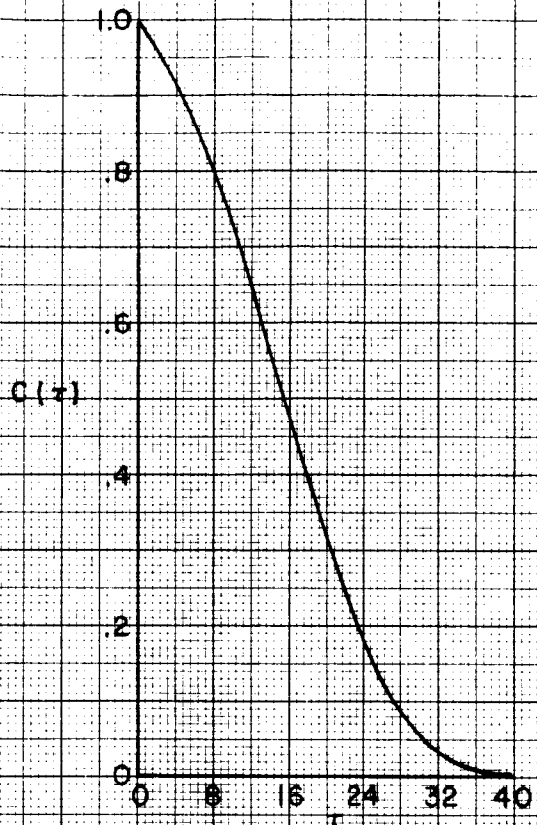


FIGURE 4.2.4.1 AUTOCOVARANCE FUNCTION

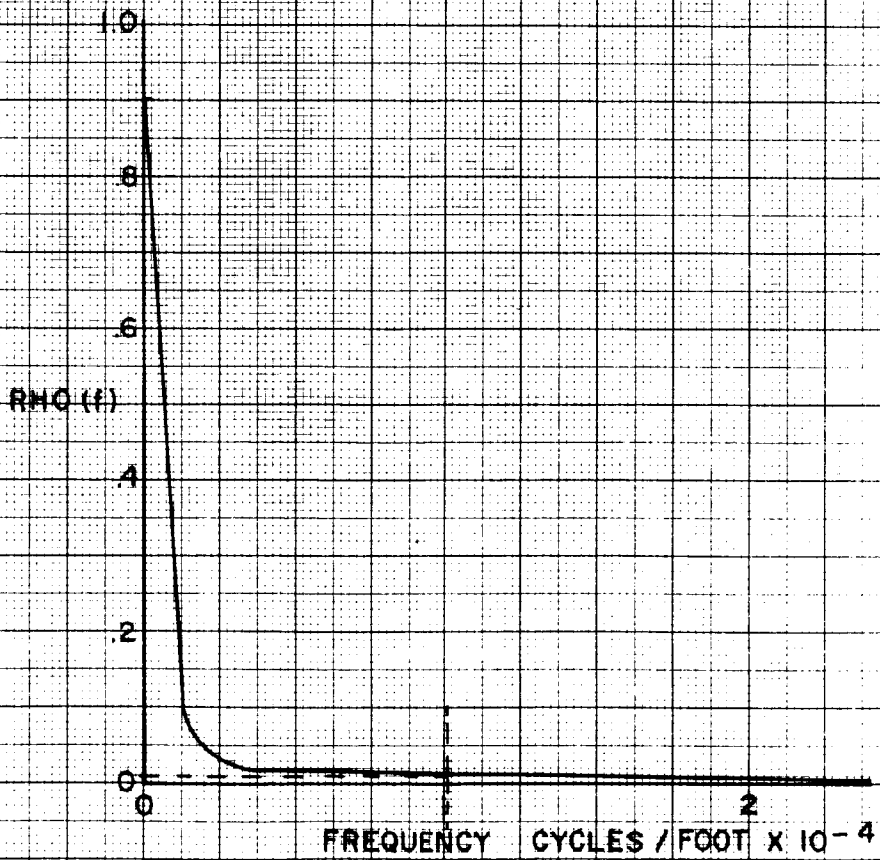


FIGURE 4.2.4.3.1-2 POWER SPECTRAL DENSITY

cycles/foot; therefore,

$$GIm = \frac{1}{2 \times 10^{-4}}$$

$$GIm = 5,000 \text{ feet.}$$

Any grid interval less than 5,000 feet will be sufficient for this analysis. Past experience has shown that by dividing the GIm by two and subtracting a safety factor of 100 feet the best results are obtained. The LUCOM grid interval was determined to be 1,660 feet.

Having selected the grid interval, the lunar surface model elevation points are interpreted at each grid intersection. This is accomplished by an automatic reading process which punches IBM cards for each of the grid intersections.

4.2.4.3.2 Antenna Mask

Each beamwidth considered in this analysis requires an antenna mask. The construction of the antenna mask begins with the antenna pattern at a specified beamwidth. For purposes of this analysis, the antenna pattern is assumed to be a $\frac{\sin x}{x}$ function. The beamwidth is incremented by

small angles, with weighting functions assigned to each incremental angle, Figure 4.2.4.3.2-1. The weighting functions represent a process by which the pattern can be displayed in digital form for the digital computer analysis. The digital representation of the antenna pattern is as shown in Figure 4.2.4.3.2-2 and Figure 4.2.4.3.2-3 where the latter figure is the plan view which is centered over each grid intersection of the lunar surface model. By placing the antenna mask over each grid intersection and quantizing the transmitted pulse width, return video build-up of the surface model is evaluated relative to area and time.

4.2.4.3.3 Area Depth Transformation

For determination of system sensitivity for the lunar model and various parameters under investigation, the Area Depth Transformation (A/D Transformation) is employed. The A/D Transformation is a computer developed program (IBM 7090) which is essentially a simulation of the power returned to a vertical incidence pulsed LUCOM radar sensor. The purpose of the A/D Transformation is to determine, for the lunar

θ = BEAMWIDTH

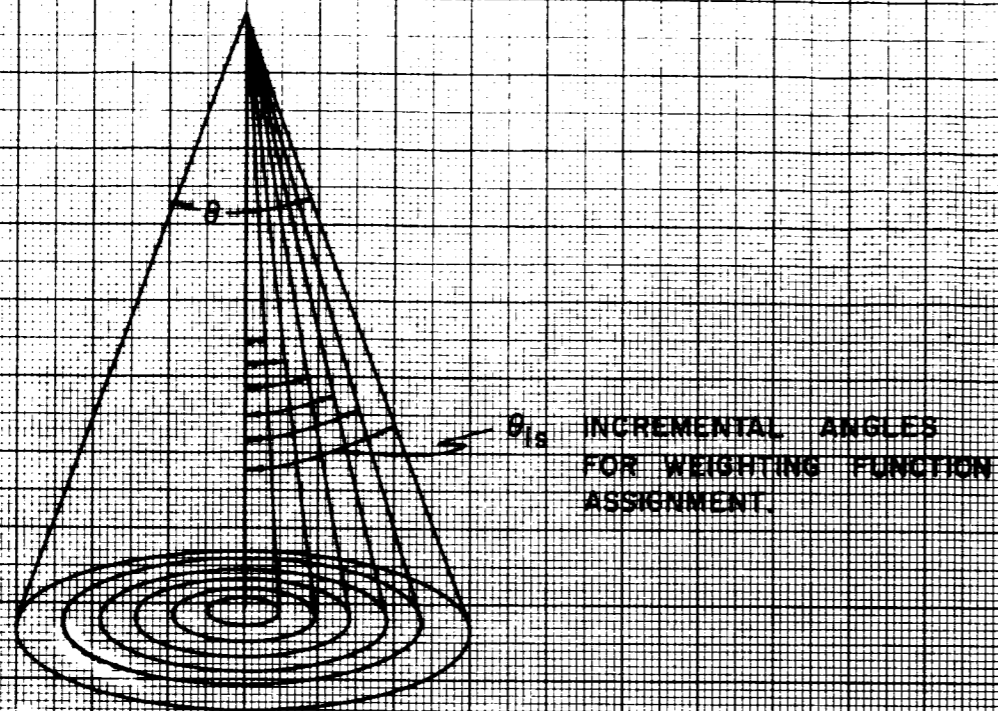


FIGURE 4.2.4.3 WEIGHTING FUNCTION DESCRIPTION

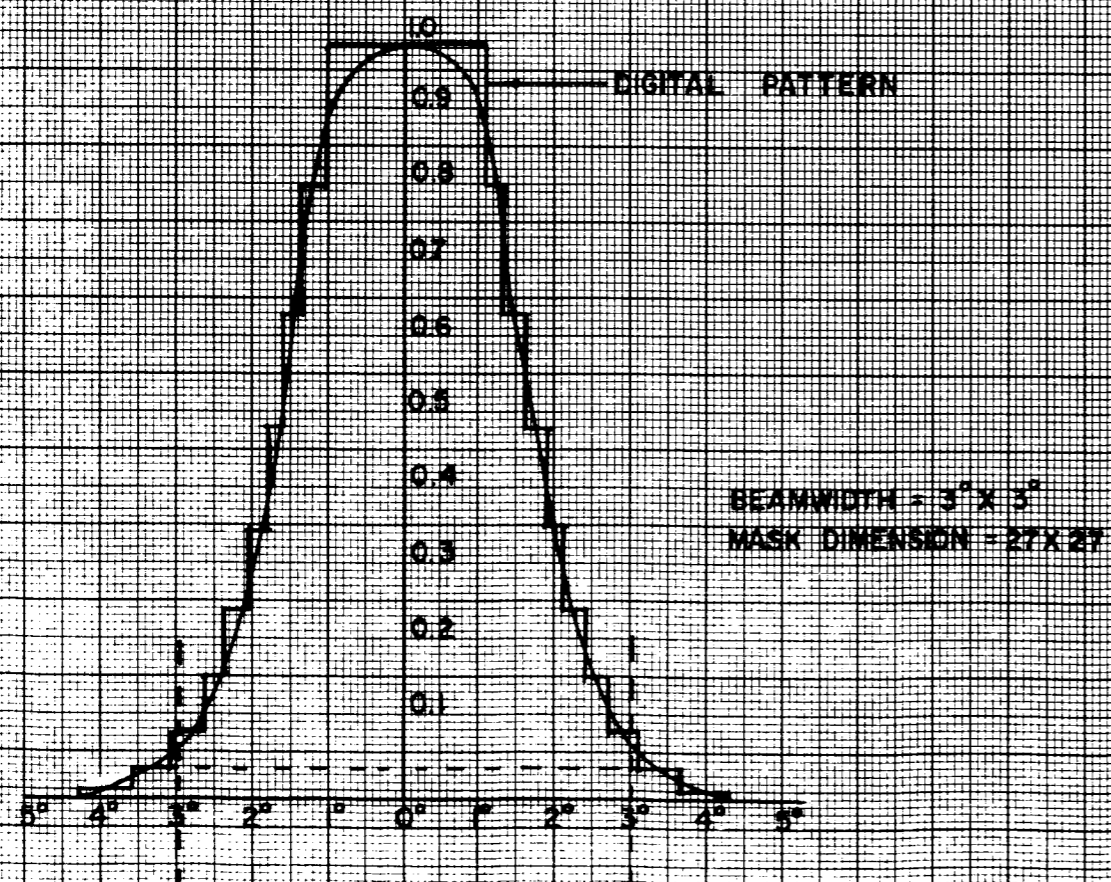


FIGURE 4.2.4.3.2-2 DIGITAL ANTENNA PATTERN

BEAMWIDTH = 3°
NUMERICAL VALUES
REPRESENT % OF
RECEIVED POWER

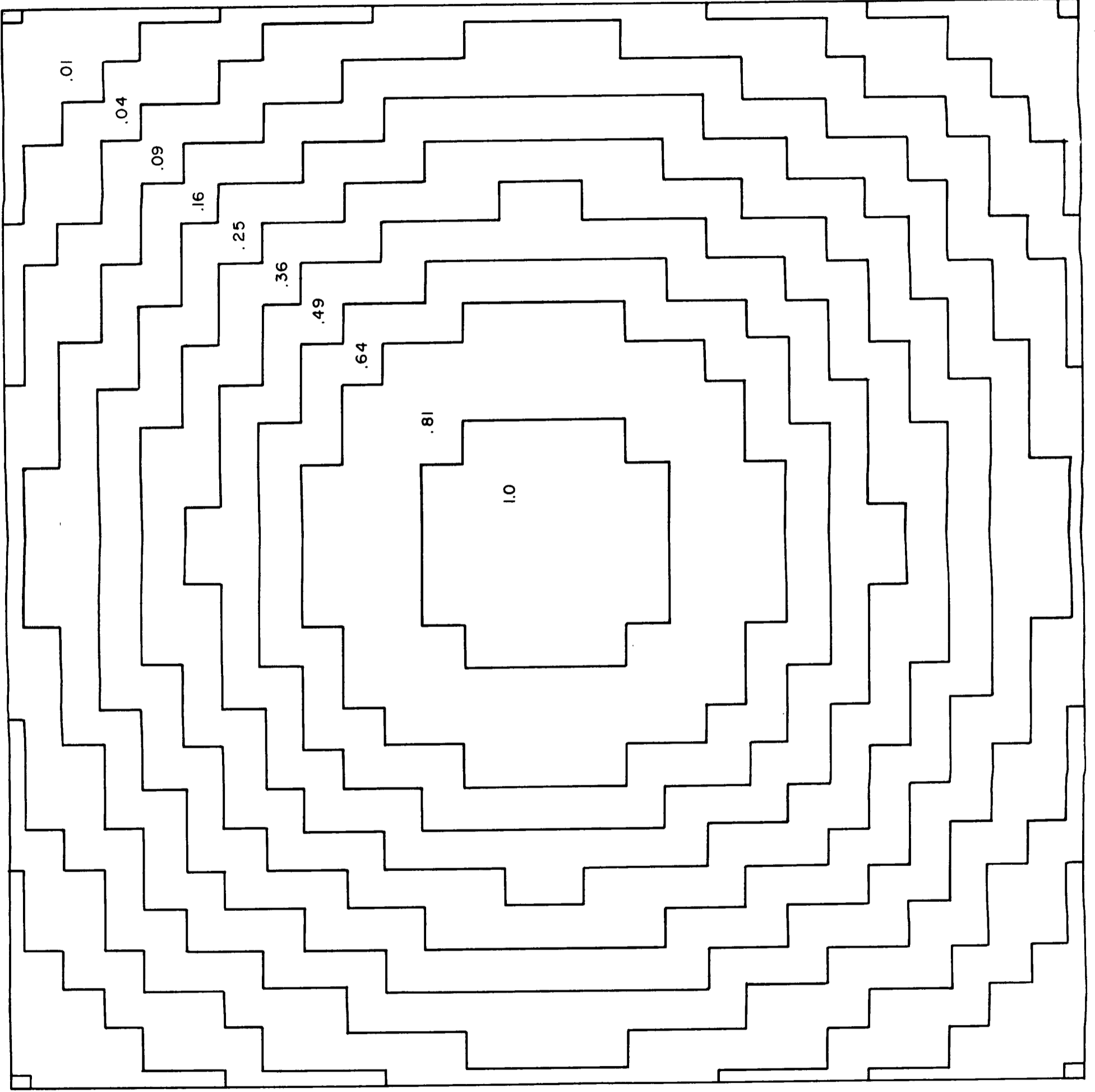


FIGURE 4.2.4.3.2.-3 27X27 ANTENNA MASK

surface model and the radar sensor parameters, the apparent lunar surface profile as viewed by the radar sensor. Time and distance are equated in the pulsed LUCOM radar sensor and the wave front may be thought of as penetrating the average terrain relief to a given depth in order to illuminate a given area. The illustration shown in Figure 4.2.4.3.3-1 shows the effects of pulse width limiting on the area build-up. When the trailing edge of the pulse arrives at the point of first contact, then the area intercepted by the trailing edge from that time on subtracts from the total area and does not contribute to the received power. The power received at altitude (H) is proportional to $\int f^2(\theta, \phi)$ where $f(\theta, \phi)$ is the antenna pattern. The integral $\int f(\theta, \phi)$ is the effective area build-up as the pulse propagates over the lunar surface model. The A/D Transformation output is the apparent elevation of a point under the vehicle as determined by the area build-up for the surface model being analyzed. The surface area of interest is quantized into incremental areas. A time history of the pulse propagating over the surface is required, which is accomplished by the quantization of the pulse width. The surface model matrix is considered as a group of points in three-dimensional rectangular cartesian system coordinates. The position in the matrix of an incremental area and the elevation number provide the coordinates of the area location. Considering the vehicle fixed over the grid intersections of the ground matrix and at the orbit altitude, the simulation process calculates the distance of the grid intersections, altitude and all possible incremental areas. All these distances are stored and scanned to find the shortest range measurement (R). The number of distances between (R) and (R + q), where (q) is quantization grain of the pulse width, is counted and recorded. The quantization grain for the LUCOM surface model is 5 feet for the 3° and 5° beamwidths, and 25 feet for the 1° beamwidth. The information that is counted and recorded is the number of incremental areas illuminated by a pulse width of γ . This process is continued in steps of (q) until the desired tracking area is realized. As the trailing edge of the pulse reaches (R), then the number of ranges in the first increment (q) is removed from the process and the areas in the next new increment of (q) are added in, which simulates pulse width limiting. This counting of areas in incremental pulse width γ continues until the desired tracking area is reached. The location of the leading edge of the pulse is $[R + N(q)]$, where (N) is the number of steps required. The apparent and simulated elevation of the point at each grid intersection is then altitude $[(\text{orbit}) - R + N(q)]$. This process continues point by point until the complete matrix of apparent elevations is constructed. Transformation at several beamwidths can be made to determine the effects of beamwidth on system sensitivity.

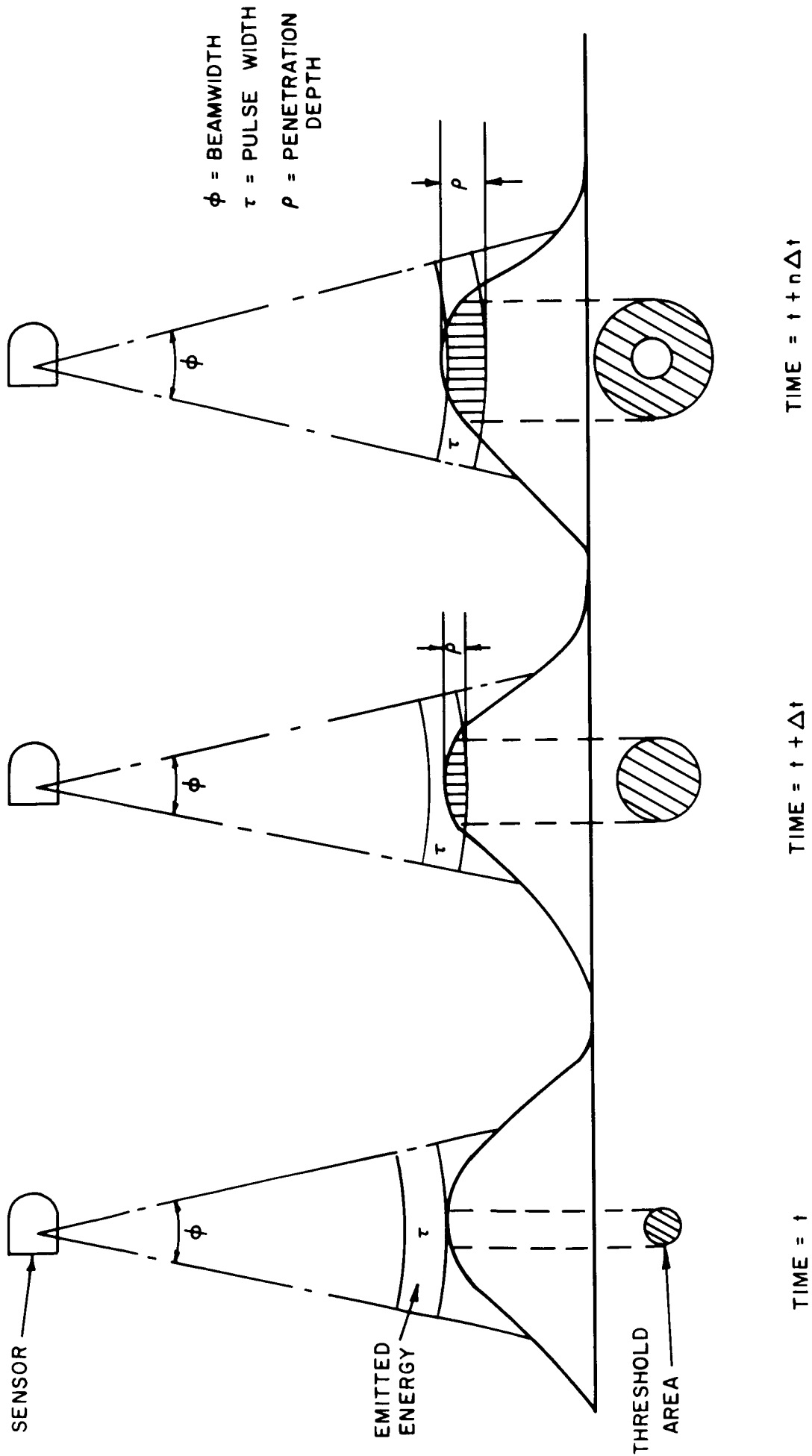


FIGURE 4.2.4.3.3-1 AREA DEPTH RELATIONSHIP (TYPICAL)

4.2.4.4 Analytical Results

Initial implementation of the analysis, following the grid interval and antenna mask analysis, requires the use of the A/D Transformation and selection of a beamwidth. The selection of a 5° beamwidth seems reasonable due to the altitude of the orbit and the resulting large area illuminated. Considering the fact that reconstruction of the illuminated surface into a profile is greatly perturbed by the use of large areas of illumination, other parameters of the radar system could be analyzed and the results would yield an improvement factor in the profile reconstruction. In order to determine the trend of the improvements attainable, a reduction of beamwidth and/or reduction of the threshold tracking area were analyzed as a function of pulse width and beamwidth.

4.2.4.4.1 Pulse Width

By reducing the broad spectrum of beamwidths to the realistic value of 5 degrees and by the use of the A/D Transformation routine (described in paragraph 4.2.4.3.3), the effects of a pulse width as a function of tracking area can be investigated. The determination of a specific pulse width requires an analytical evaluation of the matrix rows of the lunar surface model as a function of penetration depth. Selecting a very narrow pulse width of 0.1 microsecond and permitting the antenna mask to traverse a row of the matrix, a video build-up is obtained for each grid intersection. Specifically, the video build-up is obtained when the antenna mask is positioned over a specific intersection permitting the pulse to penetrate the surface model for a period of time. The specific finite time period used in this analysis was 2.0 microseconds, which is a range pulse width of approximately 1000 feet and considered as an upper limit. The results of the area as a function of time is observed at each grid intersection by recording the column numbers of the row under investigation. The corresponding row, used for the 0.1 microsecond pulse width as shown in Figure 4.2.4.4.1-1 is row 14, which corresponds to the profile of Figure 4.2.4.4.2-1. The results obtained for a 0.1 microsecond pulse width (Figure 4.2.4.4.1-1) indicate that a tracking area (approximately 6×10^6) is too small to detect the return power from a surface which has steep slopes that are closely spaced. In other words, the return signal would be lost in the system noise. The results of the 0.1 microsecond pulse width analysis indicate the pulse width will have to be larger in order to obtain more signal power, that is, an increase in tracking area. Following the same procedure employed in the analysis of 0.1 microsecond pulse width, larger pulse widths of 0.5, 1.0 and 1.5 microseconds were analyzed. The results of these larger pulse widths are shown graphically in Figures

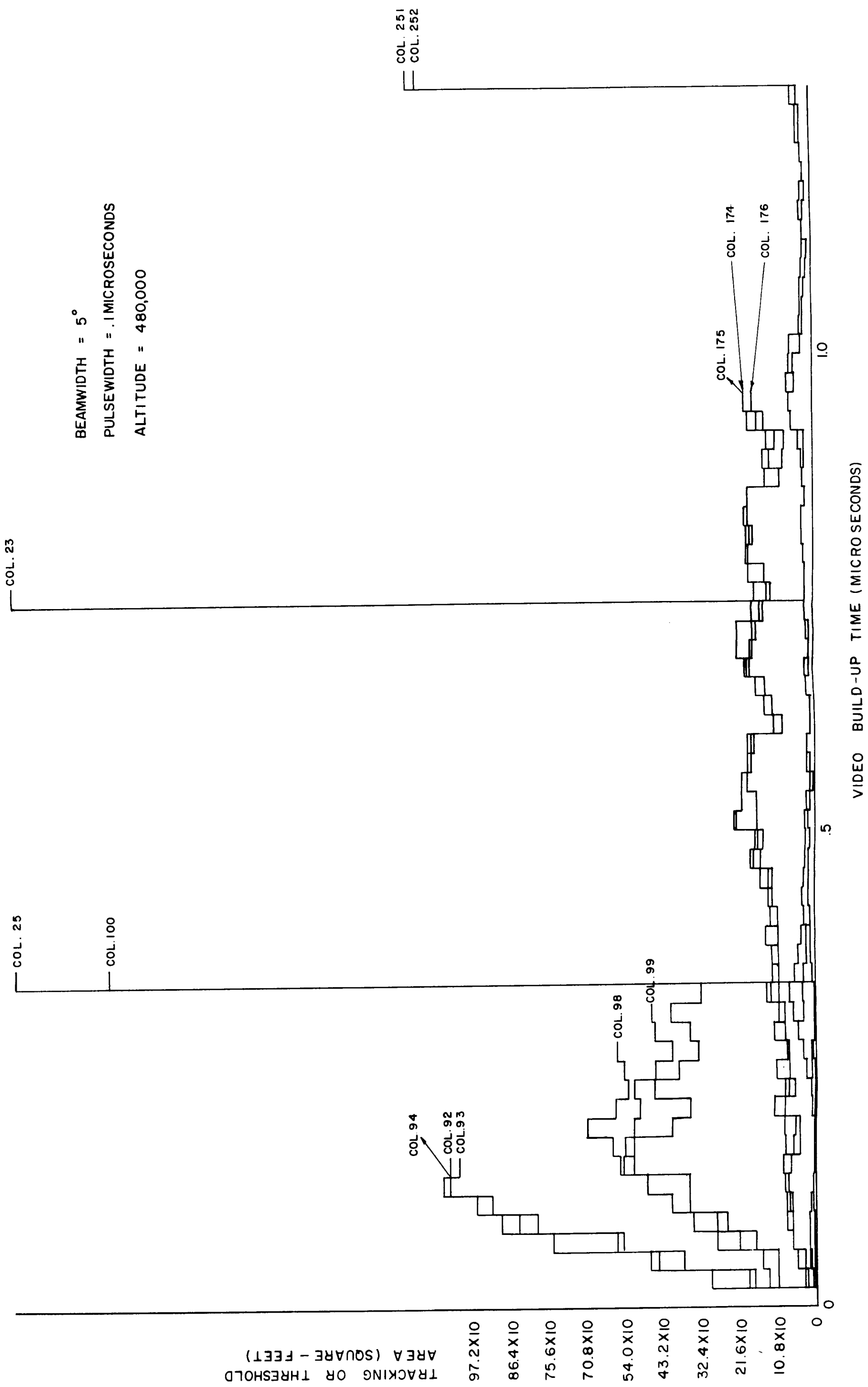


FIGURE 4.2.4.4.1-1 QUANTIZED BUILD-UP VS AREA

4.2.4.4.1-2 through 4.2.4.4.1-4, respectively. The results of the use of 0.5 microsecond pulse width (Figure 4.2.4.4.1-2) show no significant change in signal power (tracking area) over the 0.1 microsecond pulse width. Holding all parameters constant and increasing the pulse width to 1.0 microsecond has increased the tracking area to approximately 32×16^6 feet², which is sufficient for detection (Figure 4.2.4.4.1-3). Considering the worst case of this analysis, the areas of steep slopes where previous pulse widths did not produce sufficient return power (tracking area), the 1.0 microsecond pulse width did attain sufficient return power, but another variable has to be considered; this is the time required for the build-up of the tracking area. At this point, it has been determined that a pulse width larger than 1.0 microsecond will be required and the logical approach is to reach a desired tracking area (power) in as short a time period as possible. The short time period requirement is based on the inherent character of radar detection, that is, the faster a return signal reached a desired tracking area or threshold and is detected as a return signal, not as noise, the less the fluctuations of the signal. By minimizing the return signal fluctuation, the detection error is reduced to a minimum. Also, the larger the return signal, the greater the probability of detection, realizing that the system noise will remain a constant parameter. Therefore, the trade-off parameters are, short rise time and large tracking area (return power). After analyzing the results of the 1.0 microsecond pulse width, it seems apparent that a change in the threshold (tracking area) determines the rise time of the return pulse to a specific threshold. By enlarging the pulse width to 1.5 microseconds, and following the same procedure described previously, the results obtained over the same worst case surface indicated a slight improvement in the rise time of the return pulse. This improvement is due to the fact that a pulse width limiting condition exists, that is, operating over steep slopes which are closely spaced, the return power is a direct function of the pulse width penetration depth, (reference Figure 4.2.4.3.3-1 and A/D Transformation, paragraph 4.2.4.3.3). Obviously, the trade-off parameters of rise time, pulse width and tracking area could continue using larger pulse widths; however, analytical concepts must coincide with practical aspects, such as, the larger the pulse width, the more power required for transmittal, therefore, the larger the radar sensor. Other system requirements must be considered, viz. power requirements, size, weight, and volume. Considering these system requirements coupled with the results obtained, a pulse width of 1.5 microseconds was selected (Figure 4.2.4.4.1-4). However, should the power requirement be out of proportion to the other system parameters, the pulse width could be reduced to 1.0 microseconds, realizing that a greater detection error would be introduced which would reduce the system performance.

COL. 23

BEAMWIDTH = 5°
 PULSEWIDTH = .5 MICROSECONDS
 ALTITUDE = 480,000

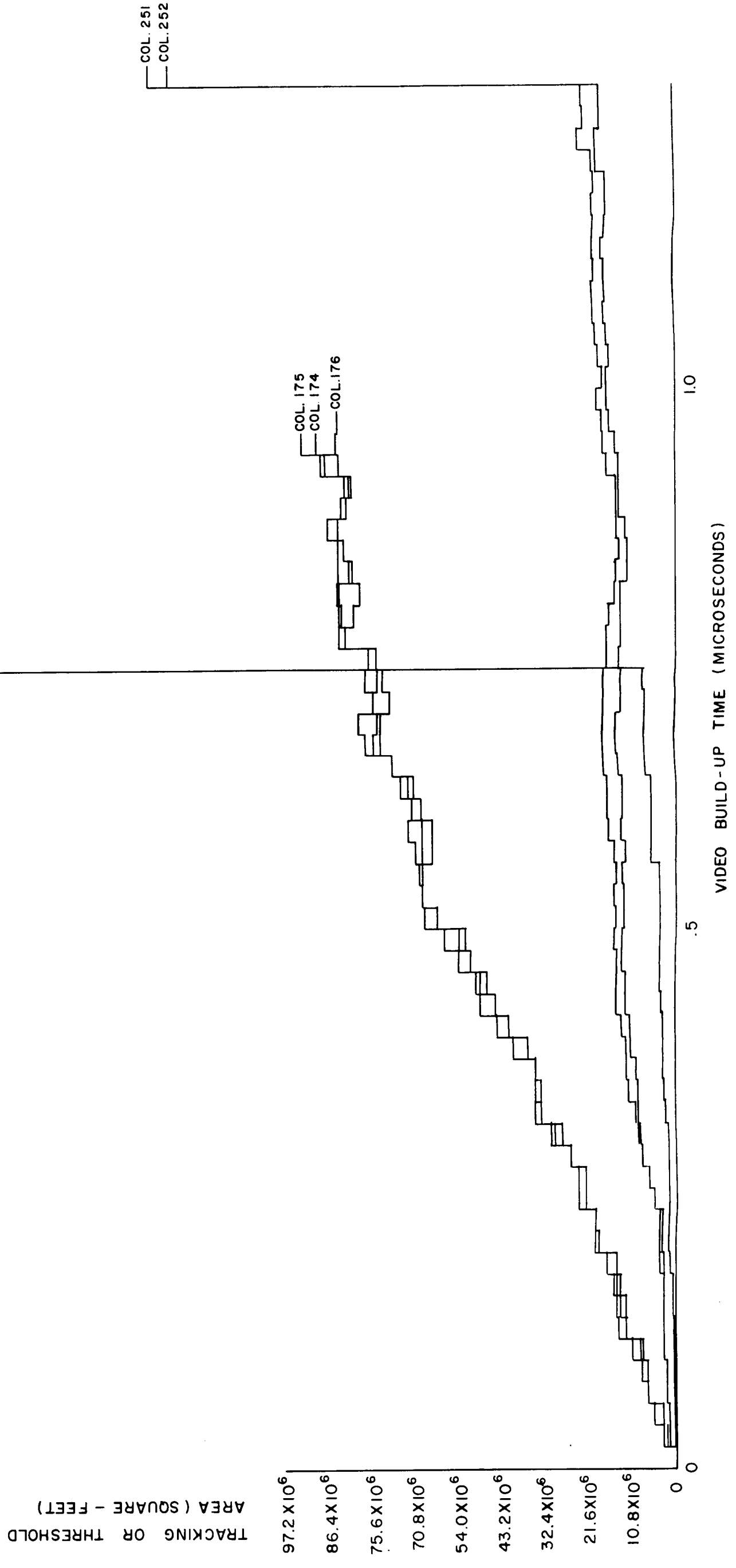


FIGURE 4.2.4.4.1-2 QUANTIZED BUILD-UP VS AREA

BEAMWIDTH = 5°
 PULSEWIDTH = 1.0 MICROSECONDS
 ALTITUDE = 480,000 FEET

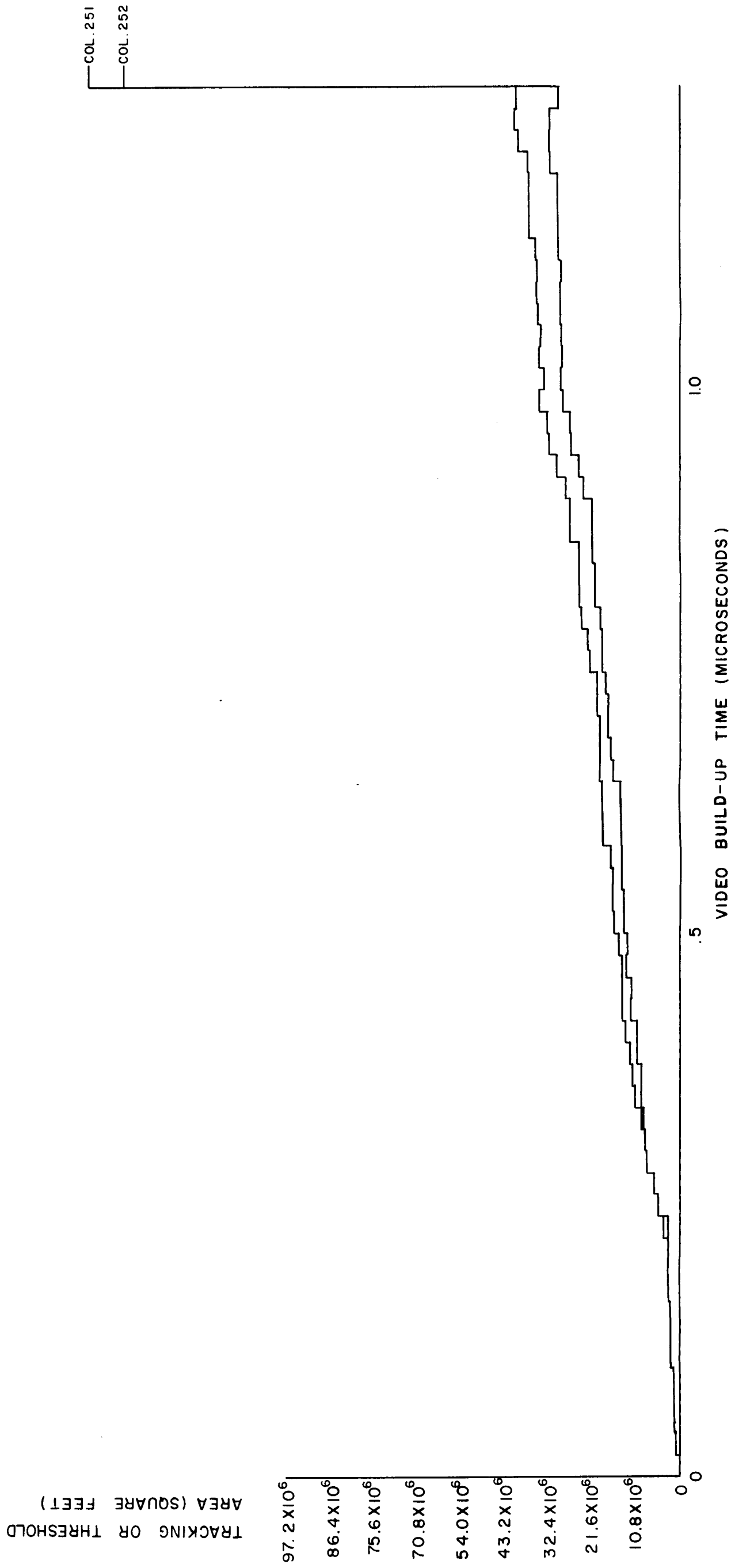


FIGURE 4.2.4.4.1-3 QUANTIZED BUILD-UP VS AREA

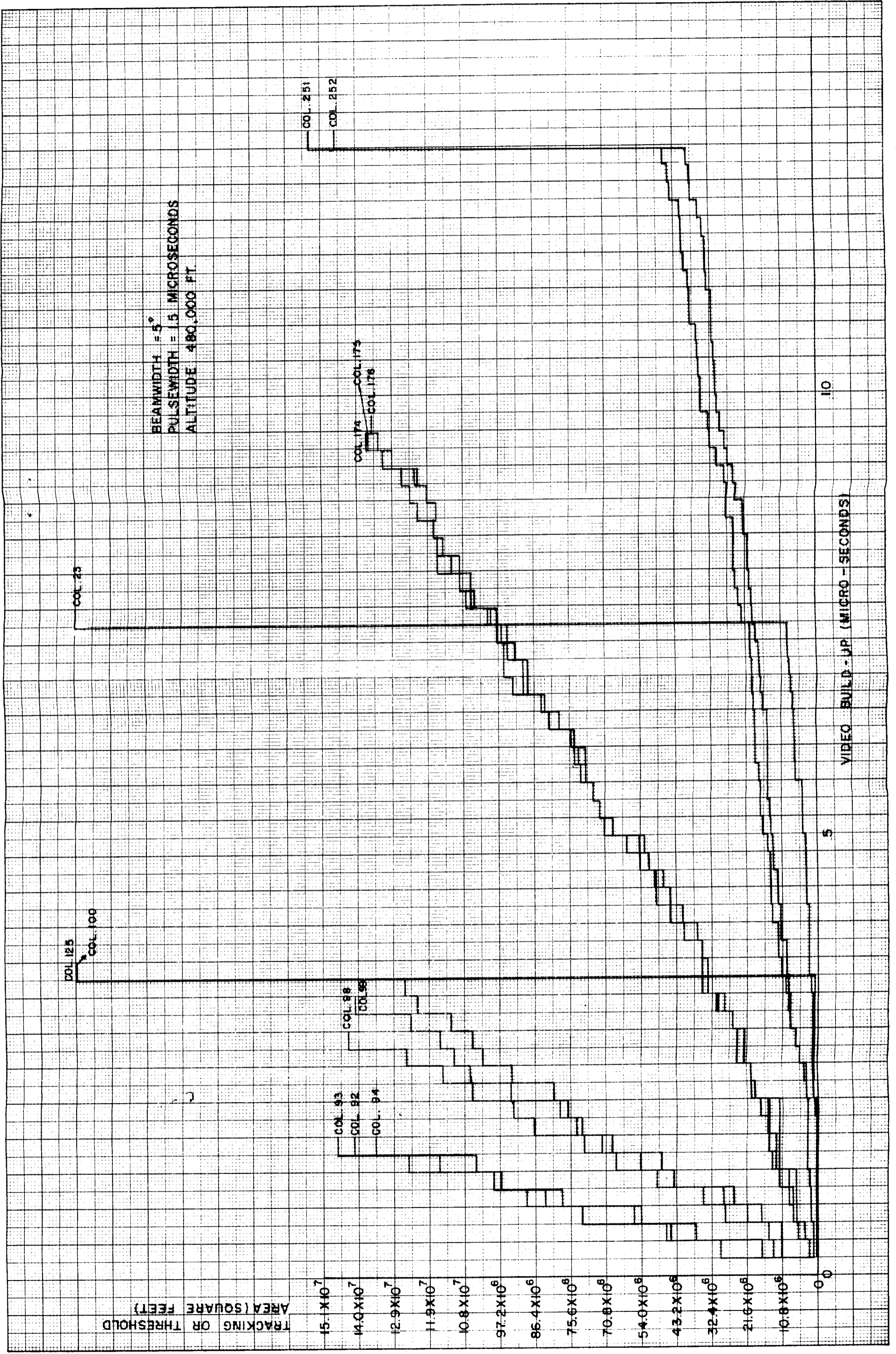


FIGURE 4.2.4.4.1-4 QUANTIZED BUILD-UP VS AREA

4.2.4.4.2 Beamwidth

The beamwidth selection follows the analytical evaluation of the pulse width. After selection of a pulse width at a specific beamwidth, the problem can be reduced to analytical evaluation of variable beamwidths as a function of tracking area. Considering a beamwidth larger than 5° does not indicate a practical approach directed toward meeting the LUCOM System requirement. That is, at the orbit altitude (80 n.m.), the illuminated area would become extremely large and the transmitted power required would constrain the radar system design. Selecting the same surface profile which was used in the pulse width analysis, beamwidths of 3° and 1° were evaluated. To determine the profile reconstruction as a function of tracking area, the 1.5 microsecond pulse width and a beamwidth of 3° were analyzed. To perform this analysis required the A/D Transformation routine and the previously specified parameters. The objective of this analysis was to show how the transformed profile compares to the original surface profile by varying the threshold (tracking area). The results are shown in Figure 4.2.4.4.2-1, which further defines the A/D Transformation concept. That is, as the transmitted energy pulse penetrates the surface, the effects of threshold tracking area as a function of the surface detail is observed. As the tracking area increases, more detail of the surface is developed. This can be observed in Figure 4.2.4.4.2-1 where the left end of the surface profile becomes more pronounced as the tracking area increases. As seen in Figure 4.2.4.4.2-2, which shows the results obtained from the upper and lower limits of the tracking areas being investigated, the effects of the A/D Transformation on the surface model are evident. As a result of past experience in terrain analysis, the A/D Transformation provides a realistic evaluation of the effects of smoothing as a function of altitude. A definite trend requiring the use of a small beamwidth is evident from the results as shown in Figure 4.2.4.4.2-2. Although the larger threshold area provides more penetration of the surface and improves the profile, the energy continues to build from the Ptolemaeus Crater rim. Specifically, the antenna mask is centered at each column intersection in the row, the antenna weighting functions are isotropic, as the antenna mask progresses down a row, the previous intersection contributes to the return signal power. The degree of contribution is a function of the surface characteristics. Using a very narrow beamwidth permits the return signal to be derived from the surface vertical to the antenna. Here again, the practical aspects must be considered. If the beamwidth is small, the vehicle stability must be good, and the angular excursion limited to a close tolerance, as well as an increase in the power requirements of the radar sensor. In order to investigate the trend towards a small beamwidth, a 1° beamwidth was selected for further analysis. This analysis used the same procedure as was applied to the

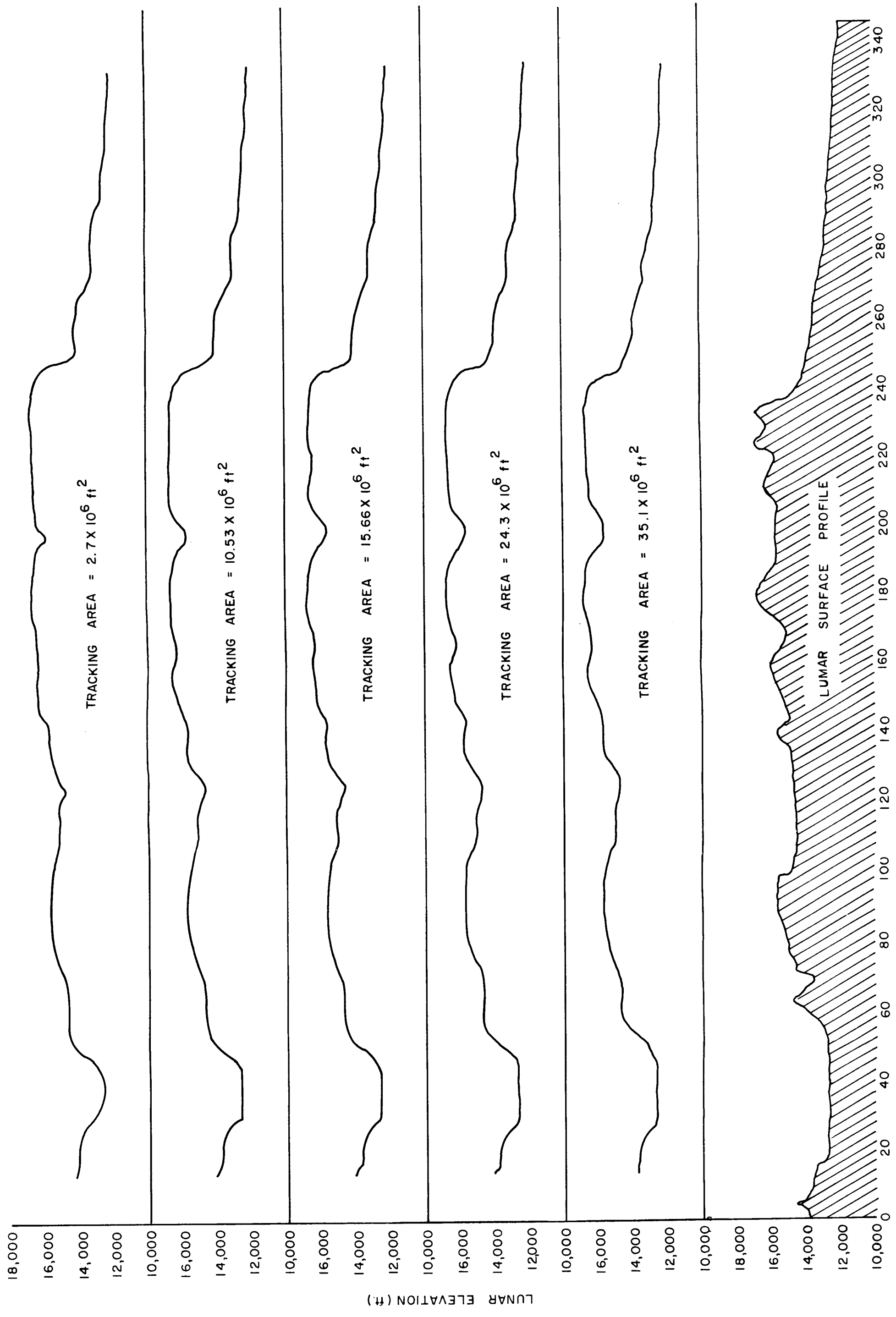


FIGURE 4.2.4.4.2-1 GROUND TRACK (S.M.)

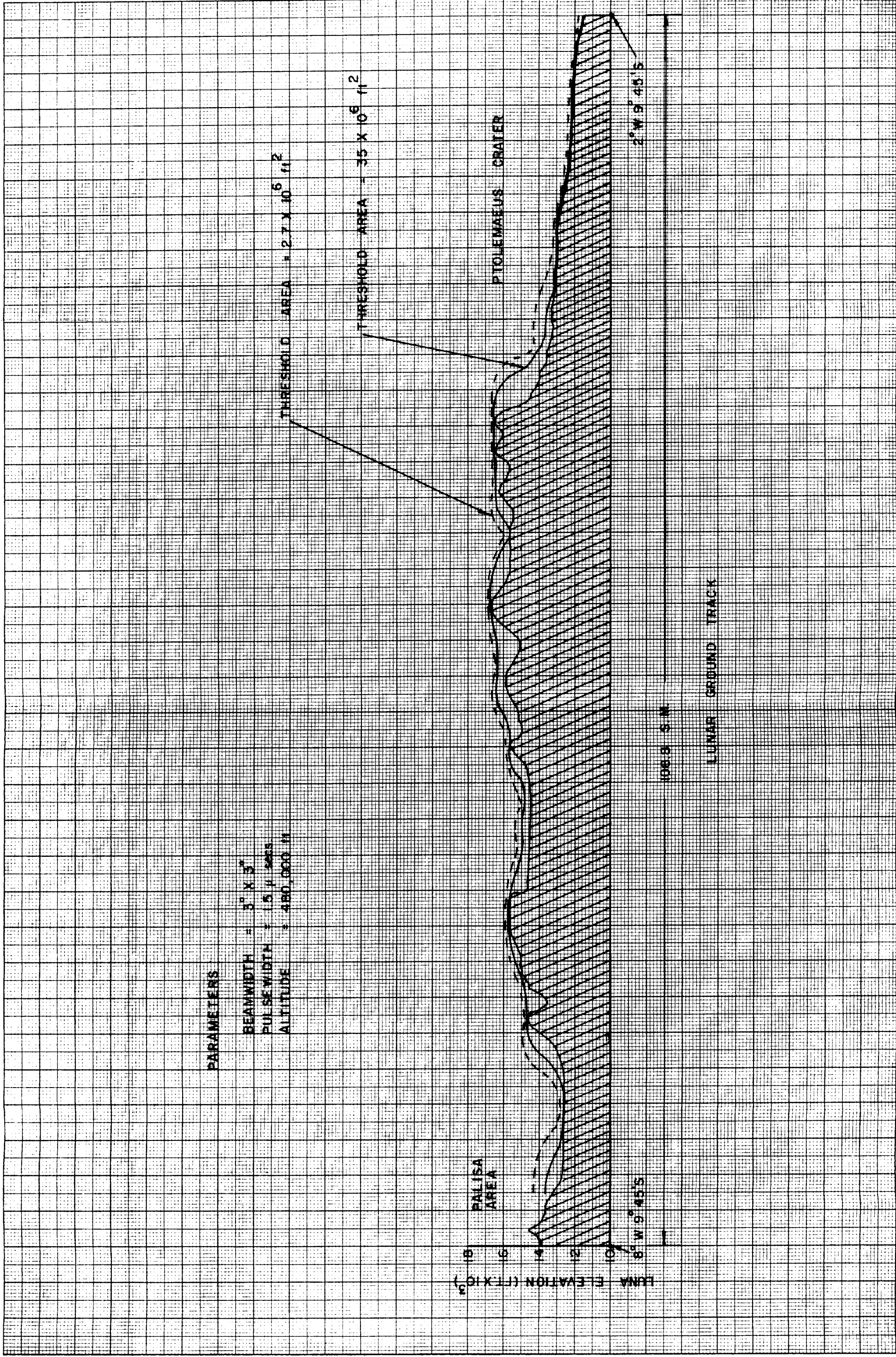


FIGURE 4.2.4.4.2-2 A/D TRANSFORMATION VS THRESHOLD AREA

3° and 5° beamwidths, as well as the same row from the lunar surface model. The results of this analysis are shown in Figure 4.2.4.4.2-3. The A/D Transformation was accomplished using a tracking area of approximately 50×10^6 feet². Video build-ups were obtained for five of the row-column intersections of the lunar surface model as shown at the top of Figure 4.2.4.4.2-3. The circled numbers marked on the surface model represent row-column intersection compatibility to the columns shown in Figure 4.2.4.4.2-1. The indications obtained from the 1° beamwidth analysis are: the smaller beamwidth does provide more surface detail, the use of a 1.5 microsecond pulse width does permit the use of a smaller tracking area less than the 50×10^6 feet² which was used, and the final selection of an operational beamwidth lies between 1 and 3 degrees. Due to the constraints that are imposed on the LUCOM System and the vehicle by the use of a 1 degree beamwidth, a 3 degree beamwidth is recommended at this point in time.

4.2.4.5 Conclusions

Analysis of the hundreds of profile plots (produced by the IBM 7090 computer in digital format and hand-plotted), shows that as the beamwidth decreases, fidelity of the reconstructed radar profile increases. This result was not unexpected, however, the improvement in surface representation gained by increasing the tracking area is less obvious. The choice of a pulsewidth of 1.5 microsecond and a tracking area of 35×10^6 feet² was fairly straight forward, and was indicated in the early computer results, but the selection of an optimum beamwidth demanded further investigation. Two additional factors were considered prior to choosing either a 3° or 1° beamwidth as a major parameter for subsequent error analysis and design; antenna characteristics and vehicle stabilization. Because of the increased antenna aperture required for the narrow beamwidth (and consequently the increased antenna weight and size), and the potential error in return signal caused by moderate changes of vehicle attitude, the 3° beamwidth was selected as a point-of-departure. The optimum beamwidth may actually fall somewhere between one and three degrees.

4.3 RADAR SENSOR DESIGN

The objectives of the radar sensor study were to: (1) develop block diagram of mapping sensor, (2) develop trade-off curves and relations that indicate design trends, which would be utilized in a sensor design when Apollo specifications are released, and (3) draw general conclusions from these relations.

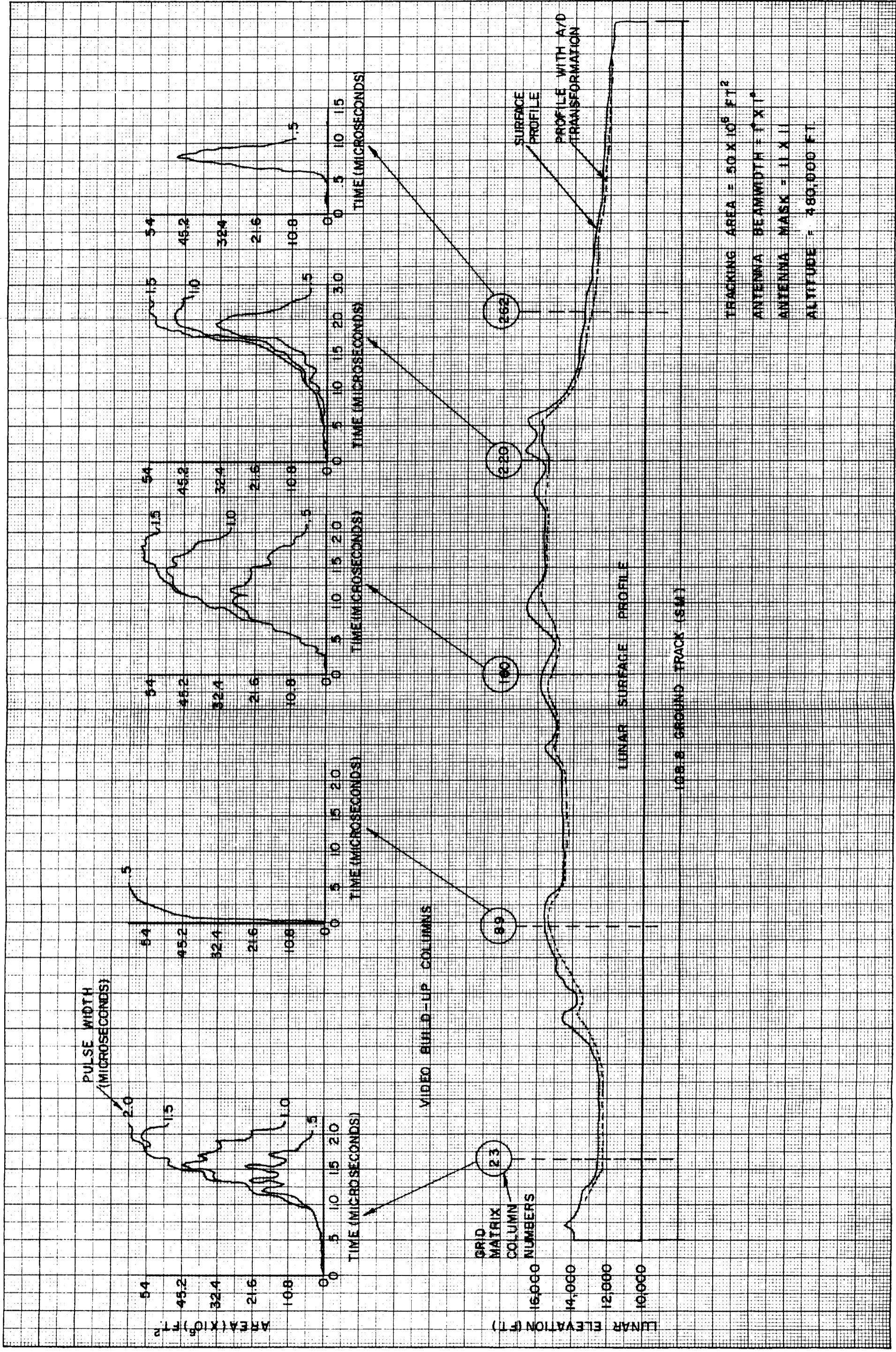


FIGURE 4.2.4.4.2-3 A/D TRANSFORMATION OF 1° BEAMWIDTH AND VIDEO BUILD-UP

The procedures followed in the study were: (1) evaluation of types of radar sensors that are applicable to the lunar contour mapping missions, (2) establishment of a radar sensor block diagram for analysis purposes, (3) determination of a detection criterion for the sensor, (4) generation of general trade-off curves on sensor system peak and prime power, carrier frequency, and pulse repetition frequency, weight, and volume requirements, (5) application of the general trade-off relations to specific cases that were examined in the lunar model profile analysis, and (6) implementation of an error analysis on the sensor.

4.3.1 EVALUATION OF TECHNIQUES

The two basic forms of radar sensors that lend themselves in a practical manner to fulfillment of LUCOM objectives are FM-CW and pulsed RF. The high altitude requirement of 80 nautical miles imposes relatively high output power requirements regardless of type of sensor.

4.3.1.1 FM-CW Type Radar

The FM-CW type operates by generating a continuous signal which is frequency modulated, and by comparing the modulation of the returning echo with the signal being transmitted. Since the modulation of the echo is the same as the modulation which was transmitted a known time before, the relative phase is indicative of the time and therefore the altitude. The pulse type operates by generating a short burst of RF energy and measuring the time of arrival of the echo pulse from the surface. Since an FM-CW system is continuously transmitting and receiving, there are two practical effects which limit the amount of transmitter leakage power which can be tolerated at the receiver. These are:

- (a) The maximum amount of power the input circuitry can withstand before it is physically damaged or its sensitivity reduced, and
- (b) The amount of transmitter noise due to hum, microphonics stray pickup, and instability which enters the receiver from the transmitter.

Although isolation between transmitter and receiver can be obtained with a single antenna by using a hybrid junction, circulator, or turnstile junction, greatest isolations require two antennas physically separated. For space-borne vehicles isolations of 50-70 db can be achieved in this manner. For the narrow beamwidths being considered, however, antenna weight

and volume make up the major portion of the sensor weight-volume. The requirement for two antennas is not practicable in consideration of the design goals for minimum weight and volume. Also, the FM-CW radars examined exhibited an altitude measurement error of 1 to 5 percent of the altitude. The most serious limitation of this type radar for mapping applications is the weighting inherently accorded the signal return from the periphery of the illuminated area, whereas the objective is to measure the delay time of the direct ray.

4.3.1.2 Pulse Type Radar

Since the pulse type only transmits for a short period of time and then receives for a short period of time, cyclically, its receiver can be isolated and protected from any damaging effects of the transmitted pulse by a transmit-receive (TR) switch, which blanks the receiver input during the transmission period. The decision circuitry can also be made inoperative except during the receive period; this technique provides isolation from noise. The pulse type exhibits no errors that are direct functions of altitude, and the signal processing technique is simple since it makes only a time measurement between the transmitted pulse and the leading edge of the reflected signal. The use of short receive time also increases return detection; this short time is analogous to reduction of receiver noise bandwidth. For these reasons, a pulsed-RF radar sensor was chosen for the LUCOM application. To summarize, the LUCOM sensor that was chosen to be evaluated was: a pulsed RF type with leading edge detection with a narrow range gate to track, utilizing a data processor for range memory, setting PRF, and accumulation of the altitude measurement in digital form.

4.3.2 SYSTEM DESIGN DISCUSSION

4.3.2.1 Components

The sensor system consists of an antenna, transmitter-receiver, and data processor. The antenna types examined for the LUCOM mission were the waveguide slot array and the parabolic reflector. The waveguide slot array was selected because of its smaller size and higher gain for a given beamwidth (a detailed comparison of the types are presented in Section 4.3.4.3). The transmitter consists of the RF power generating tube and its modulator. Power generators consist of two general classifications: self-excited power oscillators or power amplifiers driven by low-power oscillators. The

magnetron and the stablitron are self-excited oscillators. Example of radar power amplifiers are:

Klystron

Traveling-wave Tube

Amplitron

Grid-controlled Tubes

Magnetron oscillators provide the best trade-offs between peak power, size, weight, efficiency, and complexity. Since these parameters are prime considerations in the LUCOM mission, a magnetron oscillator and modulator transmitter was selected for the LUCOM sensor. Receivers commonly employed in radar applications include the superheterodyne, super-regenerative, crystal video and the tuned radio frequency types. The superheterodyne type receiver was chosen for the LUCOM analysis because of its sensitivity, high gain, selectivity, and reliability. The data processor controls the blanking of the receiver during transmission, signals the modulator to transmit, records transmission timing mark, controls open time of receiver for reception timing mark from threshold circuit when return is detected, and determines the altitude measurement digitally.

4.3.2.2 Functional Characteristics

Figure 4.3.2.2-1 reflects the sensor system block diagram established for analysis. The data processor sends a trigger to the modulator at the predetermined pulse repetition frequency (PRF). The modulator, in turn, enables and disables the magnetron to form the transmitted RF pulse. The outgoing energy is detected and a signal that the pulse has been transmitted is returned to the data processor. This method of creating a begin-of-range-measurement timing mark eliminates range measurement error due to variance in firing delay or transmitter jitter. The receiver front-end is opened to receive the return echo by a signal from the data processor. The point in time when the return echo is expected is referenced to the time of the previous echo. The front end is opened a fixed amount of time ahead of the expected return. This time is a function of maximum deviation in echo leading edge, relative change of altitude, and system jitter, all on a pulse-to-pulse basis. If C or X-band frequency is chosen, a low noise RF amplifier (probably a tunnel diode amplifier) will follow the switch in order to improve receiver noise figure. The RF frequency of the return signal is translated to an IF frequency by the

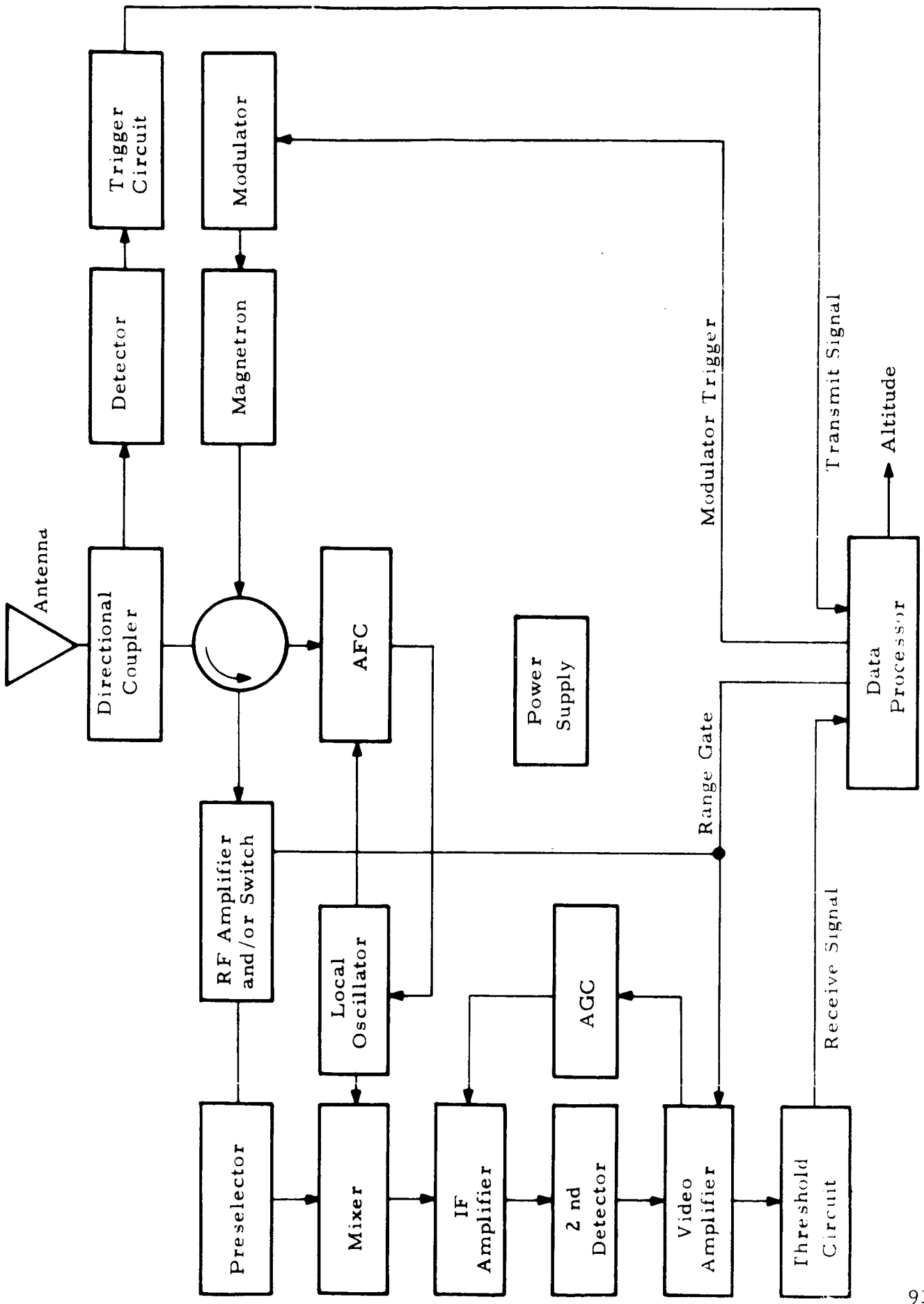


FIGURE 4.3.2.2-1. PRELIMINARY LUCOM RADAR SENSOR

mixer and amplified by the IF amplifier. The RF mixing frequency is provided by a local oscillator, whose frequency is forced to track the drift in the transmitted frequency by an AFC (automatic frequency control) loop. The video modulation is extracted from the carrier by the second detector and is amplified in the video amplifier to threshold striking levels. When an echo has been detected, a signal is sent to the data processor as an end-of-range-measurement timing mark. The time interval between transmission and reception of a pulse is measured digitally and the altitude measurement is transferred to the telemetry section. The receiver and transmitter are duplexed into a single antenna output connector by means of a conventional ferrite circulator. The preselector, operating in conjunction with the IF amplifier, limits the range of RF frequencies to which the LRS receiver will respond. This range is a small band of frequencies that is centered about the LRS transmitter frequency. The bandwidth requirement of the preselector is determined in part by requirements necessitated by the AFC lock-on range. Frequency variations that occur in the magnetron and local oscillator as a function of service, environment, and aging are considered in the selection of the AFC capture and lock-on range. The AFC is the constant difference type in which the receiver's local oscillator frequency and the receiver's signal frequency. This difference is the IF frequency. The automatic gain control (AGC) circuit receives output signals from the video amplifier, peak detects these pulses and furnishes the DC output signal for gain control.

4.3.3 TRADE-OFFS AND ERROR ANALYSIS

In the trade-off analysis general relations were derived for peak output power, weight, volume and sensor performance against the detection criterion (the detection criterion and general trade-offs are discussed in detail in Appendix 4.3). In this section resulting trade-off curves are discussed for the specific cases analyzed.

4.3.3.1 Trade-Off Analyses

The classic radar range equation can be expressed in the following form to indicate peak output power dependence on other system and mission requirements.

$$P = \frac{(4\pi)^3 K T B_n NF S/N h^4}{G^2 \lambda^2 \sigma_r A} \quad (4.3.3.1-1)$$

where

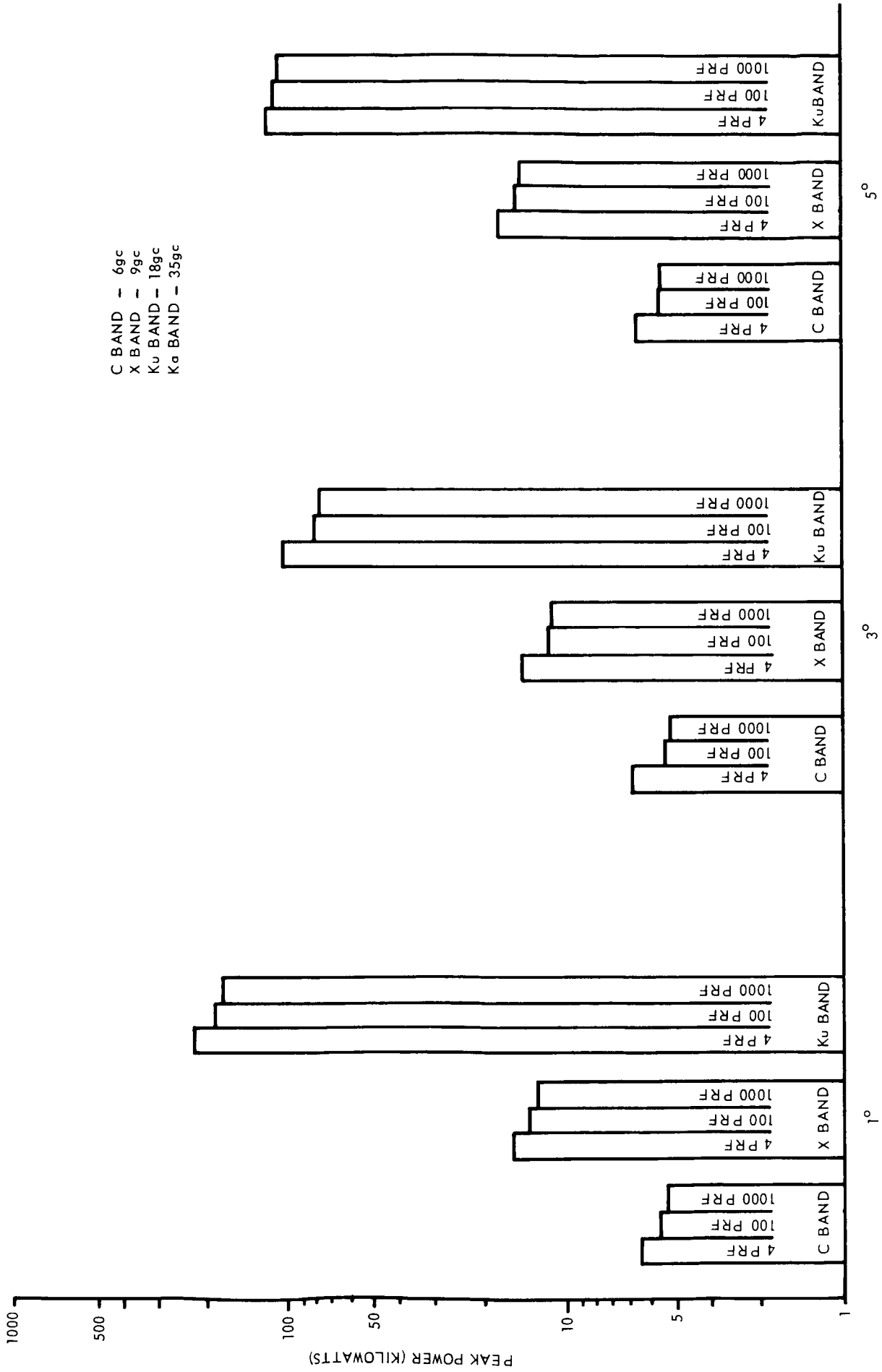
P_t	=	Peak transmitted power
G	=	Antenna Gain
λ	=	Wavelength
A	=	Surface illuminated area
σ_r	=	Lunar scattering-reflection coefficient
B_n	=	Receiver noise bandwidth
NF	=	Noise Factor
S/N	=	Signal-to-noise ratio
h	=	Altitude
K	=	Boltzman's constant
T	=	Noise temperature in ° Kelvin

All parameters are discussed in detail in Appendix C.

For the cases considered in the lunar model profile analysis for 5°, 3° and 1° beamwidths, Figure 4.3.3.1-1 illustrates in bar chart form the dependency of peak power on beamwidth, frequency, and the pulse repetition frequency (or PRF). As expected from the classic radar range equation, power requirements increase with frequency for a fixed beamwidth--due to the λ^2 term in the equation.

In the actual calculations, specific frequencies were considered. The frequencies evaluated were:

6 gc in C band	18 gc in Ku band
9 gc in X band	35 gc in Ka band



C BAND - 6gc
 X BAND - 9gc
 Ku BAND - 18gc
 Ka BAND - 35gc

FIGURE 4.3.3.1-1. PEAK OUTPUT POWER

BEAMWIDTH (DEGREES)

Ka band is not pictured on any of the figures in this section because the power requirement at those frequencies were in excess of 1 megawatt; transmitter power requirements of this magnitude are not compatible with present off-the-shelf space-borne equipment. The power requirements in the Ku band are 100-200 kilowatts. Presently, there is limited off-the-shelf capability at 100 KW at this frequency. For this reason, Ku band will be carried through the trade-offs but definite conclusions regarding this band will not be drawn.

This chart also shows the power dependency on pulse repetition frequency. Three distinct cases were considered--a PRF of 4 pulses per second represents approximately the grid interval simulated in the profile analysis (reference Section 4.2.4); a PRF of 1000 represents an absolute theoretical unambiguous maximum used in the analysis; and the PRF of 100 was analyzed as a projected nominal frequency. As can be observed, there is very little peak power reduction by increasing PRF from 100 to 1000 pulses per second. For the cases considered, the 3° beamwidth requires the least output peak power in general.

For these same cases, sensor plus antenna weights and volumes were determined (Figure 4.3.3.1-2). The results were derived from off-the-shelf equipment and standard circuitry, i.e., micro-circuitry was not included in the trade-offs. As noted earlier, the standard waveguide slot array antenna would be used for trade-off purposes. Since this type of antenna can be flush-mounted, some of its physical parameters can be absorbed by the vehicle structure. For the LUCOM mission, the proportion of the antenna weight and volume that could be so treated was not known; so the total weight-volume of the antenna was included for trade-off purposes.

Figure 4.3.3.1-2 reflects the reduction of physical requirements with increase in frequency and antenna beamwidth, where the dash line bars represent volume, and the solid line bars represent weight. No differences are indicated in the weights and volumes by a change in PRF (as was shown on the power chart--Figure 4.3.3.1-1). This again is caused by the great influence of the antenna on the sensor system's physical parameters.

As can be seen, the greatest incremental change in weight or volume is gained by going from the 1° beamwidth case to the 3° case:

For C band: Greater than a 400 pound reduction in weight
and 63,000 cubic inch reduction in volume.

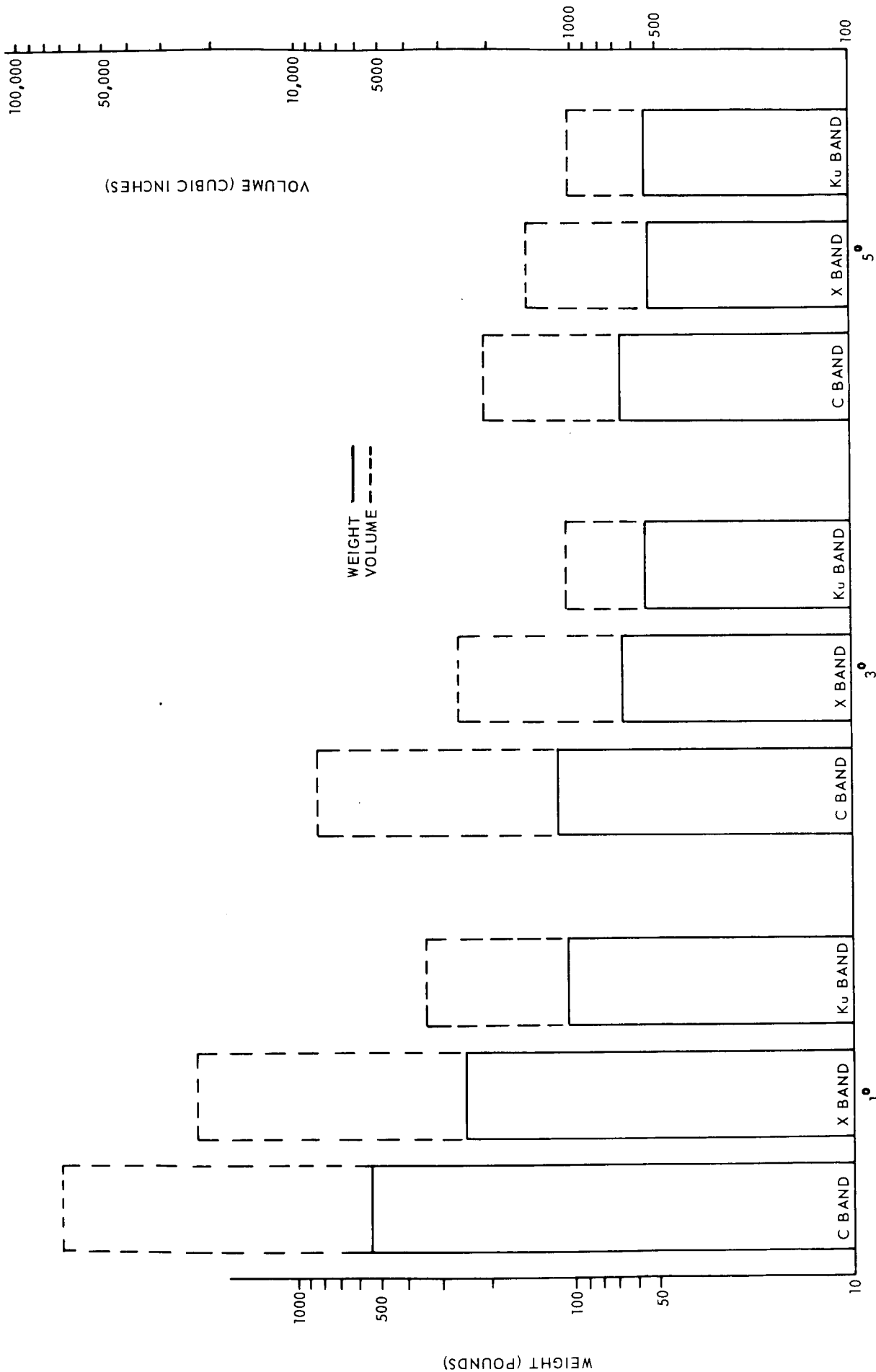


FIGURE 4.3.3.1-2. SENSOR & ANTENNA WEIGHT & VOLUME

For X band: Greater than a 170 pound and 21,000 cubic inch reduction.

For Ku band: Around a 50 pound and 2,300 cubic inch reduction.

This can be compared with the incremental changes in increasing beam-widths from 3° to 5° of

C band: Less than a 50 pound reduction in weight and 6,300 cubic inch reduction in volume.

X band: Less than a 15 pound and 1,200 cubic inch reduction.

For Ku band: Insignificant reduction in either parameter.

Since the type of prime power source was not known for the LUCOM mission, its weight-volume parameters were not included in the trade-offs. However, prime power requirements were included. Figure 4.3.3.1-3 shows the dependency of prime power on frequency and PRF. Prime power requirements increase with PRF because of the increase of the average output power. The increased requirement in peak power with increased frequency is again reflected in the prime power requirements. For low prime power consumption then, a low frequency and low PRF is indicated.

4.3.3.2 Error Analysis

An error analysis was performed on the LUCOM radar sensor and included as a trade-off input. The sources of error evaluated were:

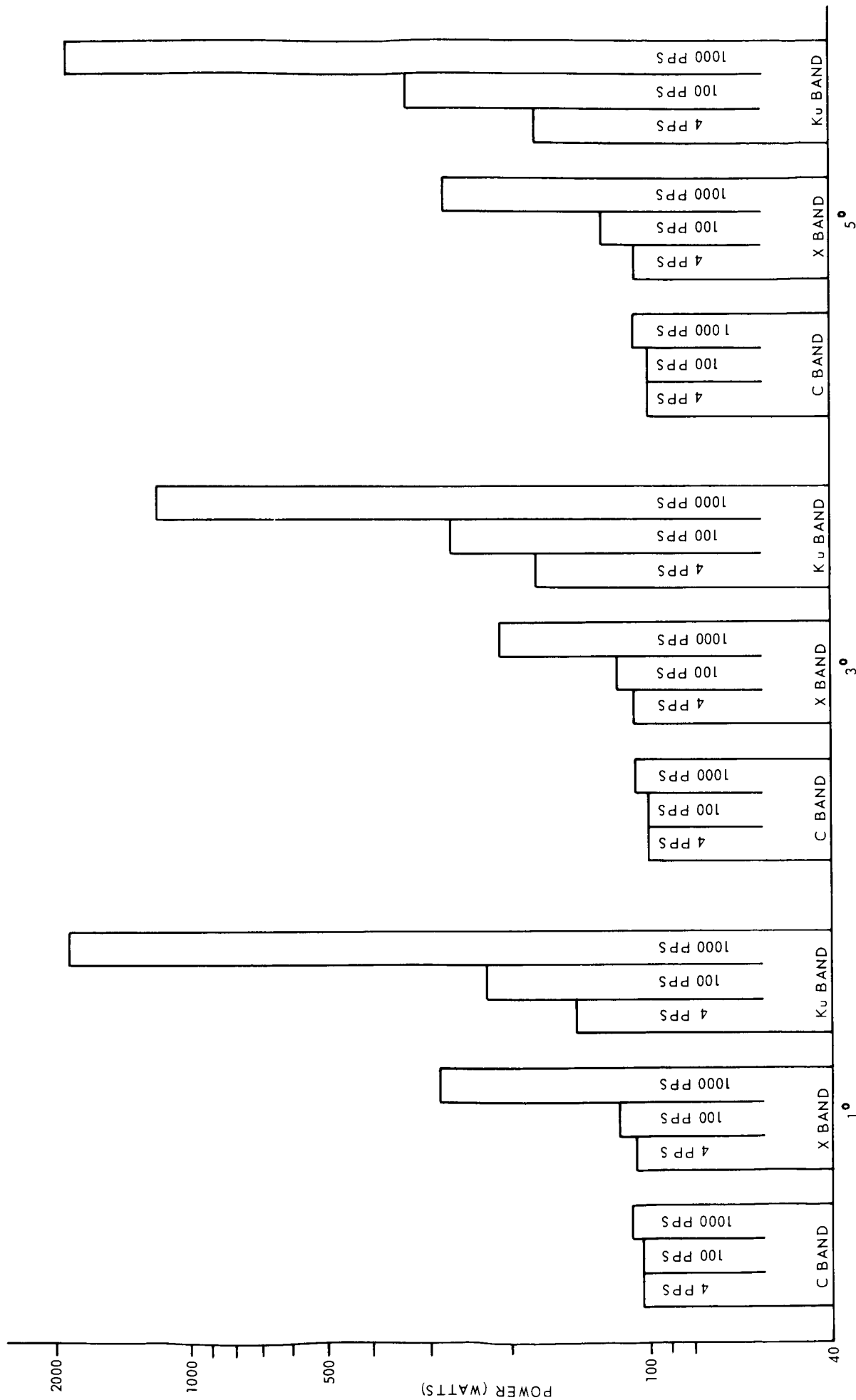
Return signal variation--which includes noise jitter and statistical variation of the reflected signal.

Verticality

AGC limitations

Threshold detector variation

Gate jitter



BEAMWIDTH (DEGREES)
FIGURE 4.3.3.1-3. PRIME POWER

Clock frequency stability

Quantization error

The analysis showed no significant dependence on frequency or PRF. A detailed discussion of the error sources and their evaluation are included in Appendix 4.3-H. Figure 4.3.3.2-1 reflects the results of an analysis on an X-band system at PRF = 100 pps for 5°, 3°, and 1°, beamwidths.

The uppermost points on the solid lines for the N=1 case represent the rms altitude error in feet for the cases presented in the previous charts at 5°, 3°, and 1° beamwidths. These points show a reduction in error with increasing weight and volume that accompanies a decreasing beamwidth. The lowermost points on the solid lines for the N=1 case represent a lower error for a peak power increase causing a 10% increase in weight, for the 5° and 3° cases; for the 1° case the increase in peak power to reduce error was limited by the maximum considered in the trade-offs (in the neighborhood of 200 kw). These N=1 curves show considerable reduction in error as the beamwidth is decreased from 5° to 3° and the corresponding increase in weight and volume. A somewhat smaller reduction in error by decreasing the beamwidth even further to 1° is accompanied by quite a substantial increase in weight and volume.

Another approach taken in reducing the rms error in a mapping sensor of this type is to average a number of measurements for the altitude reading given to the telemetry section. This technique reduces the mean square of pulse-to-pulse errors that are independent by a factor equal to the number of return measurements averaged. Specifically, the pulse-to-pulse errors in this analysis that demonstrate pulse-to-pulse independence are the variations in the return signal and the quantization error. Using this method, the remaining lines on Figure 4.3.3.2-1 reflect the error reduction by averaging, where N is the number of measurements averaged. The N=1 case then, is the individual pulse measurement case. Substantial reduction in the error can be observed. Again, the 3° case offers the greatest reduction for the smallest increase in weight and volume.

By averaging only 2 returns in the 5° case, the lower error approaches that gained by increase in weight and volume for the single pulse case. For the 3° case, averaging of 4 returns results in a lower error than that achieved by increasing weight and volume.

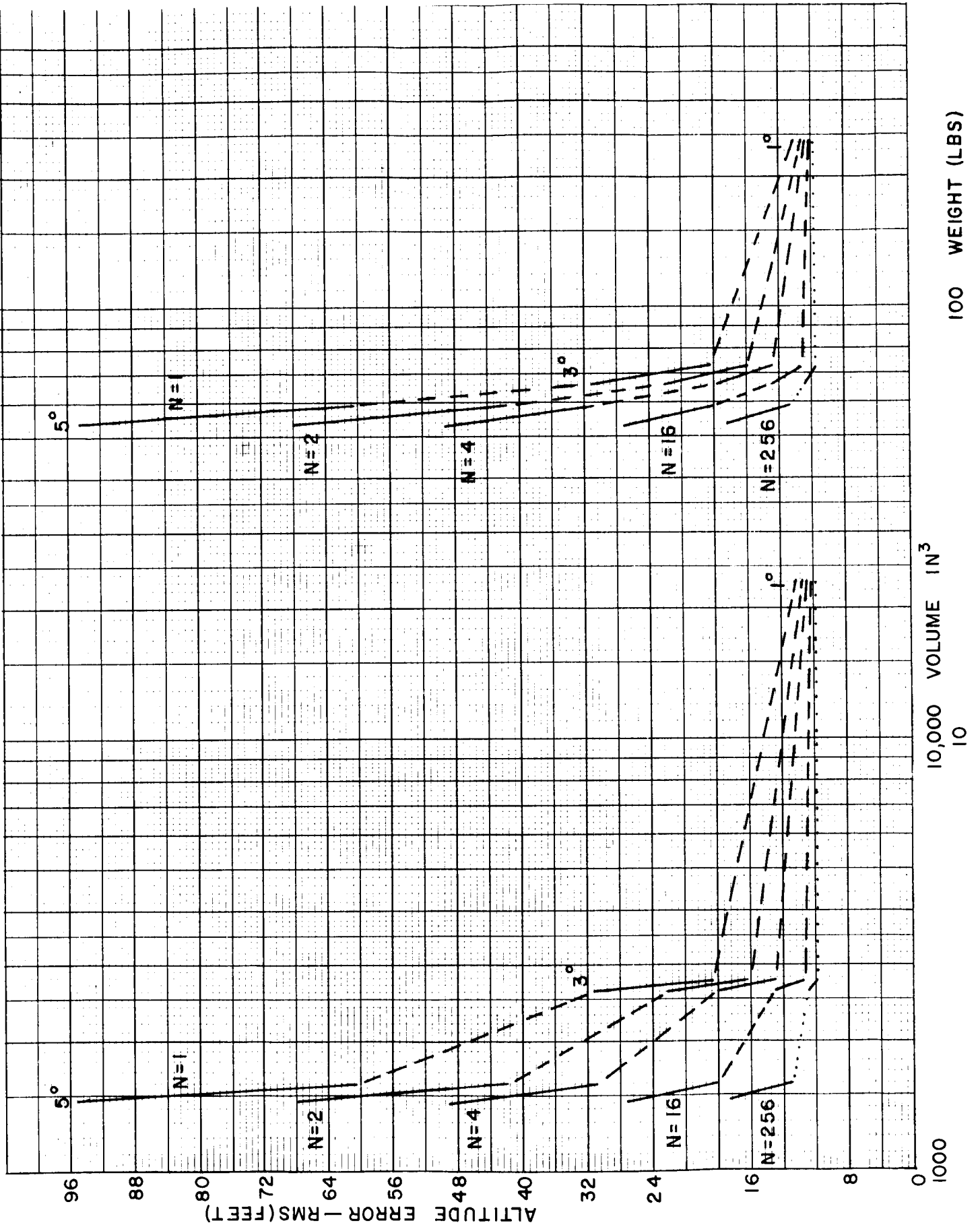


FIGURE 4.3.3.2-1 RMS ERROR

4.3.3.3 Analyses Summary

To summarize, the LUCOM Radar Sensor trade-offs indicate for the cases considered:

A low frequency, high PRF, and a 3° beamwidth for minimum peak power.

A high frequency and wide beamwidth for minimum weight and volume.

A low frequency and low PRF for minimum prime power consumption.

A narrow beamwidth and return averaging for minimum altitude error.

These results although not conclusive, point to a radar sensor with the following parameters:

Frequency	X to Ku band
PRF	Approximately 100 pps
Beamwidth	3° or less
Pulsewidth	Approximately 1.5 us

4.3.4 SELECTION OF COMPONENTS

Based on the results drawn from the total analysis described in previous sections, and requiring a single set of characteristics for subsequent sensor design, the following parameters were selected as optimum for LUCOM:

Frequency	X band
PRF	100 pps
Antenna beamwidth	3°
Transmitted pulsewidth	1.5 us
Peak output power	11.5 kw

Prime power	117 watts
Sensor weight and volume	42 lbs. 577 in. ³
Antenna weight and volume	24.5 lbs. 2000 in. ³
Antenna aperture	2.6 ft.

The following sections show the incremental breakdown of the sensor's physical parameters, as well as a more complete discussion of the data processor and the antenna.

4.3.4.1 Transmitter-Receiver

A breakdown of components in the transmitter and receiver are listed below:

	<u>Weight (lbs.)</u>	<u>Volume (in.³)</u>
Magnetron	2.36	45.6
Modulator	2.92	40.5
Circulator	.56	28.8
Tunnel Diode Amplifier & Switch	2.07	40.0
Preselector	.50	2.0
Mixer	.25	5.9
Local Oscillator	1.28	34.9
Receiver Group	3.50	72.5
Data Processor	7.50	183.0
Power Supply	8.00	124.0
Case	13.00	-0-
TOTALS	41.94	577.2 = 0.3 ft ³

The volume values here and in the trade-offs were component values only; increase in volume due to packaging was not included. A sensor similar to this has been developed by LTV Military Electronics Division; its total packaged volume is about 0.7 ft³.

4.3.4.2 Data Processor

The three major functions of the data processor are:

- (a) To derive timing pulses to be used to trigger the sensor modulator.
- (b) To derive a control signal to be used for opening and closing the receiver RF switch.
- (c) To measure the time interval between the transmit pulse and its received return and provide range measurement output to the telemetry section.

The data processor can thus be divided into three sections, each section fulfilling the function of one of the objectives. Figure 4.3.4.2-1 is a functional block diagram of the data processor showing signal flow.

The predetermined pulse repetition frequency information is programmed into the PRF section to set the time between triggers to the modulator. This section also provides a back-up feature that causes a wider than normal front end open time in the case when no return is received after a specific number of consecutive attempts. The PRF also provides a subsystem sync to both the range and accumulator sections. The range section determines when the receiver front end should be opened to receive a return echo based on the time between transmission and reception of the previous pulse, i. e., the range gate tracks the return (range gate action is discussed in Appendix 4.3-C). When the return is detected, the range section signals for the closing of the front end. The time interval between transmission and reception of a pulse is measured in the accumulator section. Any time averaging performed to acquire a range measurement is performed in this section. The accumulator section provides a binary output of the range measurement to the telemetry section. The clock is the incrementing mechanism for the data processor and its speed sets the minimum readout resolution of the range. Present state-of-the-art clocks and counting circuitry allow altitude measurement increments as low as 10 feet.

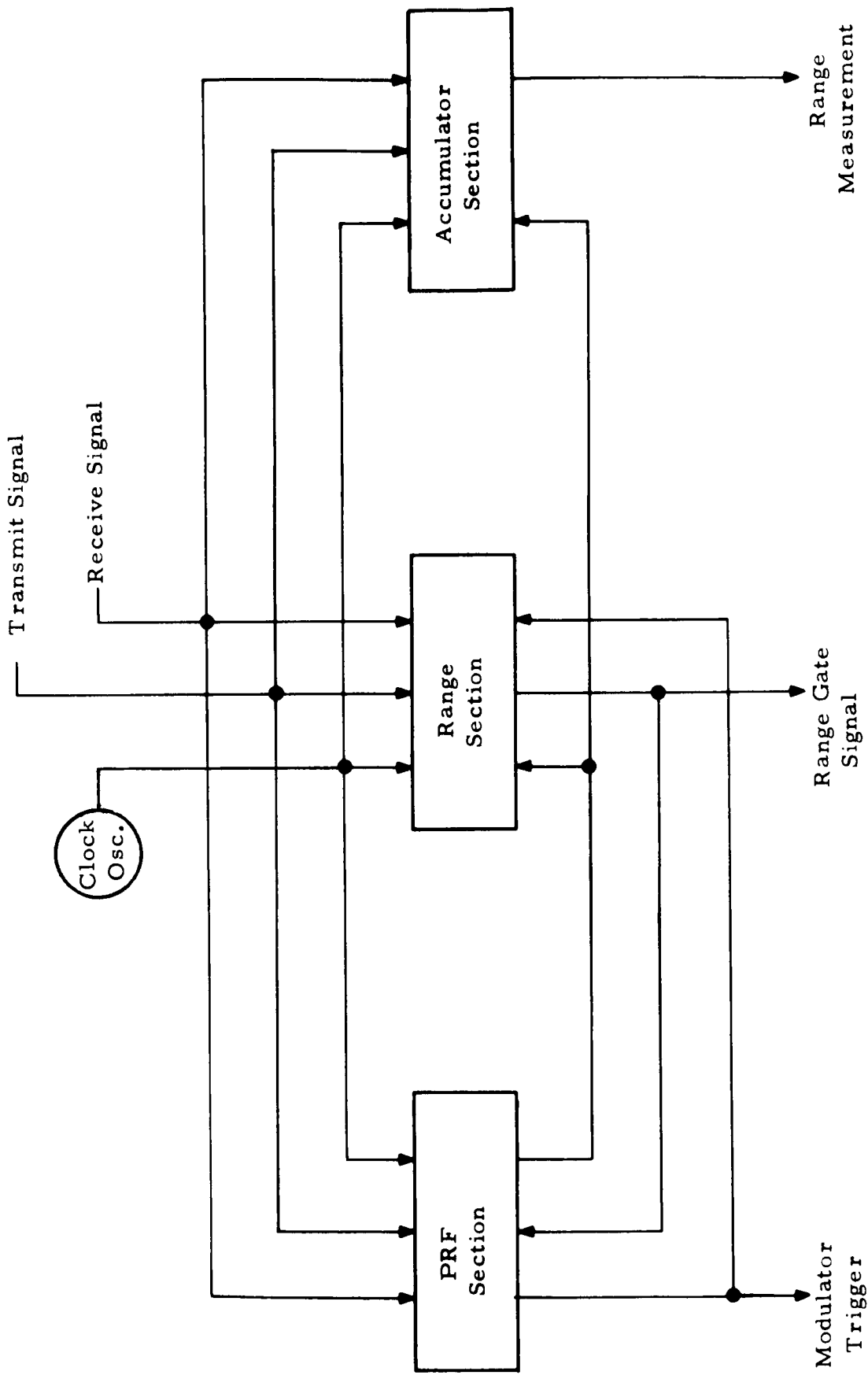


FIGURE 4.3.4.2-1. PRELIMINARY LUCOM DATA PROCESSOR

As indicated in section 4.3.3.1 standard circuits were being considered in the trade-offs. LTV Military Electronics Division has developed an applicable microelectronic data processor (Figure 4.3.4.2-2) with a 2.5 cubic inch volume.

4.3.4.3 Antenna

To provide a basis for a system trade-off study for the LUCOM program, antenna parameters for various beamwidths and frequencies for two antenna types have been considered. Those parameters important to the overall system trade-off study are size, weight and gain. The specific 3 db beamwidth range of interest was 1° to 5° and frequencies from 6 Gc to 35 Gc. The parameters that are essentially fixed are as follows:

Narrow Frequency Band

Power Handling Requirements

Linear Polarization

Single Beam-Transmit and Receive

The two general types of antennas that are considered for this application are:

Waveguide slot array

Parabolic reflector

The slot array has the advantage of being more readily adaptable to flush mounting in streamlined shapes; additionally, the radiation pattern can be altered considerably by changing the distribution on the aperture. The parabolic reflector is the simpler to construct but the aperture illumination is somewhat fixed. In general, for the same beamwidth, the parabola will have to have a larger aperture since the illumination cannot be uniform without large spillover. The parabola, with the tapered illumination, has lower side lobe levels than the slot array with uniform illumination. All these considerations are taken into account when choosing an antenna.

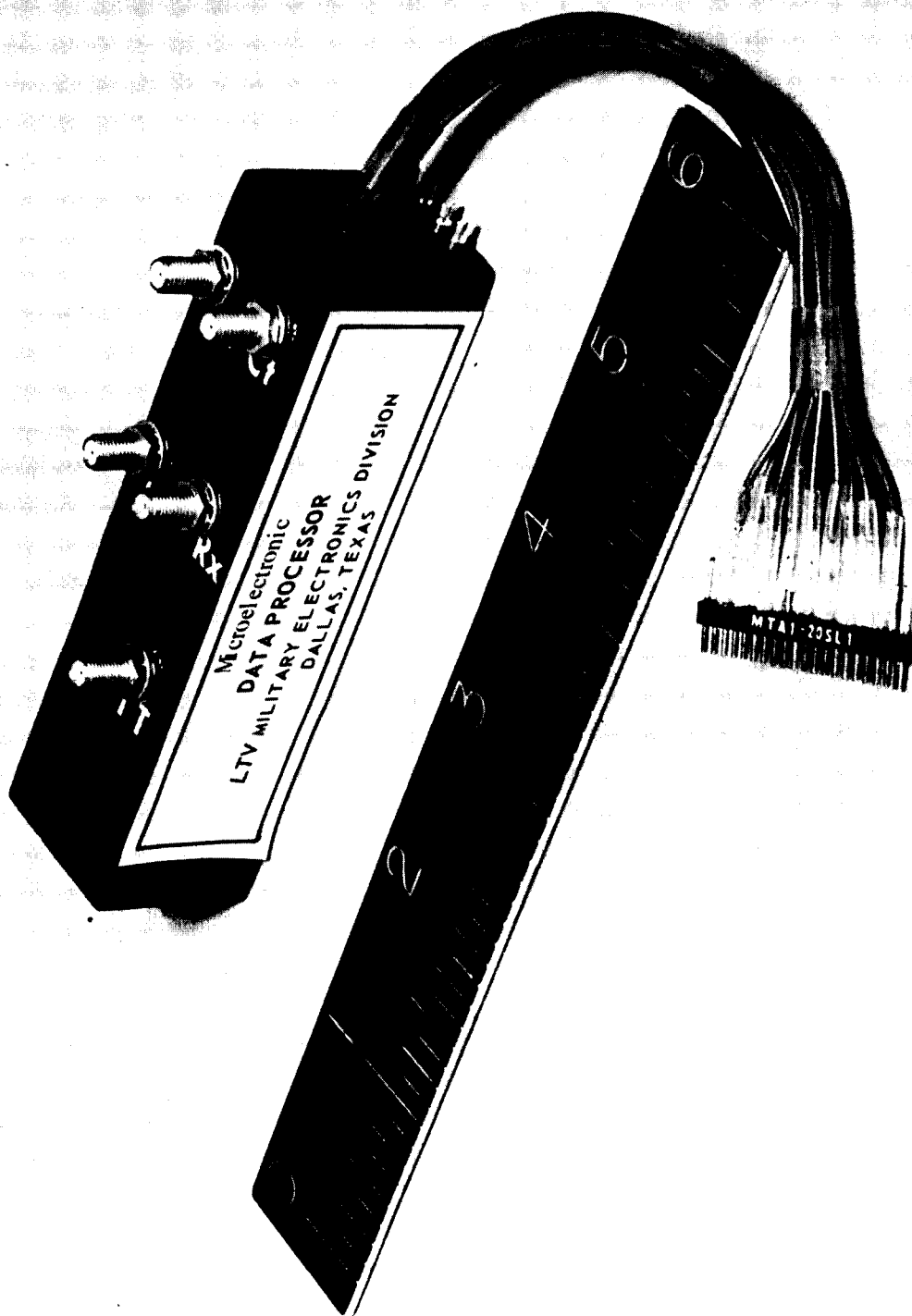


FIGURE 4.3.4.2-2 MICROELECTRONIC DATA PROCESSOR

To determine the aperture size required for the slot array, Silver's derivation was used, i. e., the number of elements in a linear array of isotropic elements spaced $\lambda/2$ is related to the half-power beamwidth by:

$$n = \frac{101.8^\circ}{\theta} \quad (4.3.4.3-1)$$

where: θ = half power beamwidth in degrees

n = number of elements

For an antenna with equal E & H beamwidths, an array of n by n elements would be required.

If the elements of the array are not isotropic but have some directivity then the total array beamwidth is not given by:

$$1/\theta_T^2 = 1/\theta_A^2 + 1/\theta_E^2$$

where: θ_A is the half-power beamwidth of the array with isotropic elements.

θ_E is the half-power beamwidth of the elements.

It can be seen that if $\theta_E > 10 \theta_A$ then:

$$1/\theta_T^2 \approx 1/\theta_A^2$$

or: $\theta_T = \theta_A$

Since the range of interest for θ_T is 1° to 5° and θ_E would be in the range of 90° (a dipole pattern), the approximation of $\theta_T = \theta_A$ is valid.

The size of the array would then be:

$$D = n \lambda/2$$

or $D = 50.9 \lambda/2$

using equation 4.3.4.3-1.

This equation is plotted in Figure 4.3.4.3-1.

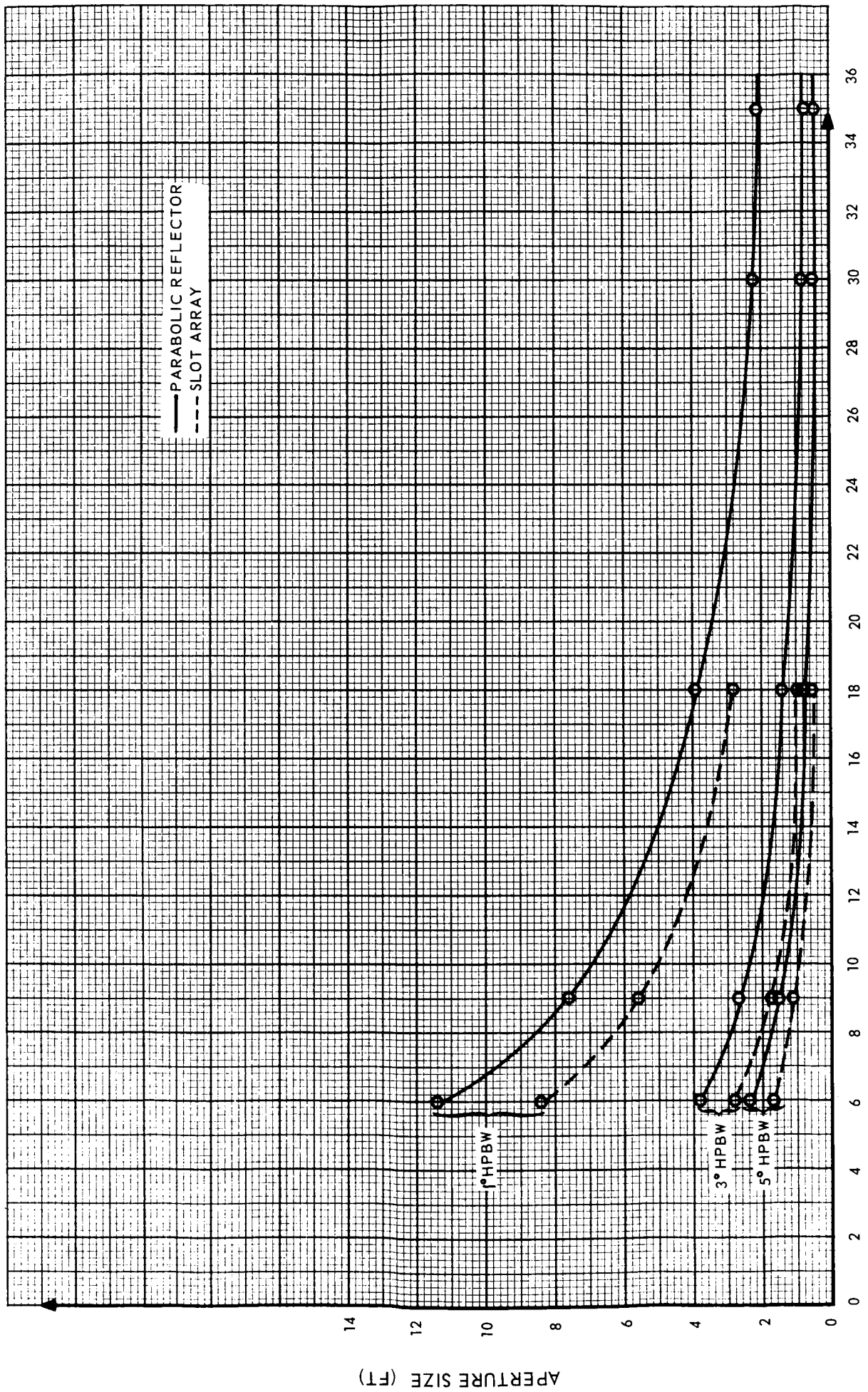


FIGURE 4.3.4.3-1. APERTURE SIZE VS. FREQUENCY

FREQUENCY (GC)

APERTURE SIZE (FT)

— PARABOLIC REFLECTOR
 - - - SLOT ARRAY

1° HPBW

3° HPBW

5° HPBW

To determine the aperture size of the parabola, Silver's derivation which relates half-power beamwidth to diameter can be used again. This relationship depends upon the shape of the aperture distribution. The distribution used is usually of the form $(1-r^2)$ which gives:

$$\theta = 72.6 \lambda / D$$

where: θ = half-power beamwidth in degrees

λ = wavelength

D = diameter of parabola

This equation is also plotted in Figure 4.3.4.3-1.

The previous statements have been directed towards aperture size. The depth of each antenna can be determined as follows. The depth of the slot array, including the corporate feed structure is about 3.5 times the wide dimension of the waveguide used. The depth of the parabola is just slightly more than its focal length, or 1.2 times the focal length can be used as its depth. Since focal length divided by the diameter will be about 0.3 db the depth is then 0.36 times the diameter. These depths for the four frequencies of major interest are shown below. Note that the slot array depth is not a function of the half-power beamwidth while the parabola is:

		Parabola		
		1°	3°	5°
6 GC	0.44	4.15	1.37	.83
9 Gc	0.29	2.74	.90	.54
18 Gc	0.15	1.37	.45	.27
35 Gc	-0-	.74	.24	.15

TABLE 4.3.4.3-1
Antenna Depth (Feet)

The gain of antenna is related to the beamwidth by the general equation:

$$G = E \frac{41253}{\theta_E \theta_H}$$

where: θ_E = half-power beamwidth (E plane)

θ_H = half-power beamwidth (H plane)

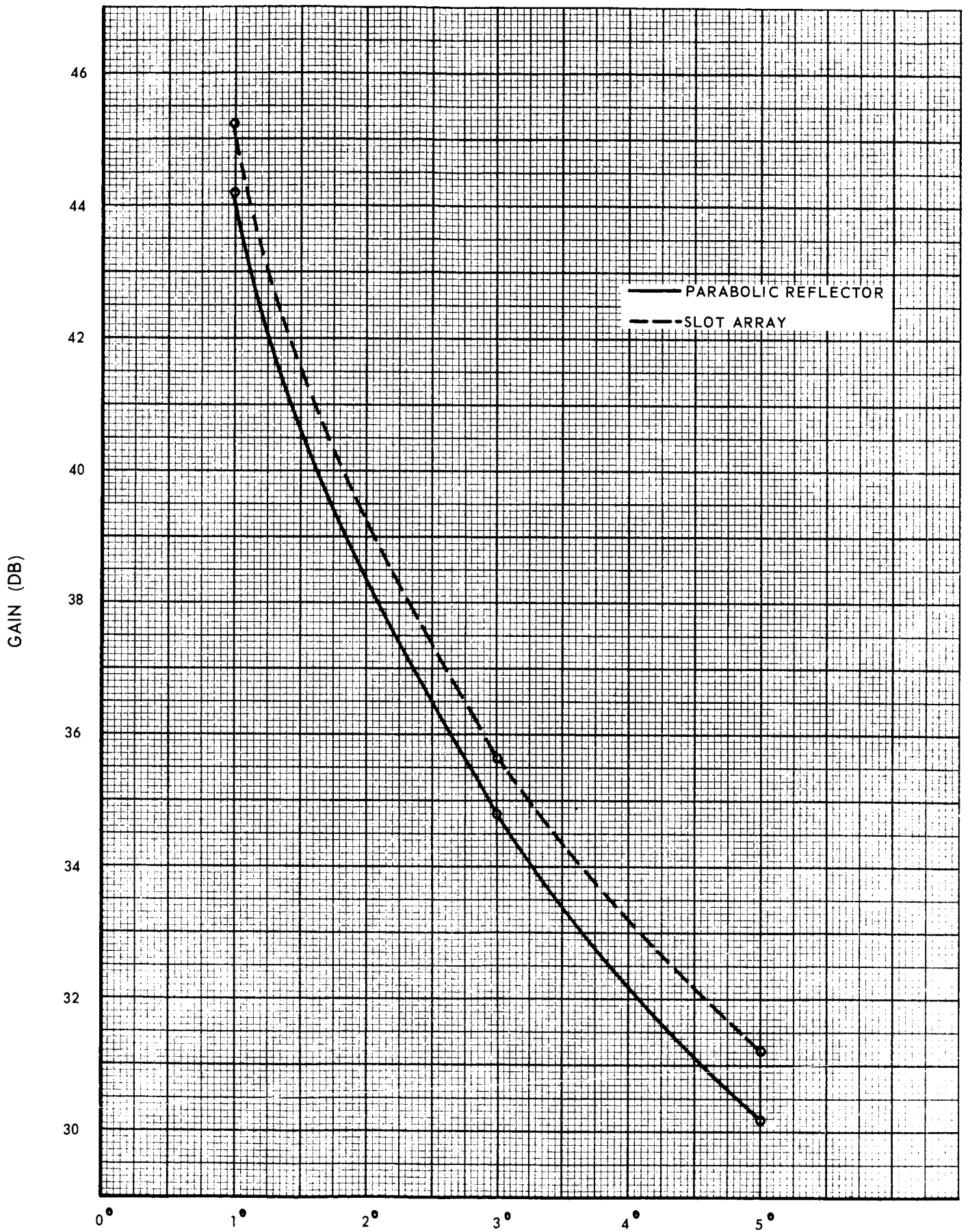
E = efficiency factor

G = power ratio

The efficiency factor, E, depends on the type of antenna, the losses in the antenna structure, the main beam shape and the side lobe structure. For an antenna with no internal losses all the energy radiated in a beam of constant amplitude of size θ_E by θ_H , E is 1.0 as shown by Kraus. From previous experience it has been found that waveguide slot arrays with uniform illumination and fabricated from aluminum waveguide have an E of approximately 0.80. For a parabolic antenna an E value of 0.55 is normally used. This includes the effects of spillover, blockage, edge taper and feed losses. Figure 4.3.4.3-2 is a plot of the gains using the above information.

Since weight as well as size is an important factor, the weight of the antenna needs to be considered. From previous experience, it has been found that the weight of a waveguide slot array is approximately twice the weight of the waveguide alone. That is, the weight of the structure to hold the waveguide together is about the same as the weight of a waveguide. For the parabolic antenna a survey was made of published data by various manufacturers. This data shows that for at least up to 12 ft. diameter the weights are approximately the same as a 0.10 thick aluminum disk of the diameter of the parabola. These weight values are plotted in Figure 4.3.4.3-3.

Since this application requires the antenna to transmit power, it is natural to consider the power handling limitations. However, upon examination of the causes of breakdown, it is found that the presence of air is the problem. Breakdown is caused by an unbalance of ionization vs. recombination of the gas molecules, as discussed by Gildden and Gould. In a perfect vacuum breakdown need not be considered and for all practical purposes this is the situation in the 80 nautical mile orbit around the moon. No pressure figures are available for this orbit, but using the figures available for 500,000 feet above the earth, the power handling capability of standard waveguide is about 2.5 megawatt peak at 6 Gc and 9.0 megawatt peak at 35 Gc. For pressures less than those found at about 100,000 ft. above the earth, the power handling capability varies inversely with the pressure. Since the



3db BEAMWIDTH
 FIGURE 4.3.4.3-2. ANTENNA GAINS

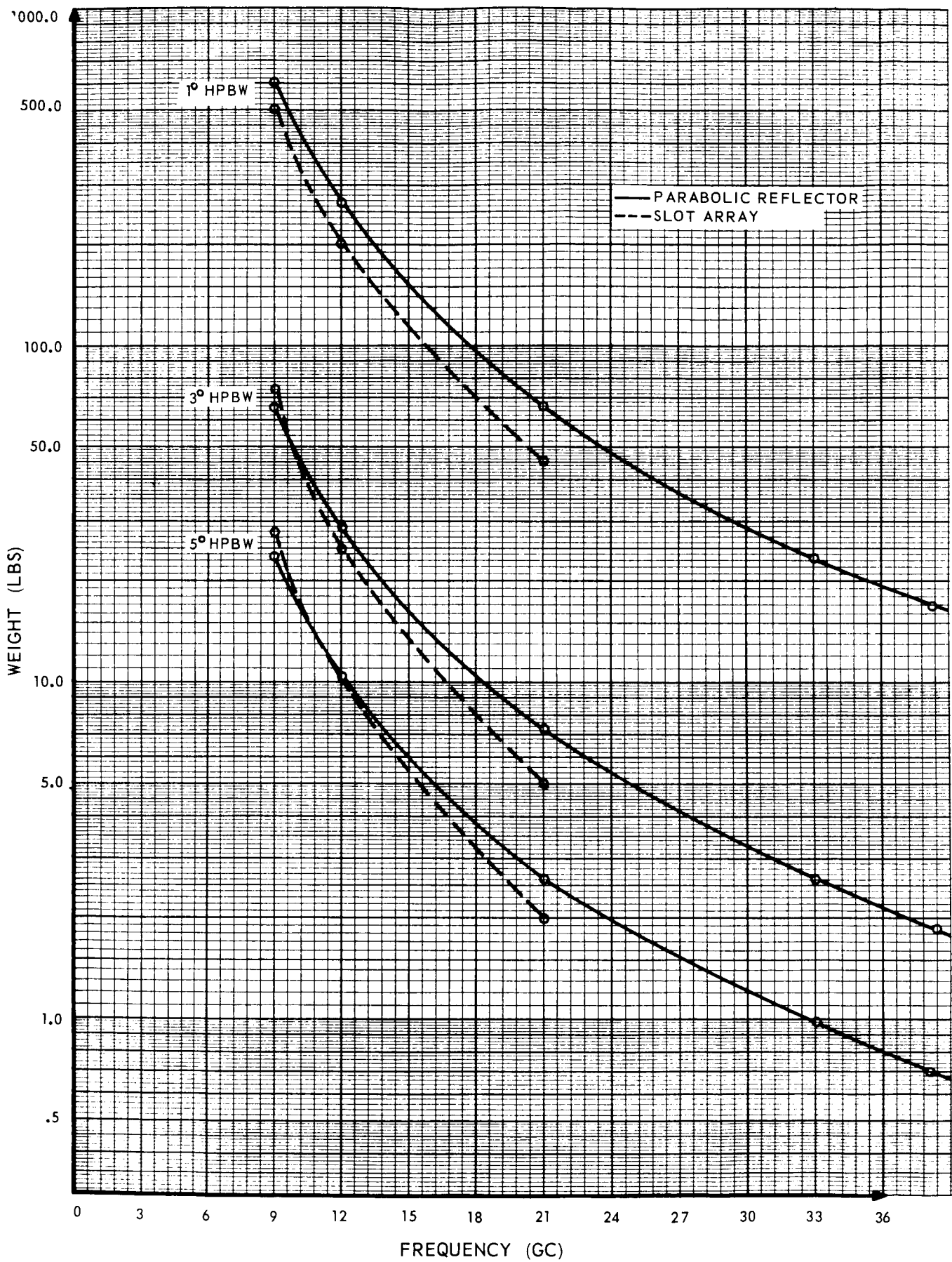


FIGURE 4.3.4.3-3. ANTENNA WEIGHTS

pressure near the moon will be less than that near the earth, the peak power related above are lower limits on the maximum power handling capabilities of standard waveguide. Since standard waveguide is the building block of the slot array, these figures apply for the total array. For the parabolic antenna, the most vulnerable spot is the waveguide to the feed, so again the above figures apply for the total antenna.

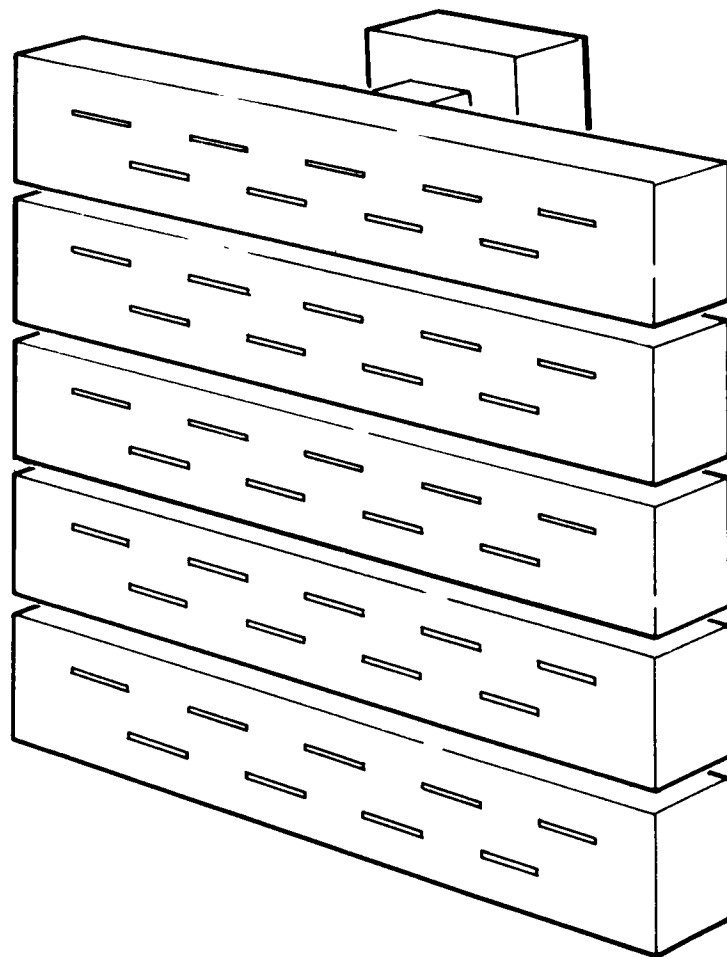
To provide linear polarization, the parabola is fed with a linearly polarization. The polarization requirement is met then by both antennas equally well.

No specific side lobe requirements exist from an overall system viewpoint. However, the parabola and the uniformly illuminated slot array have considerably different side lobe structure. The parabola will have about 20 db sidelobes while for the array they will be only about 13 db down. This is to be expected just by examining the aperture distribution on each antenna. Since the parabola must have a tapered distribution, it must have a larger diameter to give the desired beamwidth, but at the same time, the side lobes are made smaller by the process. To obtain the smallest aperture for a given beamwidth, a uniform illumination is used (the slot array), but the overall performance suffers if low side lobes are required.

If the 13 db side lobes are not detrimental to system performance, then the slot array is preferable because of its smaller size and higher gain. It will be noted that no real difference exists between the two antennas when considering weight. Although Figure 4.3.4.3-3 shows the slot array to be lighter than the parabola it must be remembered that these numbers are based on a particular design and an average. Once a detail design is selected these weights could change considerably.

It will be noted in Figures 4.3.3.4-1 and -3 that data for the slot array are not included for frequencies above 18 Gc. This is somewhat an arbitrary point above which it is not considered practical to fabricate a slot array. It is considered necessary to keep the slot width less than $\lambda / 20$ for proper electrical performance. At 18 Gc this is 0.033 inches and is considered the minimum for accurate fabrication.

The antenna trade-off curves show that for the cases considered the waveguide slot array is the most applicable standard design antenna for frequencies 18 Gc and less and that the parabolic reflector antenna should be considered for frequencies in excess of 18 Gc. Figure 4.3.4.3-4 pictures a standard slot array antenna.



5.0 DATA HANDLING

5.1 TELEMETRY STUDY

The data link study was performed to determine a method for accomplishing the following objectives:

1. Gather the altitude data that is acquired by the LUCOM altitude sensor.
2. Monitor the performance of the LUCOM altitude sensor.
3. Provide time correlation between the LUCOM altitude data and tracking data as well as any other data required to determine the position of the vehicle.
4. Provide data storage.
5. Transmit the data to earth receiving stations.

5.1.1 CONSTRAINTS

Several constraints are placed upon the data link by the LUCOM system. The characteristics of the mission, the lunar orbit and the altitude sensor accuracy play a significant part in determining the data link concept. The constraints were defined in the study where possible, but in some cases, assumptions were made in the absence of definitive information.

The constraints imposed by the mission characteristics are that data is continuously acquired throughout the 48-hour mission, the transmission path from the lunar orbit to the earth is 215,000 nautical miles, and the possibility that a Lunar Surveying Module or other excursion vehicle might gather data and transmit to the Command Service Module for relay to the earth. Maximum separation of these two vehicles is assumed to be 100 nautical miles.

The constraints imposed by the lunar orbital characteristics are that line-of-sight conditions between the vehicle and earth exist a maximum of one-half the time, and the orbital period is 6900 seconds for a circular 80 nautical mile orbit. Since continuous transmission to the earth is not possible, the storage of data when no transmission can occur must be accommodated. It should be noted that additional data storage is required when previously stored data is being transmitted, in order to assure continuous data acquisition. This infers the need for two independent data storage devices.

The third group of constraints is imposed upon the data link by the altitude sensor accuracy requirements. It is important that the data link should not significantly degrade the altitude data from the sensor. Thus, the resolution of the sensor coupled with the maximum altitude, the sensor accuracy, and the rate of change of altitude data constrain the performance requirements of the data link. Timing and time correlation accuracy play an important part in determining the correct position of the vehicle at the instant an altitude measurement is taken. A timing error of 1 millisecond represents an error in orbital position of approximately 5.5 feet.

5.1.2 DATA STORAGE

A survey was made of magnetic tape recorder state-of-the-art capabilities to determine the quantity of data that can be stored in one missile-borne recorder. A tape recorder is under development for Gemini Program that will pack 2730 bits per inch, and will record 4 hours of data at 1-7/8 inches per second, for a total data storage of 73.71 million bits. The LUCOM system requires two tape recorders operating in alternate sequences in order to transmit continuously acquired data with no dropouts during rewind and playback functions. It is desirable that each recorder store data for a minimum of one CSM orbit (6900 seconds). A tape recorder similar to the Gemini recorder with a bit packing density of 2730 bits per inch will store 2 hours (7200 seconds) of data at a tape speed of 3-3/4 inches per second. The storage capacity of 73.71×10^6 bits represents a maximum bit rate of 10,240 bits per second for 7200 seconds and will be compatible with LUCOM requirements.

5.1.3 VEHICLE DATA LINK

A pulse code modulation (PCM) technique was chosen for the LUCOM telemetry. PCM telemetry offers several advantages over other telemetry methods:

1. The primary altitude data from the sensor is in digital form. Therefore, no conversion errors are introduced by the PCM.
2. Signal to noise performance is good.
3. Time correlation is easily accomplished.
4. Ground data processing stations are available which convert the PCM format to computer format for automatic data processing.

Two data link block diagram models were developed. Model Number 1 provides a telemetry link between an altitude sensor located within the LSM or other excursion vehicle and the CSM, which stores the data until it can relay to earth based ground stations. Model Number 2 provides storage and transmission to the earth of data that is acquired by an altitude sensor located within the CSM. Since the data link configuration is dictated by the data rate and the quantity of data to be stored when line-of-sight conditions do not exist between transmitting and receiving stations, several assumptions have to be made. These assumptions are:

1. The number of altitude measurements will not exceed 1000 per second.
2. The minimum altitude increment represented by the least significant bit will be 3 meters for an 80-mile orbit or 6 meters for an orbit not to exceed 160 miles maximum altitude.
3. The LSM or other excursion vehicle is in continuous line-of-sight with the CSM.

In addition to the above assumptions, two assumptions were made which determine the LUCOM interface with the vehicle:

1. The telemetry antennas are a necessary part of the vehicle telemetry and are available for multiplexing with the LUCOM telemetry. Therefore, the LUCOM data link does not include telemetry antennas.

2. Command functions to initiate the tape recorder sequences are performed by an astronaut, or automatically by the vehicle guidance or command network.

5.1.3.1 Design Concept - Model Number 1

The data link design concept is based upon the assumptions listed previously. Figure 5.1.3.1-1 is a preliminary data link block diagram with the radar sensor located in the LSM or other excursion module. Since continuous line-of-sight between LSM and CSM have been assumed, no data storage is required in the LSM. The digital altitude from the radar sensor as well as analog and bi-level housekeeping signals are conditioned as required for compatibility with the multiplexer-encoder. The multiplexer-encoder time division multiplexes 11 high-level analog inputs and 72 bi-level inputs. These signals are encoded into 8-bit binary words which are combined with an internally generated frame synchronization code. The resulting serial binary wavetrain is converted to a split-phase PCM code form and pre-modulation filtered prior to being fed to the telemetry transmitter. A VHF telemetry link is utilized for data handling from the LSM to the CSM. This is compatible with existing Apollo techniques for communication between the CSM and a lunar excursion module. The telemetry clock and time code generator are used to establish running time increments from some arbitrary starting point (time t_0). This t_0 should be made to represent either the time when the radar sensor begins to gather data or some fixed correlation point with Apollo or earth reference time. The telemetry clock is shown in the block diagram as a LUCOM module. However, further study may indicate the desirability of eliminating the LUCOM telemetry clock and interfacing with the LSM clock or time reference in order to simplify time correlation with LSM photography and guidance.

The VHF receiver and the electronics necessary to store and subsequently transmit the LUCOM data to earth are located in the CSM. Referring again to Figure 5.1.3.1-1, the VHF antenna and multi-coupler are assumed to be in existence in the CSM and available for LUCOM use. The VHF receiver output supplies the video PCM signal to a bit synchronizer and data regenerator. This unit obtains synchronization with the incoming PCM wavetrain, generates a bit rate clocking signal, and regenerates a noise-free PCM wavetrain at the same bit rate that is suitable for tape recording. Although the

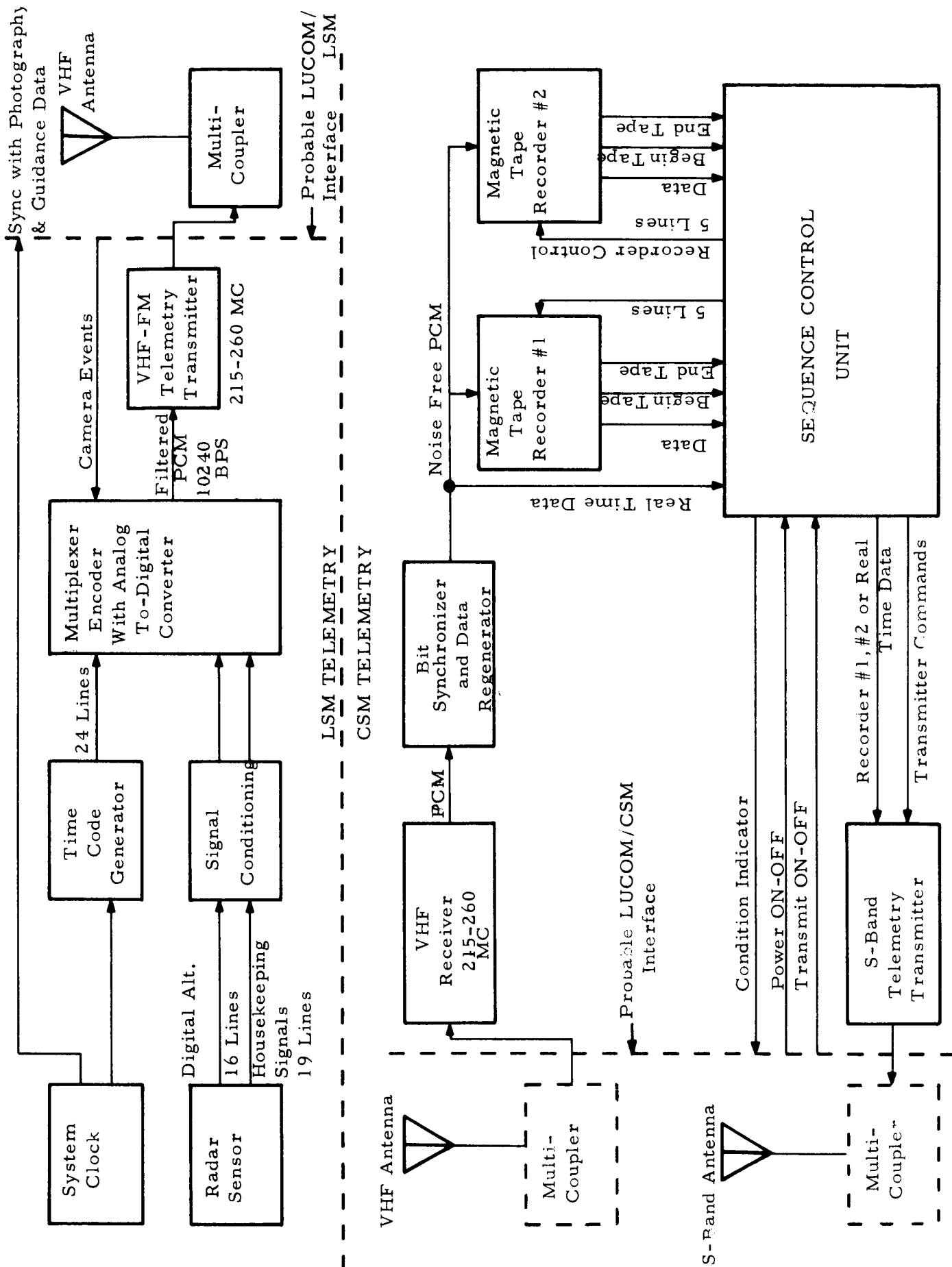


FIGURE 5.1.3.1-1. DATA LINK BLOCK DIAGRAM MODEL NO. 1

PCM code forms have not been studied to determine the optimum code forms for VHF transmission and magnetic tape recording, it is presently assumed the two codes will be identical. If not, a code form converter can be included within the bit synchronizer and data regenerator. The magnetic tape recorders alternately record, playback, and erase upon command from the sequence control unit. Accelerated rewind and playback speeds of 30 inches per second will allow 2 hours of data to be rewound in 15 minutes and played back in 15 minutes. Real time data is transmitted through the S-band telemetry link during recorder rewind functions to allow some redundancy as well as time correlation between LUCOM data and earth range time. If the Deep Space Information Facility (DSIF) has the capability of handling reversed PCM data, the recorders can play back during the rewind cycles. This eliminates 30 minutes of full power recorder operation per orbit and simplifies the Sequence Control Unit switching functions.

5.1.3.2 Design Concept - Model Number 2

Figure 5.1.3.2-1 is a data link block diagram in which the altitude sensor is located within the CSM. The data link is simplified from Figure 5.1.3.1-1 in that the VHF link and the bit synchronizer and data regenerator are eliminated. The multiplexer-encoder connects directly into the tape recorders and sequence control unit.

5.1.3.3 Component Description

The LUCOM data link is composed of the functional blocks as shown in Figure 5.1.3.1-1. The blocks are the signal conditioning, multiplexer-encoder which includes the clock and time code generator, the VHF telemetry transmitter, VHF receiver, bit synchronizer and data regenerator, tape recorders, sequence control unit and S-band telemetry transmitter. The tape recorders have been discussed previously.

5.1.3.3.1 Signal Conditioner

The signal conditioner accepts data from the altitude sensor and conditions it to a level that can be sampled by the multiplexer-encoder. Event type information from the vehicle is buffered when necessary. Signal conditioning state-of-the-art is highly developed, and analog accuracies of 1 percent and better are common. The following list describes some typical signal conditioners and their possible uses in the LUCOM data link:

CSM TELEMETRY

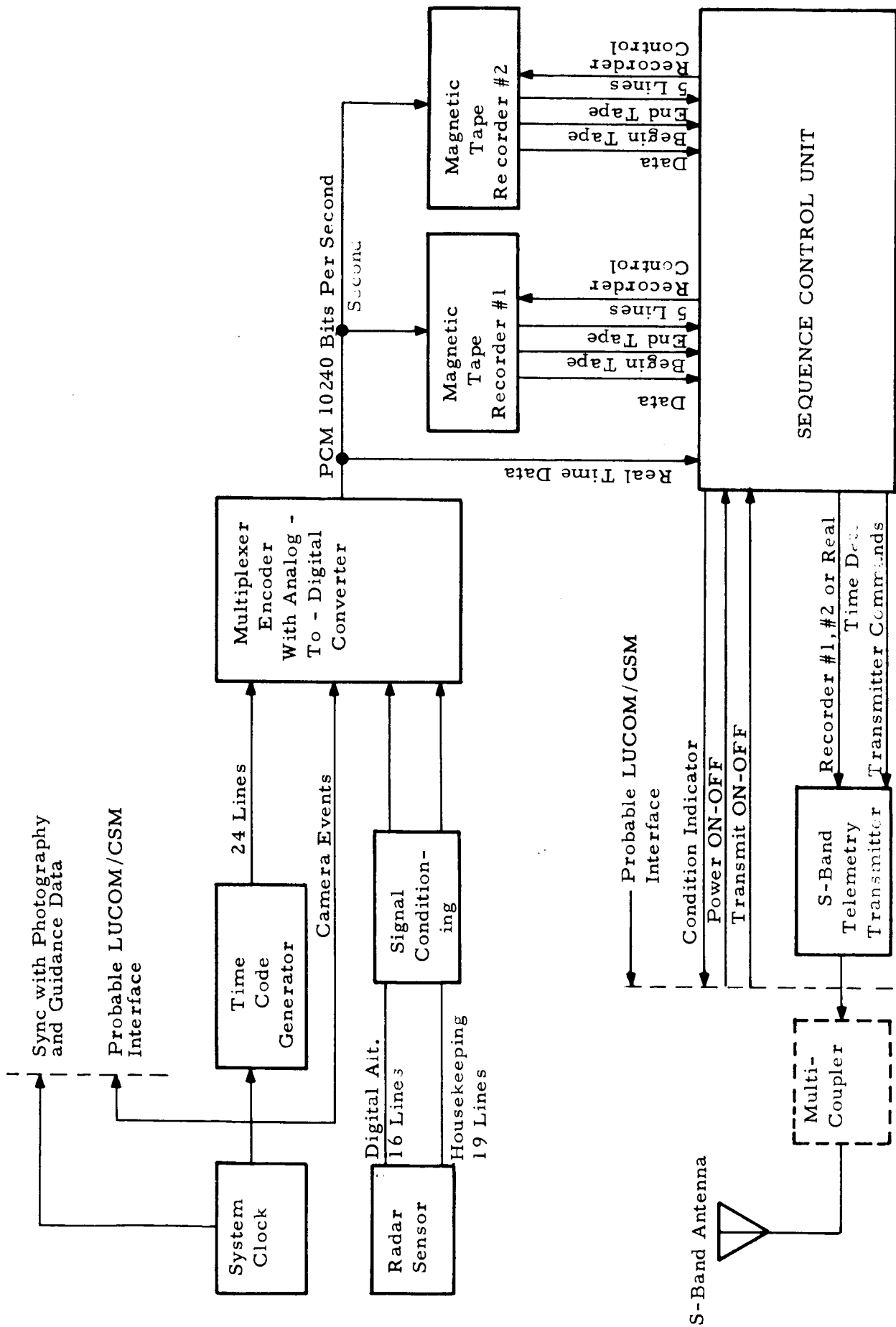


FIGURE 5.1.3.2-1. DATA LINK BLOCK DIAGRAM MODEL NO. 2

<u>Conditioner</u>	<u>Use</u>
DC Amplifier	Amplifies low-level DC voltages.
Analog Buffer	Provides impedance isolation between signal source and multiplexer-encoder.
RF Power Detector	Converts detected video pulse to a DC level which represents the peak pulse power.
Temperature Converter	Converts thermocouple output to a DC level which represents the temperature of the thermocouple.
Active Attenuator	Provides impedance isolation and reduces high level DC voltages to be compatible with the multiplexer-encoder.
Digital Buffer	Provides impedance isolation and logic level change to the multiplexer-encoder.

5.1.3.3.2 Multiplexer-Encoder

A typical multiplexer-encoder block diagram is shown in Figure 5.1.3.3.2.-1. The 11 analog inputs are applied to an 11-channel analog multiplexer. The pulse-amplitude-modulated (PAM) output of the analog multiplexer is applied through an isolation amplifier to a sample-and-hold circuit. The sample-and-hold output is coupled through another isolation amplifier into an 8-bit analog-to-digital converter. The analog-to-digital converter, along with the analog readout circuitry, encodes each channel of the PAM unit to obtain an 8-bit serial binary code which is proportional to the analog input amplitude.

The 72 bi-level inputs are composed of up to 24 altitude bits, 24 time code bits, and up to 24 bi-level events which include events used to time correlate the altitude data with the photography and guidance data that is a part of the Apollo data link. The bi-level inputs are applied to the bi-level multiplexer. The bi-level multiplexer groups

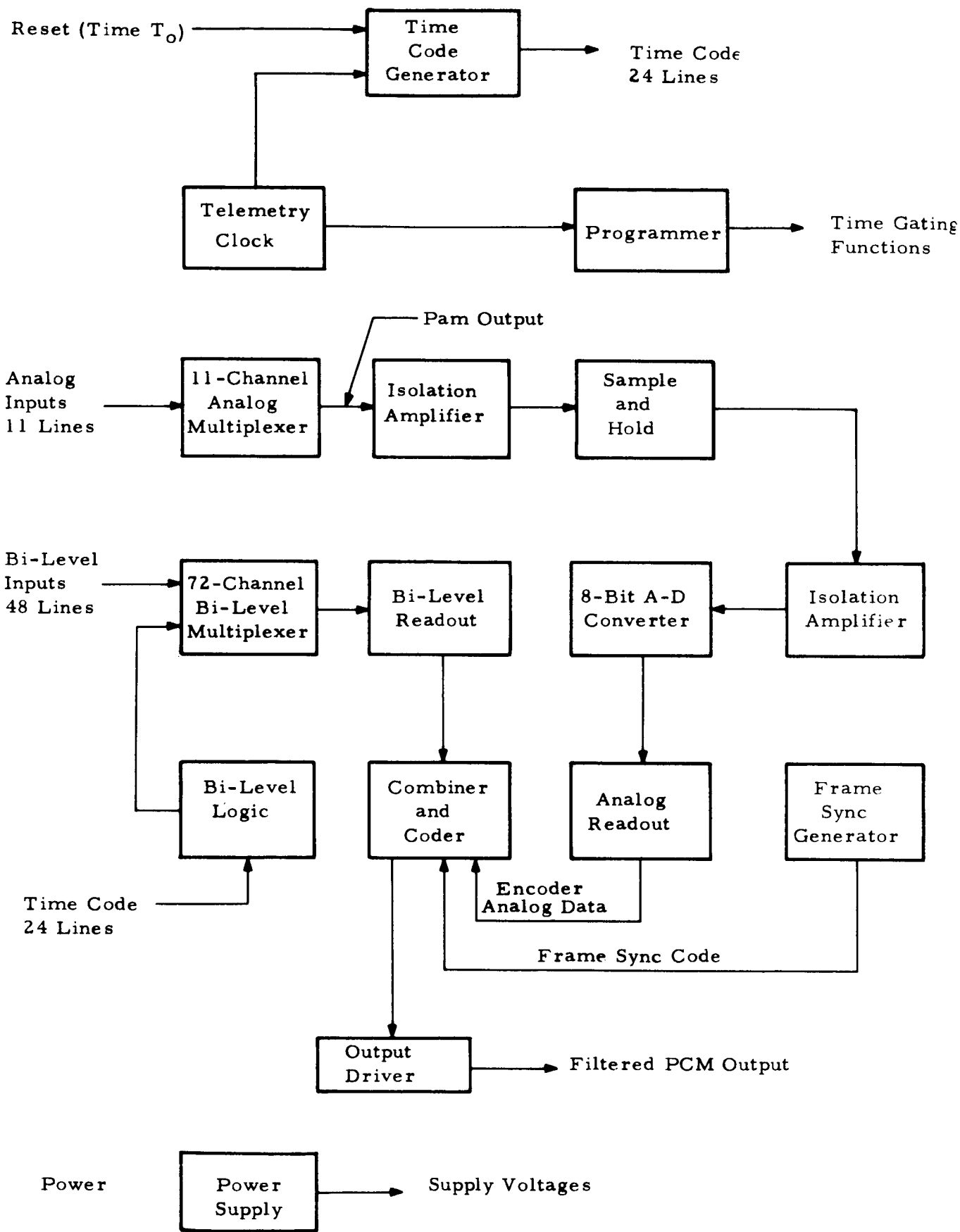


FIGURE 5.1.3.3.2-1. MULTIPLEXER - ENCODER BLOCK DIAGRAM

the bi-level inputs into nine 8-bit, parallel binary words. These nine parallel binary words are converted into serial binary codes by the bi-level readout circuitry. The 24-bit frame synchronization code is generated in the frame sync generator.

The encoded analog data output of the analog-to-digital converter, encoded bi-level outputs from the bi-level readout, and frame sync generator output are intermixed in the combiner to obtain a composite NRZ serial binary wavetrain. The NRZ output is converted to the appropriate split-phase code form by the coder. This split-phase output is premodulation-filtered to drive the VHF transmitter.

The required amplitudes, impedance, etc., are provided by the output driver circuitry. Time gating functions required by the system are provided by the programmer. The telemetry clock and time code generator shown in Figures 5.1.3.1-1 and 5.1.3.2-1 will be incorporated into the multiplexer-encoder if the telemetry clock is a part of the LUCOM system, but a separate encoder clock will be used to drive the programmer in the event the time code generator is driven by the vehicle timing system.

5.1.3.3.3 VHF Transmitter

The VHF transmitter which is to be used on Model Number 1 only can be either frequency or phase modulated. It is used to transmit the PCM wavetrain to the CSM. A large selection of VHF transmitters are on the market as off-the-shelf devices. The primary differences between the units is their capability for operating under environmental extremes and their DC to VHF efficiency.

5.1.3.3.4 VHF Receiver

The VHF receiver is used in Model Number 1 to receive the signal from the LSM and detect the PCM wavetrain. A number of off-the-shelf receivers are available in subminiature configuration suitable for use in space environments.

5.1.3.3.5 Bit Synchronizer and Data Regenerator

The Bit Synchronizer and Data Regenerator obtains bit synchronization with the noisy PCM wavetrain from the VHF receiver and generates a noise-free and jitter-free PCM signal at the same bit rate to the S-band transmitter or magnetic tape recorders. Figure 5.1.3.3.5-1 is a

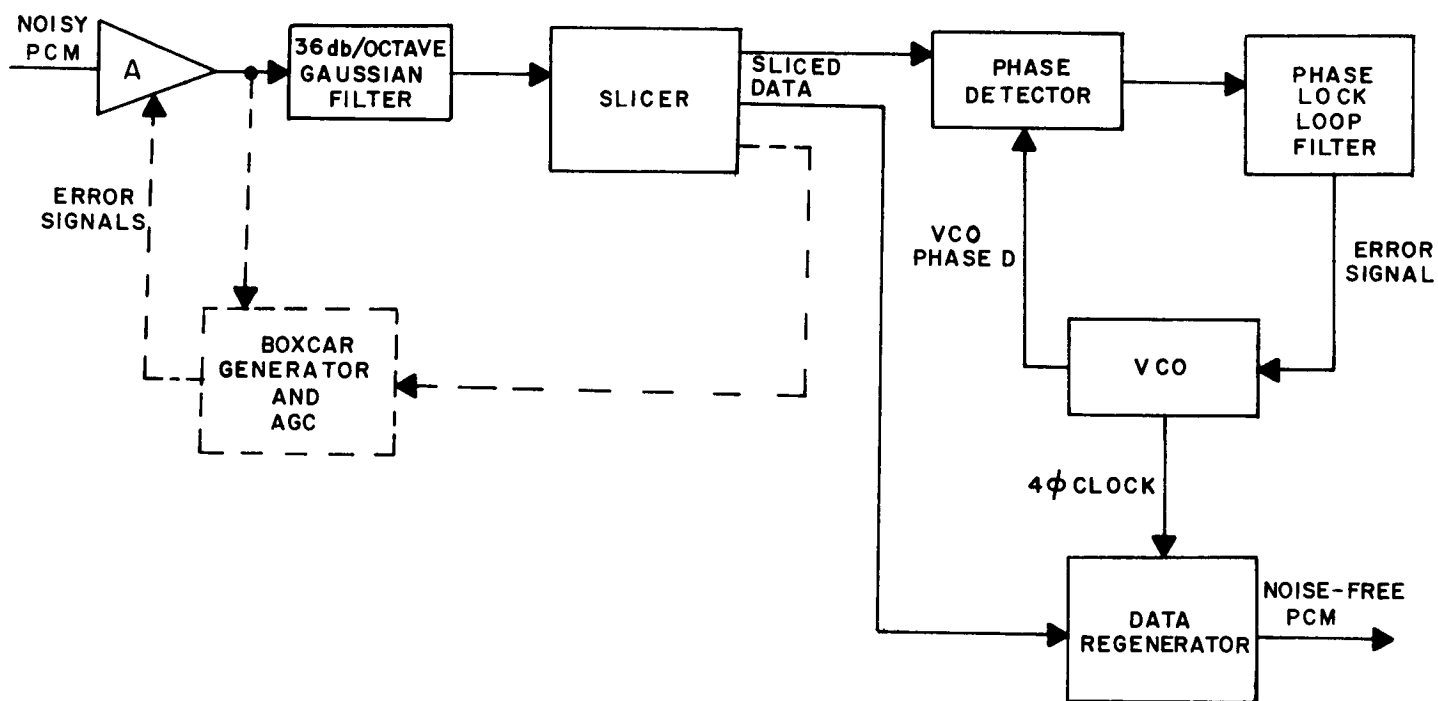


FIGURE 5.1.3.3.5-1 TYPICAL BIT SYNCHRONIZER AND DATA DETECTOR

block diagram of a typical bit synchronizer and data regenerator. The noisy PCM signal from the VHF receiver is fed to the input amplifier where the signal is amplified to a useable level. The amplified signal is filtered by a 36 db per octave Gaussian filter with a cutoff of 1.5 times the bit rate. The filter is shown in the block diagram following the input amplifier. Because the gain of active filter sections is usually low, it is desirable to reduce the effect of their noise contribution by placing them in location where the signal level is high. The filtered data is sliced at the zero crossings and amplified to produce a squared-up signal which represents a 0.6 volt slice of the original data. The slicer output rise time is in the vicinity of 0.1 microsecond, but the sliced data is a direct representation of the input signal intelligence. The noise components have been converted to jitter at the leading and trailing edges of the waveform. Figure 5.1.3.3.5-3 is a phase diagram of the waveforms throughout the Bit Synchronizer and Data Regenerator. A phase detector is gated ON when the sliced data is positive and compares the sliced data with phase D of the voltage controlled oscillator (VCO). An error signal is generated by the phase detector that has a positive DC component when the VCO lags the sliced data and a negative DC component when the VCO leads the sliced data. The phase lock loop filter provides very high amplification of the DC component while lowering the AGC gain. The filter bandwidth is optimized to the operating bit rate. The error signal from the loop filter corrects the phase by slightly changing the VCO frequency. When the sliced data and VCO are in phase, there is no DC component from the phase detector. Once bit synchronization is obtained, the four VCO phases and regenerating the data. The VCO operates at twice the bit rate. Phases A, B, C, and D are at bit rate and are separated by 1/2 bit in phase. The flip-flop that samples the data is clocked by a negative-going transition of the VCO. The sliced data is sampled at the 1/4 and 3/4 position of each bit period. The block diagrams and phase diagrams are for split phase code form. It should be noted that various code forms and even code form conversion can be accommodated by rearranging the VCO phase assignment to the phase detector and data regenerator clock. The boxcar generator and agc of Figure 5.1.3.3.5-1 are not a necessary part of the circuit, but with a 20 percent variation in VHF receiver output the agc can improve the signal-to-noise performance of the unit by 1.6 db.

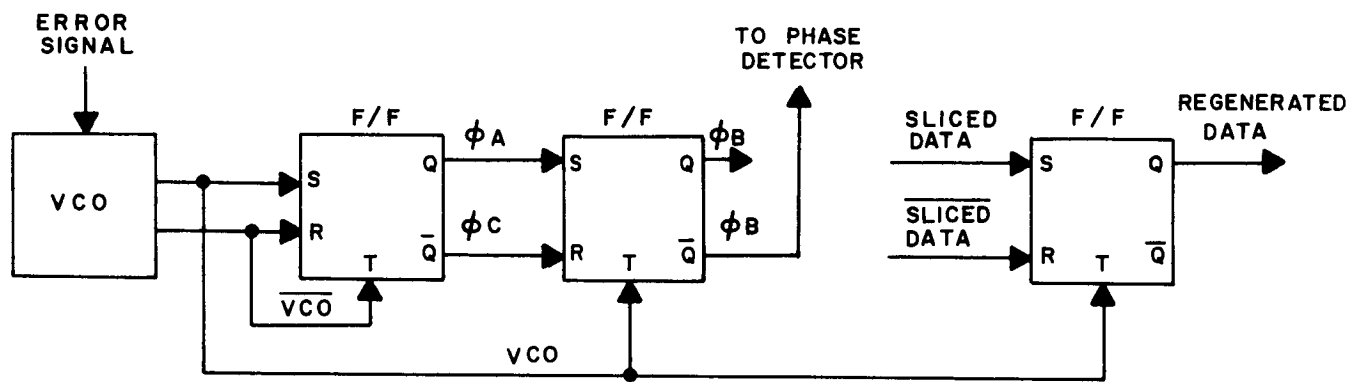


FIGURE 5.1.3.3.5-2 VCO AND DATA REGENERATOR

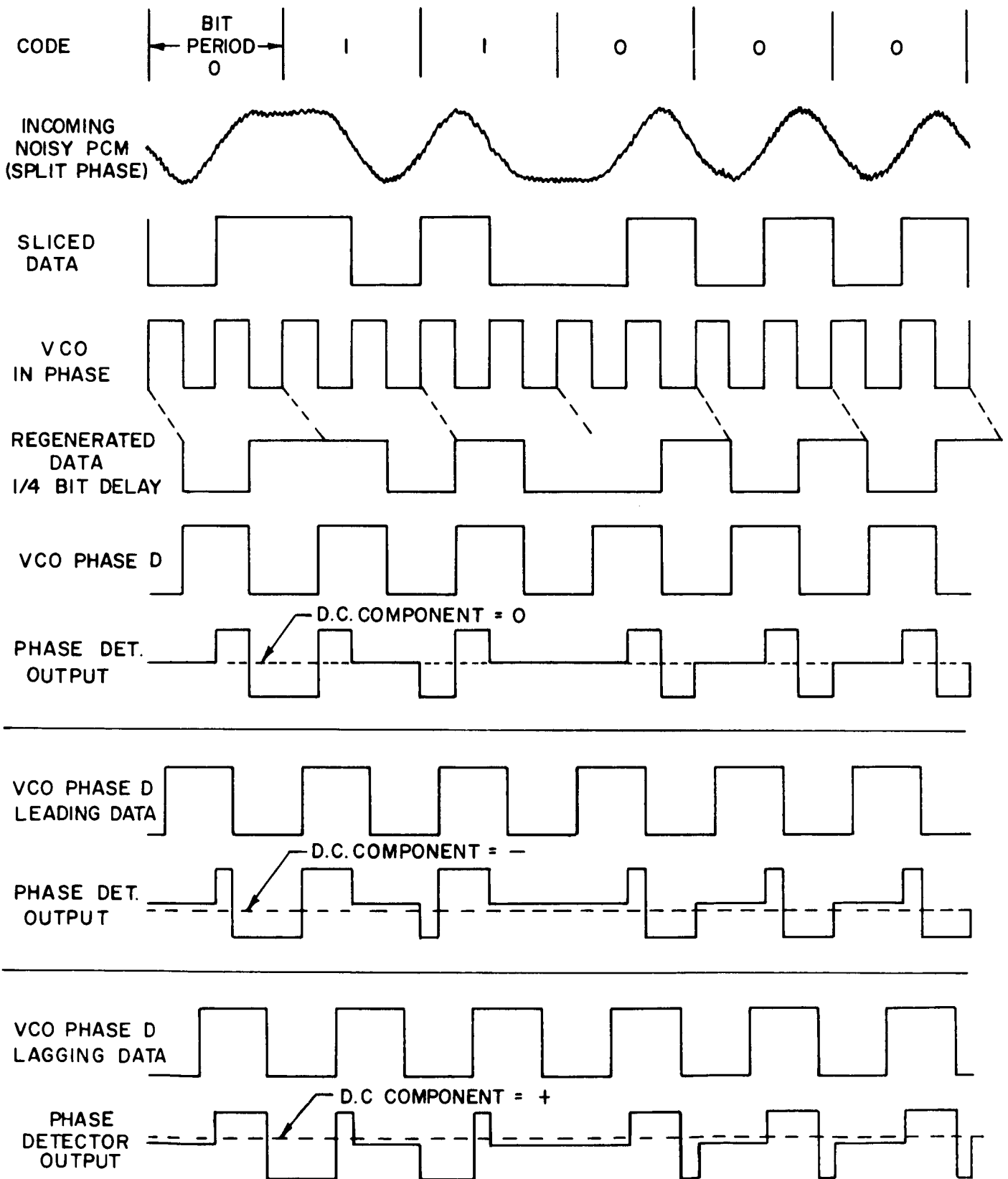


FIGURE 5.1.3.3.5-3 PHASE DIAGRAM

5.1.3.3.6 Sequence Control Unit

The Sequence Control Unit (SCU) determines the sequence of transmitting the information from Recorder No. 1, Recorder No. 2, or the real time data output from the Bit Synchronizer and Data Regenerator. In all cases the output is presented to the S-band transmitter. The logic design is based upon system requirements as presented in Table 5.-AI. It is expected that future changes in system requirements can easily be phased into the present SCU design. The various methods available for implementing the SCU logic design have not been considered, although a combination of solid state and electromechanical switching devices is likely.

Input-Output Signals

The input-output signals are shown in Figure 5.1.3.3.6-1. Definitions for the logic symbols and a state diagram are included in Appendix 5-BI.

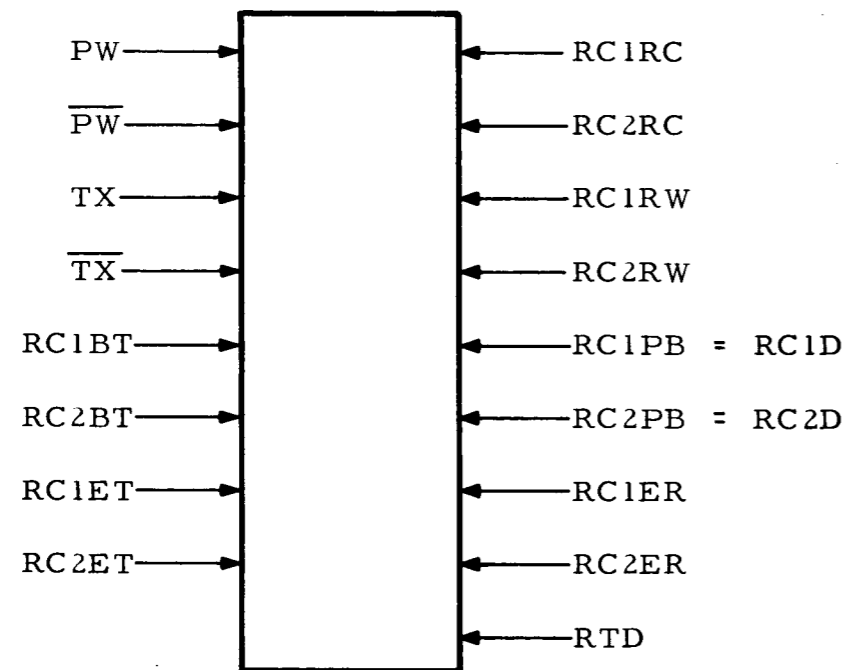


Figure 5.1.3.3.6-1

Circuit Description

The circuits employed in Figure 5.1.3.3.6-2 are flip-flops, A, B, C, D, E, and F for state control, flip-flops M, N, P, and Q for generating

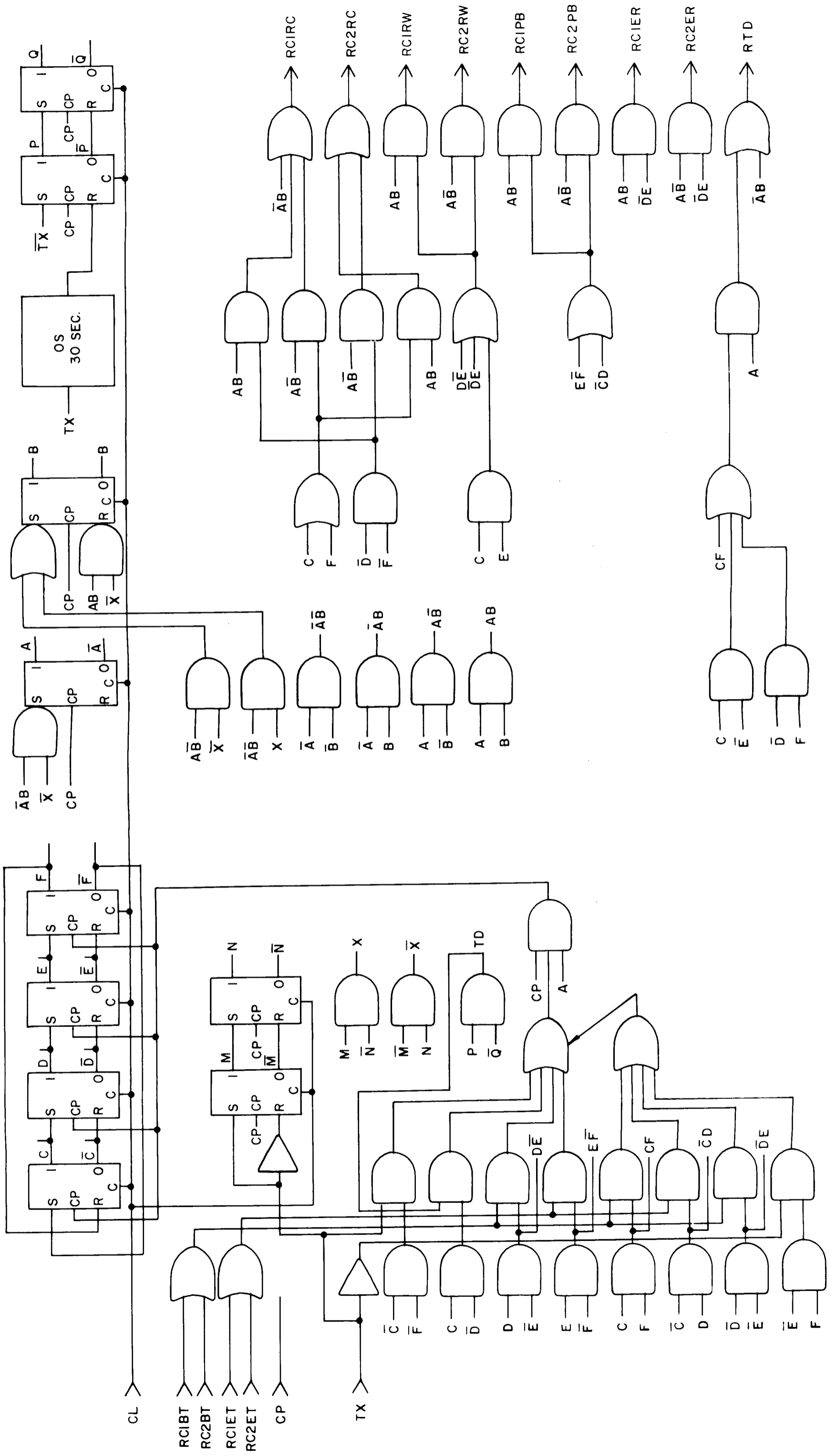


FIGURE 5.1.3.3.6-3 SEQUENCE CONTROL UNIT LOGIC DIAGRAM

logic signals, a one-shot, and various AND-OR gates for combining different signals.

State Control

State control is provided by flip-flops, A, B, C, D, E, and F. In general, A and B outputs determine whether the SCU is in Standby, pre line-of-sight, odd orbit, or even orbit. The C, D, E, and F flip-flops make up an 8-count Johnson counter and designate the 8 different output states during the odd and even orbits. The primary advantage of the Johnson counter over the conventional binary counter is that only two stages out of four need be decoded to detect any one count output while three stages out of three are required for the conventional binary type.

Signal Generation

Flip-flops M and N are used to generate X and \bar{X} signals from the TX input. Flip-flops P and Q are used along with a 30 second time delay multivibrator (OS) to generate the TD signal from the TX input. The logic involved in generating these signals is shown on the Logic Diagram.

Gates

There are 8 gates used to generate the output functions. Other gates are used to generate flip-flop clock pulses, R-S inputs, and generally perform basic logic functions. The equations for the more difficult logic functions are shown in Appendix 5-BII.

5.1.3.3.7 S-Band Transmitter

The S-band transmitter operates in the 2290 to 2300 megacycle region in order to be compatible with the Apollo unified S-band system. The PCM wavetrain from the tape recorders is transmitted at a bit rate of 81.9 kilobits per second. Real time data from the sequence control unit is transmitted at 10.24 kilobits per second. A variety of S-band transmitters are available or under development.

5.1.4 PCM FRAME FORMAT

A sample PCM frame format, shown in Table T-AII, was generated which, although not optimized to provide minimum bandwidth, will

satisfy LUCOM data requirements and allow a basis to determine altitude data rates from the tape recorder performance information. Based upon this sample format, a maximum bit rate of 10.24K bps and a maximum altitude word rate of 160 digital altitude measurements per second can be handled. This represents a radar sensor PRF of 160 pps with no averaging, or 1280 pps with 8 samples per altitude readout. An alternate frame format is shown in Table 5-AIII which can accommodate 210 altitude words per second. Several trade-offs are available to increase the data handling to cover the assumed 1000 altitude measurement per second. They are:

1. Sequence the recorders to record only 1/2 orbit instead of one full orbit.
2. Incorporate multiple track recording features into the tape recorders to sequentially change tracks at each end-of-tape sensing.
3. Optimize the PCM frame format to include sub-commutation techniques and record only the least significant bits of the altitude during the sub-frames.

5.1.5 R. F. LINK ANALYSIS

Tables 5-AIV and 5-AV are the RF Link Analysis for the VHF and S-band links. In the VHF link, a receiver IF noise figure of 12.8 db was used to determine the receiver noise power of -191 dbw. The calculation based on an ideal receiver is -208 db, which allows a circuit margin of +23 db.

5.1.6 DATA LINK ERRORS

An analysis has been made of the LUCOM data link to determine the altitude errors that may be injected into the LUCOM system by the data link. The two data link configurations studied were data link block diagrams, Model No. 1 and Model No. 2. The analog signals and analog-to-digital conversion were not considered in the error analysis because the altitude readings will be provided to the telemetry in digital form and will not be associated with analog measurements.

The data link errors that contribute to erroneous altitude readings can be grouped into three categories:

1. Quantization errors in the spaceborne data re-generator due to noise in the VHF telemetry link.
2. Bit errors due to signal dropouts in the magnetic instrumentation tape.
3. Quantization errors in the ground data processing due to noise in the S-band telemetry link.

Figure 5.1.6-1 shows curves of bit error probability vs. peak signal-to-rms noise for pre-modulation filtered PCM signals. Curve I utilizes a 36 db/octave Gaussian filter detector.¹ The polarity of the output at the midpoint of the bit period is the bit decision. Curve II utilizes a slicer following the 36 db/octave Gaussian filter. The level of the slicer at the midpoint of the bit period is the bit decision. The slicer improves the performance by approximately 1.5 db. Derivation of the curves of Figure 5.1.6-1 are found in Appendix 5-C.

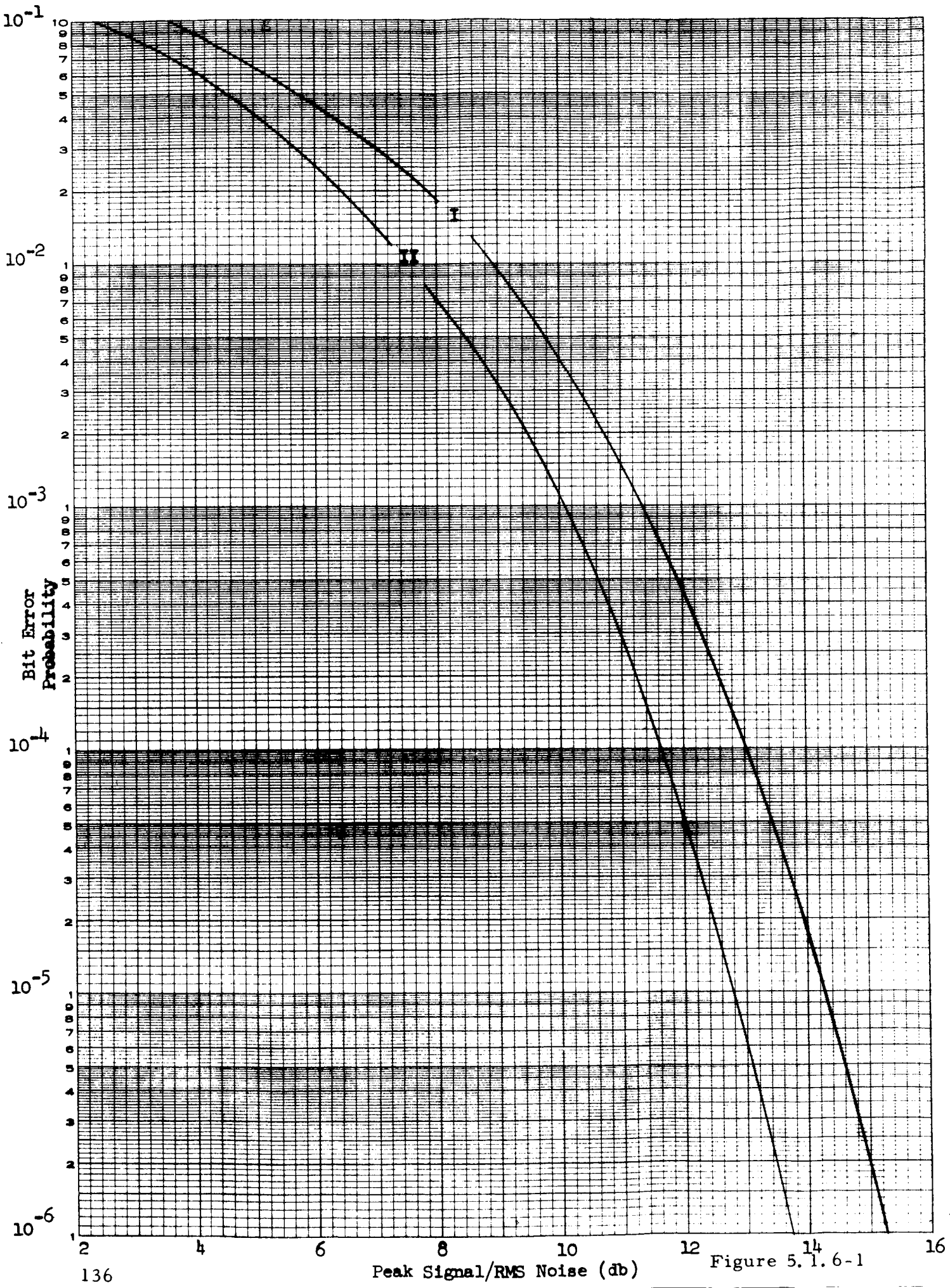
The RF Data Link Analyses of Tables 5-AIV and 5-AV allows a +15 db signal-to-noise ratio. For the spaceborne data regenerator, a bit error rate of 2×10^{-6} from Curve I is a very conservative worst case analysis, since Table 5-AIV contains a +10 db circuit margin and Curve I can be refined to give a 1.5 db improvement. Considering the ground station data regenerator and subtracting 10 db from the circuit margin of Table 5-AV because of possible signal fading due to earth atmospheric conditions, a signal-to-noise ratio of 14.5 db results. From Curve I, the associated bit error probability is 6.5×10^{-6} for the ground station.

The bit errors attributed to signal dropouts in the instrumentation tape also follow a Gaussian distribution. Published data for the Gemini tape recorder give a bit error rate of 1×10^{-5} at a bit packing density up to 3200 bits per inch. The LUCOM recorder will pack up to 2730 bits per inch.

The data link bit error probability is the sum of the three categories, or:

$$\text{Model No. 1: } p_e = 2 \times 10^{-6} + 1 \times 10^{-5} + 6.5 \times 10^{-6} = 1.85 \times 10^{-5}$$

$$\text{Model No. 2: } p_e = 1 \times 10^{-5} + 6.5 \times 10^{-6} = 1.65 \times 10^{-5}$$



Assuming an 80 nautical mile lunar orbit with ± 3 meters resolution, an altitude word contains 16 bits. The probability of error in any one or more of 16 consecutive bits is:

$$P_e(16) = 1 - (1 - p_e)^{16}$$

and Model No. 1: $P_{e(16)} = 2.96 \times 10^{-4}$ altitude errors per transmitted altitude word

Model No. 2: $P_{e(16)} = 2.64 \times 10^{-4}$ altitude errors per transmitted altitude word

At an altitude word rate of 160 words per second, the above probabilities correspond to 21.1 and 23.7 seconds between altitude errors for Models No. 1 and 2, respectively.

An error source of a different nature that should be included in the LUCOM system error analysis is the time correlation error. The result of a time correlation error is the incorrect positioning of the radar sensor on the lunar coordinate system at the instant an altitude measurement is taken. Twenty-four bits of the PCM frame have been reserved for time code. A 24-bit binary counter can count 16,776,216 increments before recycling. If the counter has to run the entire 48 hour mission without recycling, the minimum available time increment is 10.3 milliseconds. At an orbital path velocity of 5460 feet per second (80 N.M. circular orbit), the orbital path position error is 56.2 feet. If the counter is allowed to recycle once per orbit, (6900 seconds) the minimum available time increment is 0.4 millisecond and the orbital path position error is 2.2 feet. For ease of utilization, it would be desirable to use 1 millisecond increments (5.5 feet error). A basic clock accuracy of 1×10^{-5} and a clock stability of 1×10^{-6} can be expected. Assuming the clock errors can be corrected once per orbit when real time data is being transmitted to earth, the cumulative error due to basic clock inaccuracy is 69 milliseconds per orbit and due to the clock stability is 6.9 milliseconds per orbit. Since the basic clock inaccuracy results in a linear error accumulation, a correction factor can be applied at any desired time to reduce the error. For example, five equally spaced corrections per orbit will reduce the cumulative error to 14 milliseconds.

A summary of the time correlation errors and the associated orbital path errors for an 80 N.M. orbit are listed below:

<u>Description</u>	<u>Time Error</u>	<u>Distance Error</u>
LUCOM time increments	.001 second	5.5 ft. /increment
LUCOM clock accuracy	.069 second/orbit	376.7 ft. /orbit
LUCOM clock accuracy linearly corrected 5/orbit	.014 second	76.4 ft.
LUCOM clock stability	.0069 second/orbit	37.7 ft. /orbit
Assumed range time total accuracy	.001 second	5.5 ft.

5.1.7 EQUIPMENT PERFORMANCE CHARACTERISTICS

Tables 5-AVI through 5-AXIII specify the performance characteristics for each functional block of the data link block diagram of Figure 5.1.3.1-1.

5.1.8 TRADE-OFF ANALYSES

Two initial assumptions were made which stated that the altitude measurements will not exceed 1000 per second, and the minimum altitude increment will be 3 meters for an 80-mile orbit. A PRF of 1000 pulses per second represents the absolute, unambiguous maximum sampling rate that is determined by the length of time required for a radar pulse traveling at the speed of light to make the round trip from the vehicle to the lunar surface. With a least significant bit resolution of 3 meters, 16 bits will be necessary to provide a binary representation of the altitude. This establishes an information rate of 16,000 bits per second, considering only the altitude data with no housekeeping data or formatting bits. The single track recorder which was previously described will accommodate a bit rate of only 10240 bits per second in recording for one complete orbit. Several alternate approaches were suggested to increase the data storage capability. However, consider the sensor trade-off curve of Figure 4.3.3.1-3 in which a PRF in the vicinity of 100 pulses per second appears to be a much better choice from the standpoint of sensor prime power consumption. In addition, the sensor trade-off curve of Figure 4.3.3.2-1 shows that averaging the returns results in improved altitude measurement accuracy. The data link is presented the averaged altitude measurement which occurs at a rate equal to the PRF divided by the number of samples per measurement. Since Figure 4.3.3.1-3 indicates that a PRF below 1000 pps is

desirable, and Figure 4.3.3.2-1 indicates that averaging the pulse is advantageous, it is reasonable to assume that the sensor data rate will be 160 measurements per second or less. The data link can handle this rate adequately. Figure 5.1.8-1 shows the data rate vs. altitude measurement rate for the VHF link (model no. 1) for twenty-one 8-bit auxiliary channels and a 24-bit frame synchronization code. The number on the curve represents the number of times an altitude measurement is taken within each PCM frame, or the supercommutation factor. The curve numbered 4 corresponds to the sample PCM format of Table 5-AII. From curve 4, it may be seen that at the maximum tape recorder capability of 10,240 bits per second, the altitude rate is 160 measurements per second. The curves of Figure 5.1.8-2 take into account the accelerated tape recorder playback rate. At an altitude rate of 160 measurements per second, from curve 4, it may be seen that the S-band data rate is 81,920 bits per second.

The effect of increasing the data rate is to increase the noise bandwidth, so that for a given signal to noise ratio, an increase in data rate requires more transmitter power. Figure 5.1.8-3 shows transmitter power versus data rate for the VHF and S-band links. For the data rates mentioned previously, a VHF transmitter power of 5 watts and an S-band transmitter power of 5.5 watts are required.

Insufficient transmitter power results in increased altitude measurement errors. From the data link error analysis the altitude error rate of 2.96×10^{-4} for model no. 1 was based upon 5-watt transmitters in both VHF and S-band links. Figures 5.1.8-4 and 5.1.8-5 show the dependence of altitude error rate upon the altitude measurement rate and transmitter power. The limit of the family of curves at 1.6×10^{-4} is due to tape recorder restrictions so that increasing the transmitter power will not improve the error rate beyond that point. Assuming that an altitude error rate of 10^{-3} (1 error per 1000 measurements) is acceptable; a minimum transmitter power of 2 watts for each link will be sufficient.

The final trade-off that was considered is the size and weight reduction that can be accomplished by utilizing integrated circuitry and advanced packaging techniques. Several considerations require evaluation that cannot be performed at this time, so the results are presented in Tables 5-AXIV and 5-AXV without drawing conclusions. These considerations are the reliability factors for integrated versus conventional circuitry, lead times for subsystems development, and cost factors.

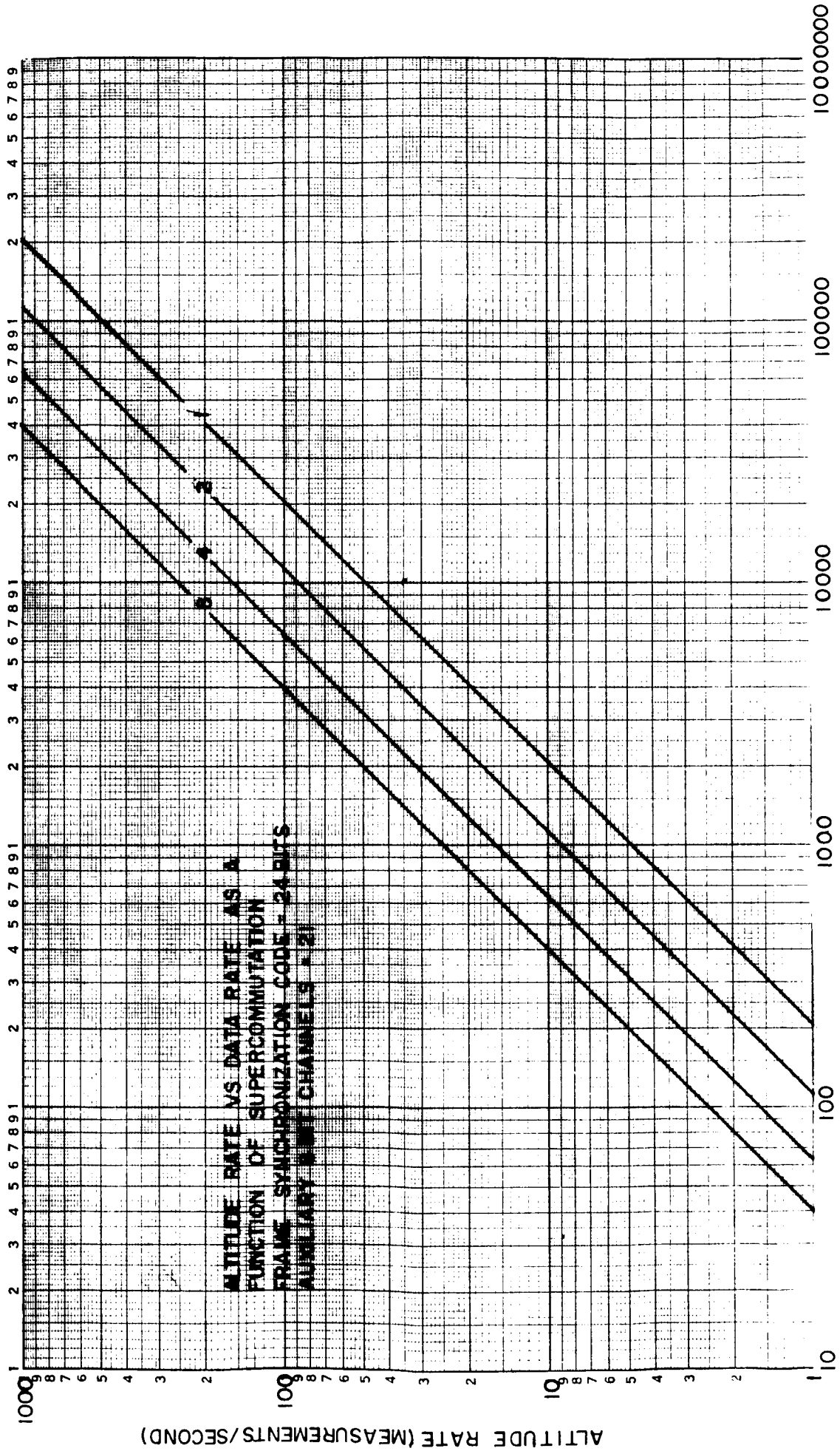
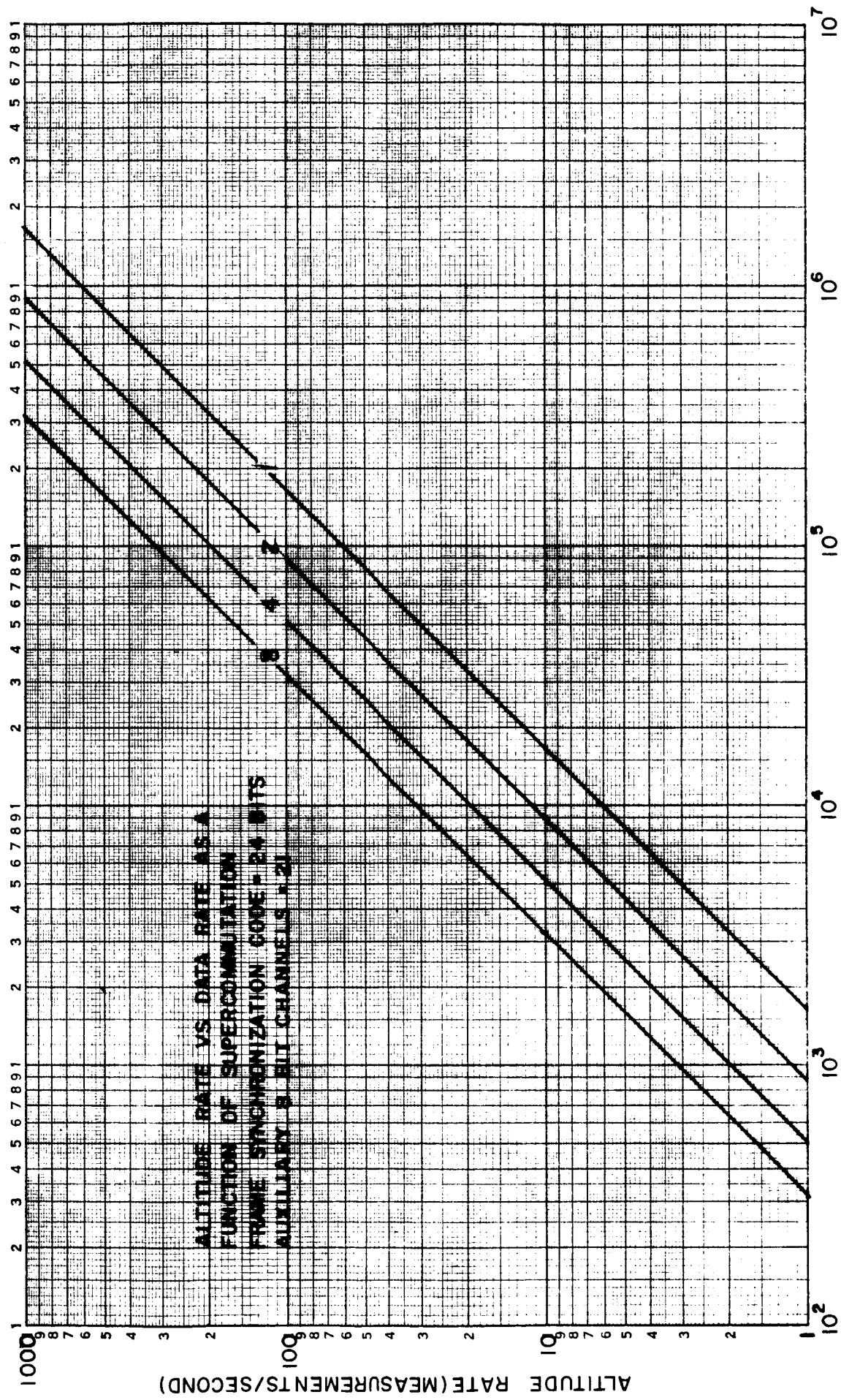
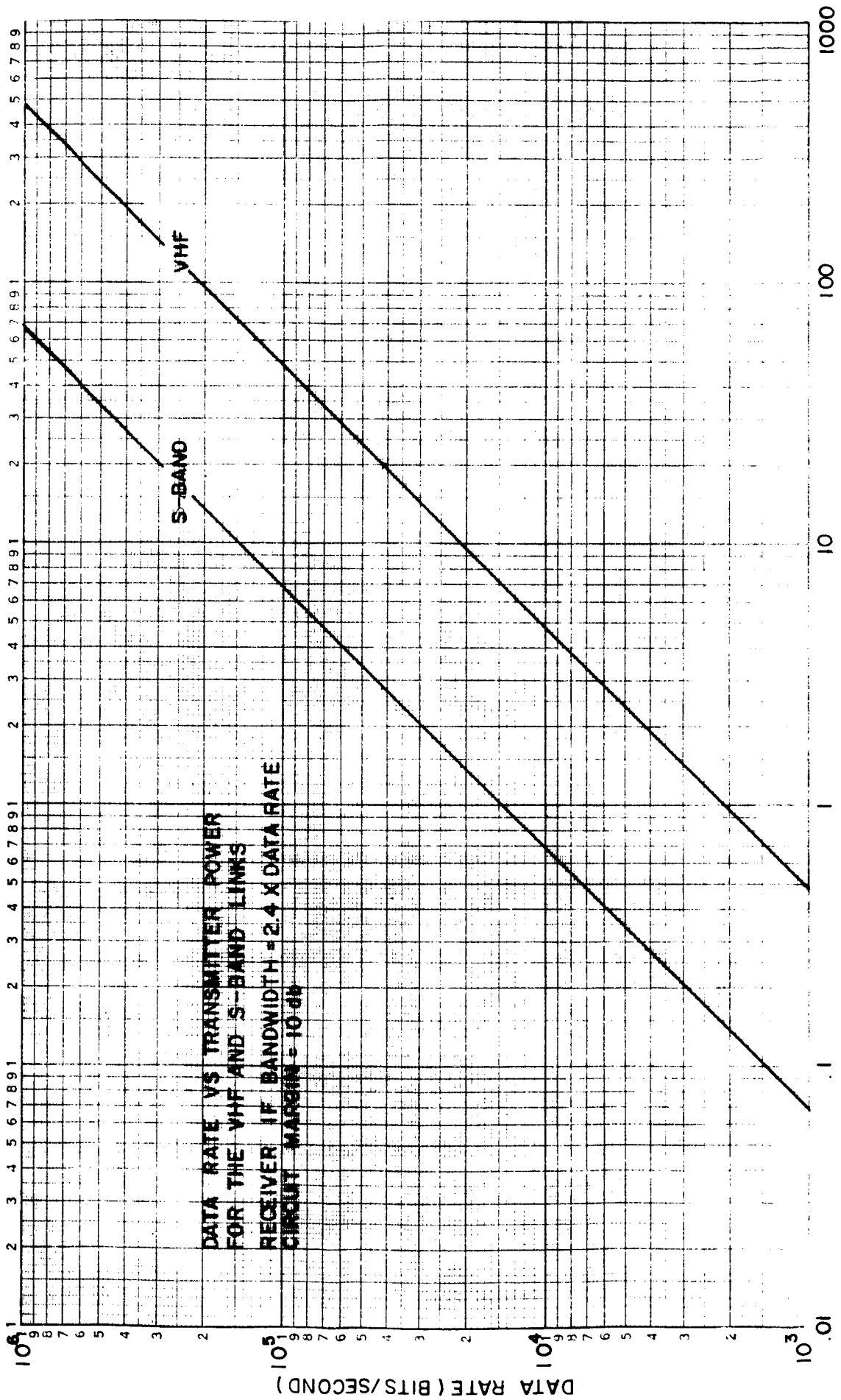


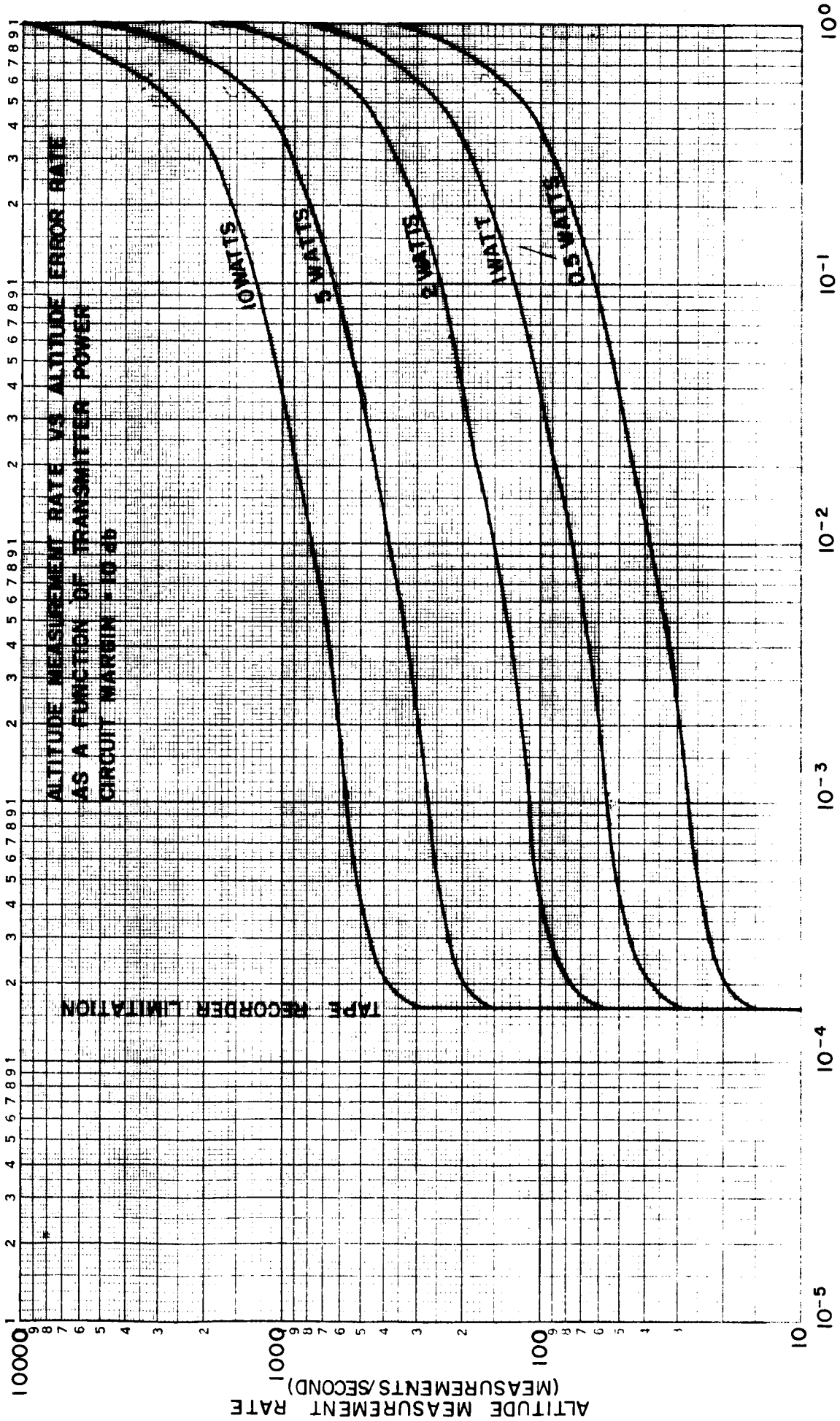
FIGURE 5.3-1 VHF DATA LINK



DATA RATE (BITS / SECOND)
 FIGURE 5.3-2 S-BAND LINK



TRANSMITTER POWER (WATTS)
FIGURE 5.3-3



ALTITUDE ERROR RATE (ERRORS/MEASUREMENT)
FIGURE 5.3-4 DATA LINK MODEL NO. 1

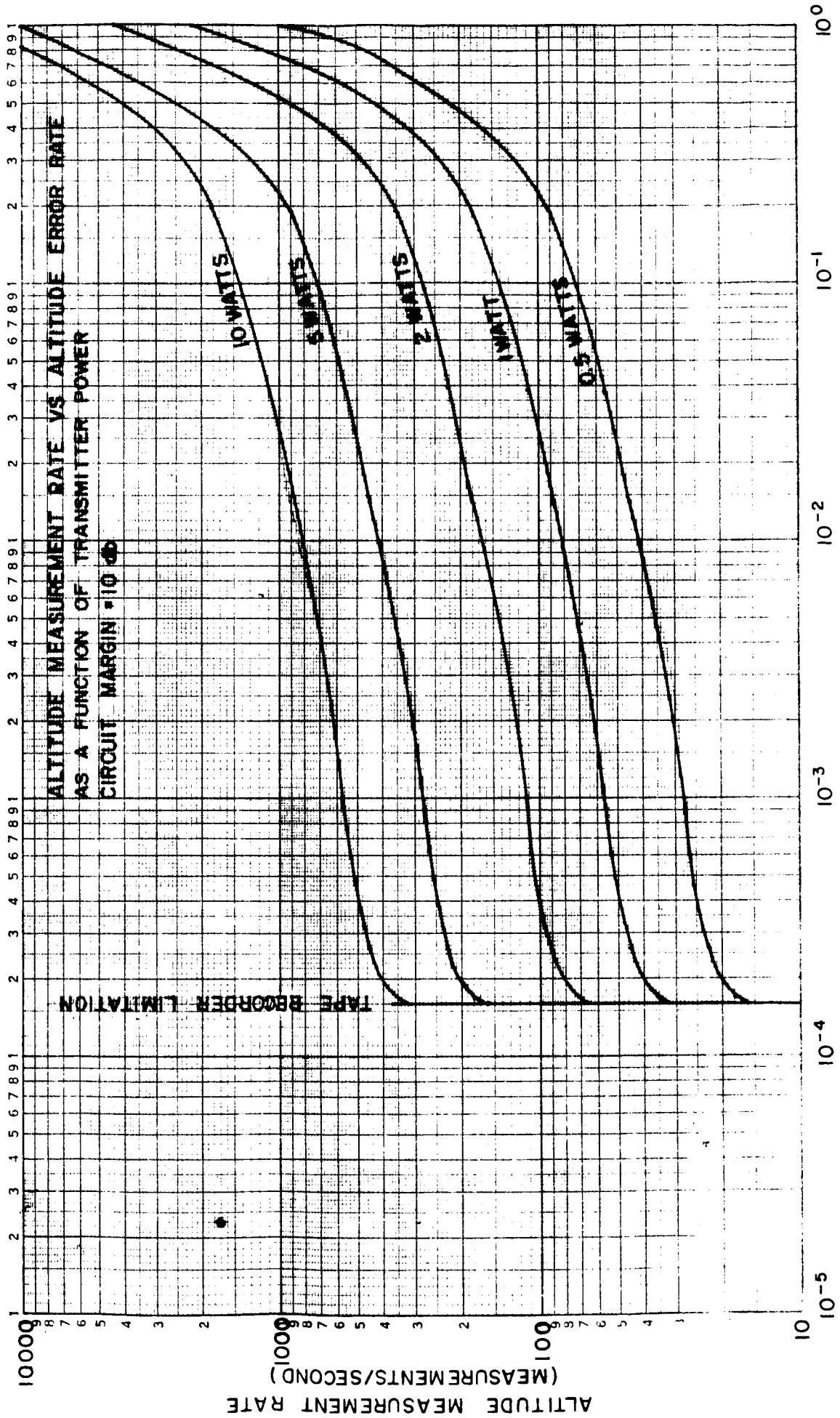


FIGURE 5.3-5 DATA LINK MODEL NO. 2

6.0 DATA UTILIZATION

This task consisted of devising methods for using the data provided by the LUCOM System to accomplish the LUCOM scientific objectives, which are:

- (a) Determination of the lunar figure.
- (b) Vertical control for photography.
- (c) Determination of slopes and surface relief, especially on back side of moon.
- (d) Establishment of interim selenodetic control.

6.1 DETERMINATION OF THE LUNAR FIGURE

The basic method consists of obtaining altimetry data of the lunar surface, utilizing the Apollo orbit for a base line, and by subtraction, obtaining the geometrical figure of the moon in the sub-orbital tracks. Auxiliary data will be provided by the Apollo Guidance System.

The data obtained from the LUCOM System will be processed in the data reduction center after completion of the mission. Since it is not a real time activity, sophisticated techniques, programs and equipment can be used to convert the collated information into useable scientific knowledge. Some of the techniques investigated during this program are described in the following paragraphs.

6.1.1 IMPROVEMENT OF THE APOLLO ORBIT

The first step in the data reduction process is to effect an improvement in the orbit elements. The Apollo Guidance System will provide the following information:

A_0 = semi-major axis

ω_o = average angular velocity

T_o = time of passage of periselenium

E_o = eccentricity

The LUCOM System will provide measurements of two points in the orbit. Two additional points may be obtained from occultations of the space craft. Referring to Figure 6.1.1-1 below, these occultations occur at points 1 and 3. Point 1 occurs at the time when communications with the earth and the CSM are interrupted and point 3 occurs when communications with the earth and the CSM begin again.

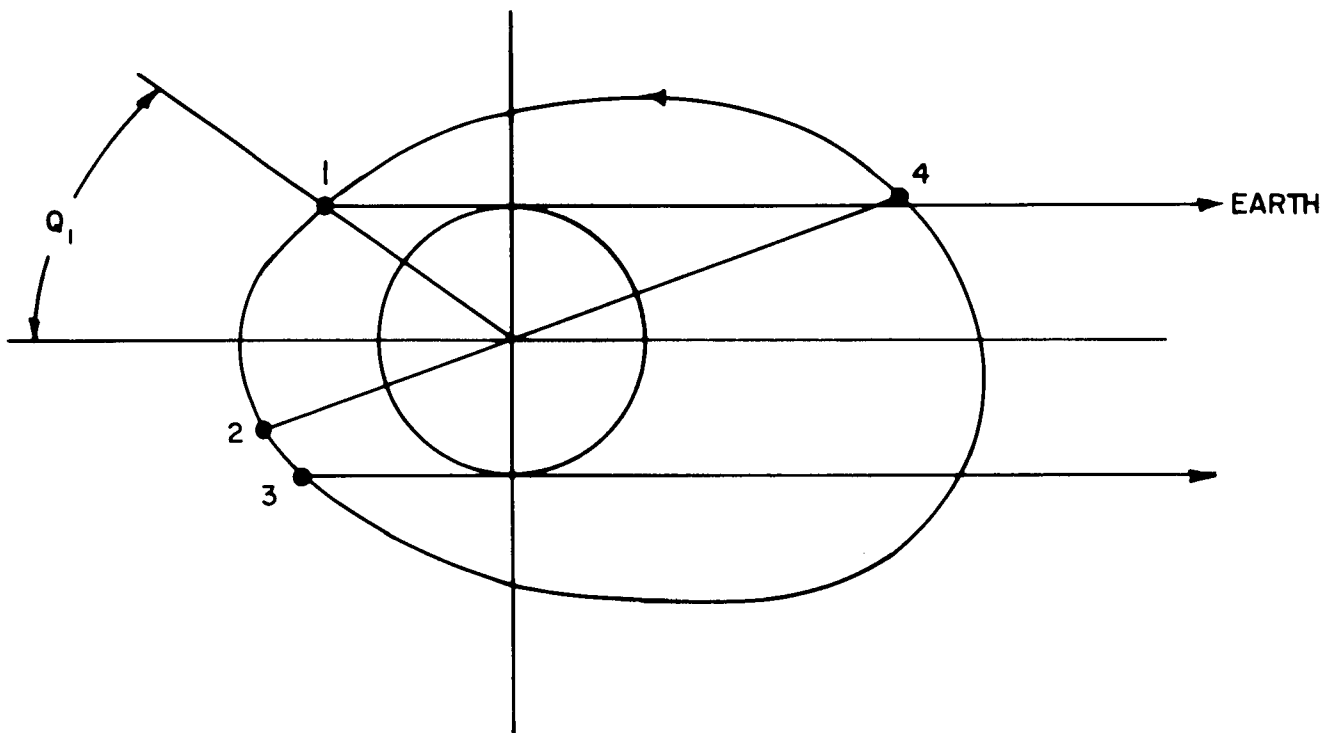


FIGURE 6.1.1-1

The average angular velocity may be conveniently obtained by averaging the time between the occurrence of point 1 over N orbits. If zero time is defined to occur at point 1 at the beginning of the first orbit, and the time of the second occurrence of point 1 is denoted by t_{11} and, in general, the $(N + 1)$ th occurrence of point 1 is denoted by t_{1N} ; and t_{31} denotes the first

time point 3 occurs and t_{3N} denotes the Nth occurrence of point 3, then the average angular velocity may be obtained from the average:

$$\omega_1 = \frac{2\pi}{t_{ave}}$$

$$t_{ave} = \left[t_{11} + (t_{12} - t_{11}) + \dots + t_{1N} - t_1 (N - 1) + \dots \right. \\ \left. (t_{32} - t_{31}) + \dots + t_{3N} - t_3 (N - 1) \right] / 2N$$

The other two points, 2 and 4, are obtained by correlating the terrain profiles. Referring back to Figure 6.1.1-1, in the region of maximum inclination, the ground track crossings are practically coincident. This fact can be used to correlate the radar terrain profiles with each other to obtain a fixed point in the orbit, related to time. The orbit is centered at the center-of-mass of the moon, while the moon is rotating at approximately one-half degree per hour. Figure 6.1.1-2 below illustrates the path of the orbit. The curves y_1 , y_2 , and y_3 represent the lunar terrain. Each curve is actually the same section, but each curve is shifted horizontally because of the moon's rotation. Actually there is no vertical shift, but this was done for clarity in the illustration. The radar altitude readings for the first pass are denoted by y_{1K} , for the second pass by y_{2K} , and so on. One way to correlate the passes is by the mean square difference criteria, that is:

$$MSD(\tau) = \frac{1}{n} \sum_{K=1}^n (y_{1K} - y_{2K} + \tau)^2 \quad \tau = 1, 2 \dots N$$

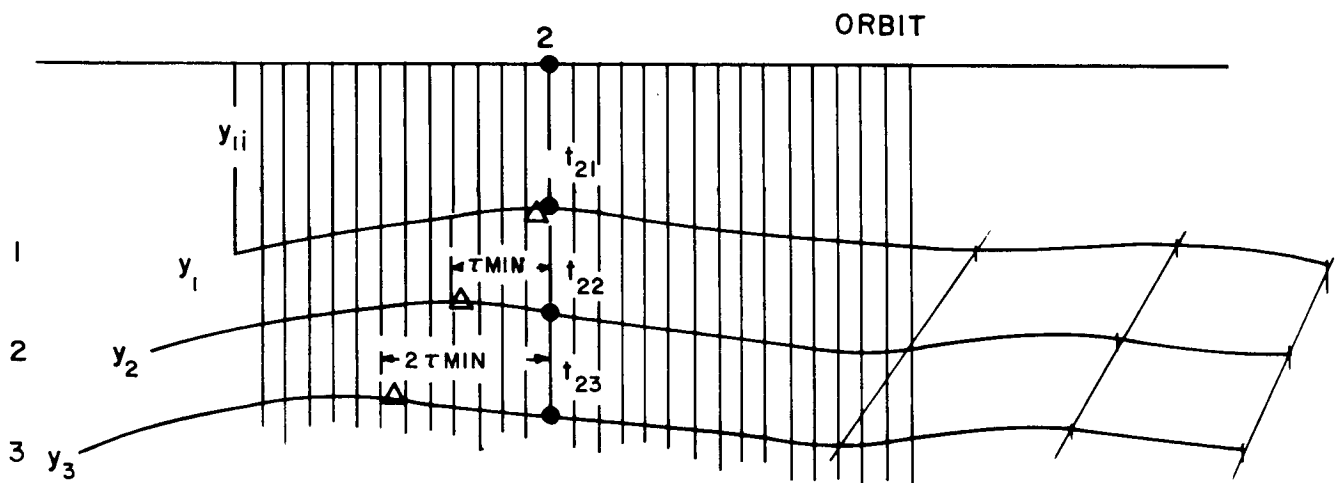


FIGURE 6.1.1-2

The value of T for which the MSD is a minimum is equal to the time between the passing over of a particular point on the lunar surface from one pass to the next. Thus, T_{min} is caused by the rotation of the moon. If the moon did not rotate, T_{min} would be equal to zero. The MSD operation is performed on the y's for the other passes. This procedure allows the times, t₂₁, t₂₂, ... at which a given point in the orbit occurs, to be determined. The point 4 is obtained by a similar correlation process on the opposite side of the moon where the ground tracks are approximately coincident. Now that the time of occurrence of four positions of the orbit have been determined, these measurements may be averaged over N orbits to improve the estimates of the orbit elements furnished by the Apollo guidance system.

The expression for the true anomaly in terms of the mean anomaly is:

$$Q_{mi} = Q_{mio} + \frac{\partial Q_{mio}}{\partial E_0} (E_1 - E_0) + \frac{\partial Q_{mio}}{\partial T_0} (T_1 - T_0) + \dots$$

This expression is a Taylor's series with only first order terms retained. The coefficients are:

$$Q_{mio} = \omega_1 (t_{mi} - T_0) + 2E_0 \sin W_1 (t_{mi} - T_0) + \dots$$

where T₀ and E₀ are determined by the Apollo guidance system.

$$\frac{\partial Q_{mio}}{\partial E_0} = 2 \sin \omega_1 (t_{mi} - T_0) + \dots$$

$$\frac{\partial Q_{mio}}{\partial T_0} = -\omega_1 - 2 E_0 \omega_1 \cos (t_{mio} - T_0) + \dots$$

where M = 1, 2, 3, 4, the four points on the orbit,

i = 1, 2, ... N, the number of orbits.

Also

$$\sum_m^4 Q_{mi} = 2\pi$$

The equations of condition are:

$$2\pi - \sum_m^4 Q_{mio} = \sum_m^4 \frac{\partial Q_{mio}}{\partial E_0} (E_1 - E_0) + \sum_m^4 \frac{\partial Q_{mio}}{\partial T_0} (T_1 - T_0)$$

i = 1, 2, ... N

Let
$$R_i = 2\pi - \sum_m^4 Q_{mio}$$

$$A_i = \sum_m^4 \frac{\delta Q_{mio}}{\delta E_0}$$

$$B_i = \sum_m^4 \frac{\delta Q_{mio}}{\delta T_0}$$

$$[AA] = \sum_i^N A_i^2$$

$$[AB] = \sum_i^N A_i B_i$$

etc.

The normal equations are:

$$\begin{aligned} [AA] (E_1 - E_0) + [AB] (T_1 - T_0) &= [RA] \\ [AB] (E_1 - E_0) + [BB] (T_1 - T_0) &= [RB] \end{aligned}$$

$(E_1 - E_0)$ and $(T_1 - T_0)$ are solved by Cramer's Rule. The semi-major axis A is determined from the relation

$$\omega_1 = \frac{\sqrt{GM_m}}{A_1^{3/2}}$$

where $M_m =$ mass of the moon.

6.1.2 GROUND TRACK ERROR AS A FUNCTION OF ORBIT ELEMENTS

The position of the ground track on the lunar surface may be expressed in a lunar coordinate system by the vector:

$$\begin{aligned} \underline{P}' &= R_m (\cos \varphi \cos \psi + \sin \varphi \sin \psi \cos \theta) \underline{1}_{xm} \\ &+ R_m (\sin \varphi \cos \psi \cos \theta - \sin \psi \cos \varphi) \underline{1}_{ym} \\ &+ R_m (\sin \varphi \sin \theta) \underline{1}_{zm} \end{aligned}$$

R_m is the radius vector from the center of the moon to the surface. ψ is well defined and is equal to ω_{mt} . θ is called the true anomaly and is related to the mean anomaly by the expression:

$$\varphi = M + 2 E \sin M + 5/4 E^2 \sin 2M + \dots$$

For a particular point on the lunar surface, R_m , φ , ψ , and θ will be known to a certain degree of accuracy. Represent these quantities by a bar placed over the quantity. These will be referred to as computed quantities. An estimate of the probable error of these quantities should be available. An estimate of the ground track error may be obtained by expanding the expression for the components of the ground track vector about the computed quantities in a Taylor series. The result is:

$$\begin{aligned} \underline{P}' &= \left\{ \bar{R}_m (\cos \bar{\varphi} \cos \bar{\psi} + \sin \bar{\varphi} \sin \bar{\psi} \cos \bar{\theta}) \right. \\ &+ (\cos \bar{\varphi} \cos \bar{\psi} + \sin \bar{\varphi} \sin \bar{\psi} \cos \bar{\theta}) (R_m - \bar{R}_m) \\ &+ \bar{R}_m (-\sin \bar{\varphi} \cos \bar{\psi} + \cos \bar{\varphi} \sin \bar{\psi} \cos \bar{\theta}) (\varphi - \bar{\varphi}) \\ &+ \bar{R}_m (-\cos \bar{\varphi} \sin \bar{\psi} + \sin \bar{\varphi} \cos \bar{\psi} \cos \bar{\theta}) (\psi - \bar{\psi}) \\ &+ \left. \bar{R}_m (-\sin \bar{\varphi} \sin \bar{\psi} \sin \bar{\theta}) (\theta - \bar{\theta}) \right\} \underline{1}_{xm} \\ &+ \left\{ \bar{R}_m (\sin \bar{\varphi} \cos \bar{\psi} \cos \bar{\theta} - \sin \bar{\psi} \cos \bar{\varphi}) \right. \\ &+ (\sin \bar{\varphi} \cos \bar{\psi} \cos \bar{\theta} - \sin \bar{\psi} \cos \bar{\varphi}) (R_m - \bar{R}_m) \\ &+ \bar{R}_m (\cos \bar{\varphi} \cos \bar{\psi} \cos \bar{\theta} + \sin \bar{\psi} \sin \bar{\varphi}) (\varphi - \bar{\varphi}) \\ &+ \bar{R}_m (-\sin \bar{\varphi} \sin \bar{\psi} \cos \bar{\theta} - \cos \bar{\psi} \cos \bar{\varphi}) (\psi - \bar{\psi}) \\ &+ \left. \bar{R}_m (-\sin \bar{\varphi} \cos \bar{\psi} \sin \bar{\psi}) (\theta - \bar{\theta}) \right\} \underline{1}_{ym} \end{aligned}$$

$$\begin{aligned}
& + \left\{ \bar{R}_m \sin \bar{\varphi} \sin \bar{\theta} \right. \\
& \quad + \sin \bar{\varphi} \sin \bar{\theta} (R_m - \bar{R}_m) \\
& \quad \left. + R_m \cos \bar{\varphi} \sin \bar{\theta} (\varphi - \bar{\varphi}) \right\} \frac{1}{z_m}
\end{aligned}$$

The uncertainty in ground track position varies as a function of the position of the ground track along the lunar surface. An examination of the above equation reveals the following facts.

The uncertainty in vertical distance from the surface varies from a maximum of $R_m - \bar{R}_m$ to a minimum of $(R_m - \bar{R}_m) \cos \bar{\theta}$. For small angles of $\bar{\theta}$ the uncertainty in height is almost independent of longitude.

The uncertainty in downtrack distance is a maximum at $\bar{\varphi} = \pi/2$ and is equal to:

$$\bar{R}_m (\psi - \bar{\psi}) - (\varphi - \bar{\varphi})$$

The uncertainty in crosstrack distance is a maximum at $\bar{\phi} = \pi/2$ and is equal to $(R_m - \bar{R}_m) \sin \bar{\theta}$. All of these errors are basically composed of two quantities: radar altitude and time.

These analyses can be performed on the reduced data from the operational mission.

Orbital computation is made in a computer program of the general form:

```

C      LUCOM ORBIT CALCULATIONS
      DIMENSION R(400), Q(400)
      CALL F1TYIO (1, A, E)
      JMAX=360
      DO 4 J=1, JMAX
      H=J/57.3
      P=.50-COSF(H)/E-.5*COSF(2.*H)
      R(J)=A*(1+E*E *P)
4      Q(J)=H+2.*E*SINF(H)+E*E*1.25*SINF(2.*H)
      CONTINUE
      N1=1
      NN=5
      PUNCH102

```

```

102  FORMAT(9X,24H LUCOM ORBIT CALCULATIONS)
6    PUNCH 100, N1, (R(I), I=N1, NN)
     PUNCH 101, N1, (Q(I), I=N1, NN)
     N1=NN+1
     NN=NN+5
     IF(NN-364)6, 6, 105
105  CONTINUE
100  FORMAT(3HR--, I4, 5X, 5F10.4)
101  FORMAT(3HQ--, I4, 5X, 5F10.4/)
     END
     EOF

```

where the printouts shown in the dimension statement (on the second line of the program) are R, the radius vector of the vehicle position, and Q, the angular position in the orbit in radians. This may be referenced to the line of nodes to represent the true anomaly. This program, or a similar one, would furnish the base line for the LUCOM measurements.

6.1.3 FOURIER SERIES TECHNIQUE

A possible method for determination of the lunar surface figure is to represent the data by a Fourier series. A computer program can be devised to determine the coefficients of the series by numerical integration, and by the use of a least squares fitting routine, the most probable shape of the lunar spheroid can be derived.

The computer program shown below is typical. This program will determine the coefficients of a Fourier series to any desired number of harmonics both odd and even. This particular program does not include the least squares fitting routine; however, that addition would be similar to the program shown in section 6.1.4.

```

          DIMENSION X(500)
          CALL F3TYIO (1, L)
          READ 2, N, (X(K), K=1, N)
2        FORMAT (I4/(F8.4))
          DO 1 J=1, L
          A=0.0
          B=0.0
          DO 3 I=2, N, 4
          ARG = 6.28318*I*J/N
          B=B+SINF(ARG)*X(I)

```

```

3      A=A+COSE (ARG)*X(I)
      B=2.0*B/N
      CALL F1TYIO (0, B)
      PUNCH 4, B
4      FORMAT (E15.9)
      A=2.0*A/N
      CALL F1TYIO (0, A)
1      PUNCH 5, A
5      FORMAT (E15.9)
      END
      EOF

```

The orbit elements $A_1, \omega_1, E_1,$ and T_1 are determined as discussed in 6.1.1. Point 1 is designated as zero time and the equation for the orbit is expressed in the form:

$$R = \frac{A_1 \sqrt{1 - E_1^2}}{1 + E_1 \cos(Q - Q_1)} \quad (6.1.3-1)$$

where $Q_1 = -\omega_1 T_1 - 2 E_1 \sin \omega_1 T_1$

Q is then computed for those values of time at which radar readings were taken according to:

$$Q_{NK} = \omega_1 (t_{NK} - T_1) + 2 E_1 \sin \omega_1 (t_{NK} - T_1), \quad (6.1.3-2)$$

the corresponding radar altitude is Y_{NK} . Then the lunar spheroid at t_{NK} is:

$$R_{MNK} = R_{NK} - Y_{NK}$$

$R_{MNK}(Q_{NK})$ is the expression for the lunar spheroid. It is convenient to represent the moon's figure in the form of a Fourier series. The coefficients are evaluated by the method of least squares. This procedure has the advantage of averaging out radar altitude errors. The expression for the figure becomes:

$$R_{MNK} = C_0/2 + \sum_r^r C_r \cos r Q_{NK} + \sum_r^r B_r \sin r Q_{NK}$$

R_{MNK} is determined from equations 6.1.3-1 and 6.1.3-2. N refers to the N th orbit and K refers to the K th reading of the N th orbit. One advantage

of this approach is that the number of harmonics that are chosen is arbitrary, but in any case, the method of least squares will determine the most probable values of the coefficients. For illustrative purposes, consider only the first harmonic. The equation of condition for the Nth orbit becomes:

$$R_{MN1} = C_0/2 + C_1 \cos Q_{N1} + B_1 \sin Q_{N1}$$

$$R_{MN2} = C_0/2 + C_1 \cos Q_{N2} + B_1 \sin Q_{N2}$$

$$\begin{matrix} \cdot & \cdot & \cdot & \cdot \\ \cdot & \cdot & \cdot & \cdot \\ \cdot & \cdot & \cdot & \cdot \end{matrix}$$

$$R_{MNK} = C_0/2 + C_1 \cos Q_{NK} + B_1 \sin Q_{NK}$$

The problem is to find the most probable values of C_0 , C_1 , and B_1 . Let

$$[AA] = \frac{1}{2^2} K$$

$$[BB] = \sum^k \cos^2 Q_{NK}$$

$$[CC] = \sum^k \sin^2 Q_{NK}$$

$$[RB] = \sum^k R_{MNK} \cos Q_{NK}, \text{ etc.}$$

The normal equations are:

$$[AA] C_0 + [AB] C_1 + [AC] B_1 = [RA]$$

$$[AB] C_0 + [BB] C_1 + [BC] B_1 = [RB]$$

$$[AC] C_0 + [BC] C_1 + [CC] B_1 = [RC]$$

Next find C_0 , C_1 , and B_1 by Cramer's Rule. The result is the most probable value of these coefficients.

The next step in the study was to utilize the altimeter data against the Apollo orbit base line to perform a simulated data utilization problem in determining the lunar figure. One procedure studied involves the use of an astronomically determined lunar radius as a point-of-departure for improvement.

For a given time, the true anomaly is calculated. The radar altitude at this time is measured and recorded. This measured altitude is added to radius of the moon. The radius of the moon is obtained from astronomical observation. The sum of measured altitude and the radius of the moon is labeled the measured radius of the satellite. Data for the measured radius of the satellite is accumulated over several hundred measurements. A least square fit is then applied to the equation of the orbit to obtain the most probable values of the semi-major axis, A , the eccentricity, E , and the angle between the periselenium and the ascending node, ωT . The radius of the orbit is then recalculated using these new orbit elements at the original time increments. The measured altitude is then subtracted from the calculated radius. The result is the most probable shape of the moon based on a least square fit, as shown in Figure 6.1.4-1.

In order to assess the utility of this method to the problem at hand, a representative problem was set up on the computer. An orbit was assumed with the following elements:

$$A = 1124 \text{ miles}$$

$$E = .032$$

$$\omega T = .785$$

This corresponds to an orbit with a maximum altitude of 80 miles and a minimum altitude of 8 miles. The results are presented in Table 6.1.4-1. The radius and true anomaly were computed for 365 equal increments of time. The results were printed at intervals of ten. In the table, R is the radius in miles and Q is the true anomaly in radians. For purposes of setting up the problem, it is assumed that the true shape of the moon in the plane of the orbit is an ellipse with a semi-minor axis of 1080 miles and a semi-major axis of 1080.6 miles.

In the actual reduction of data after the completion of the LUCOM mission, this shape is not known, and is in fact the parameter being sought. Also, this method is in no way dependent on the shape of the moon being represented by a simple analytical expression. In this representative problem,

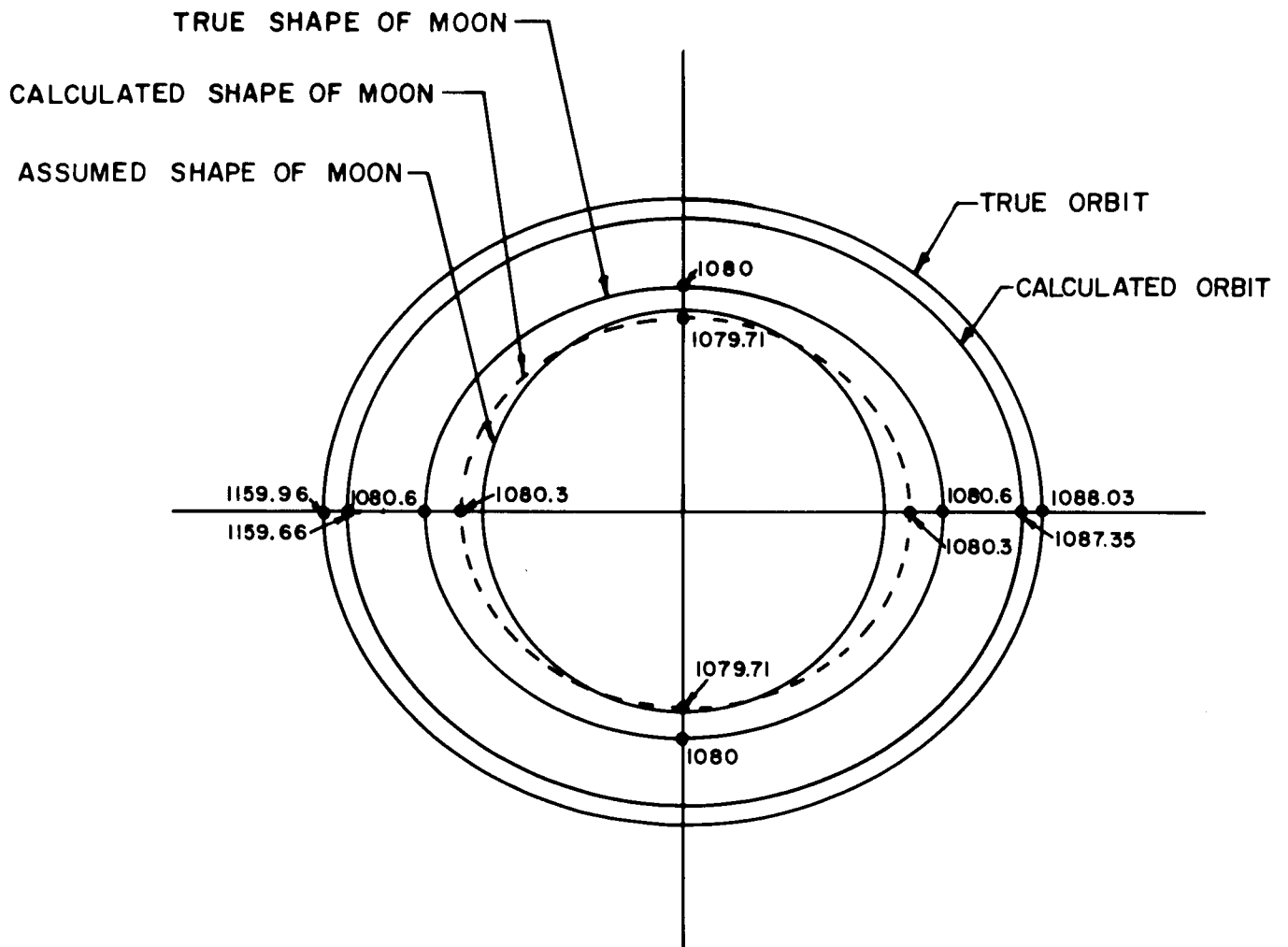


FIGURE 6.1.4-1

LEAST SQUARES FIT PROBLEM

the moon was assumed to be an ellipse merely for convenience in programming the problem. At any rate, the radius of the moon was computed for the same increments of anomaly as the satellite. These results appear under the column headed R1. Then the radius, H, that the altimeter would measure is R minus R1. In the problem, it was assumed that the best estimate of the shape of the moon was a circle of radius 1080 miles. The measured radius of the satellite was defined to be 1080 plus H. These values of measured radius were substituted into the equation of the orbit and new estimates of the orbit elements were obtained by the method of least squares. The results were:

$$A1 = 1123.7 \text{ miles}$$

$$E1 = .03200$$

$$\omega T1 = .78540$$

These new values for the orbit elements were substituted into the equation for the orbit to obtain new estimates of the radius and true anomaly of the orbit. These values appear under the columns headed RN and QN. The probable shape of the moon is then obtained from RN - H. The true error is obtained from RN - R. This value, of course, will not be known in the actual LUCOM mission.

The general character of the results is revealed in Figure 6.1.4-1. For this problem, in which it was assumed that the true shape of the moon in the plane the orbit was an ellipse and that the estimated shape was a circle, the resulting most probable shape (the dotted curve) passes through the assumed and actual shapes.

It will be noted that the error is distributed around the assumed shape at the limbs as well as the geometrical center. This was a natural result of the mode of operation of the program in which the true shape of the moon was not made to control at any point. In actual operation it might be possible to provide a weighting function for the data taken at the limbs where determinations from earth have more confidence.

In that case, the least squares fit would be made to pass through the limbs. It should be emphasized that the result reported was based on a single run of the data. Repeated runs should be made until the most probable shape is obtained.

The computer program used, which is typical of those which would be used in the LUCOM operational program, is shown below:

```
LUCOM ORBIT CALCULATIONS
DIMENSION R(365), Q(365), R1(365)
COMMON R
CALL F1TYIO(1, A, B, C, E, START, DELTA)
CALL F3TYIO(1, J1, J2)
AA=0.
BB=0.
CC=0.
BC=0.
AB=0.
AC=0.
A11B1=0.
A12B1=0.
A13B1=0.
DO50N=1, J1
AMWT=(START+(N-1)*DELTA-45.)/57.29578
AEE=A*E*E/2.
R(N)=A+AEE-AEE*COSF(AMWT*2.)-A*E*COSF
(AMWT)
Q(N)=AMWT+2.*E*SINF(AMWT)+1.25*E*SINF
(AMWT*2.)*E
QM=Q(N)+.7854
T=COSF(QM)*COSF(QM)/(C*C)+SINF(QM)*SINF
(QM)/(B*B)
R1(N)=1/SQRTF(T)
A11=R(N)/A
A12=-COSF(AMWT)-E*COSF(2.*AMWT)
A12=A12+E
A13=-SINF(AMWT)-E*SINF(AMWT*2.)
B1=B-R1(N)+UNIF(0, .04, -.04)
AA=AA+A11*A11
BB=BB+A12*A12
CC=CC+A13*A13
BC=BC+A12*A13
AB=AB+A11*A12
AC=AC+A11*A13
A11B1=A11B1+A11*B1
A12B1=A12B1+A12*B1
A13B1=A13B1+A13*B1
CONTINUE
D=AA*BB*CC+AB*BC*AC+AC*AB*BC-AC*BB*
AC-BC*BC*AA-CC*AB*AB
```

```

XO=A11B1*BB*CC+AB*BC*A13B1+AC*A12B1*BC
  -A13B1*BB*AC-BC*BC*A11B1-CC*A12B1*AB
YO=AA*A12B1*CC+A11B1*BC*AC+AC*AB*A13B1
  -AC*A12B1*AC-A13B1*BC*AA-CC*AB*A11B1
ZO=AA*BB*A13B1+AB*A12B1*AC+A11B1*AB*BC
  -AC*BB*A11B1-BC*A12B1*AA-A13B1*AB*AB
WT=.7853975+AO/(D*A*E)
A1=A+XO/D
E1=E+YO/(D*A)
PUNCH 102
PUNCH 103
PUNCH 104
PUNCH 105
PUNCH 109, D, XO, YO, ZO
PUNCH 110, WT, A1, E1
PUNCH 106
DO60N=1, J1, J2
ANGLE=START+(N-1)*DELTA
AMWT1=ANGLE/57.29578-WT
P1=.5-COSF(AMWT1)/E1-.5*COSF(AMWT1*2.)
RN=A1*(1+E1*E1*P1)
QN=AMWT1+2.*E1*SINF(AMWT1)+1.25*E1*E1*
  SINF(AMWT1*2.)
U=RN-R(N)
S=U+R1(N)
60 PUNCH107, ANGLE, R(N), Q(N), R1(N), RN, QN, S, U
102 FORMAT(9X, 24HLUCOM ORBIT CALCULATIONS/)
103 FORMAT(2X, 45HDETERMINATION OF THE SELE-
  NOID WITH AN ASSUMED)
104 FORMAT(2X, 46HSHAPE BY MEASURING ORBIT
  ALTITUDE AND APPLYING)
105 FORMAT(2X, 27HTHE METHOD OF LEAST SQUARES)
109 FORMAT(4H D =, E11.5, 6H XO =, E11.5, 6H
  O =, E11.5, 6H ZO =, F9.4)
106 FORMAT(3X, 5HANGLE, 8X, 1HR, 7X, 1HQ, 10X,
  2HR1, 9X, 2HRN, 6X, 2HQN, 7X, 4HRN-H, 5X, 4HRN-R)
107 FORMAT(2F11.5, F8.5, 2F11.5, F8.5, F11.5, F8.5)
110 FORMAT(4HWT =, E11.5, 6H A1 =, E11.5, 6H
  E1 =, E11.5)
END
EOF

```

LUNAR ORBIT CALCULATIONS

DETERMINATION OF THE SELENOID WITH AN ASSUMED SHAPE BY MEASURING ORBIT ALTITUDE AND APPLYING THE METHOD OF LEAST SQUARES

D = .11800E+08 X0 = -.34038E+07 Y0 = -.55288E+04 Z0 = 1542.80*
 WT = .78540E+09 E1 = .11237E+04 A1 = .32000E-01

ANGLE	R	Q	RI	RN	QN	RN-H	RN-R
0.00000	1099.14227	-.87065	1080.24897	1098.86059	-.83194	1079.96730	-.28168
10.00000	1094.91540	-.68516	1080.35962	1094.63485	-.64878	1080.07907	-.28055
20.00000	1091.60749	-.49402	1080.46501	1091.32782	-.46436	1080.18534	-.27967
30.00000	1089.33468	-.29836	1080.54811	1089.05561	-.27901	1080.26904	-.27907
40.00000	1088.17761	-.09979	1080.59404	1087.89883	-.09307	1080.31526	-.27878
50.00000	1088.17761	.09979	1080.59404	1087.89881	.09306	1080.31524	-.27880
60.00000	1089.33468	.29836	1080.54811	1089.05555	.27900	1080.26898	-.27913
70.00000	1091.60749	.49402	1080.46501	1091.32773	.46436	1080.18524	-.27977
80.00000	1094.91540	.68516	1080.35962	1094.63472	.64877	1080.07894	-.28068
90.00000	1099.14227	.87065	1080.24897	1098.86044	.83193	1079.96714	-.28183
100.00000	1104.14192	1.04994	1080.14848	1103.85872	1.01356	1079.86529	-.28320
110.00000	1109.74467	1.22311	1080.06960	1109.45995	1.19344	1079.78489	-.28472
120.00000	1115.76467	1.39082	1080.01921	1115.47832	1.37145	1079.73286	-.28635
130.00000	1122.00741	1.55423	1080.00016	1121.71938	1.54750	1079.71213	-.28803
140.00000	1128.27705	1.71487	1080.01236	1127.98733	1.72159	1079.72263	-.28972
150.00000	1134.38308	1.87441	1080.05359	1134.09171	1.89377	1079.76223	-.29136
160.00000	1140.14614	2.03449	1080.11994	1139.85323	2.06415	1079.82703	-.29291
170.00000	1145.40271	2.19650	1080.20569	1145.10840	2.23288	1079.91138	-.29432
180.00000	1150.00863	2.36145	1080.30303	1149.71309	2.40017	1080.00748	-.29554
190.00000	1153.84192	2.52985	1080.40200	1153.54536	2.56623	1080.10544	-.29656
200.00000	1158.80365	2.70167	1080.49110	1158.50631	2.73132	1080.19376	-.29734
210.00000	1158.81952	2.87636	1080.55874	1158.52165	2.89571	1080.26087	-.29787
220.00000	1159.83987	3.05296	1080.59529	1159.54175	3.05968	1080.29717	-.29812
230.00000	1159.83987	3.23023	1080.59529	1159.54177	3.22350	1080.29719	-.29811
240.00000	1158.81952	3.40683	1080.55874	1158.52171	3.38746	1080.26093	-.29781
250.00000	1156.80365	3.58152	1080.49110	1156.50639	3.55186	1080.19385	-.29726
260.00000	1153.84192	3.75334	1080.40200	1153.54548	3.71695	1080.10556	-.29644
270.00000	1150.00871	3.92174	1080.30303	1149.71331	3.88301	1080.00763	-.29540
280.00000	1145.40271	4.08669	1080.20569	1145.10857	4.05030	1079.91154	-.29415
290.00000	1140.14614	4.24869	1080.11994	1139.85342	4.21903	1079.82722	-.29272
300.00000	1134.38308	4.40877	1080.05359	1134.09192	4.38941	1079.76243	-.29116
310.00000	1128.27705	4.56831	1080.01236	1127.98754	4.56159	1079.72285	-.28951
320.00000	1122.00742	4.72895	1080.00016	1121.71960	4.73567	1079.71234	-.28782
330.00000	1115.76467	4.89237	1080.01921	1115.47853	4.91173	1079.73307	-.28614
340.00000	1109.74467	5.06008	1080.06960	1109.46015	5.08973	1079.78508	-.28452
350.00000	1104.14192	5.23324	1080.14848	1103.85890	5.26962	1079.86547	-.28302
360.00000	1099.14220	5.41253	1080.24897	1098.86053	5.45125	1079.96730	-.28168

TABLE 6.1.4.-1

The basis on which vertical control for photographs must depend is definition of the lunar surface. This in turn depends primarily on derivation of the shape and size of the lunar spheroid as discussed in section 6.1.

The resolution of body angular motions becomes increasingly important in coordinating photographic data with the radar measurements. Although the problem has not been completely explored in this study, all the basic techniques are present or available. In the next phase, this problem should be processed in the simulator routines to determine feasibility of the methods proposed.

One problem characteristic of those encountered in this task is that for small angles of inclination of the radar beam, the radar spherical wave front strikes the ground first in the sub-orbital path directly below the vehicle so that the first radar return is from that point instead of from the nadir point of the photograph. If the ground has a significant persistent slope, the first return will be from an angle which is normal to that slope. Consequently, the radar ranges to a point which has some other relationship to the photograph than that which would be expected from the alignment and boresighting in the vehicle installation.

These problems are understood and may be resolved by going through the following steps:

- (a) Determine the orientation of the vehicle (from the Apollo guidance system) relative to the orbit plane and local vertical.
- (b) Through the coordinate transformations shown in section 3.1.4 of this report, determine the true direction of the boresight of camera and radar.
- (c) By the use of profiles of all adjacent sub-orbital tracks, determine the "persistent" slope of the terrain. This will require judgement and use of the wide angle photographs taken in orbit as well as the Pic-du-Midi photographs to avoid errors caused by local changes of slope craters or other details.
- (d) If a "persistent" slope can be determined within one-half radar beamwidth plus the vehicle resolved boresight angle determined in (b), then the geometry shown

in Figure 2.2.2-1 will give the best estimate of the point on the terrain measured by the radar at the instant in question. This process would produce an offset line of altimeter readings across the photographic record which would be the vertical for the photographs. The geometry of the coordinate transformations around the body axes would give the normal direction and plane in which the photographs would be rectified. Radar data is not subject to rectification since it consists of single point determinations.

The process mentioned in item (c) above, and indeed all the manipulations mentioned, may be automated in computer programs. One such program has been investigated during this study and seems very promising for application to LUCOM. This is an IBM 1620 program for numerical surface techniques and contour map plotting. This program is designed for quantitative description of surfaces by making numerical or analytical approximations to a set of coordinate values describing a surface. The contour data will be plotted automatically by use of the IBM 1627 plotter.

This program has the capability of taking a set of randomly spaced data in X, Y, and Z and interpolating to another set of matrix points. This would be used in the process described above to interpolate the offset altimeter data to the photographic nadir points.

This computer program in an early form was run using data from earth profiles. That program incorporated a rather simple weighted interpolation scheme, weighting the data points inversely as their distances from the computed point.

The new program has the following basic functions:

- (a) Surface Techniques Program
 - (1) Numerical approximation over a uniform grid.
 - (2) Smoothing.
 - (3) Interpolation to a finer grid.
 - (4) Grid-to-grid operations.
 - (5) Surface fitting with orthogonal polynomials.
 - (6) Equation evaluation over a uniform grid.

(b) Contour Map Plotting Program

- (1) Contouring.
- (2) Map annotation.

This program is recommended for use during the next phase in connection with the earth profile and data from the simulator.

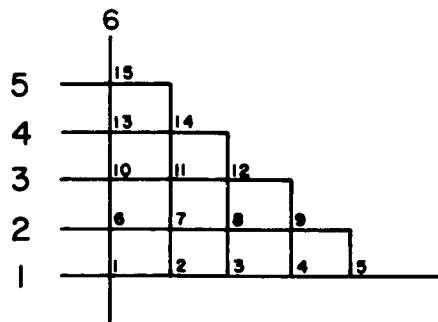
6.3 DETERMINATION OF SLOPES AND SURFACE RELIEF

The same computer program discussed in section 6.2 will be used to interpolate the data taken on the back side of the moon and in other areas where it is desirable to plot contours based on the altimetry data. Figure 3.2.1-2 shows the relationship of orbits at the point of maximum latitude. When these tracks are examined in true scale, it appears that adjacent orbits are within less than 150 feet of each other for a distance of 1° moon central angle. In the center of that interval, they cross over, so that for a distance of several miles they are within less than a hundred feet of each other. Looking at the crossing of the first and sixth orbits, it is evident that all the orbits are within a 0.188 mile latitudinal distance for a distance of about 100 miles. This same situation holds true for the other 18 orbits.

The width of the band within which all the orbit crossings occur is approximately:

$$\begin{aligned} \Delta d &= d - d \cos \varphi && (\varphi \approx 10^\circ) \\ &= 200 - 196.96 = 3.04 \text{ miles} \end{aligned}$$

The total number of orbit crossings may be obtained by considering the geometry in Figure 6.3-1 below:



This figure shows the crossings generated by six orbits. It will be noted that the figure suggests a triangular matrix. It contains a total of 15 crossings. The equation for this relationship is:

$$\begin{aligned} C &= \frac{(n - 1)^2}{2} + \frac{n - 1}{2} \\ &= \frac{n^2 - n}{2} \end{aligned}$$

where n = number of orbits.

Thus, for 24 orbits, the total crossings will be equal to:

$$C = \frac{(24)^2 - 24}{2} = 276$$

All occur within a space of approximately 3 miles by 480 miles.

It is apparent that the areas near the maximum latitude points of the orbits both on the front and back of the moon will be very closely covered, and rendering of slopes and detail in those areas will be very amenable to automatic contour plotting as proposed in the LUCOM Program.

6.4 INTERIM SELENODETIC CONTROL

To provide an improved selenodetic control network, the same IBM 1620 program and IBM 1627 plotter will be used, although it is not known at this point to what accuracy the plotter will perform. However, there is great doubt that its performance would be comparable to a dividing engine.

The program contains a least squares fitting routine so that the extrapolated output data will represent the maximum utilization of the input data. The routine will take the coordinates of the input data and extrapolate to the coordinates of the selenodetic control network. The data thus extrapolated to the selenodetic control coordinates will then form the basis for the surface network. Thus, the annotated output will form the control network regardless of the accuracy of the plotter.

The IBM 1620 computer program referenced is shown in the form of a flow diagram in Figure 6.4-1. This program has not been run in connection with the LUCOM study work, but arrangements have been made with IBM to utilize this routine when further work is authorized.

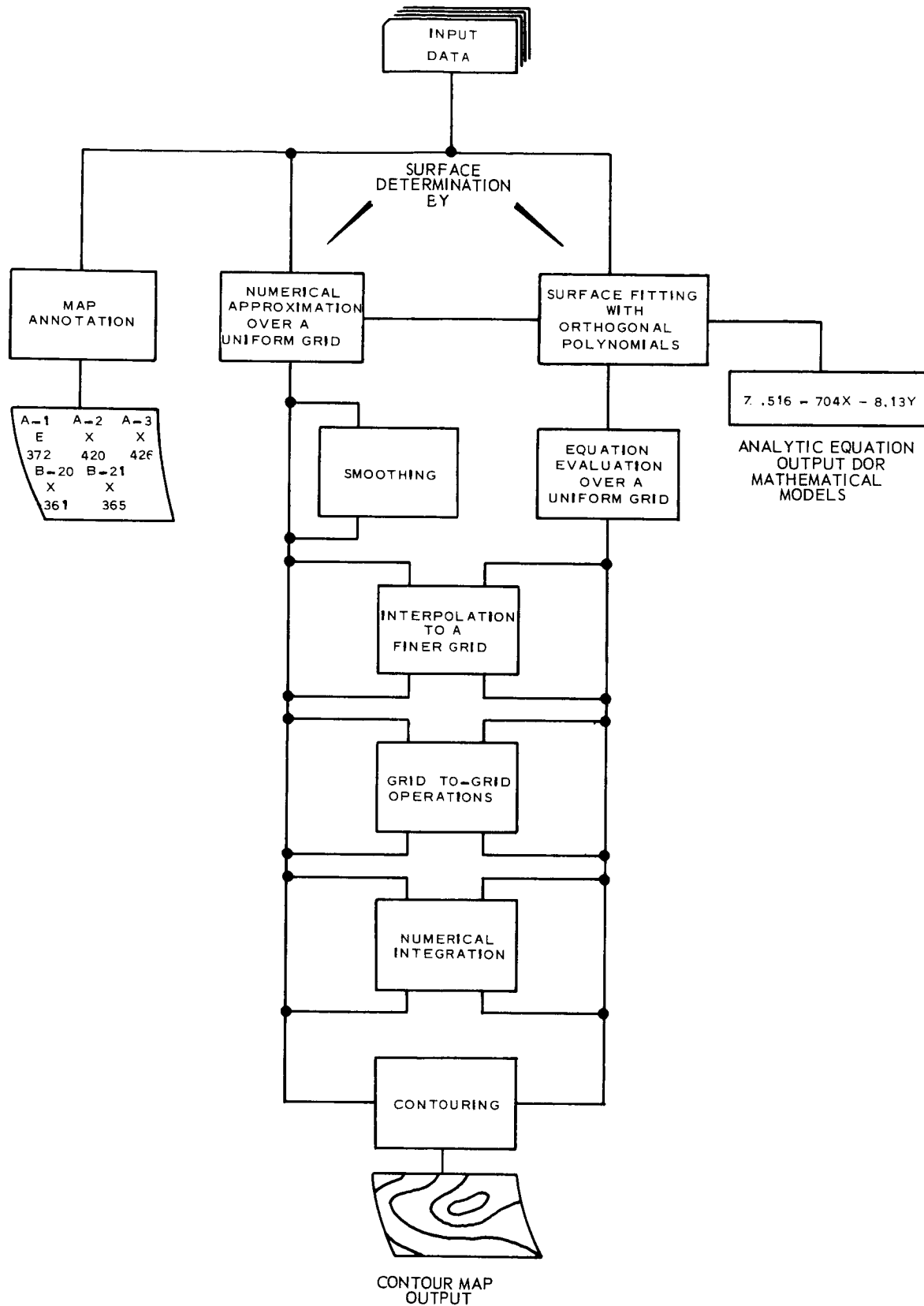


FIGURE 6.4-1 NUMERICAL SURFACE TECHNIQUES

This section would not be complete without a word about the computer programs used and planned for the LUCOM project.

ILLUMINATED AREA ROUTINE

In the beginning of the study, a program was devised to compute the relationship between altitude, h ; illuminated area, A ; pulse width, τ ; and angle of incidence of the elliptical projection of the beam on the surface, θ_i . This program supplied the indicated parameters to perform the first radar loop gain computations necessary to give a preliminary estimate of radar size, pulse width and beamwidth.

Results obtained with this program were reported in the November 11 progress report; however, to review those briefly, it was shown that pulse lengths beyond about 1.5 microseconds gave diminishing returns for a 5° beam. This subsequently proved also to be the case for the 3° beam used as a basis for the final radar parametric work as a result of the radar profile parametric analysis reported in section 4.2.4.

This computer program is shown below:

```

PUNCH 6
READ 4, ANG
W=.087266465
DO 1 1=1, 56
READ 2, H, TH
PUNCH 3, H, TH
AMAX=0.
RMAX=0.
TH=TH*.017453293
ZMAX=0.
R2MAX=0.
PMAX=0.
Z=ANG
DO 7 J=1, 700
AS=SINF(TH+W)
AC =COSF(TH+W)
BS =SINF(TH-W)
BC = COSF(TH-W)
XO =H/2.*(AS/AC+BS/BC)
XC=H*SINF(TH)/COSF(TH)
YC =H*SINF(W)/(COSF(W)*COSF(TH))

```

```

A =H/2.*(AS/AC-BS/BC)
B=A*YC/SQRTF(A*A-(SC-XO)**2)
RA=SQRTF((H/COSF(TH-Z)+246. )**2-H*H)
RB=SQRTF((H/COSF(TH-Z))**2-H*H)
C=A*A/(B*B)-1.
XA=-XO/C*(1.-A/B*SQRTF(1.+C*(RA*RA-B*B)
/XO**2))
XB=-XO/C*(1.-A/B*SQRTF(1.+C*(RB*RB-B*B)
/XO**2))
D=ATANF(XA/SQRTF(RA*RA-XA*XA))
A1A=RA*RA*(1.5707963-D-XA/RA*SQRTF(1.-
(XA/RA)**2))
E=ATANF((XA-XO)/SQRTF(A*A-(XA-XO)**2))
A2A=A*B*(1.5707963+E+(XA-XO)/A*SQRTF(1.-
((XA-XO)/A)**2))
F=ATANF(XB/SQRTF(RB*RB-XB*XB))
A1B=RB*RB*(1.5707963-F-XB/RB*SQRTF(1.-
(XB/RB)**2))
G=ATANF((XB-XO)/SQRTF(A*A-(XB-XO)**2))
A2B=A*B*(1.5707963+G+(XB-XO)/A*SQRTF(1.-
((XB-XO)/A)**2))
AT = A1A+A2A-A1B-A2B
RC=(RA+RB)/2.
R=SQRTF(RC*RC+H*H)
R2 = SQRTF(RA*RA + H*H)
P=AT/R**4
IF(P-PMAX)8,9,9
9 PMAX=P
  AMAX=AT
  RAMX=R
  R2MAX=R2
  ZMAX=Z
7 Z=Z-.0001745329
8 DB=4.343*LOGF(AMAX)
  ZMAX=ZMAX*57.29578
1 PUNCH 5, RMAX, R2MAX, ZMAX, DB
2 FORMAT(F7.0, F4.0)
3 FORMAT(6H ALT =F9.0, 2X, 8H THETA =F4.0)
4 FORMAT(F20.9)
5 FORMAT(92F10.0, F6.2, F7.2)
6 FORMAT(3X, 6H R CEN, 3X, 8H R PULSE, 2X, 2H
  Z, 4X, 5H AREA)
  END
  EOF

```

RADAR SIMULATOR ROUTINE

An advanced form of this program which is to be used as a true radar simulator routine has been written but has not yet been used in the LUCOM Program. The program incorporates the additional capabilities of: (1) provision for a radar antenna illumination pattern such as $\frac{\sin x}{x}$ or other real pattern and (2) the geometry to permit attitude angles to be programmed into the computer so that the true antenna pointing angle is resolved in terms of pitch, roll and yaw of the space craft. This program has been run in preliminary work, but has not been used in the LUCOM Study due in part to lack of knowledge of the Apollo attitude program during LUCOM data acquisition. It is planned to use this in the next phase of the program with appropriate assumptions in the event the Apollo data is still unavailable.

The preliminary form of this program is reproduced below. The constants in this specific program are for another project, e. g., antenna beam is 10.3 degrees. These are changed for each application by a simple read-in arrangement.

```

CALL F1TYIO (1, H, CON, T2, THETVE, THETA,
             PHEVE, DBA, DBT, T1)
CALL F3TYIO (1, IEXP, NT, NP, NQ)
T0=2.0325*H
COAO=COSF(THETVE)*COSF(PHEVE)*COSF
      (THETA)-SINF(THETVE)*SINF(THETA1A)
AO=ATANF(SQRTF(1./COAO/COAO-1.))
PUNCH 102
IF(SENSE SWITCH 1) 997, 996
996 IF(SENSE SWITCH 2) 91, 92
91 PUNCH 90
90 FORMAT (23HANTENNA BEAM = 10.3 DEG//)
997 PUNCH 995
995 FORMAT (18HANTENNA GAIN = 1.0//)
92 PUNCH 103
PUNCH 104, H, IEXP, CON, NT, NP, NQ, T2, THETVE,
      THETA, PHEVE, AO, T0, DBA, DBT1, T1
PUNCH 105
DT = (T2 - T1)/NT
GAIN=10. **((DBA+DBT)/10.)
H=H*1000
T=T1
R2=H+T1*492.
HS=H*H

```

```

DR2=DT*492.
SIAO=SINF(AO)
COAO=COSF(AO)
TAAOH=SIAO*H/COAO
DO 40 I=1, NT
T=T+DT
R2=R2+DR2
P2=SQR TF(R2*R2-HS)
R1=R2-246.
IF(R1-H) 10, 10, 14
10 P1=0.
GO TO 9
14 P1=SQR TF(R1*R1-HS)
9 DP=(P2-P1)/NP
P=P1-DP/2
EMM=0.
DO30J=1, NP
P=P+DP
R=SQR TF (HS+P*P)
SIGO=CON*(H/R)**IEXP
DQ=3.1416/NQ
Q=-DQ/2
IF(SENSE SWITCH 1) 999, 998
999 EM4=NQ
GO TO 30
998 EM4=0.
DO 20 K=1, NQ
Q=Q+DQ
SINQ=SINF(Q)
COSQ=COSF(Q)
TANALP=P*SINQ*COAO/(P*COSQ-TAAOH)
ALP=ATANF(TANALP)
TR=P*COAO*COAO*(P-2.*TAAOH*COSQ)
+SIAO*SIAO*(H*H+P*P*SINQ)
TANGAM=SQR TF(TR)/(H-P*COAO*SIAO*SINQ)
GAM=ATANF(TANGAM)
IF(SENSE SWITCH 2) 93, 94
93 IF(GAM-.09) 149, 149, 151
94 THETA=ATANF (COSF(ALP)*TANGAM)
SECPHE=COSF(THETA)/COSF(GAM)
PHE=ATANF (SQR TF(SECPHE*SECPHE-1.))
A=2.035*SINF(THETA)
B=COSF(THETA)
C=2.035*SINF(PHE)

```



```

        IF(THETA) 12, 11, 12
11      EH=1.
        GO TO 13
12      EH=B*SINF(8.*A)/SINF (A)/8.
13      IF(PHE) 16, 15, 16
15      EE=1.
        GO TO 20
16      EE=SINF (8.*C)/SINF(C)/8.
        GO TO 20
49      EH=1.
        EE=1.
        GO TO 20
151     EH=0.
        EE=0.
20      EM4=EM4+EH*EH*EE*EE
30      EMM=EMM+EM4*P*DP*DQ*SIGO/R**4*GAIN
        PRA=1.22E-5*EMM
        IF(PRA) 3, 3, 1
1       DB=4.343*LOGF (PRA)
        GO TO 2
3       DB=0.
2       PUNCH 108, T, P1, P2, EM4, EMM, PRA, DB
40      CONTINUE
102     FORMAT (9X, 19H  PULSE PROFILE//)
103     FORMAT (2X, 72HH  IEXP  CON  NT  NP  NQ
           T2  THETVE  THETA  A  PHEVE  1  AO  T0
           DBA  DBT  3H  T1)
104     FORMAT(F5.1, I5, F5.2, 3I4, F6.1, F8.5, F7.5,
           F6.4, F5.3, F6.1, 2F5.1, F5.3/)
105     FORMAT (70H  T  P1  P2  EM4  EMM
           1  PRA  DB/)
108     FORMAT (F9.6, 2F11.4, 3E11.5, F11.4/)
        END
        EOF

```

6.5.3 LEAST SQUARES ROUTINE

This routine has been discussed and is shown in section 6.1.

6.5.4 FOURIER COEFFICIENTS ROUTINE

This program has been discussed and is shown in section 6.1.

6.5.5 CONTOUR AND SURFACE FITTING AND PLOTTING
ROUTINE

This program has been discussed in section 6.4.

6.5.6 BENCH MARK RECOGNITION PROGRAM

The use of this program has been discussed briefly in section 3.3.2 of this report. The function of this program is to find the best correlation in some related dimension between two sets of data. In this case, it is proposed to use the altimeter profiles taken in the sub-orbital tracks where they lie superposed for long distances at the points of maximum latitude of the orbit (discussed in 6.3). This computer program is part of a proprietary technique which has been the subject of continuing work at LTV for a number of years and is completely developed and understood in theory and practice, having been extensively flight tested in sub-sonic flights. The technique has been extended in theoretical work to re-entry missile velocities and environments. Because of the great amount of theoretical and successful flight test work which has gone into this technique, it is felt to be guaranteed of success. This technique has not been analyzed in detail relative to LUCOM, but is an important task in the next phase. This will require adoption of an acceptable lunar surface model which may be used in simulator runs and analyses.

7.0 CONCLUSION AND RECOMMENDATIONS

N65-23291

Much work has been accomplished towards understanding the conceptual demands of a system which performs its tasks in two environments (space and earth) and at separate times (while in orbit and subsequently in the data-reduction center). Part of what has been accomplished remains purely theoretical, but a surprising amount of definitive data has been generated in six months. Whether these physical and functional characteristics of the system components will survive in the form presented in this report, remains purely speculative. As factual environmental data filters into the investigative efforts, and certain of the many assumptions made through necessity are proven invalid, design modifications will be inevitable. Regardless of the scope of future changes, however, the results of this Phase I LUCOM investigation indicate that: (1) a practicable radar sensor can be designed for operation at 80 nautical miles above the lunar surface; (2) the data could be converted into digital form and transmitted back to earth for processing; (3) methods and techniques can be conceived for recreating the profiles and using them to map local features; (4) altimetry readings can be used, in combination with associated Apollo data, to recompute a more accurate lunar figure; and (5) the total system can be designed within the physical limits imposed by the Apollo environment.

Yet much work remains to be done before the concept approaches reality. The Phase II Program should carry the development of the system design further towards the goal of maximum effectiveness. The "Statement of Work for Phase II Study Program" which follows in Section 8.0, contains a precise definition of LTV recommendations for continuing this effort. Parallel tasks which could lead to the fabrication of a "flyable" prototype system for aircraft tests, are not included. It is LTV's opinion, however, that such a system could be designed and made ready for high altitude flight tests within 14-16 months from contract negotiation.

Author

8.0 LUCOM PHASE II STATEMENT OF WORK

8.1 INTRODUCTION

This document has been prepared to define, in preliminary form, general study tasks for Phase II of the LUCOM Research Program. The Statement of Work outlines the LTV Military Electronics Division technical approach towards a continuing study of the LUCOM conceptual design feasibility.

Major emphasis in Phase II will be placed on the techniques and data reduction processes required to convert the raw digital profile information to useable knowledge of the lunar geophysical properties.

Additional emphasis will be placed on efforts to expand the scientific utility of the LUCOM experiment by increasing the sophistication of the radar sensor and compounding its functions. By analyzing the total structure of the return signal, including leading edge, it appears feasible to develop not only surface profile data, but also to make statistical inferences of subsurface structure and surface reflectivity. The rationale justifying extension of original LUCOM objectives to include physical characteristics other than surface relief, is based on the complex dependence of return signal structure on surface and subsurface geometry, orientation of scatterers with respect to the antenna, and electromagnetic characteristics of the scatterers. These data represent a significant contribution to the scientific investigation of the moon, and as such should be considered in constructing a final equipment configuration for the LUCOM Sensor. Investigations and studies leading to functional designs which can recover this type of information is not only pertinent to Phase II, but also represents an economical way to enhance the utility of the experiment with a minimal increase of overall development costs.

8.2 OBJECTIVES AND SCOPE

8.2.1 OBJECTIVES

The accomplishment of tasks outlined in this statement are aimed at:

- (a) Expanding and supplementing the analyses initiated in Phase I study.
- (b) Extending the systems studies to include up-dated environmental information.
- (c) Advancing the LUCOM functional design towards a more adaptable physical system in consonance with performance requirements.
- (d) Providing more comprehensive techniques for data reduction of LUCOM profile information.

8.2.2 SCOPE

The tasks in this paper are limited to analysis, investigation, and simulation. Although the ultimate goal of this effort is to develop an engineering model and/or critical hardware components, a stable basis for system fabrication must first be provided. Generally, these items represent a continuation of work performed during the initial six-month effort, but additional tasks have been introduced to broaden the analysis and to include a higher degree of sophistication in signal prediction and interpretation, sensor design, and data handling. All of the work outlined in this proposal could be performed within an 8 to 12 month period, depending on the man power loading factor used.

8.3 TASKS

8.3.1 LUNAR SURFACE RELIEF MODEL

A representative lunar surface relief model shall be established for use in statistical studies as a basis for system design parameters, and for limited assessment of the theoretical performance of the LUCOM sensor. It is not required that the model be a duplicate of the real surface in a physical sense. The model need only display physical characteristics which are typical of the surface. It can be in the form of analytical or statistical description, a digital representation, or analog simulation model. Final form and content of the model will be subject to NASA approval. Efforts directed toward developing the model will include:

- (a) Categorization of lunar relief into classes of typical surface roughness.
- (b) Definition of an electromagnetic scattering process which reasonably describes the process(es) anticipated for the lunar surface and the subsurface.
- (c) Definition of modeling equations descriptive of the system dynamics and their programming for combinations of analogue and digital simulation.
- (d) Design and construction of such acoustic simulation devices as are necessary to analogue simulation.

8. 3. 2 SYSTEM SIMULATION

Existing computer routines will be modified or extended, as required, and utilized in conjunction with the Lunar Surface Model to simulate (in a limited manner) the LUCOM System performance. An arbitrary flight profile will be assumed, and instrumentation accuracies will conform to the latest available figure published. The simulation results will provide approximate performance estimates which are required as basic input to the Data Useability Studies. The programming of model equations to provide a dynamic response to external inputs (e. g. , orbital data, vehicle perturbations, etc.), and to determine the effects of varied surface characteristics on sensor performance, will also be accomplished.

8. 3. 3 STATISTICAL SENSOR DESIGN

During Phase I, elementary statistical methods were used to analyze the LUCOM sensor performance. These methods will be applied to several detection schemes such as multiple threshold detection, pulse height analysis, total and peak signal power, etc. The mathematical processes required to extract information contained in return signal for each of the detection techniques will be defined. The objective of the task is definition of realizable detection techniques and evaluation of the techniques relative to total loop gain requirements. Included are the following sub-tasks:

- (a) Analysis of return signal structure to determine the relationships between the structure and the lunar surface characteristics.

- (b) Feasibility analysis aimed at derivation of realizable data extraction techniques for recovering "measures" of surface characteristics.
- (c) Application of statistical design methods of Communication Theory to the evaluation of the various detection schemes. These results will be used to determine signal-to-noise ratios required for detection at a practical level of accuracy.
- (d) Confirmation of theoretical results through appropriate simulation using the lunar surface model as the test input.

8. 3. 4 TRADE-OFF STUDIES

Results of the statistical analysis will be used in system trade-off studies to optimize peak power, system weight and volume, sensor error, and detection probabilities. The studies will be expanded to include a wider spectrum of radar characteristics, i. e., a greater selection of beam-widths and pulse repetition frequencies will be included, and the additional weight-volume parameters of a prime power supply will also be considered. The task objective will be met when a realizable system yielding the maximum total data consistent with overall development economy is defined.

8. 3. 5 ANTENNA STUDY

The objective of the antenna study is to provide the latest data on practical antenna configurations suitable for LUCOM application. It is anticipated that the ultimate system configuration will incorporate a large aperture and narrow beamwidth into its hardware implementation. Results of Phase I clearly indicate that antenna size and weight are controlling factors which will significantly weight the selection of an operational system. Because of their potential for light-weight, high-degree performance, particular emphasis shall be placed on inflatable type antennas.

8. 3. 6 DATA-LINK TECHNOLOGY

8.3.6.1 Storage

A detailed study of advanced state-of-the-art memory devices will be accomplished to establish definitive design goals for LUCOM data storage. Emphasis will be placed upon techniques for reducing the power consumption without sacrificing performance characteristics.

8.3.6.2 Bandwidth

A study will be made of the telemetry technique for multiplexing orthogonal pulse waveforms to improve the bandwidth efficiency by a significant factor over a conventional 8-bit PCM system. An 8:1 improvement in bandwidth efficiency has been claimed, thus allowing a 9 db reduction in transmitter power.

8.3.7 DATA USEABILITY TECHNIQUES

Four major system objectives have been described and defined in the Phase I Study, viz. ,

- (a) Recompute moon's size and shape
- (b) Provide vertical control for photography
- (c) Establish ground track profiles to map back side of moon
- (d) Provide interim selenodetic control net.

A major portion of this effort shall be devoted to continued studies of techniques and computer programs which are necessary to reduce the acquired digital data and satisfy the operational objectives listed above, as well as for reducing such additional data as can be derived from the return signal of the sensor.

8.3.7.1 Technique Refinement

The following techniques will be expanded and/or refined, and programmed for the IBM 7090:

- (a) Least-Squares Fitting
- (b) Harmonic Analysis
- (c) Time-Correlation
- (d) Bench-Mark Recognition
- (e) Occultation and Sub-orbital Correlation
- (f) Contour Surface Fitting and Plotting

8.3.7.2 Technique Simulation

Each of the Data Useability Techniques will be empirically tested to determine the feasibility of accomplishing one or more of the four system objectives.

Analytical models of sampled altimetry data will be constructed for each of the techniques to be tested. The number of data points used will vary, dependent upon the objective sought and the technique being used. In order to determine the effectiveness of the Least Squares Fitting Technique in recomputing the size and shape of the moon, for example, an entire orbit of data will be required. On the other hand, only a small matrix of sample points will suffice for testing the Contour Surface Fitting and Plotting routine.

8.3.7.3 Improved Methods

Additional methods for using the LUCOM data to update lunar knowledge will be investigated, and promising techniques shall be exploited for subsequent application to the data-reduction problem.

8.4 TECHNICAL CONSULTANTS

It is anticipated that at least two consultante will be utilized during this Phase II effort. Dr. Richard K. Moore, University of Kansas, will be required to provide technical support in the areas of Sensor Statistical Studies and Parametric Trade-off studies. Another consultant (possibly Dr. Kaula, UCLA) in the field of geophysical sciences, will be used to

assist in the formulation of methods for applying the profile data to re-creation of the lunar terrain and to the computation of the moon's figure.

8.5 SUMMARY DISCUSSION

A majority of these tasks can be accomplished independent of additional input data from the Apollo mission. These studies are of the nature of technological investigations to advance the basic knowledge of system performance. Any external information which can be fed into the analyses, however, would ultimately benefit subsequent development.

At the conclusion of this effort, program development can proceed in either of two directions; a continuation of the conceptual study, or the development of hardware for laboratory and flight testing.

4.1-A

LASER MATHEMATICAL MODEL

In the following paragraphs, the basic parameters effecting a laser altimeter system in the LUCOM application are examined. A mathematical model describing the maximum background noise to which the system would be subjected is developed first. The information produced by this model is used to determine the required number of signal photoelectrons. A mathematical model describing received signal energies as a function of transmitted signal energies is developed to determine the amount of output power needed to supply the previously determined number of signal photoelectrons. Terrain slope and ranging accuracy were both taken into account in this model.

Calculations made by industry are shown to compare the model designed especially for LUCOM with general purpose laser ranging models. Trade-off considerations are then discussed. Total system input power is the prime factor here.

4.1-A.1

Calculation of Background Noise Associated with Ranging
Off the Moon

The amount of radiant emittance reaching the moon (from the sun) is 0.14 watt/cm².⁽¹⁾ This quantity will be denoted by R_{SM} , i. e.,

$$R_{SM} = 0.14 \text{ watt/cm}^2 = 3.12 \text{ watt/ft.}^2$$

This power may be considered to have the form of a plane wave incident upon an infinite, isotropic surface⁽²⁾ of reflectivity $\eta_M = 0.1$ (the reflectivity of the moon's surface). The total power per unit area leaving the moon back into space, R_{MS} , would be given by

$$R_{MS} = R_{SM} \eta_M = 1.4 \times 10^{-2} \text{ watt/cm}^2 = 0.312 \text{ watt/ft}^2 \quad (4.1.1)$$

In space the sun's electromagnetic energy spectrum is closely approximated by a 6000 °K black body⁽¹⁾.

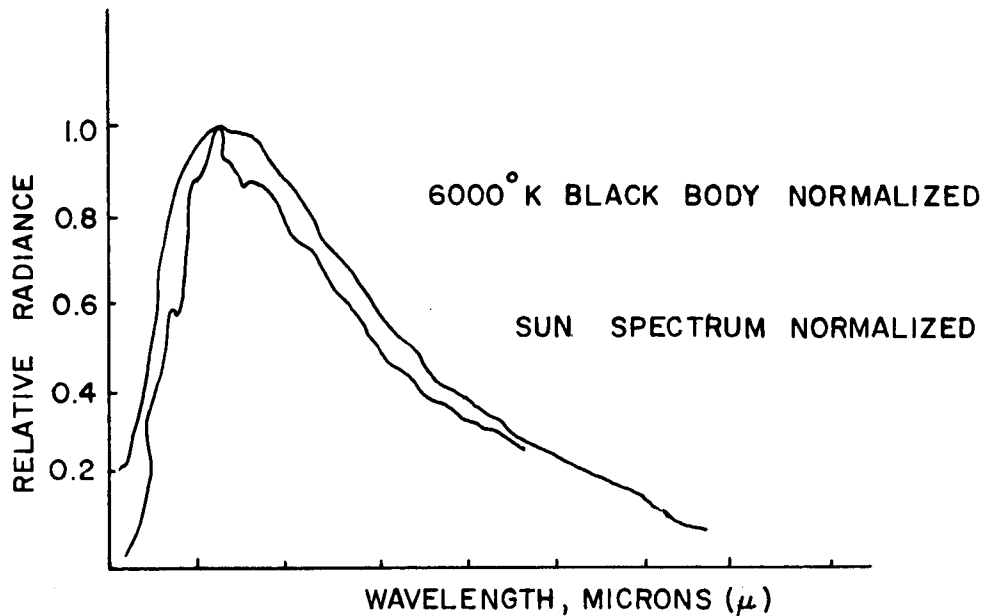


Figure 4.1-A.1-1
Sun Spectrum Outside Earth's Atmosphere vs. 6000° K
Black Body (from Ref. 1)

The amount of power from black body radiation in the $d\lambda$ region about the wavelength λ is given by Planck's law

$$W(\lambda, T) = \frac{2\pi C^2 h \lambda^{-5} d\lambda}{e^{hc/\lambda k T} - 1} \quad (4.1.2)$$

where

$$2\pi c^2 h = 3.74 \times 10^{20} \text{ watts/cm}^2 (\text{A})^4$$

$$hc/k = 1.438 \times 10^8 \text{ A}^\circ\text{K}$$

(Here h is Planck's constant, c the velocity of light, and k is Boltzmann's constant)

The total black body radiation, W , is given by

$$W = \int_0^{\infty} W(\lambda, T) d\lambda = \sigma T^4 \quad (4.1.3)$$

where

$$\sigma = 5.679 \times 10^{-12} \text{ watt/cm}^2 (\text{ }^\circ \text{K})^4$$

For a black body temperature of 6000° K,

$$W = 7.37 \times 10^3 \text{ watts/cm}^2$$

The amount of energy per unit area in the $\Delta\lambda$ region about λ is given by

$$\int_{\lambda - \Delta\lambda/2}^{\lambda + \Delta\lambda/2} W(\lambda', T) d\lambda' \quad (4.1.4)$$

This integral is closely approximated by

$$W(\lambda, T) \Delta\lambda = \frac{2\pi c^2 h}{e^{hc/\lambda kT} - 1} \lambda^{-5} \Delta\lambda, \quad (4.1.5)$$

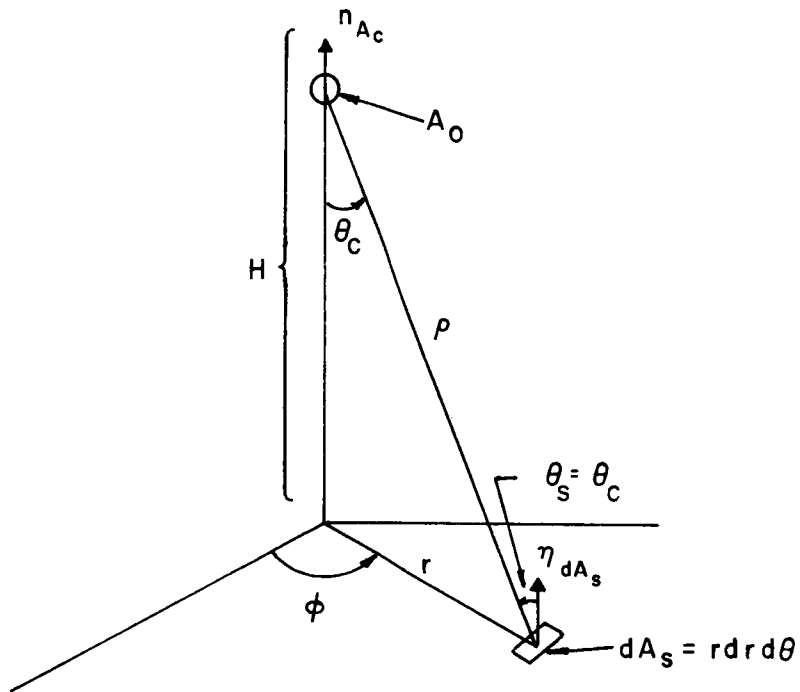


Figure 4.1. -A.1.2 Isotropic Reflection Geometry

The total power emanating from the elemental area dA_s on the surface of the moon is given by $\eta_p R_{MS} dA_s$. Lambert's law requires that the total power at the detector due to dA_s is given by⁽³⁾

$$\left(\frac{\cos \theta_s}{\pi}\right) \frac{(\eta_p R_{MS}) dA_s (\cos \theta_c) A_0}{e^2} \quad (4.1.7)$$

where $e^2 = r^2 + H^2$. The area on the ground within the field of view of the detector will have a radius \tilde{r} ($\tilde{r} \approx \frac{\omega}{2} H$) which is much less than H . Therefore $e^2 \approx H^2$ in this problem. Also both $\cos \theta_s$ and $\cos \theta_c$ are approximately equal to one. The quantity (7) is hence given by

$$\frac{\eta_p R_{ms} \omega^2 A_0}{4}$$

to a very good approximation.

For a receiver optical efficiency of η_R , the noise optical power P_{no} reaching the detector will be

$$P_{no} \approx \frac{\eta_R (\eta_p R_{ms}) \omega^2 A_0}{4} \quad (4.1.8)$$

Thus it is seen that P_{no} is independent of altitude for H much less than the radius of the moon. Each photon in the $\Delta \lambda$ region about λ will have an average energy of

$$E_p = hc/\lambda \quad (4.1.9)$$

(where h is Planck's constant and c is the speed of light),

and the detector will have a quantum efficiency of η_q (the fraction of photo-electrons produced per photon). Therefore the average number of background noise photoelectrons, N_n , will be

$$N_n = \eta_q P_{no} / E_p \quad (4.1.10)$$

This is shown for the three wavelengths

$$\lambda = 5300 \text{ \AA}, 6943 \text{ \AA}, \text{ and } 10,600 \text{ \AA}$$

in Table 4.1-A.1-1 for the particular situation:

$$\lambda = 0.53 \mu: \eta_q = 0.40, E_p = 3.73 \times 10^{-19} \text{ joule/photon}$$

$$\lambda = 0.6943 \mu: \eta_q = 0.10, E_p = 2.85 \times 10^{-19} \text{ joule/photon}$$

$$\lambda = 1.06 \mu: \eta_q = 0.010, E_p = 1.86 \times 10^{-19} \text{ joule/photon}$$

$$\eta_R = 0.4$$

$$A_o = 0.196 \text{ ft}^2$$

$$\tilde{r} = 245 \text{ ft.}$$

$$H = 490,000 \text{ ft.}$$

$\lambda \sim$ microns	0.53	0.6943	1.06
$N_n \sim$ No. of photoelectrons/sec	8.75×10^6	2.12×10^6	1.45×10^5

Table 4.1-A.1-1

Average number of background noise photoelectrons per second, N_n , for the three wavelengths of interest.

4.1-A.2 Determination of Required Number of Detected Photoelectrons

When the average number of photoelectrons produced during the resolving time of the system "is less than ten to twenty , the fluctuations may be estimated by considering the statistical probability of seeing

various numbers of pulses."⁽⁵⁾ It follows that the background noise will produce less than one photoelectron per sampling interval for all the wavelengths under consideration. Table 4.1-A.2-1 from Reference 6 shows a range of photomultiplier noise photoelectron generation rates for some typical tubes.

Tube No.	Photocathode	Equiv. Photocathode Dark Current (amp)	Photoelectrons per nanosecond (N)
RCA 7265	S-20	3×10^{-14}	1.9×10^{-4}
RCA (Dev.)	S-20	1.4×10^{-13}	8.7×10^{-4}
RCA 7102	S-1	7×10^{-12}	4.4×10^{-2}
ITT FW-118	S-1	1.4×10^{-13}	8.7×10^{-4}

Table 4.1-A.2-1

Photomultiplier Characteristics at 25° C (From Reference 6)

Note that for all the tubes except the RCA 7102, less than 0.09 noise photoelectrons will be produced. Since a S-20 surface will be used for both the 5300 Å and the 6943 Å wavelengths and a S-1 surface will be used for the 10,600 Å wavelength the values in this table will be representative of those expected. Therefore the average rates of noise photoelectrons will be increased to probably no greater than those in Table 4.1-A.2-1. A Poisson distribution estimation will allow a conservative evaluation of the probability of false alarm per sampling interval. Therefore the usual assumption made in the literature^{(7), (8)} is that the noise photoelectrons are generated randomly with nontime-varying Poisson statistics. For this distribution, the probability of false alarm per sampling interval, P_{FA} , is given by

$$P_{FA} = \sum_{r=x}^{\infty} \frac{e^{-U} U^r}{r!} \quad (4.1.11)$$

where x is the threshold number of photoelectrons required to reduce P_{FA} to some given value then the average number of noise photoelectrons generated per sampling interval is given by U . If no more than one false alarm in 1000 range measurements is allowable, then P_{FA} times the number of sampling intervals, N_i , is required to be 10^{-3} . For a ranging distance of 490,000 ft. and a ranging accuracy of 50 ft.

$$N_i = 2(490,000)/100 = 0.98 \times 10^4$$

and

$$P_{FA} N_i = P_{FA} (0.98 \times 10^4) = 10^{-3}$$

or

$$P_{FA} = 1.02 \times 10^{-7}$$

which will be the requirement in the example under consideration. After a P_{FA} has been established, a table such as Reference 9 can be used to determine the threshold setting x to be used for a particular U to give P_{FA} . If U is one noise photoelectron per sampling interval then a threshold setting of ten would give a P_{FA} of $0.3 \times 10^{-7(9)}$ (which is less than the P_{FA} of 1.02×10^{-7} established as the requirement here).

Generally Poisson statistics are also used to set the number of signal photoelectrons required for a given desired probability of detection, P_D . Perhaps the most satisfying heuristic argument for using this very conservative approach is given in Reference 5:

"Let the average number of background noise photoelectrons per second... be about 7×10^5 , and if one assumes a video amplifier 5 megacycle wide the electronic bandwidth, the incoming signal may be considered sampled independently every 0.2μ sec. (2×10^{-7} sec.). This leads to an average of 0.14 photoelectron per range sample (or sampling interval). A detection threshold is established which requires that at least η_{\dagger} photoelectrons be present in a single sample. Under

typical conditions one ordinarily expects, say, 30 signal photoelectrons back, but if the target straddles two detection cells (ranging or sampling interval), this would be reduced to 15, and there may be small blind spaces between cells which would (further) reduce the return. For the moment, let $\eta_t = 5$. That is, 5 photoelectrons are required to recognize a return.

"Now assume that return photoelectrons are random events and thus (as a conservative estimate) distributed accordingly to Poisson's formula. Then the probability of detection, P_D , is given by,"

$$P_D = \sum_{r=x}^{\infty} U_s^r e^{-U_s} \quad (4.1.12)$$

to return to the earlier notation. Here U_S is the expected number of photoelectrons produced by a return signal. According to Reference 10:

"A good highly conservative criterion for adequate power is that the returning signal be capable of providing... 25 photoelectrons out of the detector...", since number of photoelectrons and not the signal to noise ratio is the limiting criterion here. Reference 9 then gives the value of P_D associated with a threshold setting of 10 ($x = 10$) and a value of the photoelectrons generated by the return signal of 25 ($U_S = 25$).

Here

$$P_D = 0.99978$$

from the reference. This says that less than one signal in one thousand will not be detected. This is of the same order of magnitude as the number of false alarms per range sweeps. Therefore 25 signal photoelectrons generated per pulse will be established as the requirement for any system, no matter at what wavelength it operates.

In a laser altimeter system, a transmitted pulse of some pulsewidth τ_T is produced by the laser at some particular frequency ν . The very fact that the pulse is of finite width will tend to broaden the frequency spectrum of the transmitted pulse. This effect is shown in Figure 4.1-A.3-1

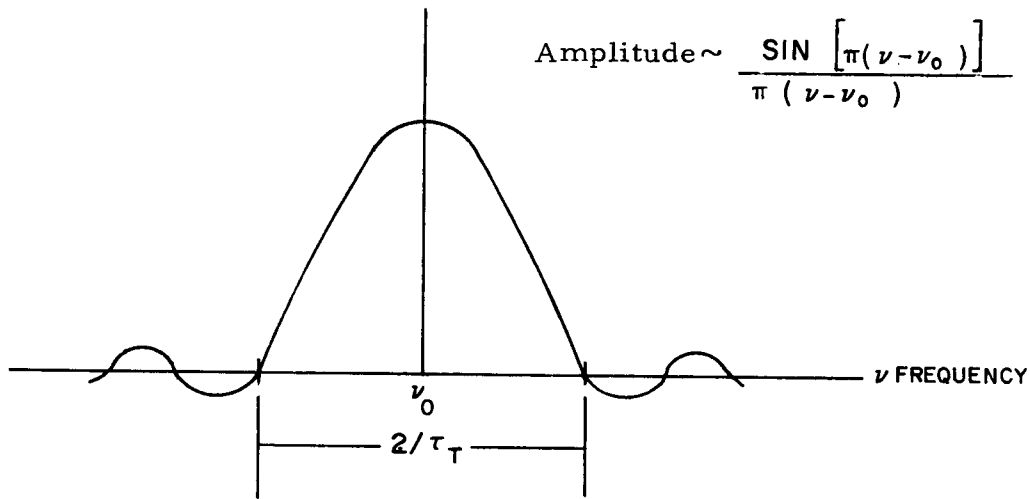


Figure 4.1.A.3-1

Frequency Spectrum of Rectangular Pulse of Length τ at Frequency ν_0

This signal is sent through a set of optics designed to reduce the beam-width of the transmitted pulse to some predetermined amount. In actuality, the pattern of the transmitted pulse will be of the form shown in Figure 4.1.-A.3-2.

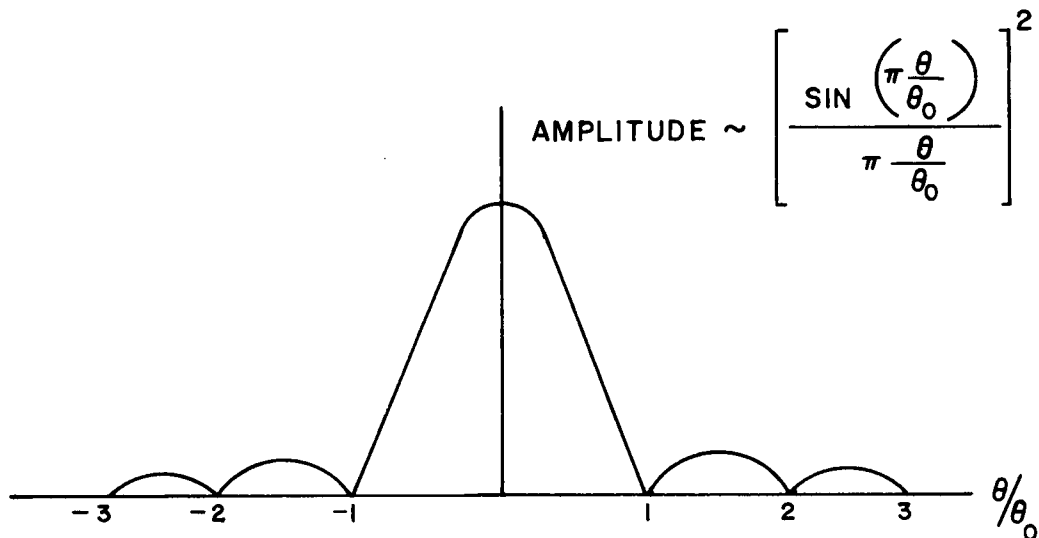


Figure 4.1-A.3-2

Intensity of a Laser Spot

However, because of source material limitations this knowledge about the antenna pattern cannot be fruitfully used at this time as it was in the radar altimeter investigation. The beam pattern will be described, therefore, by only a beamwidth, ω . In passing through the transmitter optics, the energy of the pulse will be diminished by a fraction η_T (the optical efficiency of the transmitting optics). The signal pulse will strike the moon's surface and be reflected back, having exchanged some of its energy with an isotropic surface of reflectivity η_M (taken to be 9.1 at all wavelengths under consideration). (See Reference 2). When the line of sight of the altimeter is nearly along the local vertical equation 7 holds and the return signal energy through the receiver optics is given by

$$\frac{1}{\pi} \frac{\eta_T \eta_M A_o \eta_R E_T}{H^2}$$

where A_o is the receiver effective area and η_R , the receiver optical efficiency. As in the calculation of background noise the number of signal photoelectrons generated per pulse, N_s , will then be given by

$$N_s = \frac{1}{\pi} \frac{\eta_T \eta_R \eta_q \eta_M A_o E_T}{E_p H^2} \quad (4.1.13)$$

where again, η_q is the quantum efficiency of the detector and $E_p = hc/\lambda$ is the energy of a single photon of wavelength λ . For one set of parameters N_s is shown as a function of E_T in Figure 4.1-A.3-3.

4.1-A.4 Transmitted Pulsewidth Considerations

If the line of sight of the laser altimeter does not deviate more than 0.5° from the local vertical, then the terrain slope will have the greatest effect on the duration of the return pulse. In general, return pulsewidths should not be greater than ten times the transmitted pulsewidth in order to guarantee detection of the return signal. With this in mind, a quantitative investigation of the change in return pulsewidth due to varying terrain slopes will be performed.

The duration of the return pulse, τ_R , from an altimeter will be given

$$\tau_R = \frac{2}{C} (\ell_2 - \ell_1) + \tau_T \quad (4.1.14)$$

where ℓ_2 is the distance from the altimeter to the last point on the ground the trailing edge of the pulse reaches, ℓ_1 , is the distance from the altimeter to first point on the ground the leading edge of the transmitted pulse reaches, and τ_T is the duration of the transmitted pulse. The geometry for a sloping terrain is shown in Figure 4.1-A.4-1. Using the law of sines

$$N_s = \frac{1}{\pi} \frac{\eta_T \eta_R \eta_q A_0 \eta_M}{H^2} \frac{E_T}{E_p}, \quad E_p = hc/\lambda$$

$$\eta_T = 0.9, \quad \eta_R = 0.4, \quad A_0 = 0.196 \text{ FT.}^2, \quad \eta_M = 0.1, \quad H = 490,000 \text{ FT.}$$

$$\lambda = 0.53 \mu: \eta_q = 0.4, \quad E_p = 3.73 \times 10^{-19} \text{ JOULE/PHOTON}$$

$$\lambda = 0.6943 \mu: \eta_q = 0.1, \quad E_p = 2.85 \times 10^{-19} \text{ JOULE/PHOTON}$$

$$\lambda = 1.06 \mu: \eta_q = 0.01, \quad E_p = 1.86 \times 10^{-19} \text{ JOULE/PHOTON}$$

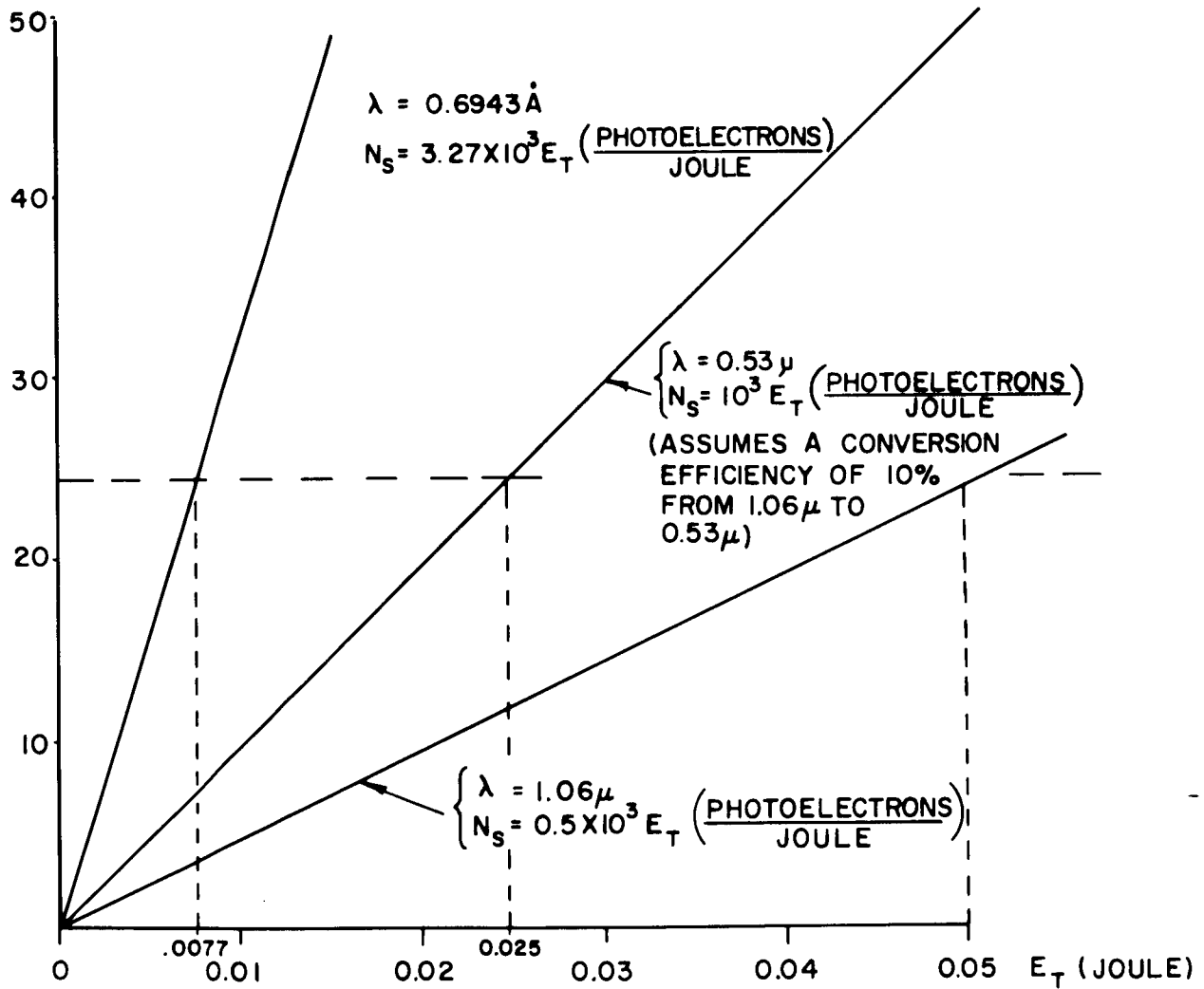


FIGURE 4.1-A.3-3. NUMBER OF RECEIVED SIGNAL PHOTOELECTRONS, N_s , AS A FUNCTION OF TRANSMITTED PULSE ENERGY, E_T

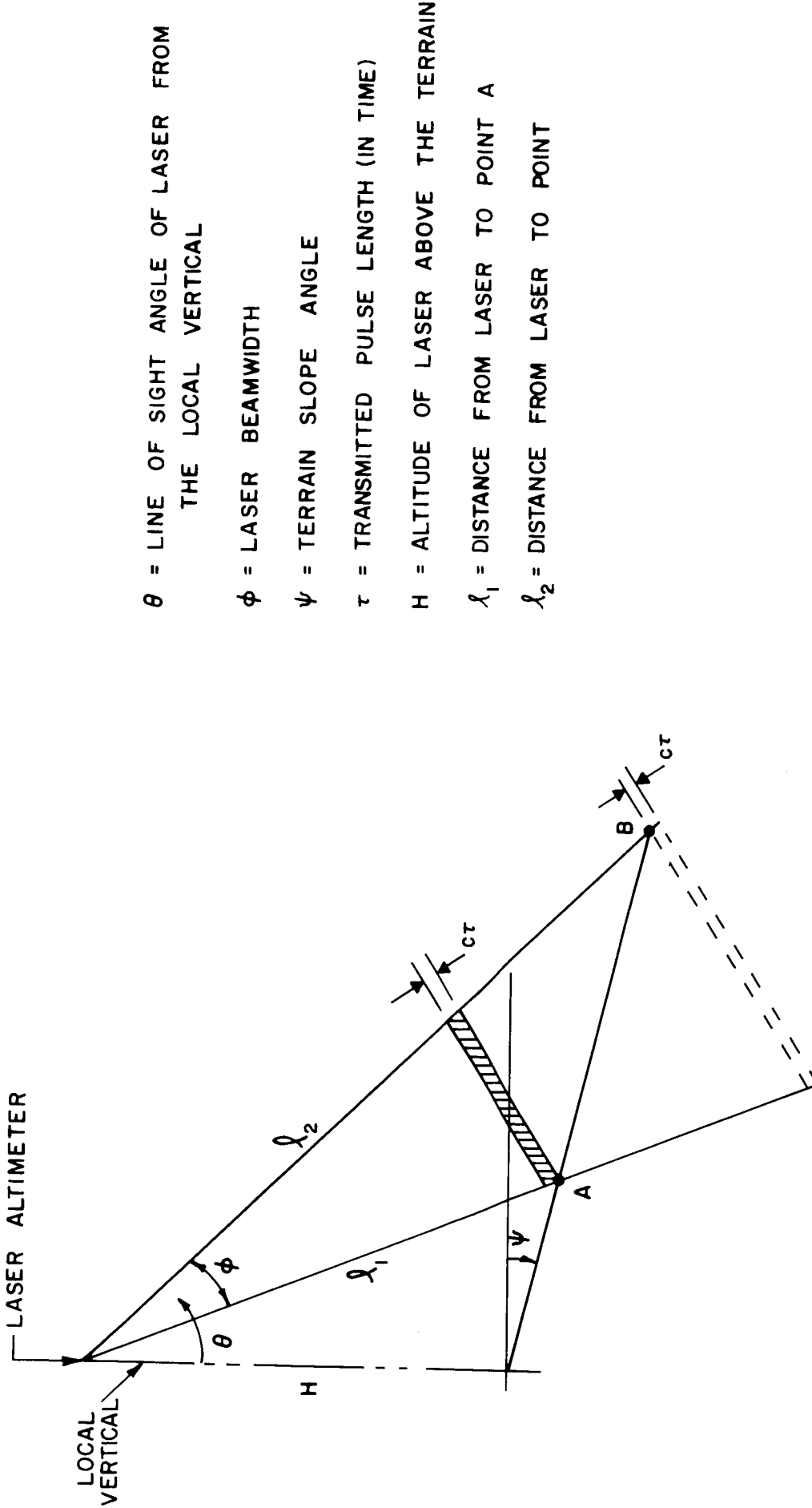


FIGURE 4.1-A.4-1. GEOMETRY OF LASER RANGING AGAINST A SLOPING TERRAIN

$$\frac{l_1}{\sin\left(\frac{\pi}{2} + \theta\right)} = \frac{H}{\sin\left[\frac{\pi}{2} - \left\{(\psi + \theta) - \phi/2\right\}\right]}$$

or equivalently

$$l_1 = \frac{H \cos \psi}{\cos\left[(\psi + \theta) - \phi/2\right]}$$

since $\sin\left(\frac{\pi}{2} \pm \alpha\right) = \cos \alpha$

Similarly

$$l_2 = \frac{H \cos \psi}{\cos\left[(\psi + \theta) + \phi/2\right]}$$

Since

$$\cos(\alpha \pm \beta) = \cos \alpha \cos \beta \pm \sin \alpha \sin \beta,$$

it follows (after some algebraic manipulation) that

$$l_2 - l_1 = H \cos \psi \left[\frac{2 \sin(\theta + \psi) \sin \phi/2}{\cos^2(\theta + \psi) \cos^2 \phi/2 - \sin^2(\theta + \psi) \sin^2 \phi/2} \right]$$

Therefore the duration of the return pulse is given by

$$\tau = \frac{\frac{4-H}{c} \cos \psi \sin(\theta + \psi) \sin \phi/2}{\cos^2(\theta + \psi) \cos^2 \phi/2 - \sin^2(\theta + \psi) \sin^2 \phi/2} + \tau_T \quad (4.1.15)$$

In Figure 4.1.A.4-2, τ_T is shown for various τ_R as a function of the terrain slope angle ψ . In all but one case the angle θ has been set equal to zero. For $\tau_T = 10$ nanosecs, τ_R was calculated for θ equal to both 0° and 0.5° . It can be seen that the two curves differ only slightly. It is apparent that the difference made by letting $\theta = 0.5^\circ$ instead of 0° would be even less for larger τ_T . Since $\theta = 0.5^\circ$ is the greatest expected deviation from the vertical, the figure can be used to estimate τ_R for the indicated τ_T and for all allowed θ .

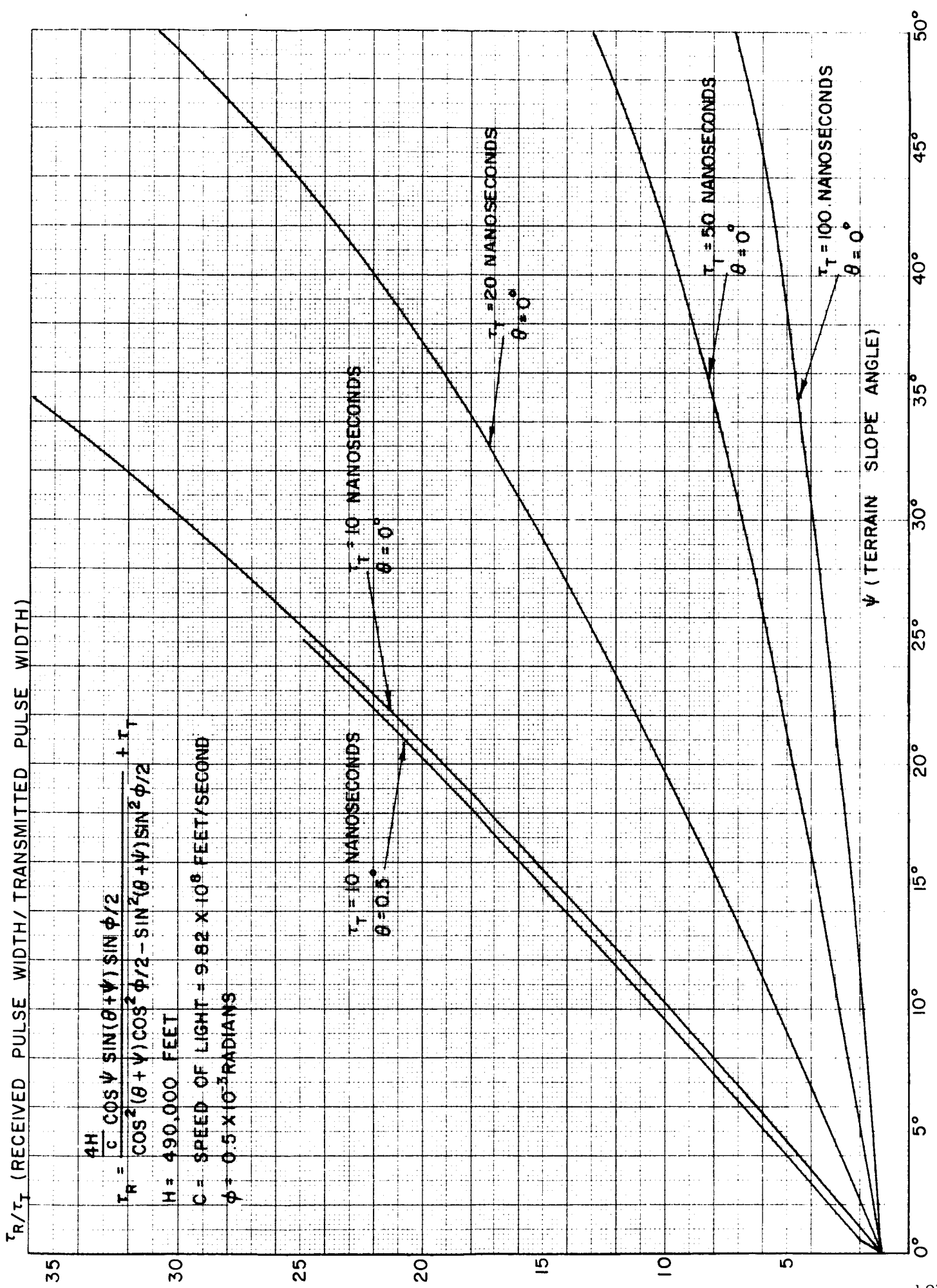


FIGURE 4.1-A.4-2. RECEIVED PULSE WIDTH NORMALIZED TO TRANSMITTED PULSE WIDTH AS A FUNCTION OF TERRAIN SLOPE

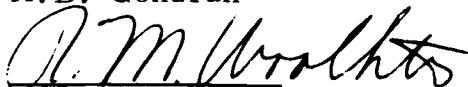
From Figure 4.1-A.4-2, it is apparent that 50 feet ranging accuracy can be maintained using a τ_T of 10 nanosecs for terrain slopes up to 10° ; whereas, this accuracy could be maintained using a τ_T of 50 nanosecs only in those areas in which the terrain slopes are less than 5.3° . On the other hand terrain slopes of up to 42° can be tolerated with a 50 nanosecs pulse, where the $10 \tau_T$ point for a 10 nanosecs pulse is only 10° . This indicates that a detailed analysis of terrain slopes at the resolution of the laser system would be required before the best choice of transmitted pulse width could be made.

AN INTRODUCTION
TO
SPECTRAL CALCULATIONS FROM DIGITAL RECORDS


8 January 1964

Prepared by:


A.D. Gondran


R.M. Woolheater

Approved by:


J.J. Stafford
Chief, Guidance Systems

AN INTRODUCTION TO SPECTRAL
CALCULATIONS FROM DIGITAL RECORDS

I. INTRODUCTION

Communications systems are invariably required to handle a large number of signals. To determine the requirements for design and utilization of these systems, the characteristic properties of these signals must be known.

Noise, signals, or other ensembles of functions (given continuously or at discrete intervals) which are approximately stationary are best studied in terms of their autocovariance and spectral density functions. Exact determinations of these quantities would, of course, require exact and continuous measurement of the desired signal for an infinite record length - an obviously impossible set of conditions to satisfy. However, a good statistical estimate of these properties can be calculated using the digital techniques set forth by R. B. Blackman and J. W. Tukey.¹

II. RANDOM FUNCTIONS

If the output of a physical random (or unpredictable) process is monitored from time to time, the resulting outputs will constitute a collection of waveforms. Each of these waveforms is referred to as a random function generated by the random process. The collection of functions is called an ensemble or class.

The processes shall be assumed to be both stationary and ergodic; that is, the averages of the ensemble do not change in time and are the same as the time averages for any one of the functions in the ensemble.

¹ R. B. Blackman and J. W. Tukey, The Measurement of Power Spectra From the Point of View of Communication Engineering, Dover Publications, Inc.

III. AUTOCOVARANCE AND SPECTRAL DENSITY

The autocovariance of a single random function at time lag, τ , is given by:

$$C(\tau) = \lim_{T \rightarrow \infty} \frac{1}{T} \int_{-T/2}^{T/2} [X(t) - \bar{X}] \cdot [X(t+\tau) - \bar{X}] dt.$$

In ensemble terms,

$$C(\tau) = \text{ave} \left\{ [X(t) - \bar{X}] \cdot [X(t+\tau) - \bar{X}] \right\}$$

The power spectral density $P(f)$ is the Fourier transform of the autocovariance function, thus,

$$P(f) = \int_{-\infty}^{\infty} C(\tau) \cdot e^{-i2\pi f \tau} d\tau$$

and

$$C(\tau) = \int_{-\infty}^{\infty} P(f) \cdot e^{i2\pi f \tau} df.$$

Since the spectral density and autocovariance are even functions of their respective arguments, these may be reduced to,

$$P(f) = \int_{-\infty}^{\infty} C(\tau) \cdot \text{COS } 2\pi f \tau d\tau$$

and

$$C(\tau) = \int_{-\infty}^{\infty} P(f) \cdot \text{COS } 2\pi f \tau df.$$

In practice, only positive frequencies and lag are considered, so that,

$$P(f) = 2 \int_0^{\infty} C(\tau) \cdot \text{COS } 2\pi f \tau d\tau$$

and

$$C(\tau) = 2 \int_0^{\infty} P(f) \cdot \text{COS } 2\pi f \tau df.$$

Given a continuous record of finite length, the autocovariance may not be estimated for arbitrarily long lags. Surely no estimates can be made for lags longer than the record; desirably, the maximum lag should not exceed ten percent of the record length. Thus, in place of

$$C(\tau) = \lim_{T \rightarrow \infty} \int_{-T/2}^{T/2} X(t) \cdot X(t+\tau) dt.$$

assuming data having a mean value of zero, we have

$$C_{00}(\tau) = \frac{1}{T-|\tau|} \int_{(-T-|\tau|)/2}^{(T-|\tau|)/2} X(t-\tau/2) \cdot X(t+\tau/2) dt$$

for

$$|\tau| \leq T_m \leq T,$$

where T is the record length and T_m is the maximum shift. $C_{00}(\tau)$ is the apparent autocovariance function.

The estimates of the power spectrum must be derived from a modified apparent autocovariance function to be meaningful. The modified autocovariance function is defined as,

$$C_i(\tau) = D_i(\tau) \cdot C_{00}(\tau).$$

Let $D_i(\tau)$ be a prescribed even function of τ , subject to the restrictions $D_i(0) = 1$ and $D_i(\tau) = 0$ for $|\tau| \geq T_m$, where $i = 0, 1, 2, 3, 4$, depending on the desired shape of $D_i(\tau)$. $D_i(\tau)$ is a window of variable transmission and called a lag window.

For any allowable lag window $C_i(\tau)$ is calculable from the data. Further, because $C_i(\tau)$ is defined for all values of τ , it has a perfectly definite Fourier transform $P_i(f)$, which should satisfy the relation,

$$P_i(f) = Q_i(f) * P_{00}(f)$$

where $Q_i(f)$ is the Fourier transform of $D_i(\tau)$; the asterisk indicates convolution², and $P_{00}(f)$ is the Fourier transform of $C_{00}(\tau)$. But $P_{00}(f)$ is not determinate, since $C_{00}(\tau)$ is not specified for $\tau \geq T_m$.

Nevertheless, since

$$\text{ave} \{ C_{00}(\tau) \} = C(\tau)$$

and

$$\text{ave} \{ C_i(\tau) \} = D_i(\tau) \cdot C(\tau)$$

where $C(\tau)$ is the true autocovariance function, it follows that

$$\text{ave} \{ P_i(f) \} = Q_i(f) * P(f)$$

$$^2 P_i(f_1) = \int_{-\infty}^{\infty} Q_i(f_1 - f) \cdot P(f) df$$

where $P(f)$ is the true power spectrum, that is, the Fourier transform of $C(\tau)$. Averaging may be done across the ensemble or along time. The explicit relation

$$\text{ave} \left\{ P_i(f) \right\} = \int_{-\infty}^{\infty} Q(f_i - f) \cdot P(f) df$$

gives the frequency averaged value of $P_i(f_1)$ of the true power spectral density $P(f)$ over frequencies near f_1 with weights proportional to $Q_1(f_1 - f)$. In a matter of speaking, $P_i(f_1)$ is the collected impression of the true power spectrum $P(f)$ obtained through a window of variable transmission $Q_1(f_1 - f)$. Therefore, $Q_1(f)$ is called the spectral window and corresponds to the lag window $D_1(\tau)$.

The lag windows enjoying most popular use are,

$$D_2(\tau) = \begin{cases} 0.5 + 0.5 \cos \frac{\pi \tau}{T_m} & \text{FOR } |\tau| < T_m \\ 0 & \text{FOR } |\tau| > T_m \end{cases}$$

called the "hanning"³ window, and

$$D_3(\tau) = \begin{cases} 0.54 + 0.46 \cos \frac{\pi \tau}{T_m} & \text{FOR } |\tau| < T_m \\ 0 & \text{FOR } |\tau| > T_m \end{cases}$$

called the "hamming"⁴ window.

IV. ALIASING

A random function $X(t)$ may be available continuously or, as is usually the case, at discrete sampling intervals. Data recorded at these equally spaced time intervals introduces the two important considerations of aliasing of frequencies and analysis involving digital rather than analog computation.

When $X(t)$ is known for,

$$t = 0, \Delta t, 2\Delta t, 3\Delta t, \dots, n\Delta t$$

$C(\tau)$ may be estimated only for

$$|\tau| = 0, \Delta t, 2\Delta t, \dots, m\Delta t, \quad m < n.$$

3 Named for Julius Von Hann.

4 Named for R. W. Hamming.

The frequency range of the estimated spectral density now will be limited to,

$$0 \leq f \leq f_N, \quad f_N = 1/2\Delta t.$$

All power contributions to frequencies above f_N (Nyquist frequency) will be folded into the range $0 \leq f \leq f_N$.

Careful consideration must be exercised in the choice of an adequate sampling interval to provide sufficient frequency range; power contributions in the vicinity of f_N must be very small relative to maximum power (i.e., about two percent). Sampling interval may be determined by trial and error or by prior knowledge.

V. DIGITAL TRANSFORMATION

Digital transformation of the $m + 1$ values, $C_0, C_1, C_2 \dots, C_m$, of the autocovariance function produces $m + 1$ estimates of the spectral density in the range,

$$0 \leq f \leq f_N$$

at equally spaced intervals of f_N/m . Smoothing modifications in the computation by weighting provide a realistic estimate of the continuous spectral density.

Transformation is effected by first computing the mean lagged products, i.e., the digital estimates of the autocovariance function,

$$C_r = \frac{1}{n-m+1} \sum_{q=0}^{q=n-m} (X_q - \bar{X}) \cdot (X_{q+r} - \bar{X})$$

for

$$r = 0, 1, 2, \dots, m, \quad m < n.$$

Subscripts are now used, since for discrete data $C(\tau)$ exists only for integral values of lag.

Applying a discrete finite cosine series transform to the sequence, C_r results in the raw power spectral density,

$$V_r = \Delta \tau \left[C_0 + 2 \sum_{q=1}^{m-1} C_q \cos \frac{qr}{m} + C_m \cos r\pi \right]$$

for

$$r = 0, 1, 2, \dots, m.$$

For the digital operation spectral windows reduce to the following sets of constants:

K_1	K_2	K_3	
0.25	0.5	0.25	(hanning set)
0.23	0.54	0.23	(Hamming set)

The smoothing operation is simply performed here:

$$P_0 = K_2 V_0 + K_2 V_1$$

$$P_r = K_1 V_{r-1} + K_2 V_r + K_3 V_{r+1} \quad 1 \leq r \leq m-1$$

$$P_m = K_2 V_{m-1} + K_2 V_m$$

VI. TERRAIN APPLICATIONS

The requirements of various systems to handle large numbers of terrain samples has aroused interest in the spectral analysis of terrain profiles. However, observation of several profiles shows that the terrain is generally neither ergodic nor stationary. To remove the effects of distance (analogous to time in prior discussion) varying mean values, a method of refinement of raw data has been developed. A least squares fit line is calculated for a piece of data exhibiting a strong upward or downward trend and the value of the line is subtracted from the data value at the appropriate distance.

The need for trend and mean value removal is shown by the following example:

Suppose a set of observed data points is known to lie between -100 and +100 with few exceptions. The standard deviation of the set would be

about 30, the variance about 900. If the average of the observations is other than zero and is overlooked in computation, an excessive amount of power is concentrated in the low frequency region of the power spectrum. The total power is the square of the average (dc power) plus the variance. Numerically, perhaps $100 + 900 = 1000$ for the supposed data with a mean value of 10. All the dc power is in the lowest frequency band whose width is,

$$\Delta f = \frac{1}{(n-m+1)} \Delta d$$

where d is distance interval.

If the data is recorded at 400 foot intervals for 399,600 feet (1000 data points), f_N equals 12.5×10^{-4} cycles per foot. The elementary frequency bands constitute $1/900$ ($1/n - m + 1$) of the frequency spread. The dc power appears in the lowest band; thus, one tenth of the total power will be concentrated in one nine-hundredth of frequency range. Trends have much the same effect, but do not contribute as much dc power. These general long period ramps are roughly analogous to zero frequency sine waves.

There is one other processing of the data that may be required before computing the lagged products. If the spectrum under study is quite steep in certain frequency ranges, the sidelobes of the hanning or the hamming windows may pass excessive power from adjacent frequency bands and corrupt the band at the center of the lag window. This problem can be minimized by processing the data so the resulting spectrum tends to be flat. This flattening of the spectrum gives rise to the name, pre-whitening, for this particular process. The process itself takes the form of moving linear combinations and autoregressive series. The result

of the processing is to multiply the spectrum by a factor depending on the processing series used, and it is a simple matter to remove the effects of the processing, leaving the derived spectral estimates. Prewhitening has not been used thus far since the particular series to be used depends on the shape of the derived spectrum. That is a fair idea of the spectrum being calculated is required. In future terrain studies a prewhitening process will be employed.

The methods presented in the preceding section may now be directly applied to the analysis of frequency content in terrain profiles and the subsequent determination of adequate sampling rates to sufficiently identify a piece of terrain.

Experience has indicated that the preliminary sampling grain should not exceed four hundred feet. This interval makes the Nyquist frequency,

$$f_N = \frac{1}{2\Delta d} = 12.5 \times 10^{-4} \text{ CYCLES PER FOOT.}$$

Approximately ten shifts and one hundred data points should be used to provide eleven estimates of the spectral density.

In practice, a United States Geological Survey map quadrangle is considered as a random process. A family of terrain profiles at random headings is read and refined to constitute an ensemble of presumably random functions.

An arbitrary cutoff frequency (f_c) has been taken as the -13 db point on the spectral density curve. That is, $\rho(f_c)/\rho(f)_{\max} = 0.05$, and the maximum sampling rate that should be used to satisfy this criterion is $1/2f_c$.

Figures 1 through 7 are plots of the spectral densities of diverse terrains including two Pacific Ocean regions. Table 1 lists the cutoff frequencies for these various areas with the maximum sample interval and refined terrain variances.

<u>Region</u>	<u>f_c Cycles/Foot</u>	<u>Sample Interval Feet</u>	<u>σ^2 (Feet)²</u>
Atoka, Oklahoma	4.81×10^{-4}	1040	3253
Bonanza King, Calif.	3.40×10^{-4}	1471	134070
China Mountain, Calif.	3.75×10^{-4}	1333	61716
Benton, Penn.	7.15×10^{-4}	699	6748
Llano, Texas	9.52×10^{-4}	525	570
Taylor, Iowa	6.35×10^{-4}	788	1180
SEACOM Area B	5.50×10^{-4}	909	68
SEACOM Area C	5.15×10^{-4}	952	552

TABLE 1

No correlation is seen to exist between the variance of a region and the sampling interval to be used in that region.

VII. EXAMPLE PROBLEM

For illustration, the following example problem is included:

Four terrain profiles at random headings were read from a map of the Llano, Texas, area; each was refined and the lag products computed. One of these profiles is shown in Figure 9; the refined data of the profile is plotted in Figure 10.

Table 2 lists the individual lag products and the average lag products. Digital transformation of these average lag products gives the composite power spectral density of Figure 4.

LLANO, TEXAS

<u>τ</u>	<u>$c(\tau)_1$</u>	<u>$c(\tau)_2$</u>	<u>$c(\tau)_3$</u>	<u>$c(\tau)_4$</u>	<u>$\bar{c}(\tau)$</u>
0	737	157	416	969	570
1	534	87	280	732	408
2	264	- 7	85	362	176
3	- 16	-48	-23	48	10
4	-184	-44	-86	-162	-119
5	-282	-12	-95	-235	-156
6	-367	7	-59	-186	-151
7	-337	6	-17	- 97	-111
8	-230	-24	-12	20	- 62
9	-120	-32	-12	66	- 25

TABLE 2

COMPOSITE POWER SPECTRAL DENSITY
ATOKA, OKLAHOMA
6 DATA LINES

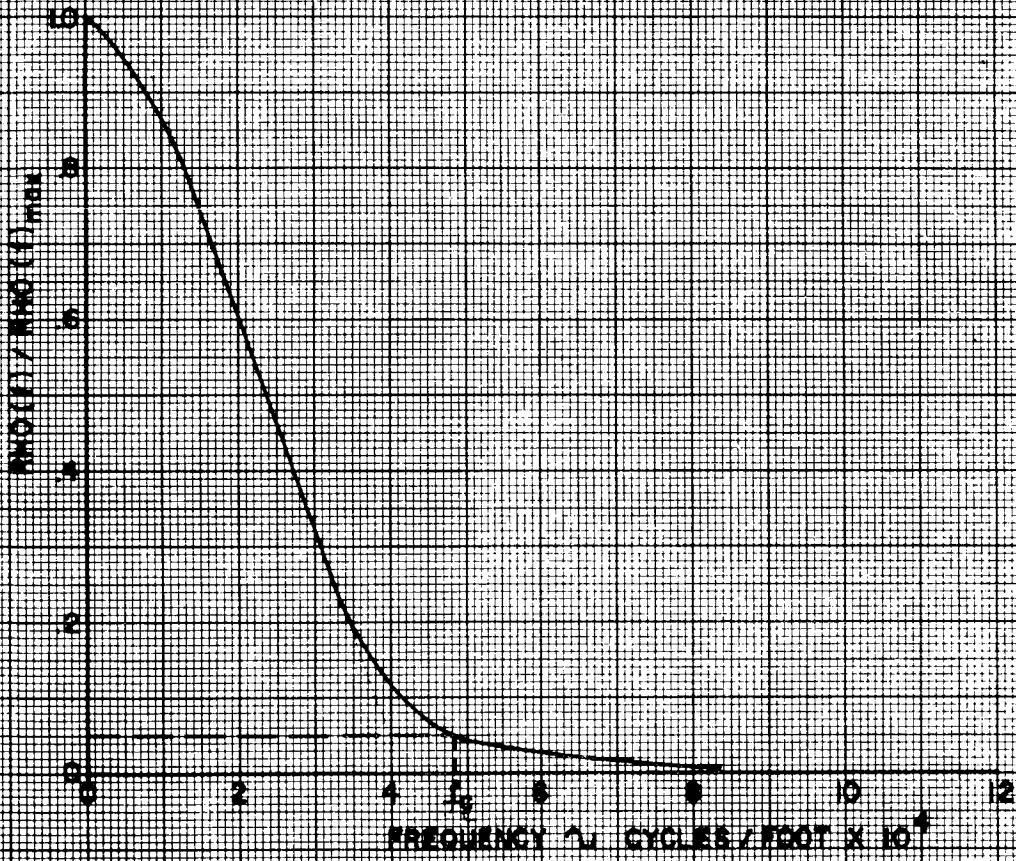


FIGURE 1

COMPOSITE POWER SPECTRAL DENSITY
BONANZA KING, CALIFORNIA
4 RANDOM LINES

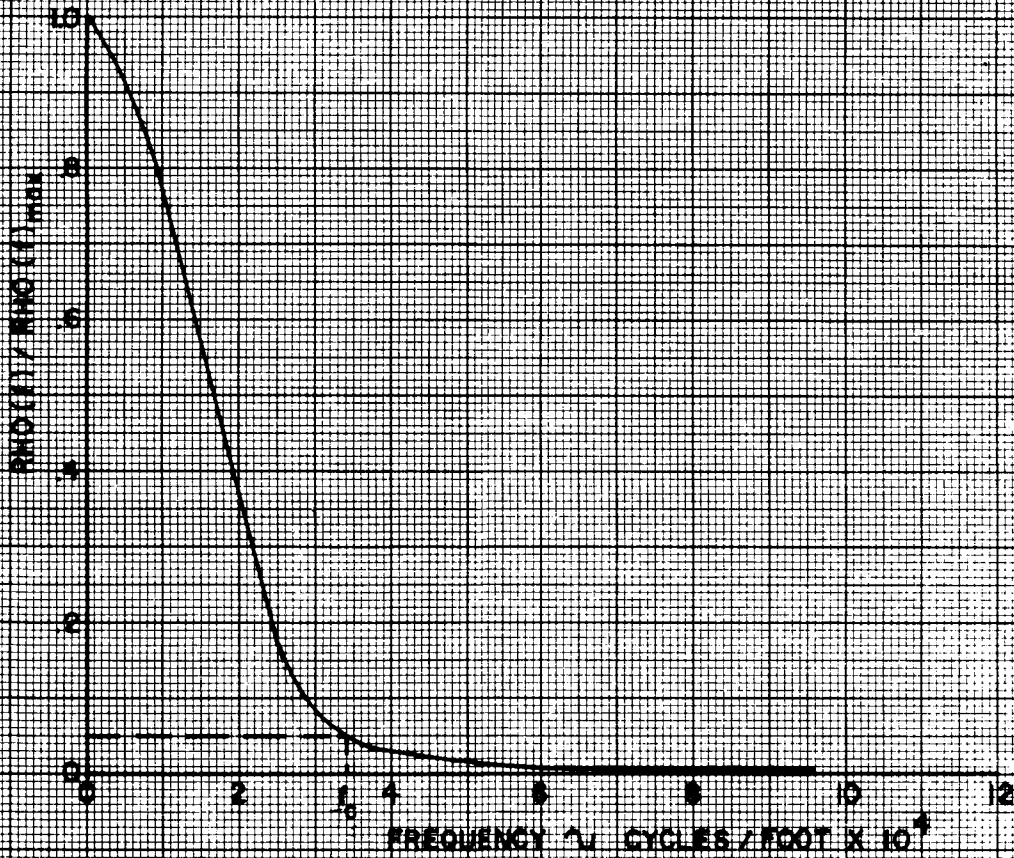


FIGURE 2

COMPOSITE POWER SPECTRAL DENSITY
CHINA MOUNTAIN, CALIFORNIA
4 RANDOM LINES

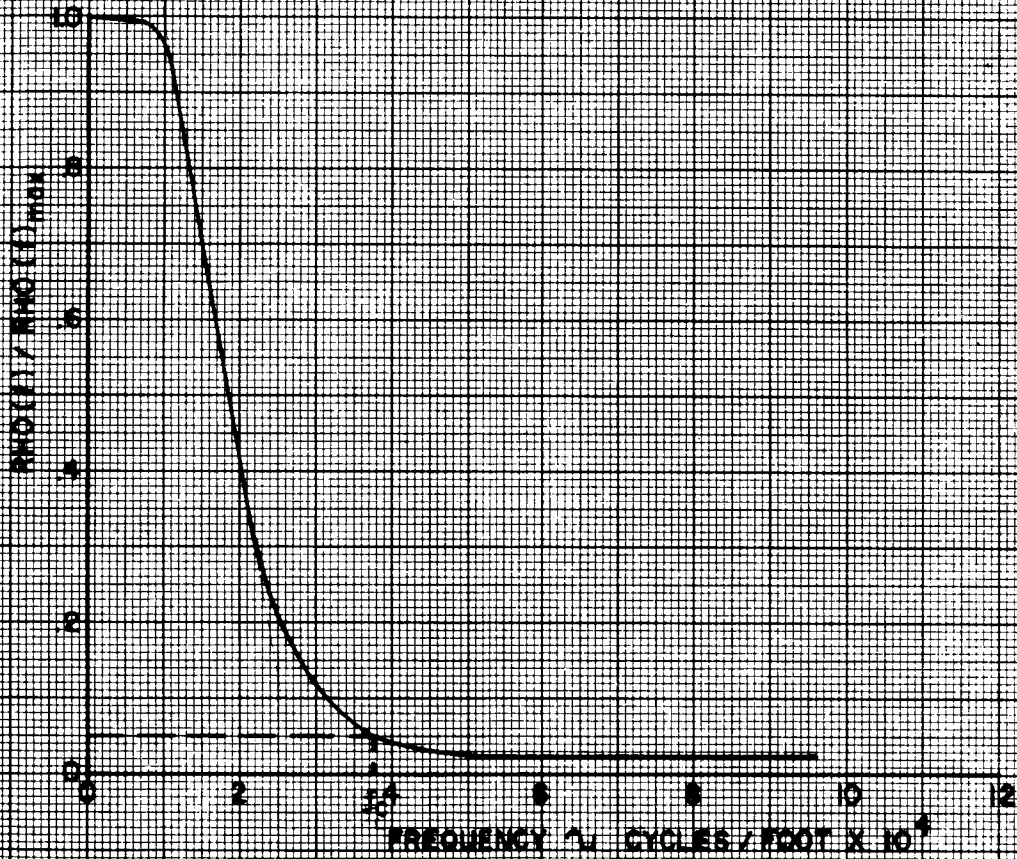


FIGURE 3

COMPOSITE POWER SPECTRAL DENSITY
LLANO RANDOM LINES

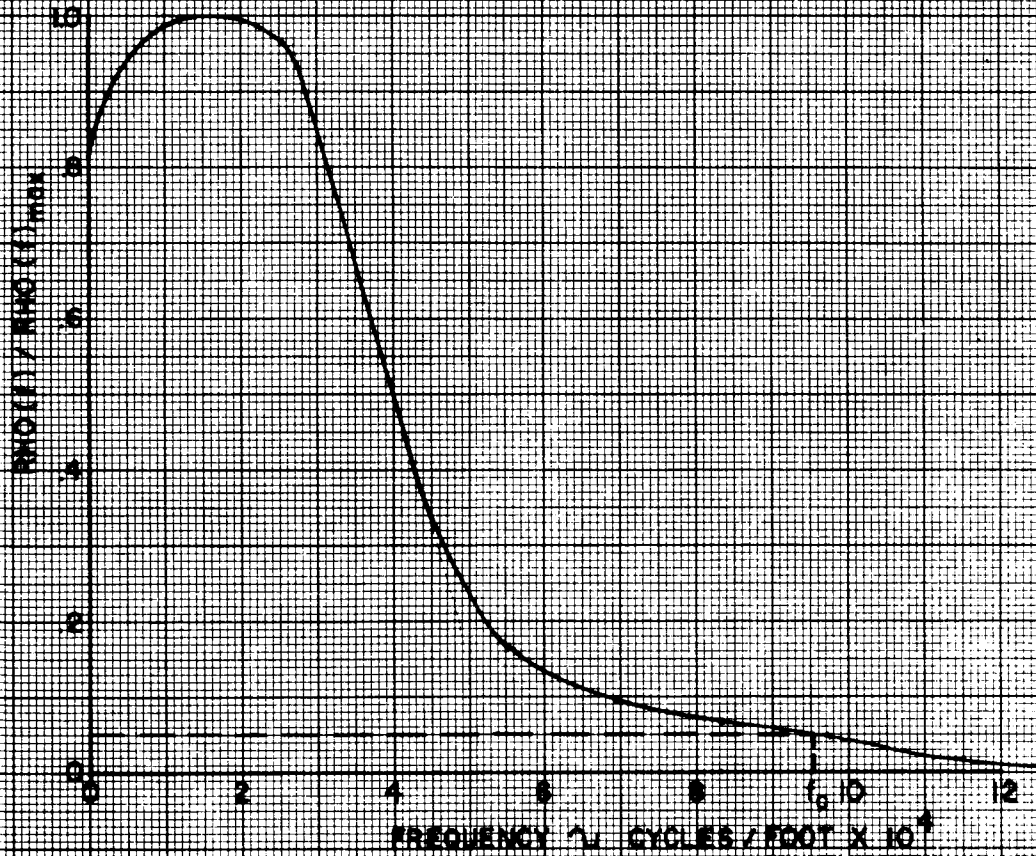


FIGURE 4

COMPOSITE POWER SPECTRAL DENSITY
BENTON, PENNA.
4 RANDOM LINES

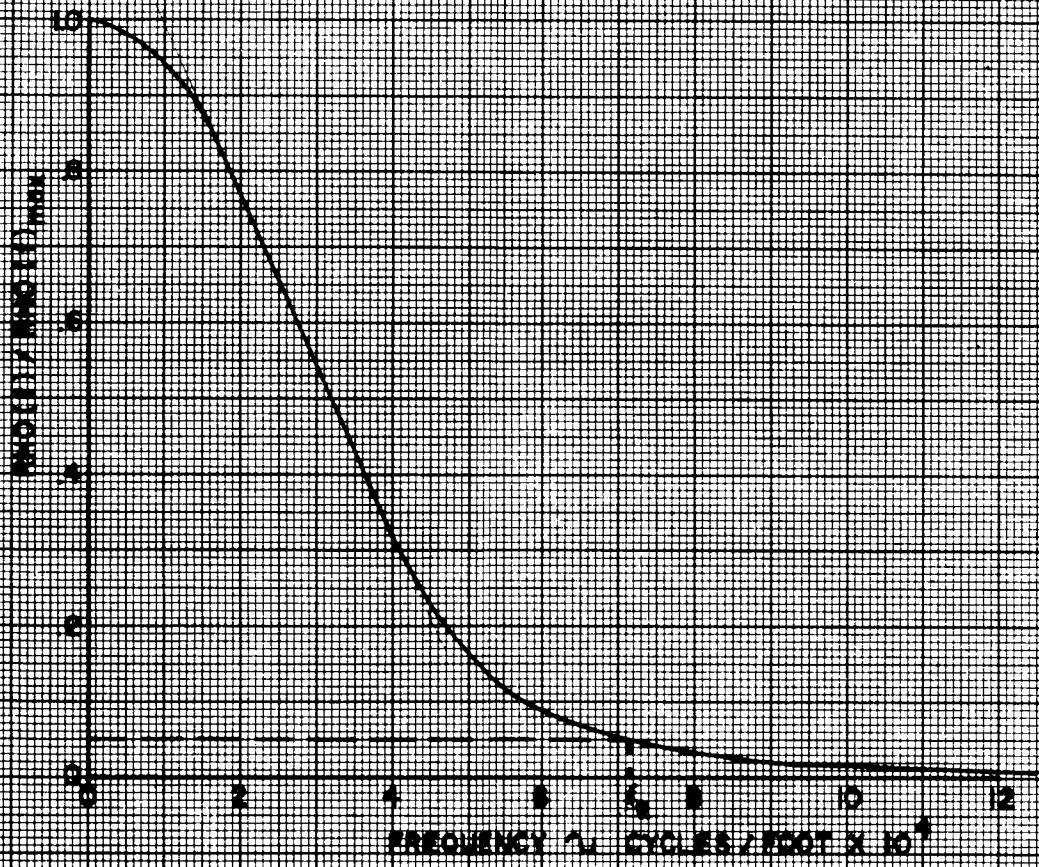


FIGURE 5

COMPOSITE POWER SPECTRAL DENSITY
TAYLOR, IOWA
4 RANDOM LINES

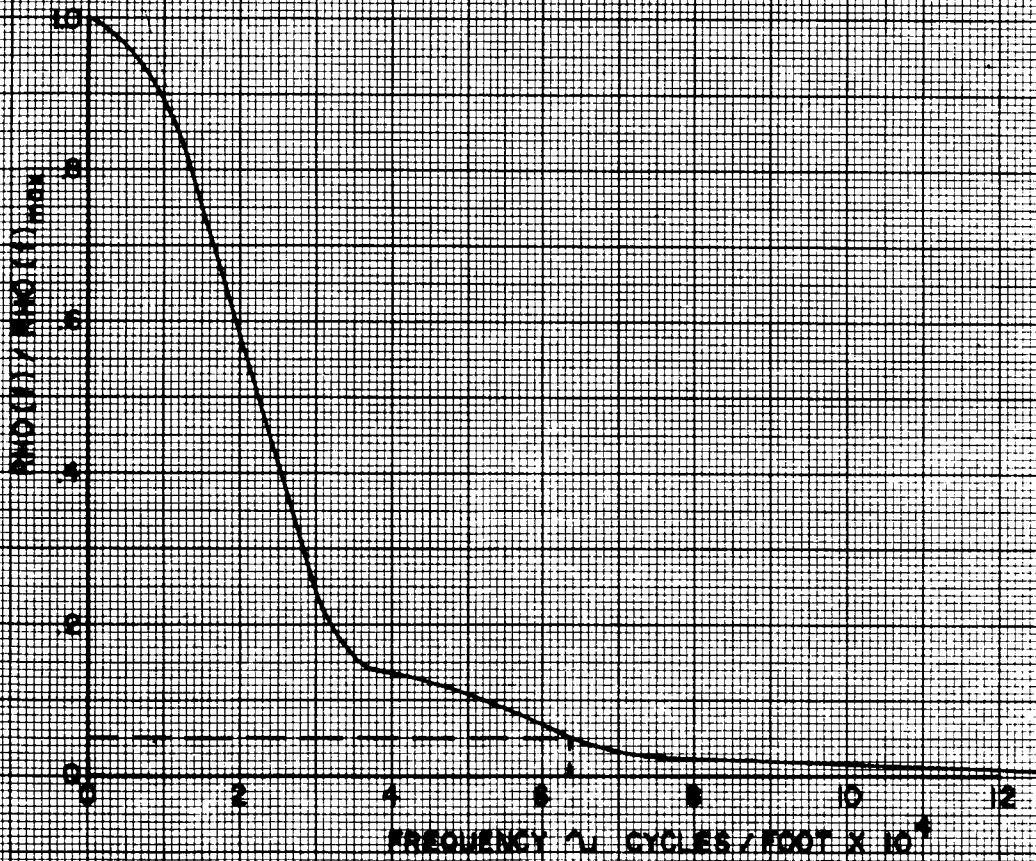


FIGURE 6

COMPOSITE POWER SPECTRAL DENSITY
SEACOM AREA B

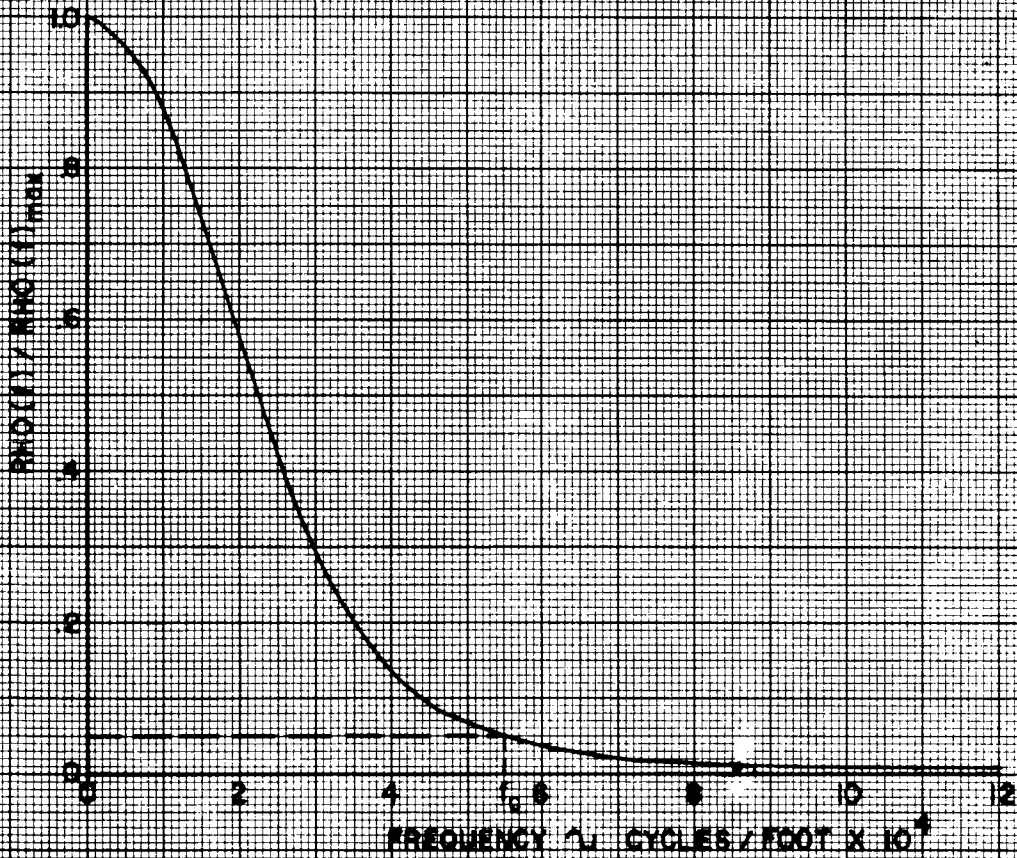


FIGURE 7

COMPOSITE POWER SPECTRAL DENSITY
SEACOM AREA C

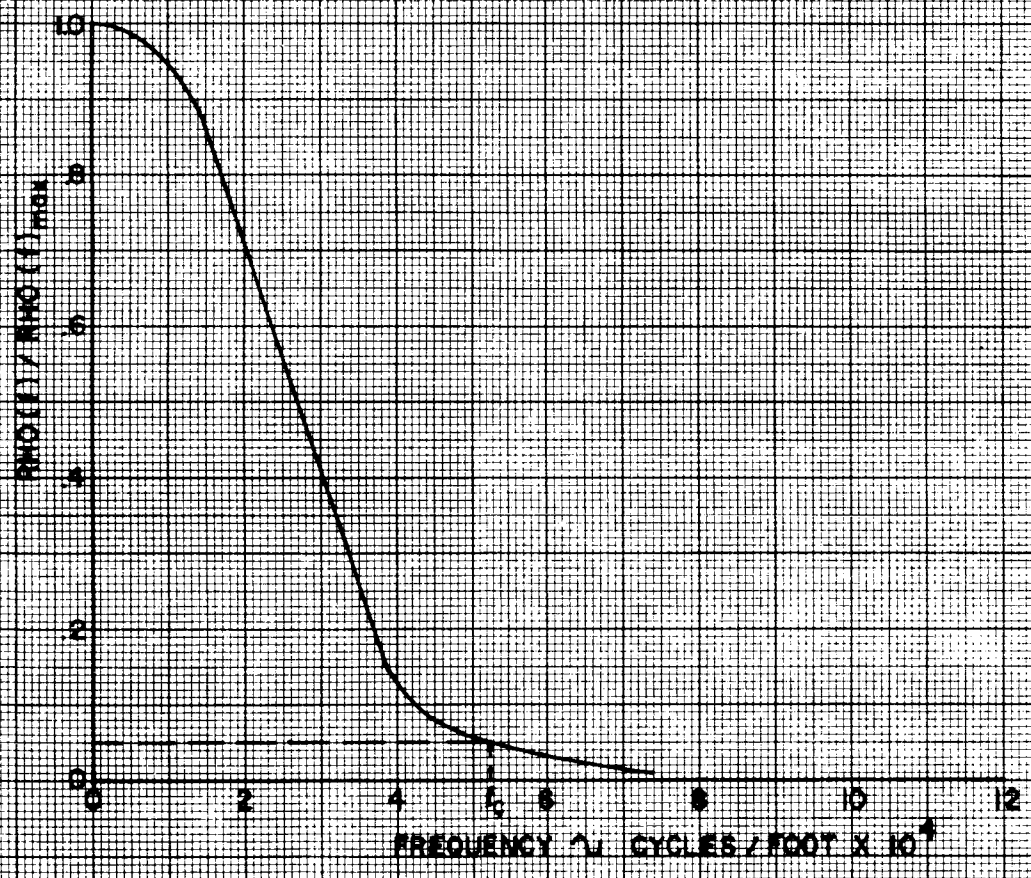
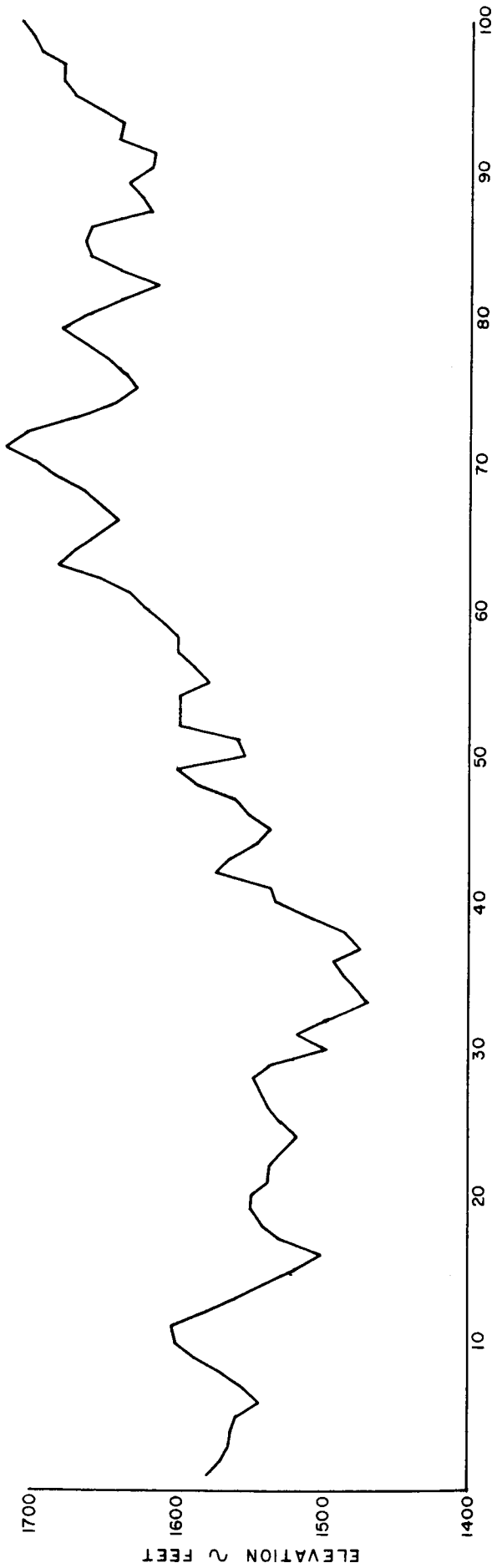


FIGURE 8

751-27



SAMPLE INTERVALS
 $I = 400$ FT.

FIGURE 9 LLANO, TEXAS RANDOM LINE NO.3

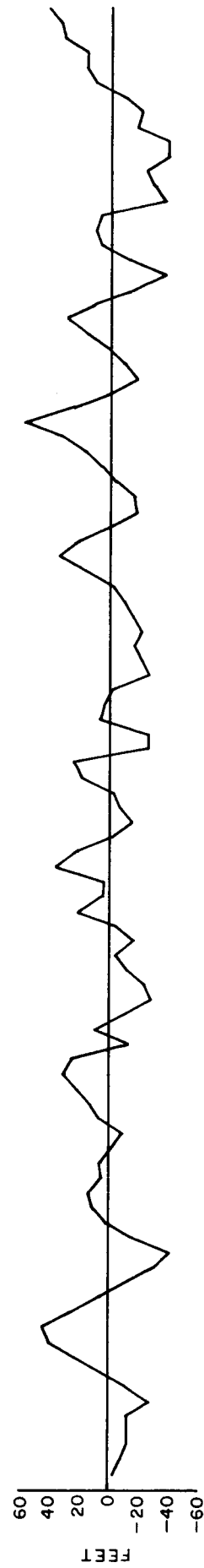


FIGURE 10 RANDOM LINE NO. 3 REFINED

APPENDICES 4.3-A through 4.3-H
RADAR SENSOR ANALYTICAL DEVIATIONS

Included in the following sections are:

List of symbol definitions

Derivations of system radar parameters

Basic weight and volume relations

Detail error analysis

SYMBOL DEFINITIONS - Appendix 4.3-A

A	=	Surface illuminated area
A_t	=	Illuminated threshold area
B_{IF}	=	IF bandwidth
B_n	=	Receiver noise bandwidth
B_v	=	Video bandwidth
c	=	Velocity of light = 9.8355923×10^8 ft./sec.
CR	=	Resolution of digital memory device
D	=	Antenna aperture size
E	=	Antenna efficiency
f_o	=	Frequency of maximum response

G	=	Antenna gain
h	=	Altitude = 490,000 ft. (80 nm)
H(f)	=	Frequency-response characteristic of IF amplifier
K	=	Boltzman's constant = 1.38×10^{-23} joules
LRS	=	LUCOM Radar Sensor
m	=	Number of noise samples per TRO
Δm	=	Number of noise samples excluded by closing range gate
n'	=	Number of noise samples per range gate
N	=	Number of returns averaged
NF	=	Noise factor (figure)
N_{fa}	=	Average number of noise samples between false alarms
P_{av}	=	Prime power necessary to provide required average transmitted power over a PRT
P_d	=	Probability of detection: probability of signal-plus-noise exceeding threshold
P_{fa}	=	Probability of false alarm per noise sample
P_o	=	Average sensor prime power independent of output power
P_p	=	Average prime power
PRF	=	Transmitter repetition frequency in pulses per second
PRT	=	Transmit-receive interval
P_v	=	Received power at which verticality error appears
P_l	=	Relative received power threshold

$P_{\text{lock-on}}$	=	Probability of lock-on
P_{max}	=	Maximum received power
$P(t)$	=	Received power as a function of time
P_t	=	Peak transmitted power
P_s	=	Probability of success during range gate
P'_s	=	Probability of success during T_{ro}
Q_{fa}	=	Probability of zero false alarms per noise sample
Q'_{fa}	=	Probability of zero false alarms in range gate
Q''_{fa}	=	Probability of zero false alarms during T_{ro}
R	=	Signal envelope amplitude
RSS	=	Root of the sum of the error mean squares
$S/N/N$	=	Signal-plus-noise-to-noise ratio
T	=	Noise temperature in °Kelvin
t_o	=	Rise time of return
T/N	=	Threshold-to-noise power ratio
t_{rg}	=	Minimum range gate width
T_{ro}	=	Maximum receiver open time
t_v	=	Maximum vertical altitude change per PRT
V	=	Volume
V_g	=	Ground speed of vehicle = 5000 ft./sec.
V_T	=	Relative threshold voltage
W	=	Weight

γ	=	Worst case surface gradient
θ	=	Half-power antenna beamwidth
θ_A	=	Half-power beamwidth of array with isotropic elements
θ_E	=	Half-power E plane antenna beamwidth
θ_H	=	Half-power H plane antenna beamwidth
ϕ	=	Verticality angle error
λ	=	Wavelength
σ_l	=	Lunar scattering-reflection coefficient = -25 db
η	=	Overall sensor power efficiency
τ	=	Pulsewidth
ω	=	Radian frequency
ψ_0	=	Mean square noise voltage

RADAR SYSTEM PARAMETERS

Appendix 4.3-B

The system parameters discussed in this section are receiver noise bandwidth, receiver noise figure, RF carrier frequency, and pulse repetition frequency.

The radar receiver is subjected to undesired front-end receiver noise which can introduce errors into the measurement of range information. The amount of noise that enters a receiver is proportional to the effective noise bandwidth (the greater the bandwidth the greater the front-end noise). Since the receiver's bandwidth has to be wide enough to preserve the radar echo's leading edge (rise time) to obtain accurate range information, the amount the bandwidth can be decreased is limited by the rise time of the return signal's leading edge. Figure 4.3-B-1 shows the conventional approximation of the front-end noise of a receiver as independent noise samples, which are spaced at intervals equal to the reciprocal of the receiver noise bandwidth (B_n).

Figure 4.3-B-2 reflects the approximated video return for the beamwidth limited cases being considered. The Laplace transform of $P(t)$, received power as a function of time, is

$$L [P(t)] = \frac{P_{\max}}{t_0} \int_0^{t_0} t e^{-st} dt + P_{\max} \int_{t_0}^{\tau} e^{-st} dt - \frac{P_{\max}}{t_0} \int_{\tau}^{\tau+t_0} (t-\tau-t_0) e^{-st} dt$$

Performing the integrations, this reduces to

$$L [P(t)] = \frac{P_{\max}}{t_0 S^2} \left(1 - e^{-st_0} \right) \left(1 - e^{-s\tau} \right)$$

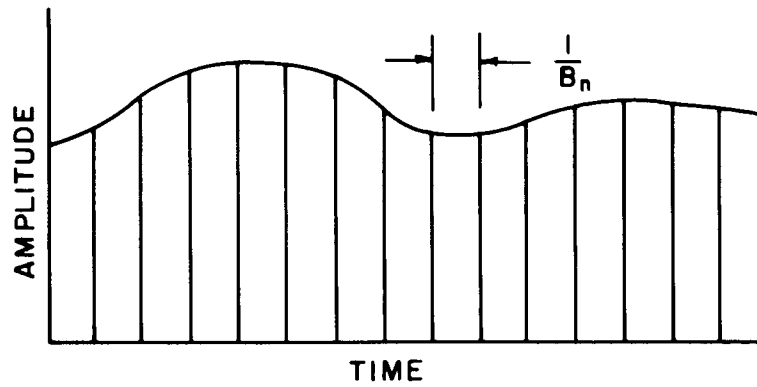


FIGURE 4.3-B-1 NOISE SAMPLES

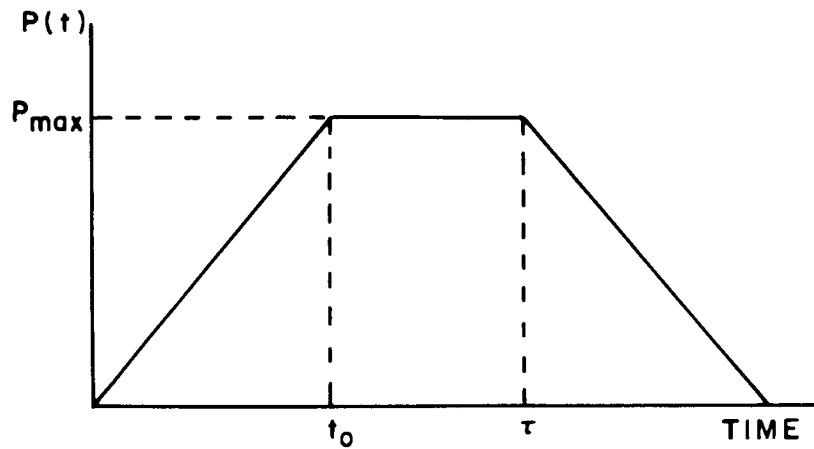


FIGURE 4.3-B-2 VIDEO RETURN

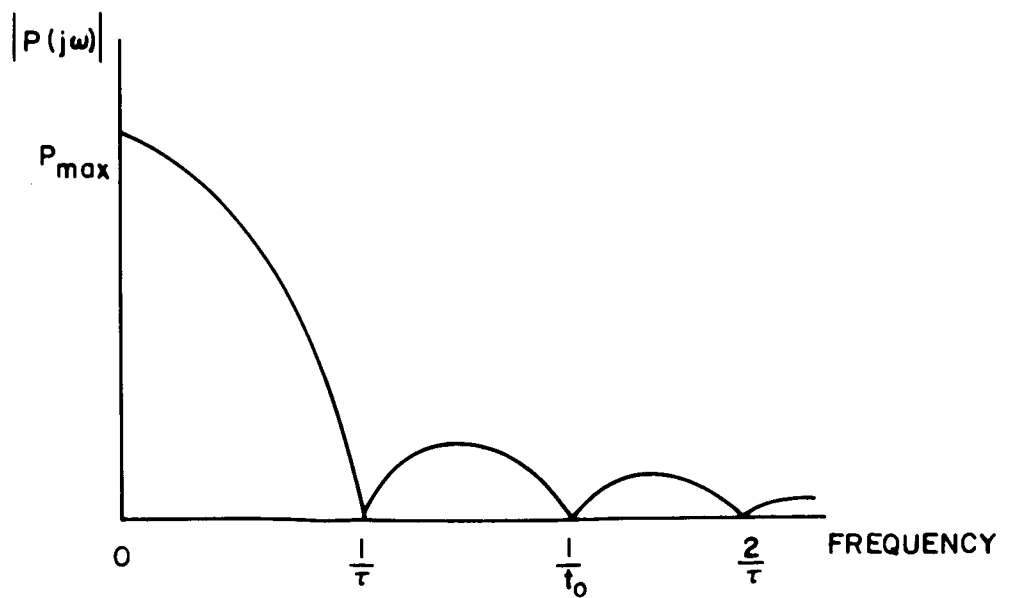


FIGURE 4.3-B-3 FREQUENCY SPECTRUM

The one-sided Fourier transform may be found by setting $s = j\omega$, i. e.,

$$F [P(t)] = P(j\omega) = \tau P_{\max} e^{-j\omega(t_0 + \tau)} \frac{\sin \frac{\omega t_0}{2}}{\frac{\omega t_0}{2}} \cdot \frac{\sin \frac{\omega \tau}{2}}{\frac{\omega \tau}{2}}$$

whose absolute magnitude is

$$|P(j\omega)| = \tau P_{\max} \left| \frac{\sin \pi t_0 f}{\pi t_0 f} \cdot \frac{\sin \pi \tau f}{\pi \tau f} \right|$$

This frequency spectrum of the video signal is shown in Figure 4.3-B-3. Since the power return is extremely dependent on the steepness of the leading edge, a video bandwidth (B_v) of $\frac{1}{t_0}$ or wider is necessary. For

this study the relation $B_v = \frac{1}{t_0}$ was used since

$$t_0 = \frac{2h}{c} (\sec \frac{\theta}{2} - 1) \quad (4.3-B-1)$$

where h = operational altitude
 c = speed of light
 θ = antenna beamwidth in degrees

The video bandwidths can be determined for a given beamwidth and altitude. For an altitude of 490,000 feet, the video bandwidths for the cases considered were:

θ	5°	3°	1°
B_v	1 mc	3.3 mc	30 mc

The required IF bandwidth (B_{IF}) is twice the video bandwidth plus a frequency tolerance for AFC tolerance and IF bandwidth stability (2.2 mc was used in the study).

A receiver's thermal noise bandwidth (B_n) is an integrated bandwidth.

$$B_n = \frac{\int_{-\infty}^{\infty} |H(f)|^2 df}{|H(f_0)|^2}$$

where $H(f)$ = frequency-response characteristic of IF amplifier

f_0 = frequency of maximum response

A comparison of noise bandwidth and filter 3 db bandwidth for various filter types is shown in Table 4.3-B-1.

<u>Type of Receiver Circuit</u>	<u>No. of Stages</u>	<u>Ratio of Noise to 3 db Bandwidth</u>
Single tuned	1	1.57
	2	1.22
	3	1.16
	4	1.14
	5	1.12
Double Tuned	1	1.11
	2	1.04
Staggered Triple	1	1.148
Staggered Quadruple	1	1.019
Staggered Quintuple	1	1.01
Gaussian	1	1.065

Table 4.3-B-1 BANDWIDTH COMPARISON

A factor of 1.2 was used to determine B_n for this study, i. e.,

0	5°	3°	1°
B_n	4.8 mc	10.2 mc	60 mc

A measure of the noise produced by a practical receiver compared with the noise of an ideal receiver is the noise figure (NF). A receiver's minimum noise figure is related to its frequency and bandwidth. Table 4.3-B-2 reflects noise figures in db as a function frequency and the beamwidth cases under consideration used in this study.

<u>Frequency Band</u>	<u>5°</u>	<u>Beamwidth 3°</u>	<u>1°</u>
C	7.0 db	7.0 db	8.5 db
X	7.5 db	7.5 db	9.5 db
Ku	10.0 db	10.0 db	15.0 db
Ka	15.0 db	15.0 db	21.5 db

Table 4.3-B-2 NOISE FIGURE (db)

In the actual calculations, specific frequencies within the bands were used. The frequencies used were C band-6 gc, X band-9 gc, Ku band -18 gc, and Ka band-35 gc.

The temperature T which appears in the radar equation is the temperature at the input to the network. In this study, the maximum lunar surface temperature of 101°C (374°K) was used as T.

The maximum pulse repetition frequency (PRF) is determined by the maximum distance between the vehicle and the lunar surface. For a maximum altitude of 490,000 ft. the maximum unambiguous PRF would be

$$\overline{\text{PRF}} = \frac{c}{2h} = 1003.6 \text{ pps}$$

where c = velocity of light (9.835592×10^8 ft./sec.)

The actual PRF would be lower than this value due to sensor signal processing time; however, a maximum PRF of 1000 pps was used for study purposes. A low PRF of 4 pps was also used to reflect that simulated in the lunar model profile analysis. Trade-offs were also analyzed at a PRF of 100 pps for trend setting purposes.

RANGE GATE

Appendix 4.3-C

To obtain a high resolution radar sensor (LRS) which has a high probability of overall system success with minimum transmitter power requirement, a narrow digital controlled electronic range gate is incorporated into the system. Range gating is the method of enabling the receiver to receive an expected return. Reducing the range gate time is analogous to decreasing the system's noise bandwidth, thereby decreasing the number of false alarms that can reach the decision making element and provides the LRS with a tracking range gate that can accept fast rate of changes in range measurements since there is no time-constant associated with the digital range gate memory device. The range gate has two modes of operation, acquisition of the lunar surface reflected signal and tracking the reflected signal on a pulse to pulse basis.

The range section of the data processor provides a search or target acquisition capability which is independent of time delays since the range gate is electronically digital controlled and not servo controlled. This is accomplished by taking no information from the range section except as a gating function. This allows the receiver blanking portion of the range gate to close in on the true lunar surface radar return excluding the false alarms which occur (in time) ahead of the previously accepted signal and progressively restrict the number of false firings which can occur, thereby causing the false alarm probability per transmit-receive interval to decrease until true target acquisition is achieved.

Since the range-gate uses no averaging process, the memory is up-dated on a pulse to pulse basis if a radar return is received and accepted by the sensor's decision making element as a true target return. After target acquisition, if one or more radar returns fail to cross the decision element's threshold, the range memory has the ability to retain the digital range information for any predetermined number of transmit-receive intervals before reverting to the target acquisition mode of operation.

The minimum range gate width (t_{rg}) which can function properly in the LRS modes of operations (acquisition and tracking) is a function of several system parameters. These parameters are antenna beamwidth, operational altitude, resolution of the range gate memory device and the delta range change that can occur from transmit to transmit interval. These system parameters make up the three components of t_{rg} , which for convenience will be designated as t_o , t_v and CR.

$$t_{rg} = t_o + t_v + CR$$

t_o = the rise time of the leading edge of the return power

t_v = the maximum vertical altitude change per PRT

CR = resolution of the digital memory device, which is a function of the standard clock

The component t_o can be found from equation 4.3-B-1 (Figure 4.3-B-2). The t_v component of t_{rg} can be found from the vehicle's ground speed (feet per second), LRS repetition frequency and the worst case terrain gradient .

$$t_v = \frac{V_g \tan \gamma}{PRF}$$

where V_g = Vehicles ground speed (feet per sec.)

γ = Worst case surface gradient

PRF = Transmitter repetition frequency in pulses per second

Since the range gate t_{rg} is opened from information acquired from the preceding transmitted pulse, two (t_v) components were incorporated into (t_{rg}) for this study to allow at least 2 PRTs without detection before reverting to the acquisition mode. The last component of t_{rg} (CR) depends upon the frequency of the standard clock in the data processor. As an illustration, for a 50 megacycle clock the digital counter's resolution would be one clock cycle or 20 nanoseconds. This is equivalent to 10 feet two-way propagation for the transmitter RF energy.

$$CR = \frac{1}{\text{Clock Frequency}}$$

A final equation for a minimum (t_{rg}) range-gate width will result.

$$t_{rg} = t_o + 2 t_v + CR$$

$$t_{rg} = \frac{2h}{c} \left(\sec \frac{\theta}{2} - 1 \right) + \frac{2V_g \tan \gamma}{\text{PRF}} + \frac{1}{\text{Clock Frequency}}$$

For the cases considered, the following parameters were used:

$$V_g = 5000 \text{ ft./sec.}$$

$$\gamma = 0.5^\circ$$

$$\text{Clock Frequency} = 50 \text{ mc}$$

Table 4.3-C-1 reflects the corresponding values of t_{rg} .

PRF (pps)	Beamwidth		
	5°	3°	1°
4	6.1 us	5.4 us	5.1 us
100	1.3 us	0.6 us	0.3 us
1000	1.1 us	0.4 us	0.2 us

Table 4.3-C-1 MINIMUM RANGE-GATE WIDTH (t_{rg})

Since the receiver is opened a finite length of time ahead of the return pulse, the detector is susceptible to a false alarm by triggering on noise and a probability is associated with the occurrence of this event. Also, there is a probability associated with the event that the return in the presence of noise will not exceed the threshold. For purposes of definition, the probability that such a noise false alarm does not occur in the delta range gate (t_{rg}) time or the probability of zero false alarms is Q'_{fa} . The probability that signal plus noise will

exceed the threshold is defined as P_d . Thus, there is a probability that if the signal is present, the signal will be detected; i. e., the probability that there is zero false alarms preceding the true return and that the return is detected. This is termed the probability of success (P_s) and is the product of Q'_{fa} and P_d .

$$P_s = Q'_{fa} P_d$$

DETECTION CRITERION

Appendix 4.3-D

In this study, a detection criterion was established to obtain receiver signal-to-noise ratios to achieve specific probabilities of detection without exceeding specific probabilities of false alarms.

The received signal consists of two parts, (1) that due to receiver generated noise and the thermal noise attributed to the antenna radiation resistance, and (2) return signal reflected from the terrain. The first or noise component is Gaussian noise, modified by the sensor bandpass characteristics. The envelope of this signal was a Rayleigh distribution of amplitude. A square law detector changes this to an exponential or chi - square distribution. The return signal from the surface may be considered as the vector sum of a large number of components from small elemental areas of the surface. For any one pulse, the amplitude and phase of each elemental contribution to the return signal may be considered as fixed. However, for successive pulses, the motion of the vehicle alters phase relations, with the result that amplitudes in successive pulses are essentially uncorrelated for the usual case. The amplitude of the elemental contributions will be Rayleigh distributed, and at video the distribution will be exponential, as was the case with noise.

Since the return signal can only be specified on a statistical basis, the threshold crossing must also be expressed statistically. This is a type of problem for which no known solution exists. Receiver operation can be simulated with a digital computer and many trials can be run to approximate the statistics of the threshold crossing. Such a simulation program has been developed "in-house" by Dr. F. E. Brooks, but was not available early enough to generate sufficient data to derive detection statistics for this study. The program was utilized to predict the rms deviation from a mean threshold crossing time. The computer program and its application for determining signal variations at the threshold are discussed in the error analysis in Appendix 4.3-H.1.

A method for setting detection probabilities for constant amplitude signal is well known. This method, which is discussed below, was utilized and a high probability of detection was imposed to allow for any reduction associated with a varying return signal.

As noted earlier the envelope of noise component of the signal is Rayleigh distributed and can be written:

$$p(R)dR = \frac{R}{\psi_0} e^{-\frac{R^2}{2\psi_0}} dR$$

where R = envelope amplitude

ψ_0 = mean square noise voltage

The probability that the envelope of the noise voltage will exceed a voltage threshold voltage V_T is

$$\begin{aligned} \Pr (V_T < R < \infty) &= \int_{V_T}^{\infty} \frac{R}{\psi_0} e^{-\frac{R^2}{2\psi_0}} dR \\ &= e^{-\frac{V_T^2}{2\psi_0}} \end{aligned} \quad (4.3-D-1)$$

Since a false alarm occurs when the noise exceeds the threshold, equation (4.3-D-1) gives the probability of false alarm (P_{fa}), or

$$P_{fa} = e^{-\frac{V_T^2}{2\psi_0}}$$

This voltage relation may be converted to a threshold-to-noise power relation, T/N :

$$P_{fa} = e^{-T/N}$$

If a sine-wave signal with amplitude A is present with the noise, the envelope then has the probability density function

$$Ps(R)dR = \frac{R}{\psi_0} e^{-\frac{R^2 + A^2}{2\psi_0}} I_0 \left(\frac{RA}{\psi_0} \right) dR$$

Where $I_0(\frac{RA}{\psi_0})$ is the modified zero order Bessel function. The probability of detection is the probability that the envelope R will exceed the threshold, or

$$P_d = \Pr(V_T < R < \infty)$$

$$P_d = \int_{V_T}^{\infty} \frac{R}{\psi_0} e^{-\frac{R^2 + A^2}{2\psi_0}} I_0\left(\frac{RA}{\psi_0}\right) dR$$

This relation has to be evaluated by numerical techniques and results in a family of curves relating the probability of detection to threshold voltage and signal amplitude, or

$$P_d = f\left(\frac{V_T^2}{2\psi_0}, \frac{A^2}{2\psi_0}\right)$$

which can again be converted to threshold-to-noise and signal-plus-noise-to-noise power relations:

$$P_d = f\left(T/N, \frac{S+N}{N}\right)$$

A more graphic illustration of the process of detection is shown in Figure 4.3-D-1. The probability density function for noise alone, $p(R)$, is plotted along with that for signal-plus-noise, $p_s(R)$, for a specific signal amplitude to rms noise voltage ratio. The cross-dotted area to the right of the threshold under the curve for signal-plus-noise represents the probability of detection, while the double-crossdotted area under the curve for noise alone represents the probability of a false alarm. As can be observed, if the threshold setting is increased to reduce the probability of a false alarm or increase the probability of zero false alarms, the probability of detection will be reduced also.

For purposes of threshold settings, the probability of zero false alarms in the range gate, Q'_{fa} , (which was introduced in the previous section) can be related to the probability of false alarm per noise sample, P_{fa} . Letting Q'_{fa} be a desired probability of zero false alarms during the range gate, the probability of zero false alarms per noise sample (Q_{fa}) can be determined from the following:

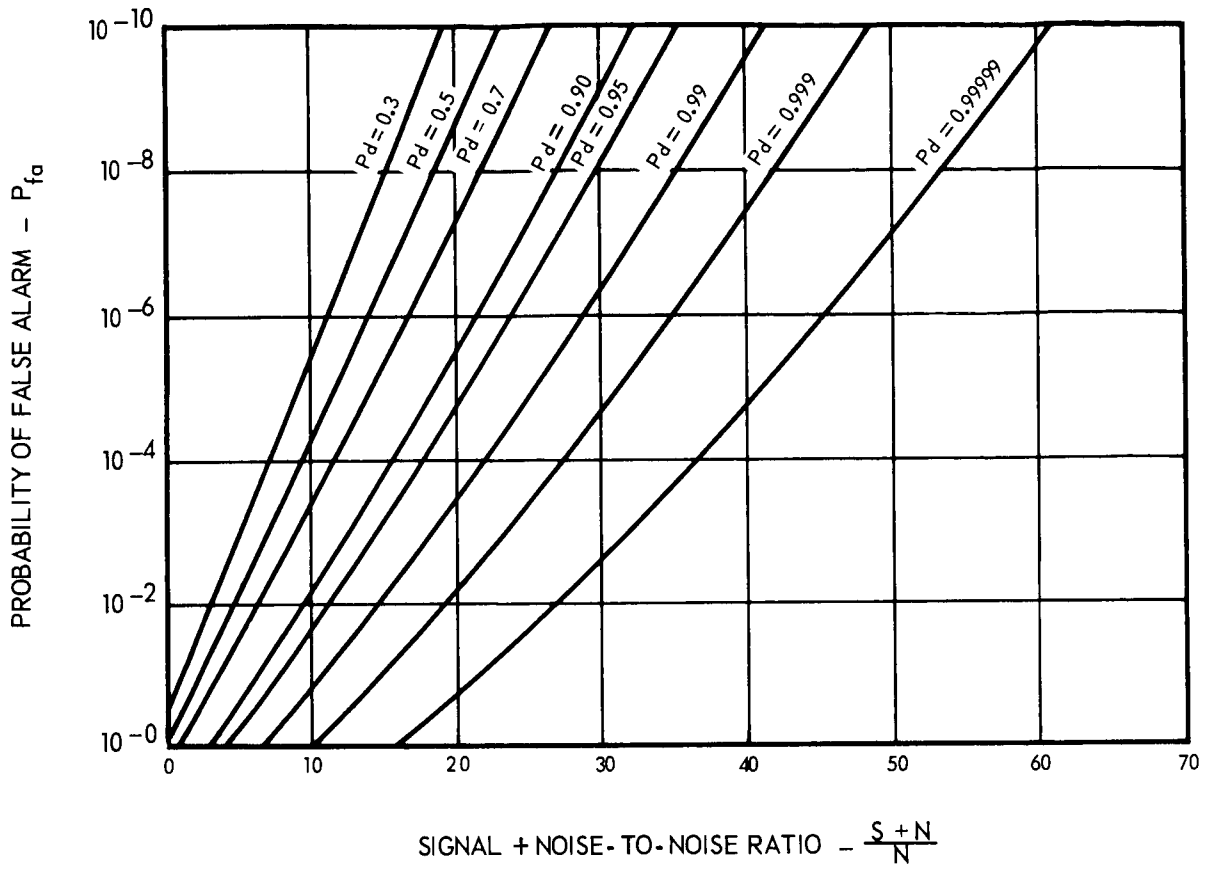


FIGURE 4.3-D-2. DETECTION PROBABILITY (P_d)

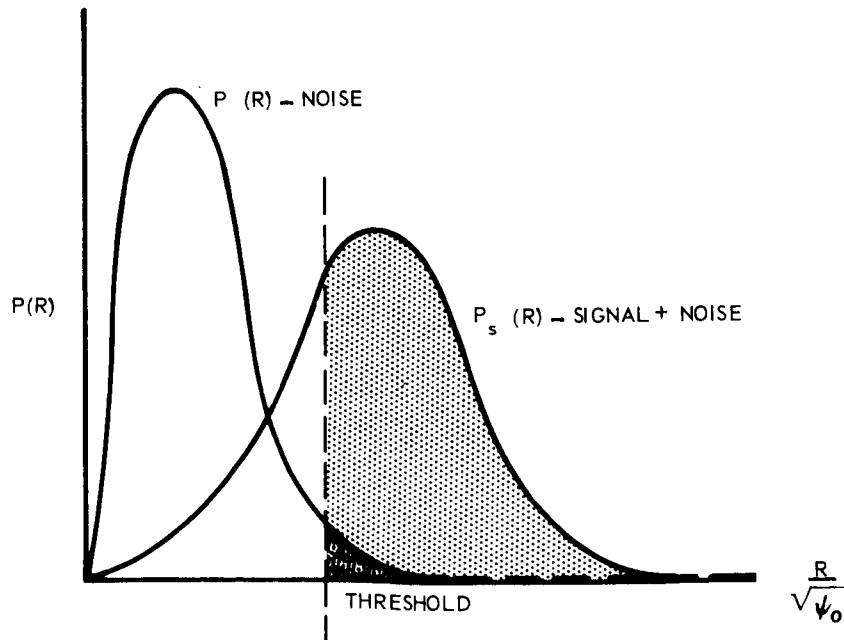


FIGURE 4.3-D-1. THRESHOLD DETECTION

$$Q'_{fa} = (Q_{fa})^{n'}$$

$$Q_{fa} = (Q'_{fa})^{1/n'}$$

Where n' is the number of noise samples during range gate:

$$n' = B_n^t \text{rg}$$

The probability of zero false alarms is also related to the probability of false alarm per noise sample by

$$Q_{fa} = 1 - P_{fa}$$

Thus since $P_{fa} = e^{-T/N}$

the threshold-to-noise setting for a specified Q'_{fa} can be determined

$$Q'_{fa} = (1 - e^{-T/N})^{n'}$$

or $T/N = -\ln (1 - (Q'_{fa})^{1/n'})$

Table 4.3-D-1 reflects values of T/N in db for values of Q'_{fa} of 50%, 85%, and 99% for the specific cases being considered.

Beamwidth Q'_{fa} (%)	5°			3°			1°			
	PRF (pps)	99	85	50	99	85	50	99	85	50
4		9.01	7.15	5.74	9.36	7.78	6.42	9.96	8.76	7.84
100		8.06	5.59	3.48	8.06	5.59	3.30	8.70	6.74	5.16
1000		7.93	5.37	3.12	7.85	5.09	2.66	8.50	6.35	4.50

Table 4.3-D-1 THRESHOLD-TO-NOISE (db)

Since $P_s = Q'_{fa} P_d'$

a high probability of detection should be imposed if P_s is to approach Q'_{fa} . For this study, a $P_d = 99.9\%$ was so imposed. From Figure 4.3-D-2 signal-plus-noise-to-noise values can be determined for the cases covered by Table 4.3-D-1.

Table 4.3-D-2 reflects these values in db:

Beamwidth Q'_{fa} (%)	5°			3°			1°			
	PRF (pps)	99	85	50	99	85	50	99	85	50
4		14.20	13.26	12.58	14.27	13.46	12.75	14.70	14.02	13.51
100		13.60	12.56	11.56	13.60	12.56	11.56	14.00	12.90	12.67
1000		13.56	12.50	11.52	13.50	12.38	11.46	13.80	12.70	12.26

Table 4.3-D-2 SIGNAL-PLUS-NOISE-TO-NOISE (db)
for $P_d = 99.9\%$

A high probability of zero false alarms during the receive interval is required for a short acquisition period and to remain in the tracking mode.

Figure 4.3-D-3 reflects the first requirement for a 3° beam-width and 100 pps PRF system. Curves I and II indicate the progressive increasing probability of target acquisition with a narrow range gate as a function of number of PRT's for Q'_{fa} of 99% and 85%, respectively. Curve III shows the acquisition probability with a constant maximum range gate for Q'_{fa} of 99%. This time is the maximum receiver open time to acquire maximum altitude variations (assumed 30,000 ft.). Similar data was generated at Q'_{fa} of 85% but low probabilities resulted for the number of PRT's in the figure, e.g., a probability of lock-on of only .01% was gained after 1620 PRT's. The results of the curves are two-fold: a range gating system such as that proposed is necessary, as well as a high Q'_{fa} .

The data for Curves I and II were obtained in the following manner. Knowing P_{fa} , the average number of noise samples per false alarm (N_{fa}) is

$$N_{fa} = \frac{1}{P_{fa}}$$

and the average time between false alarm crossings (T_{fa}) is

$$T_{fa} = \frac{1}{B_n P_{fa}}$$

The probability of lock-on ($P_{lock-on}$) for a given PRT for $m - \Delta m < n$ where

m = number of noise samples per T_{ro} interval

m = $B_n T_{ro}$

Δm = amount of receiver noise excluded by closing range gate

Δm = N_{fa} times the number of preceding PRT's

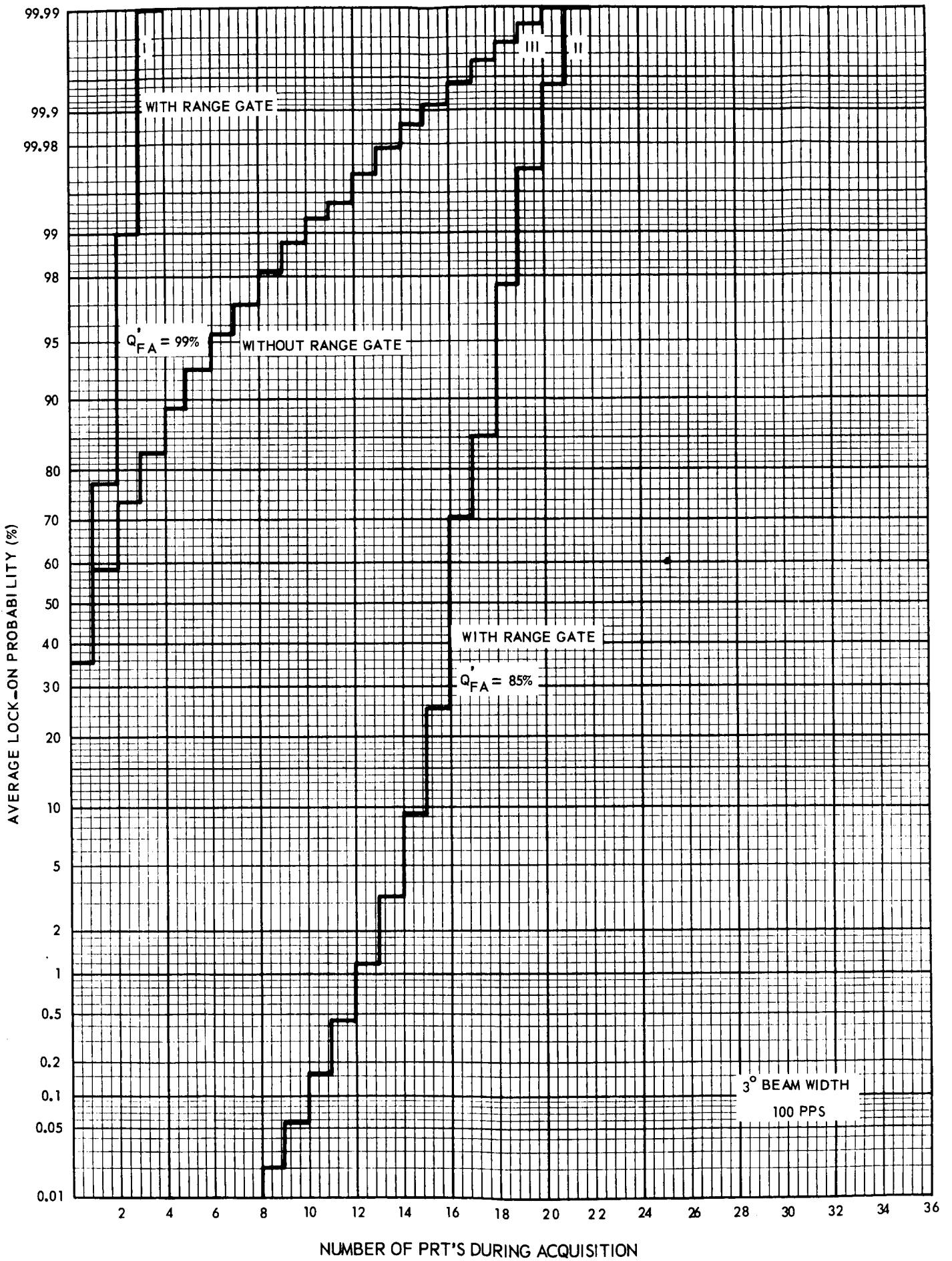


FIGURE 4.3-D-3. LOCK-ON PROBABILITY

$$\text{is } P_{\text{lock-on}} = (Q_{\text{fa}})^{m - \Delta m} \quad (4.3-D-2)$$

When the range gate has closed to its minimum, or $t_{\text{rg}}, m - \Delta m > n'$

Under these conditions, equation 4.3-D-2 becomes

$$P_{\text{lock-on}} = 1 - (1 - P'_s)^{\text{No. of PRT's}}$$

Since curve III reflects the condition without range gate action, equation 4.3-D-2 becomes the probability of finding at least one PRT which contains zero false alarms or

$$P_{\text{lock-on}} = 1 - (1 - P'_s)^{\text{No. of PRT's}}$$

where $P'_s =$ probability of success during t_{ro}

$$P'_s = Q''_{\text{fa}} P_d$$

$Q''_{\text{fa}} =$ probability of zero false alarms during T_{ro}

$$Q''_{\text{fa}} = (Q_{\text{fa}})^m$$

For all curves a P_d of 99.9% was used, so

$$P_s \approx Q'_{\text{fa}}$$

$$P'_s \approx Q''_{\text{fa}}$$

Figure 4.3-D-4 shows the relationship between the predetected threshold to noise ratio (T/N) and zero false alarm probability (Q'_{fa}) during the range gate (t_{rg}) for two specific range gate widths.

The 0.6 microsecond range gate locus is the calculated width for an antenna beamwidth of 3 degrees and a repetition frequency of 100 pps. The 1.2 microsecond range gate locus indicates the effects on the 0.6 microsecond range gate if a false alarm crossed the decision threshold when the range gate is first opened as a worst case comparison. The

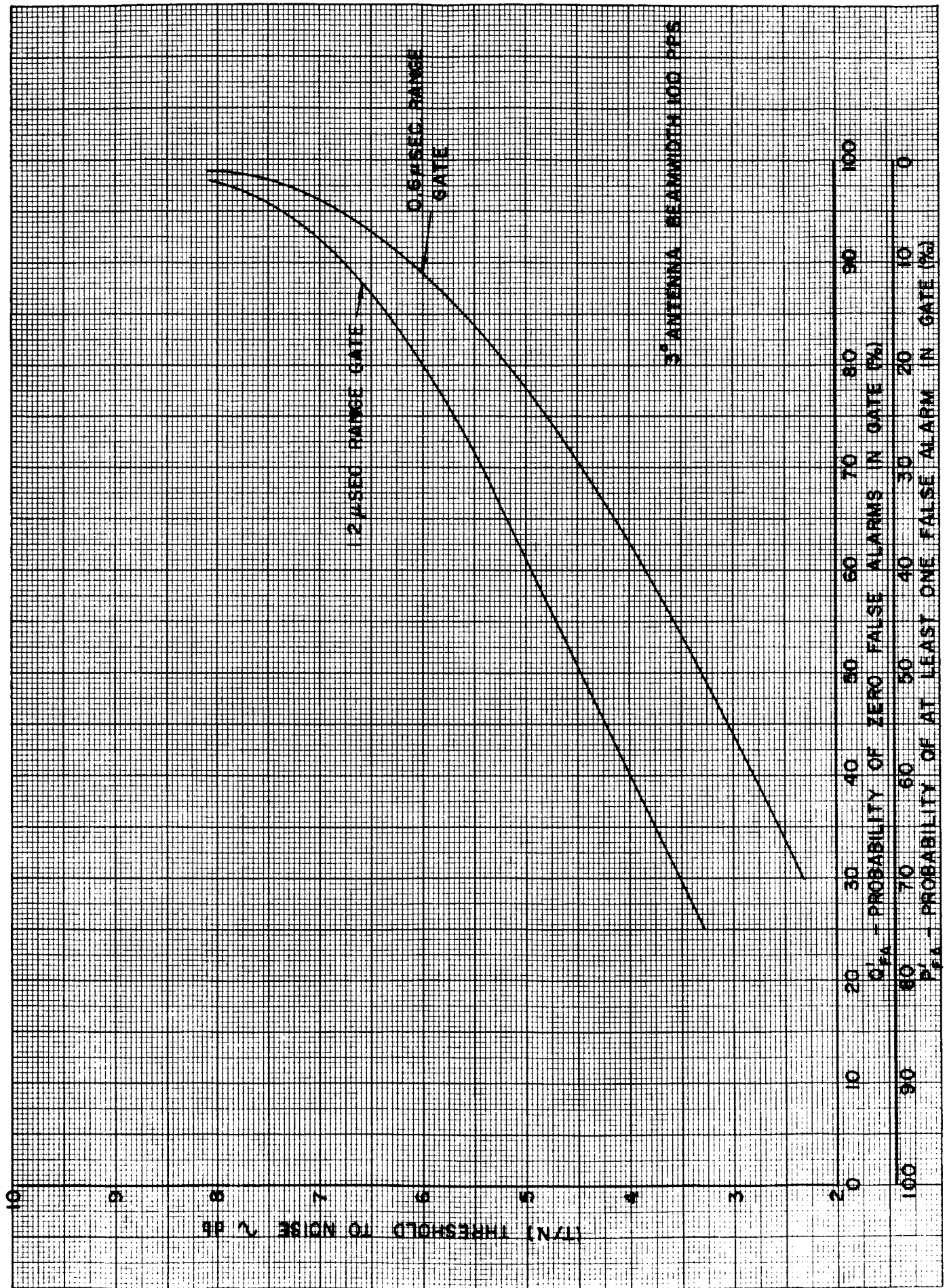


FIGURE 4.3-D-4 THRESHOLD -TO- NOISE VS FALSE ALARM PROBABILITIES

curves indicate the necessity of choosing the threshold-to-noise ratio (T/N) equal to or greater than 6.75 db if a Q'_{fa} of 90% or greater is desired. The larger the (T/N) ratio the smaller Q'_{fa} the delta probability change that will occur due to a false alarm firing during t_{rg} interval on a pulse to pulse basis.

As an example, select a T/N value of 8 db. Then the normal t_{rg} (0.6 microseconds) gives a Q'_{fa} of 99% and a worst case false alarm firing only decreases this probability to 98% or 1% delta change. Thus, for tracking purposes, a high Q'_{fa} is indicated.

PEAK POWER

Appendix 4.3-E

Using the values for T/N and the parameters of the radar equation 4.3.3.1-1 previously discussed in Section 4.3.3.1, peak output power can be determined for threshold areas. Figures 4.3-E-1 through 4.3-E-9 reflect the relationship between theoretical illuminated threshold area (A_t) and peak transmitted power necessary to obtain specific (Q'_{fa}) zero false alarm probabilities after lock-on for the various frequency (C, X, Ku and Ka) bands. Since the relationship between A_t and peak power (P_t) are functions of the repetition frequency and the t antenna beamwidth, curves were generated for 1, 3, and 5 degree beamwidths with repetition frequencies of 4 pps, 100 pps and 1000 pps.

Two additional conversions must be made in going from these general curves to the resultant bar chart of Figure 4.3.3.1-1 in section 4.3.3.1 for the three specific cases. The area buildups of the profile analysis (section 4.2.4) demonstrate a scattering coefficient. This is illustrated in Figure 4.3-E-10 where the analysis buildups (staircase curves) differ from that of a perfect spectral reflector ($\sigma = 0$ db curve). Since a constant coefficient of -25 db is applied to illuminated area in this study, the buildup areas are normalized to the ideal before the -25 db coefficient is applied. The buildups depicted represent the best case or fastest buildups over the lunar model for the particular beamwidth cases. The 1° beamwidth case exhibited no detectable difference for the time increment used in the program. An additional 6 db loss must also be added to the power requirement. This loss is broken down in the following:

Plumbing losses	3 db
Non-ideal equipment loss	2 db
Non-matched receiver loss	1 db

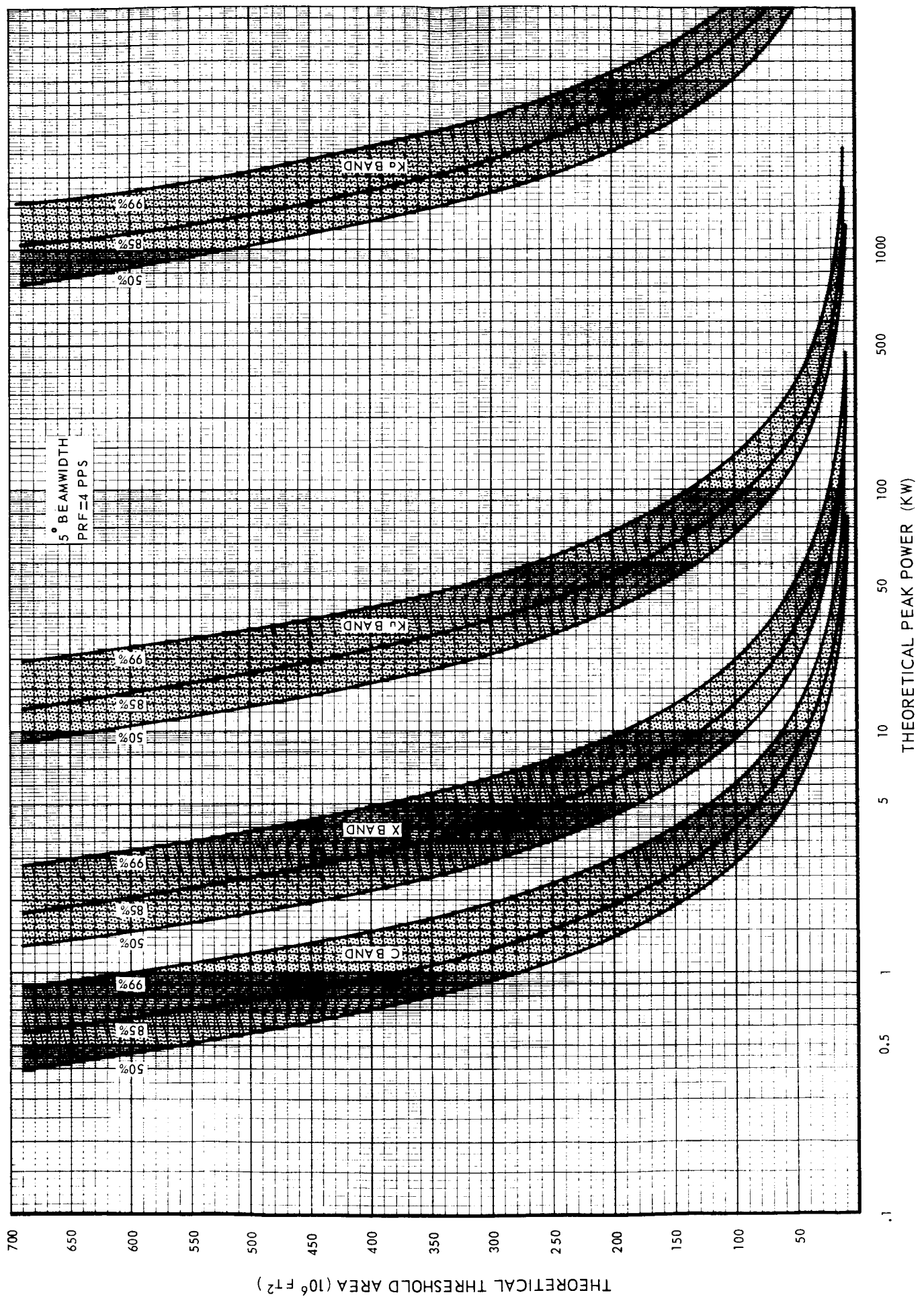


FIGURE 4.3-E-1.

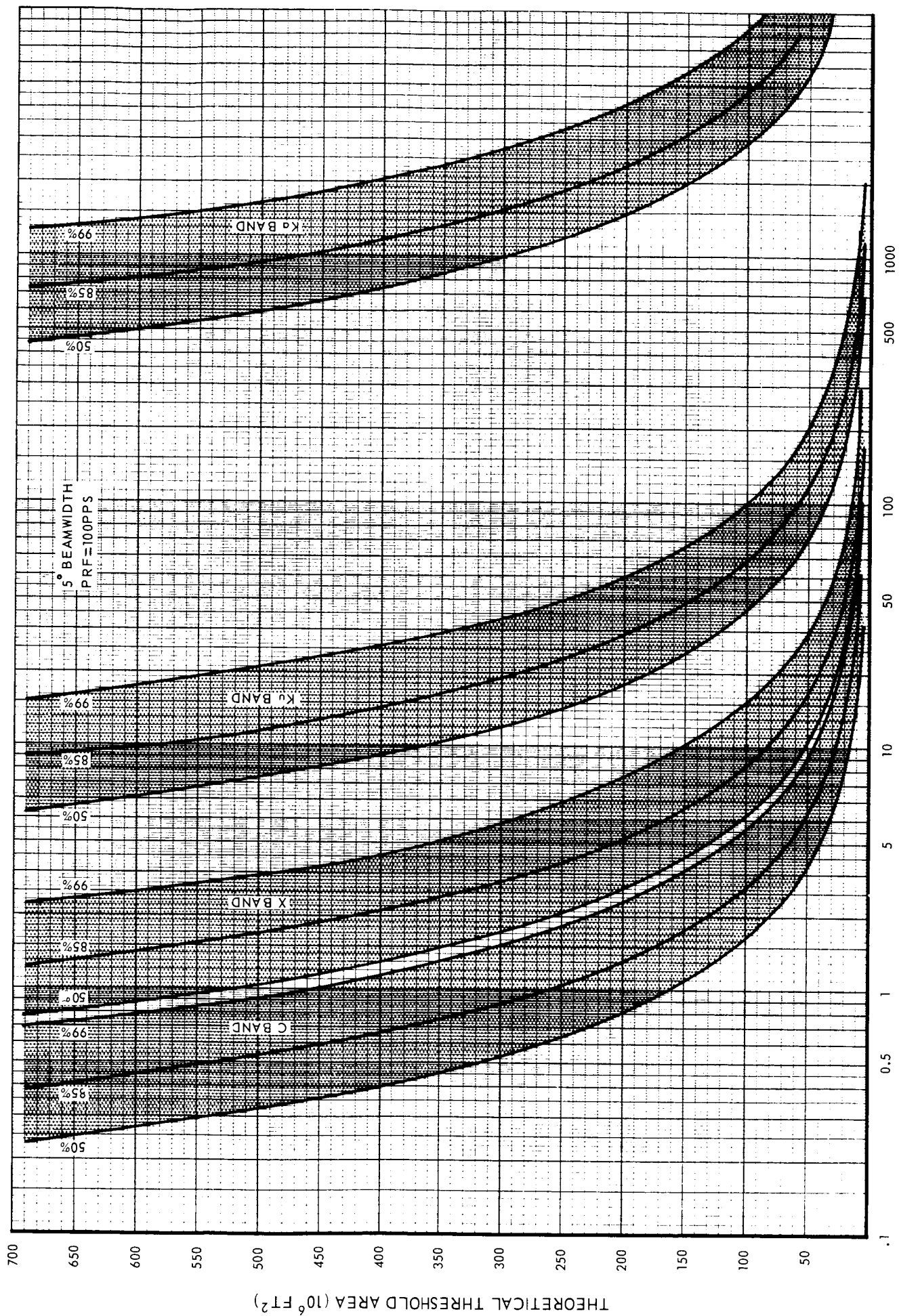


FIGURE 4.3-E-2.

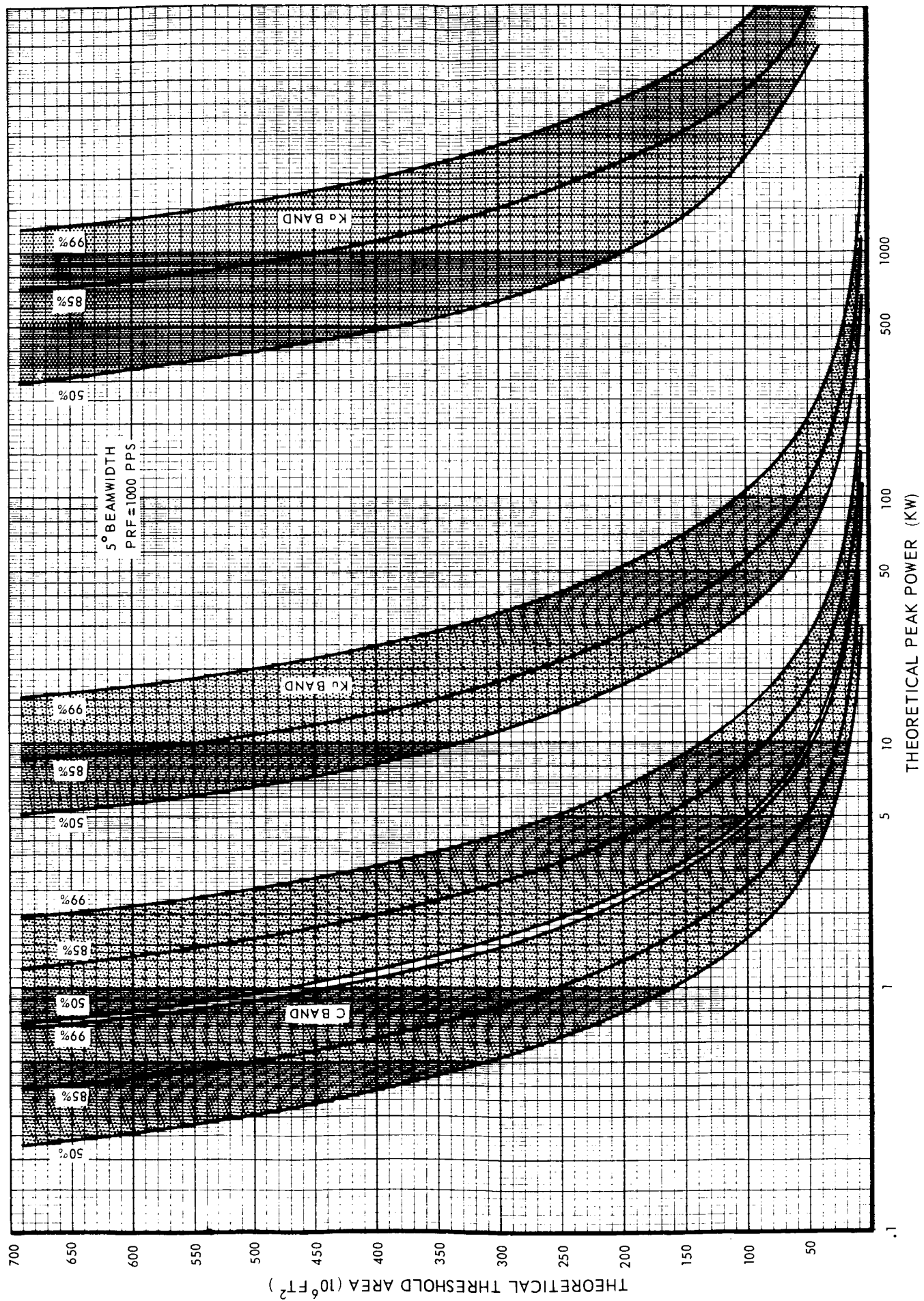


FIGURE 4.3-E-3.

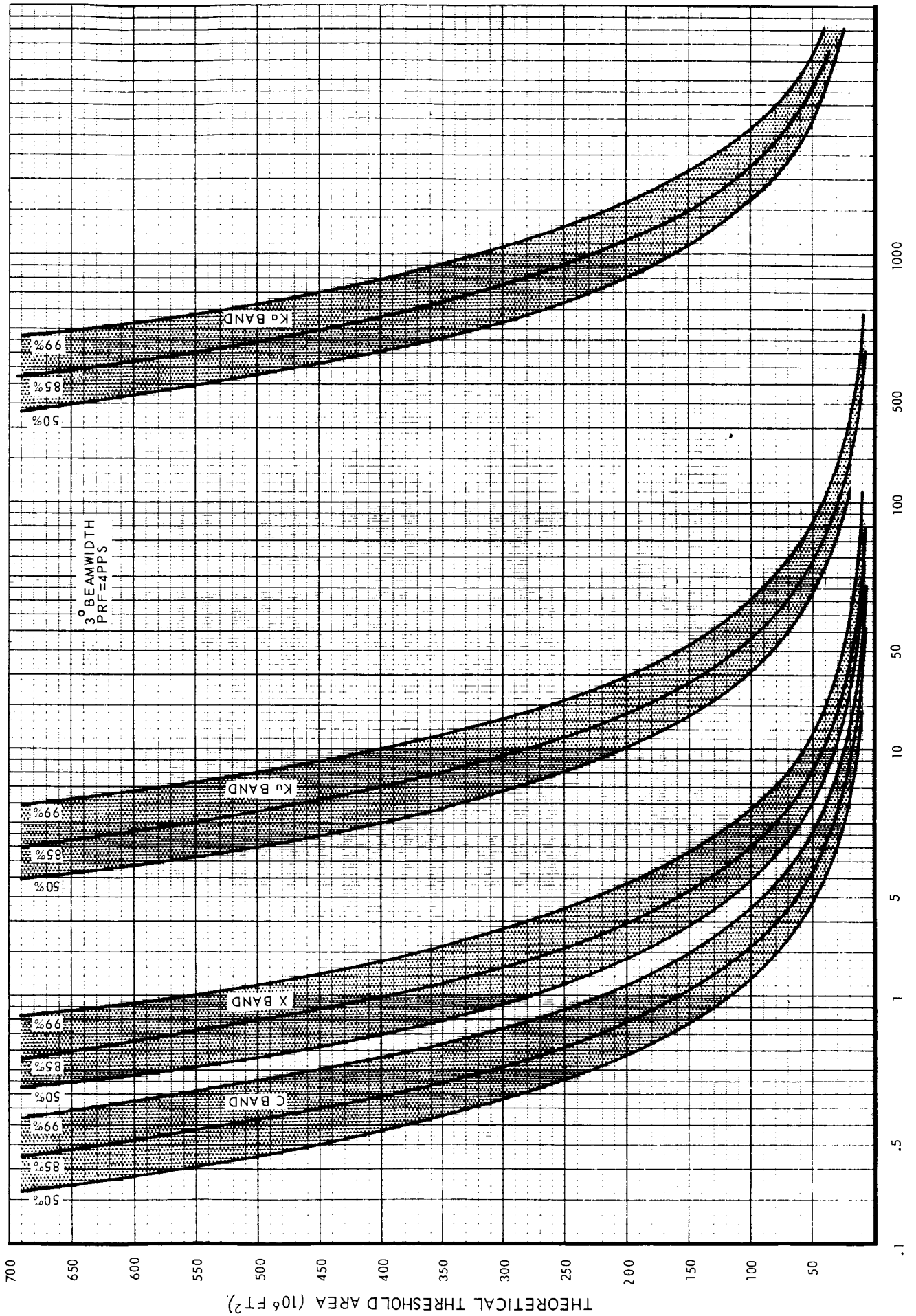


FIGURE 4.3-E-4.

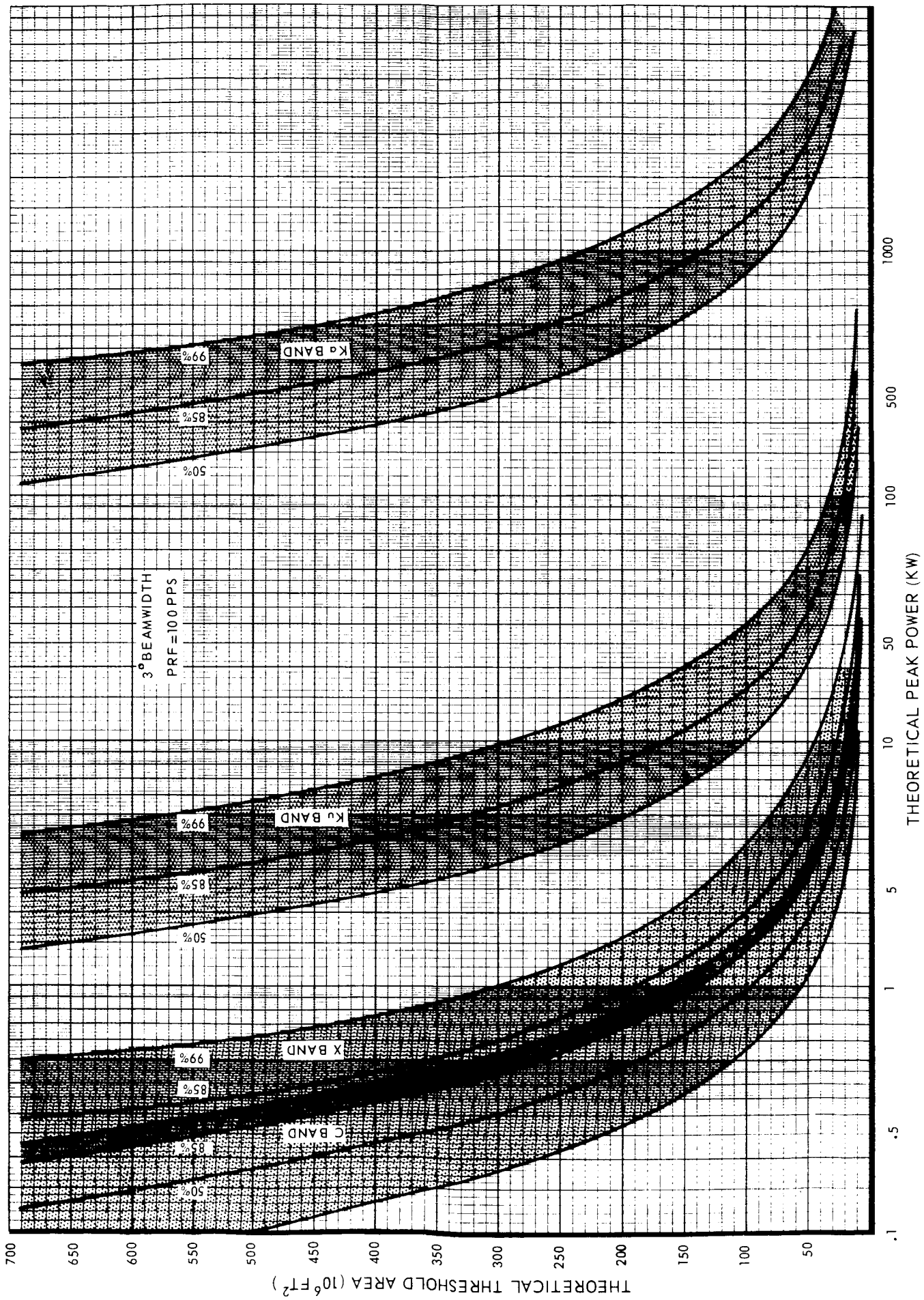


FIGURE 4.3-E-5.

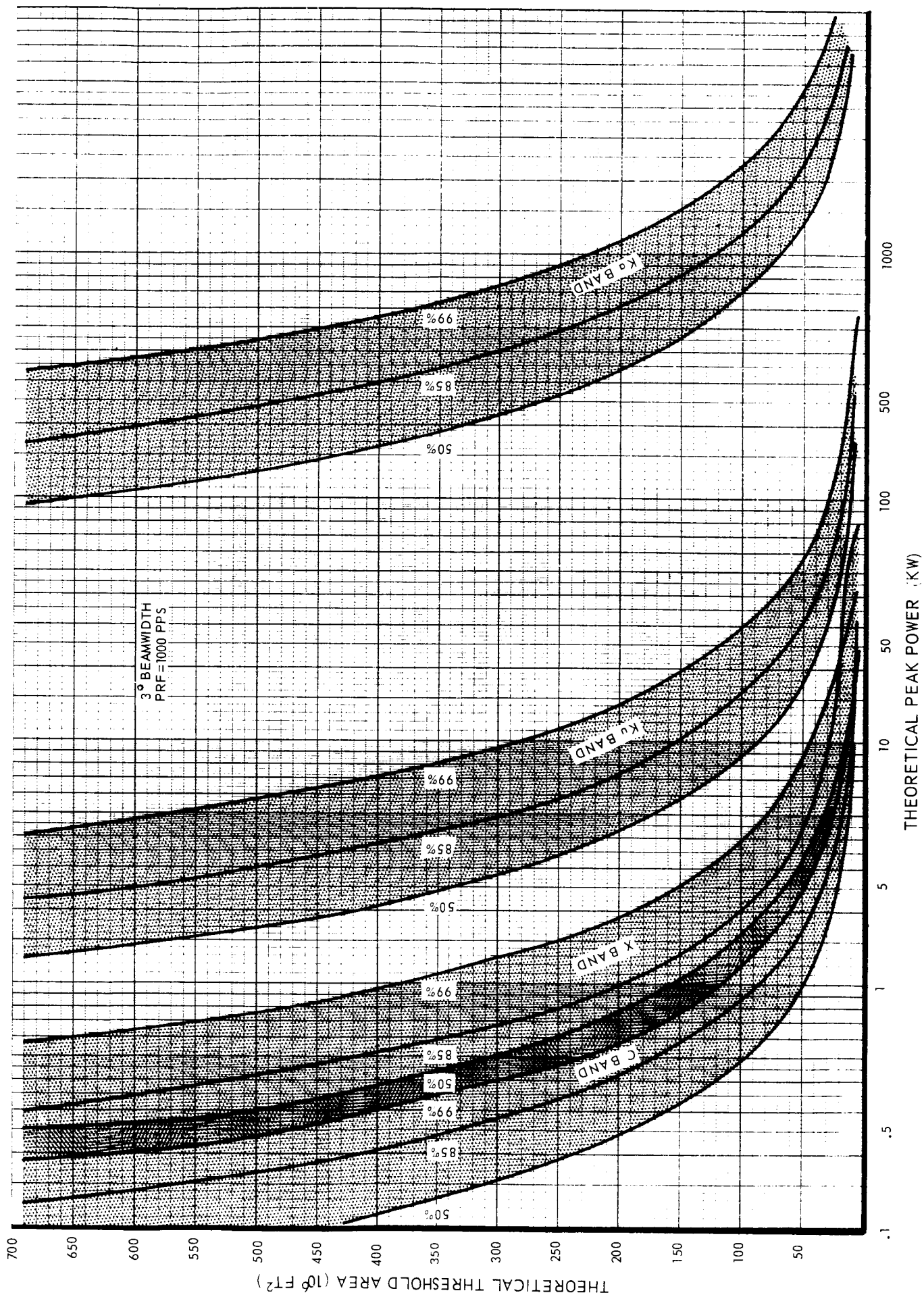


FIGURE 4.3-E-6.

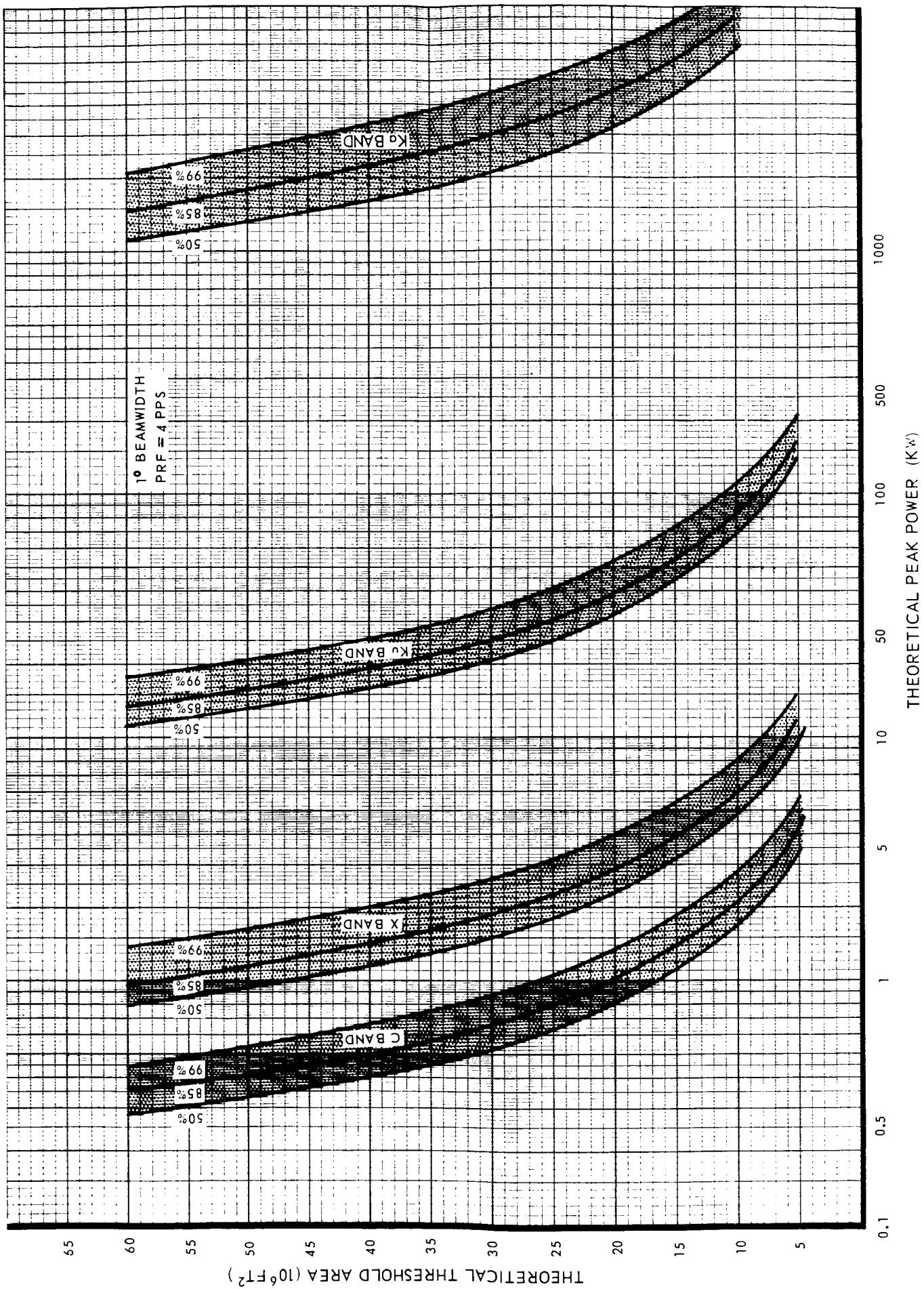
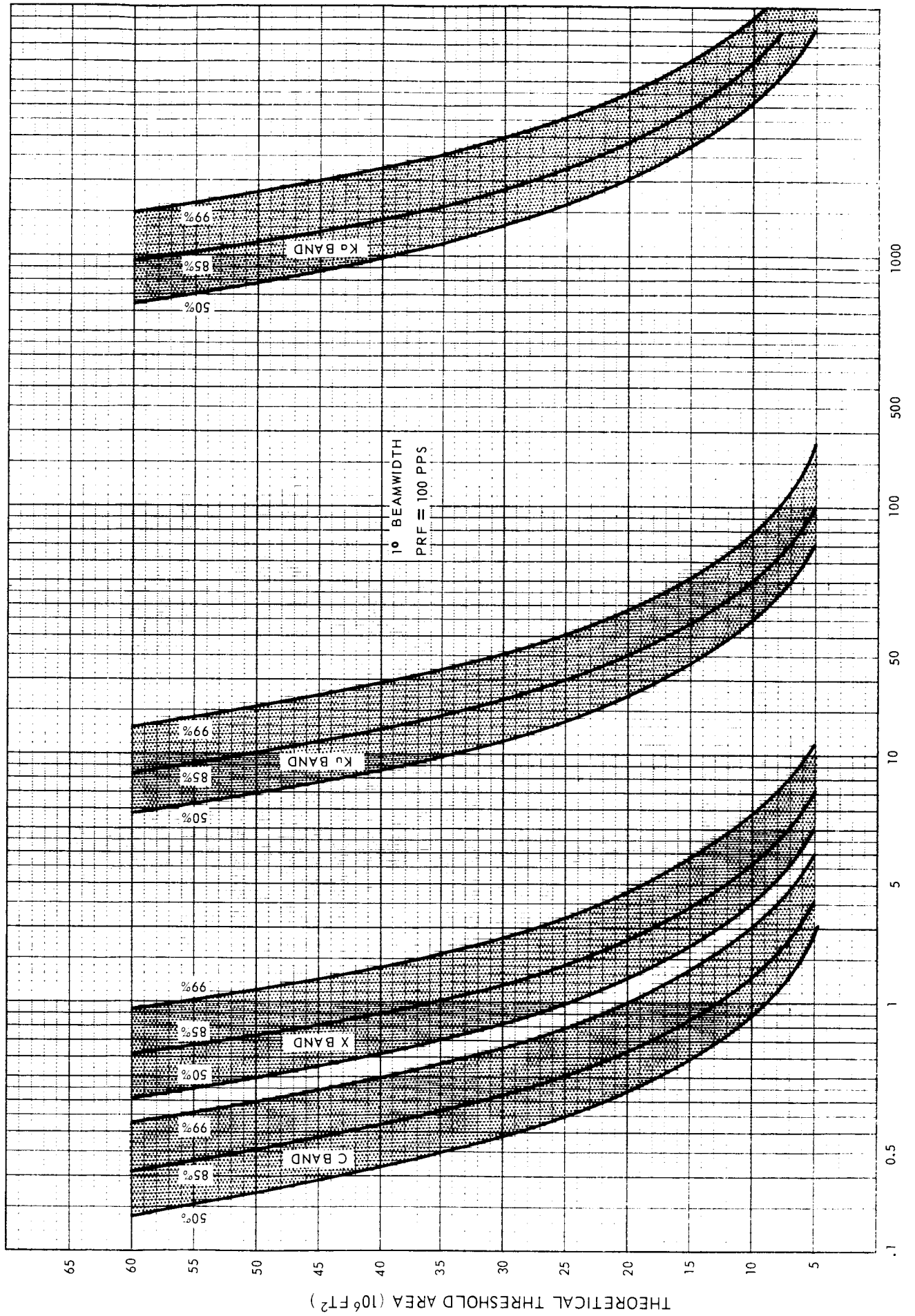
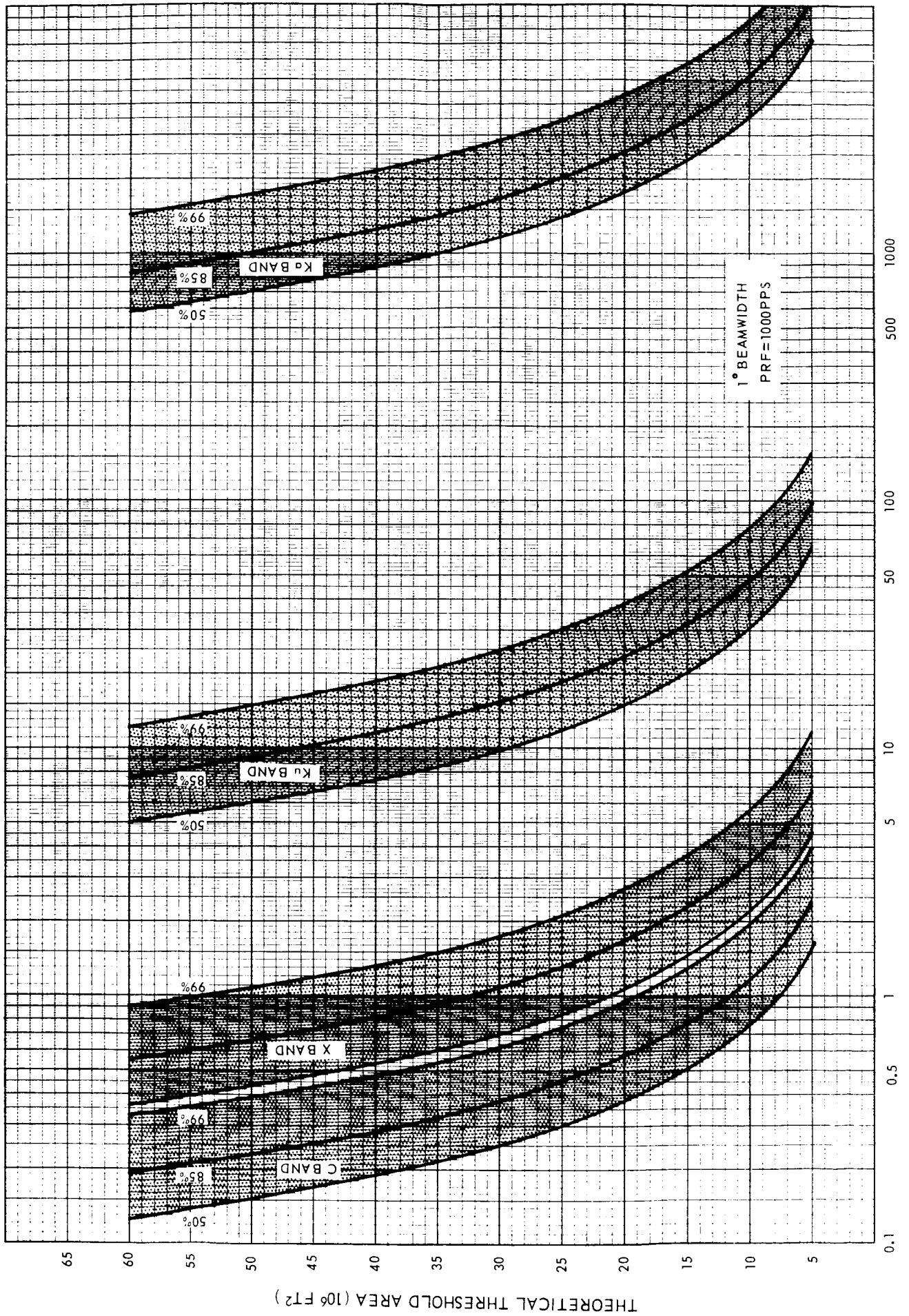


FIGURE 4.3-E-7.



THEORETICAL PEAK POWER (KW)

FIGURE 4.3-E-8.



THEORETICAL PEAK POWER (KW)

FIGURE 4.3-E-9.

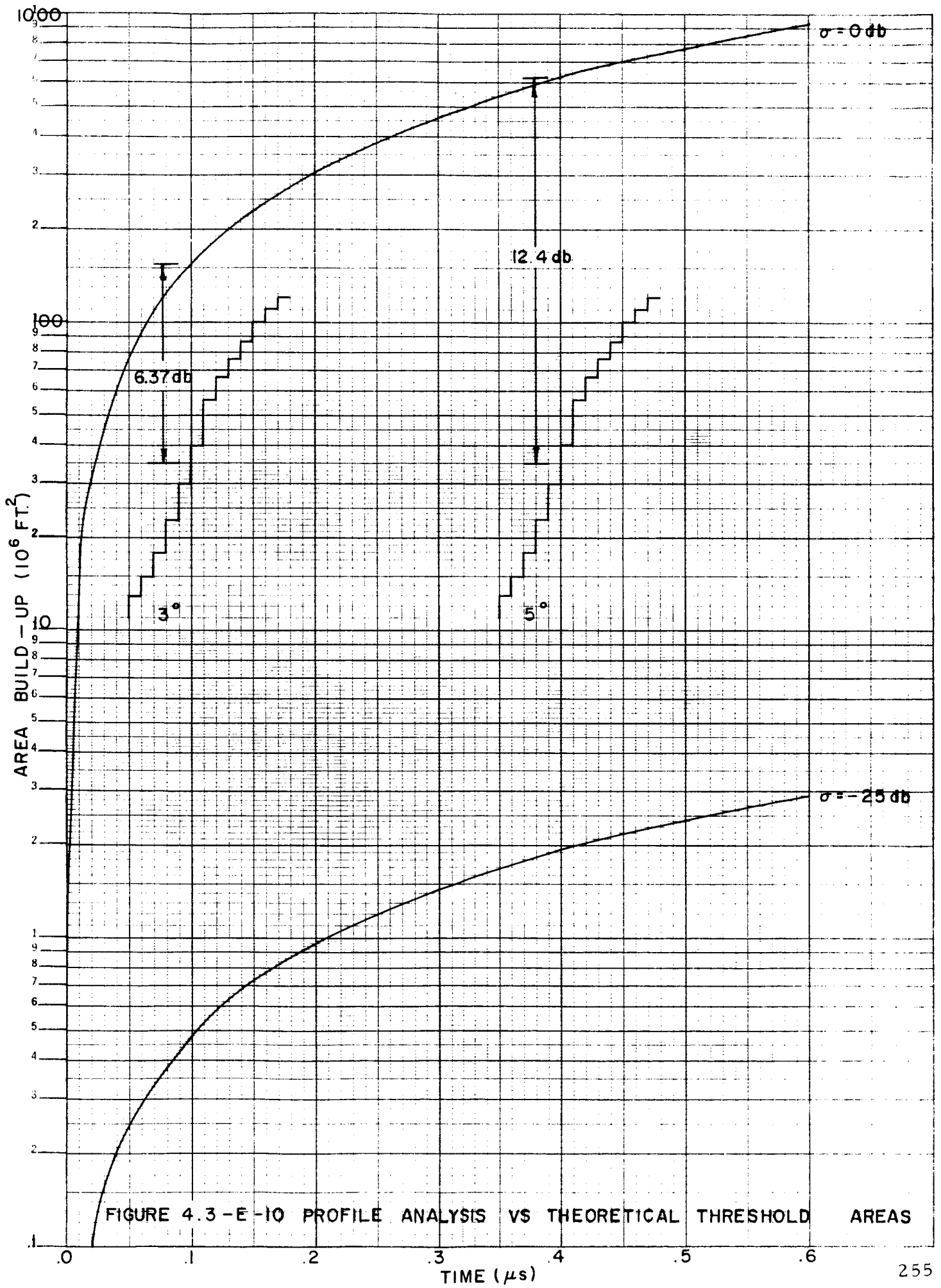


FIGURE 4.3-E-10 PROFILE ANALYSIS VS THEORETICAL THRESHOLD AREAS

When the power required for the normalized threshold area (Figures 4.3-E-1 through 4.3-E-9) is modified to account for the additional losses, the resultant peak power can be calculated for a specific case. For example, the 3° threshold area of 35 x 10⁶ ft.² is normalized to 152 x 10⁶ ft.². For a PRF of 4 pps at X band (Figure 4.3-E-4) a peak power of 3.7 kw is required. The 6 db additional requirement increases peak power to 14.8 kw.

As discussed in the previous section, a probability of detection of 99.9% was imposed on the system. The corresponding signal-plus-noise-to-noise ratios were used in conjunction with the maximum illuminated areas to determine the peak power requirements that satisfy this detection criterion. The maximum illuminated areas for the specific beamwidth and pulsewidth cases were:

$$5^\circ - 1440 \times 10^6 \text{ ft.}^2, 3^\circ - 518 \times 10^6 \text{ ft.}^2, 1^\circ - 58 \times 10^6 \text{ ft.}^2$$

Table 4.3-E-1 lists the peak power requirements in kilowatts for all the cases considered.

Beamwidth Frequency Band PRF (pps)	5°			3°			1°		
	C	X	Ku	C	X	Ku	C	X	Ku
4	5.7	18.1	128	5.9	14.8	108	5.4	15.4	217
100	5.0	15.8	120	4.6	11.5	81	4.6	12.1	185
1000	4.9	15.6	118	4.4	11.2	79	4.4	12.5	177

Table 4.3-E-1 PEAK POWER REQUIREMENTS (KW)
($Q'_{fa} = 99\%$ $P_d \geq 99.9\%$)

Figure 4.3.3.1-1 in section 4.3.3.3 reflects these values in bar chart form. For all the cases the peak power requirement at Ka band was greater than 1 megawatt.

WEIGHT AND VOLUME

Appendix 4.3-F

In this section the derivation of antenna and sensor weight-volume relations from those of individual components will be discussed.

Figures 4.3-F-1 through 4.3-F-3 show the weight (W) and volume (V) of magnetrons versus peak output power for C, X, and Ku bands, respectively. Log-log curves were "fitted" to the data. The resulting equations were used in the total sensor trade-off relations. Additional data, which will refine the curves, are being received. Table 4.3-F-1 lists the magnetron relations.

<u>Frequency Band</u>	<u>Weight (Lbs.)</u>	<u>Volume (in³)</u>	<u>Peak Power Range</u>
C	0.5	4.4	P < 2KW
C	$0.3 P_{kw}^{.788}$	$2.2 P_{kw}^{1.08}$	$2 \text{ KW} \leq P \leq 85 \text{ KW}$
X	0.63	7.0	P < 1.3 KW
X	$0.525 P_{kw}^{.615}$	$9.5 P_{kw}^{.642}$	$1.3 \text{ KW} \leq P \leq 400 \text{ KW}$
Ku	$1.31 P_{kw}^{.34}$	$14.4 P_{kw}^{.51}$	$1 \text{ KW} \leq P \leq 100 \text{ IW}$

Table 4.3-F-1 MAGNETRON TRADE-OFF RELATIONS

Figure 4.3-F-4 represents similar curves derived for the modulator. The resultant relations are:

X BAND MAGNETRONS

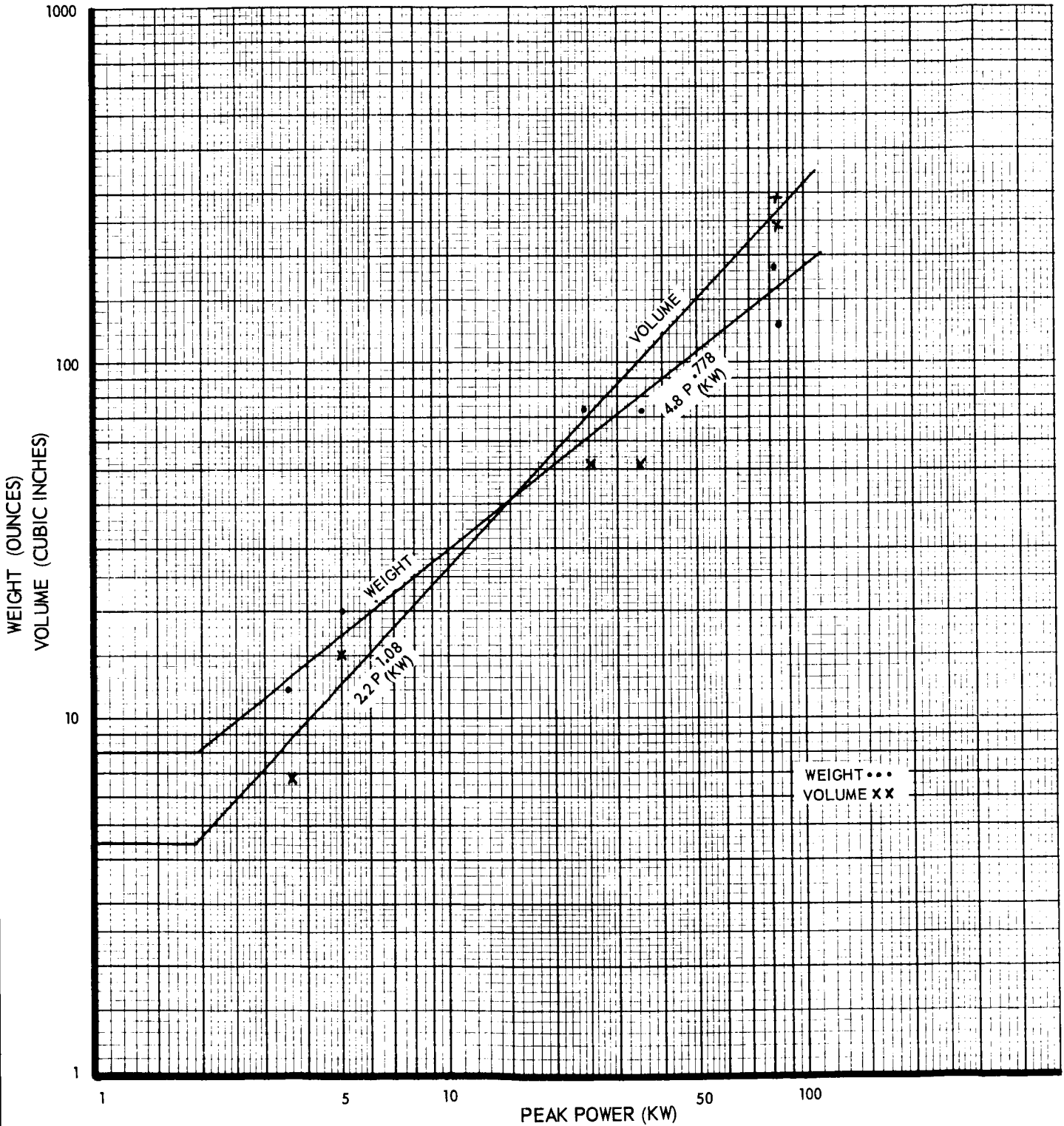


FIGURE 4.3-F-1. C BAND MAGNETRONS

X BAND MAGNETRONS

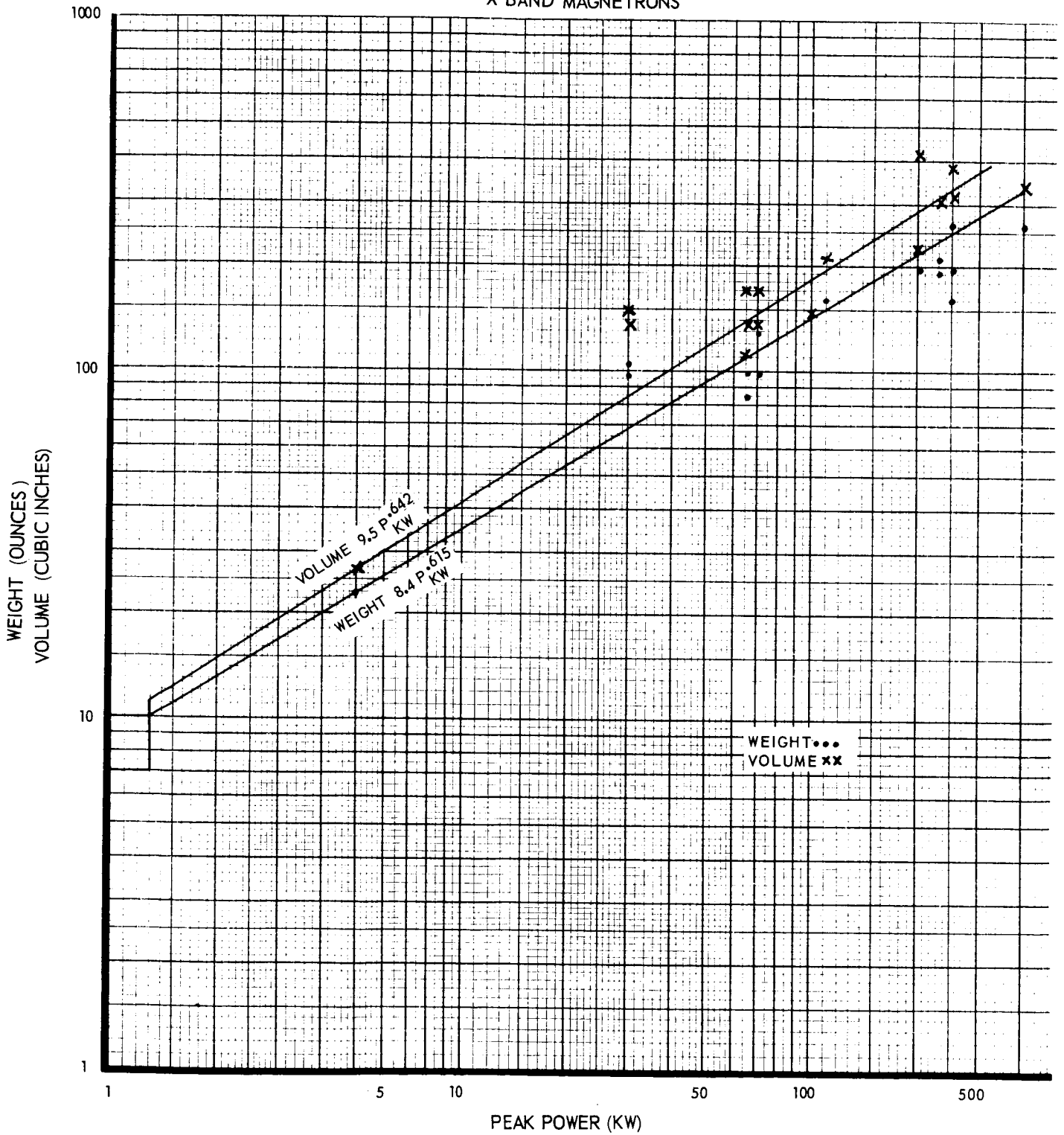


FIGURE 4.3-F-2. X BAND MAGNETRONS

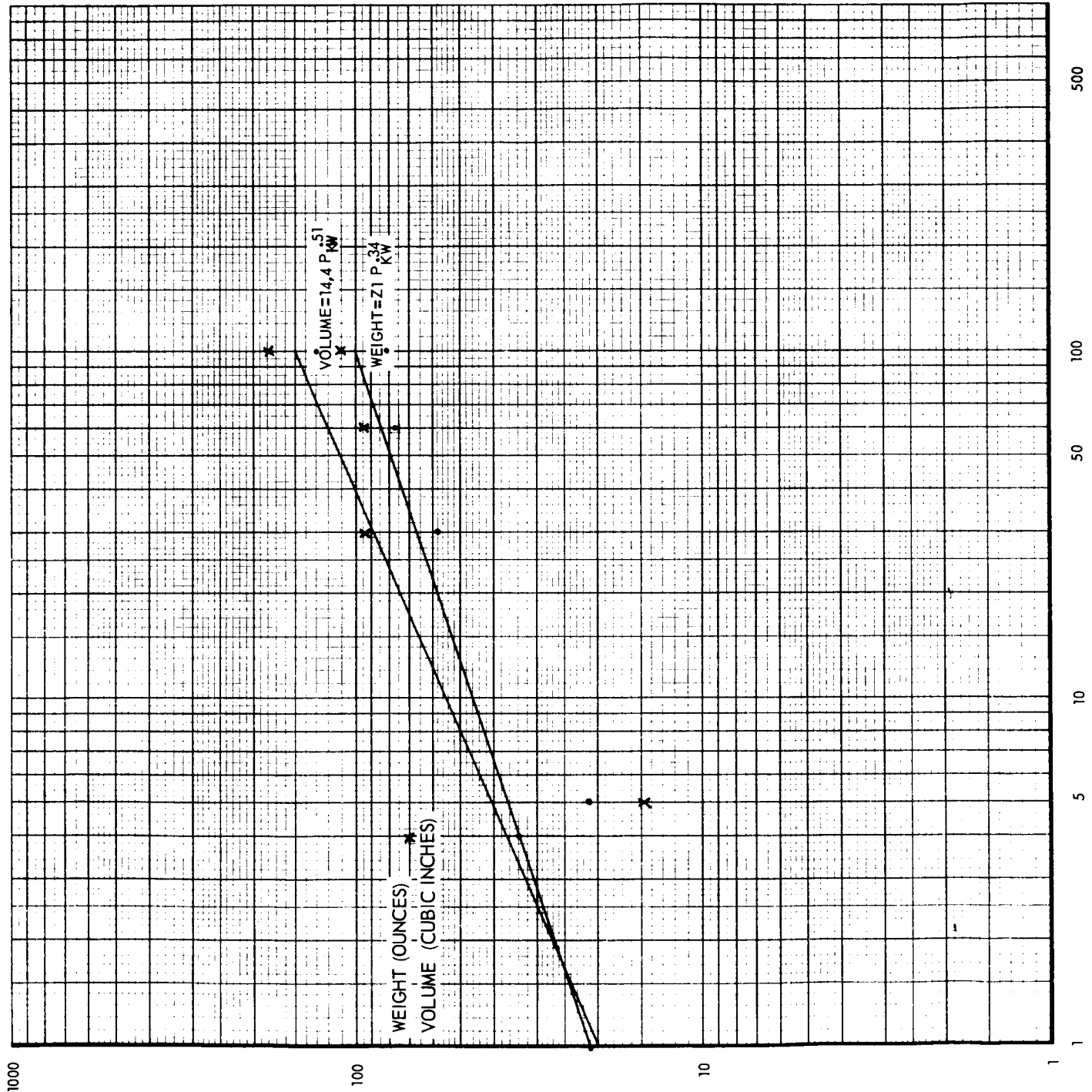


FIGURE 4.3-F-3. K_u BAND MAGNETRONS

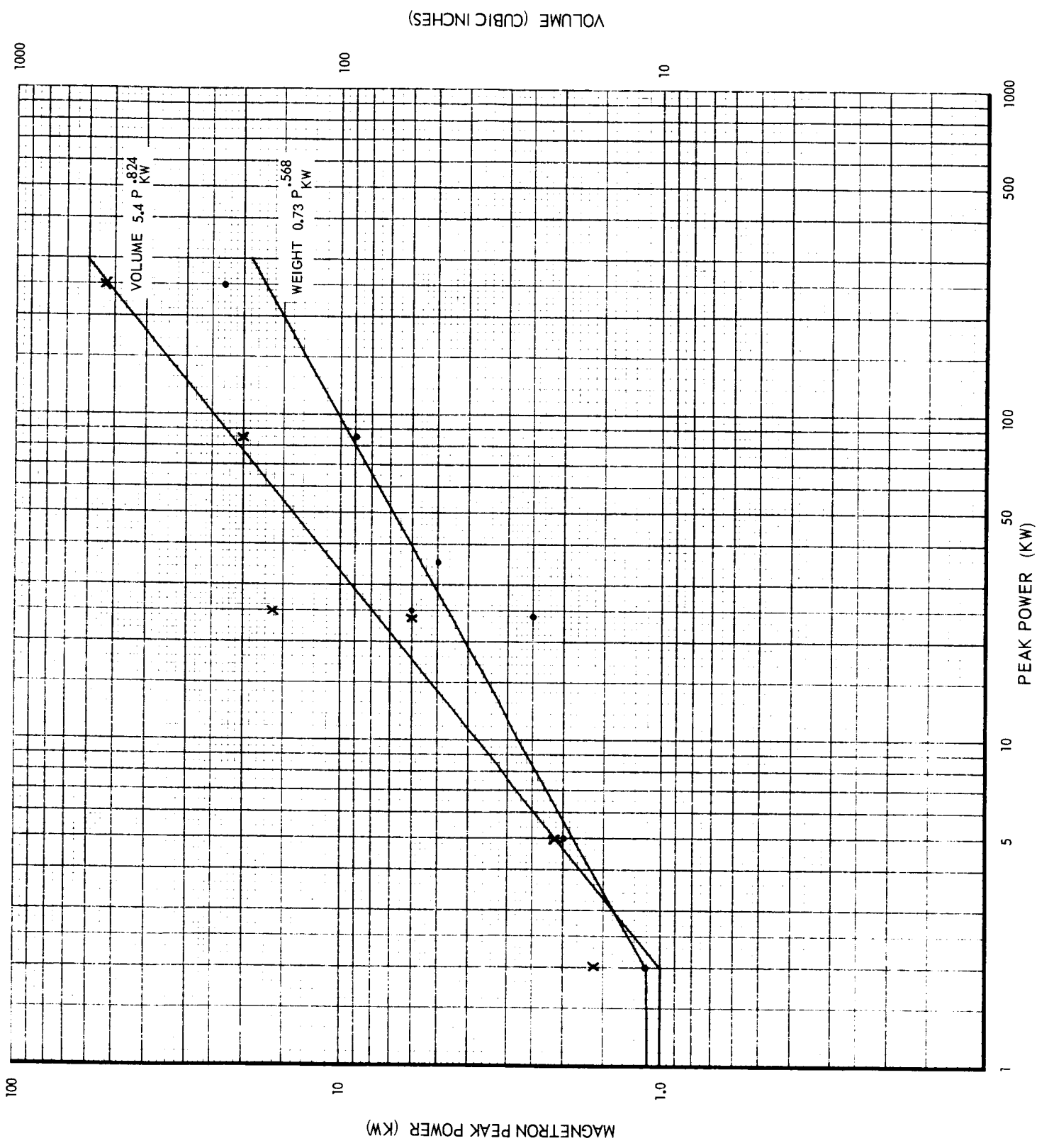


FIGURE 4.3-F-4. MODULATORS

$$W = 1.1 \text{ lbs.} \quad V = 10 \text{ in}^3 \text{ for } P < 2 \text{ KW}$$

$$W = 0.73 P_{\text{kw}}^{.568} \quad V = 5.4 P_{\text{kw}}^{.824} \text{ in}^3 \text{ for } P \geq 2 \text{ KW}$$

The remaining components were:

	<u>Weight</u>	<u>Volume</u>	<u>Band</u>	
Preselector	0.57	3.00	C	
	0.50	2.00	X	
	0.10	0.25	Ku	
RF Switch (P < 4 KW)	1.55	22.70	C	
	1.00	13.30	X	
	0.50	6.12	Ku	
	(4 KW ≤ P ≤ 100 KW)	2.06	28.40	C
		1.33	17.70	X
		0.60	8.03	Ku
Circulator, TDA, Local Oscillator, Mixer, Receiver, Data Processor	14.00	347.00	all	
Power Supply	8.00	124.00	all	

The total sensor weight-volume versus peak power relations for the three frequency bands (Figures 4.3-F-5 and 4.3-F-6) are:

$$\begin{aligned} \text{C band} \quad \text{Weight} &= 37.6 + 0.73 P_{\text{kw}}^{.568} + 0.3 P_{\text{kw}}^{.788} \text{ lbs.} \\ \text{Volume} &= 532 + 5.4 P_{\text{kw}}^{.824} + 2.2 P_{\text{kw}}^{1.08} \text{ in}^3 \\ \text{X band} \quad \text{Weight} &= 36.8 + 0.73 P_{\text{kw}}^{.568} + 0.53 P_{\text{kw}}^{.615} \text{ lbs.} \\ \text{Volume} &= 511 + 5.4 P_{\text{kw}}^{.824} + 9.5 P_{\text{kw}}^{.642} \text{ in}^3 \\ \text{Ku band} \quad \text{Weight} &= 35.7 + 0.73 P_{\text{kw}}^{.568} + 1.3 P_{\text{kw}}^{.34} \text{ lbs.} \\ \text{Volume} &= 479 + 5.4 P_{\text{kw}}^{.824} + 14.4 P_{\text{kw}}^{.51} \text{ in}^3 \end{aligned}$$

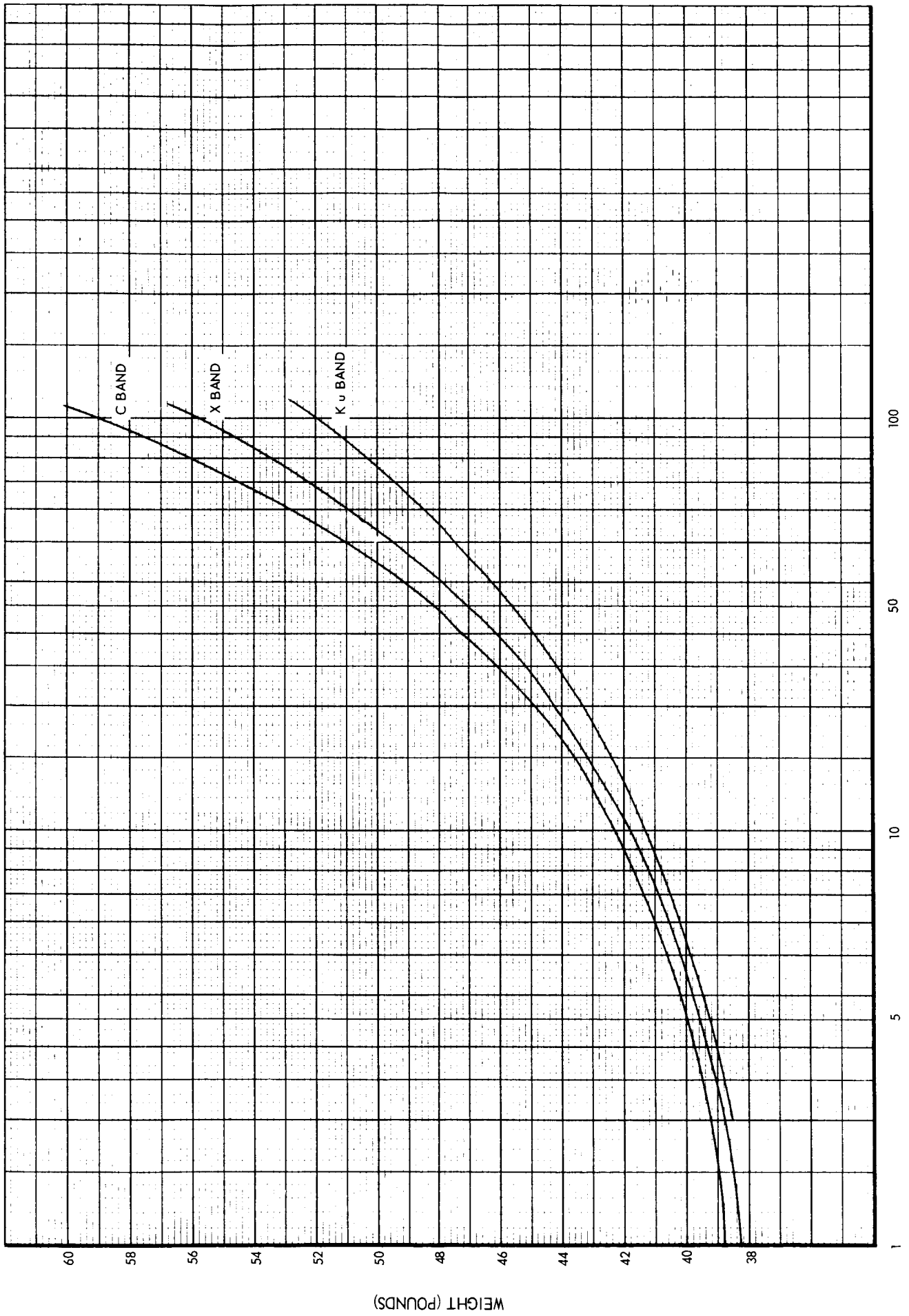


FIGURE 4.3-F-5. SENSOR WEIGHT

PEAK POWER (KW)

WEIGHT (POUNDS)

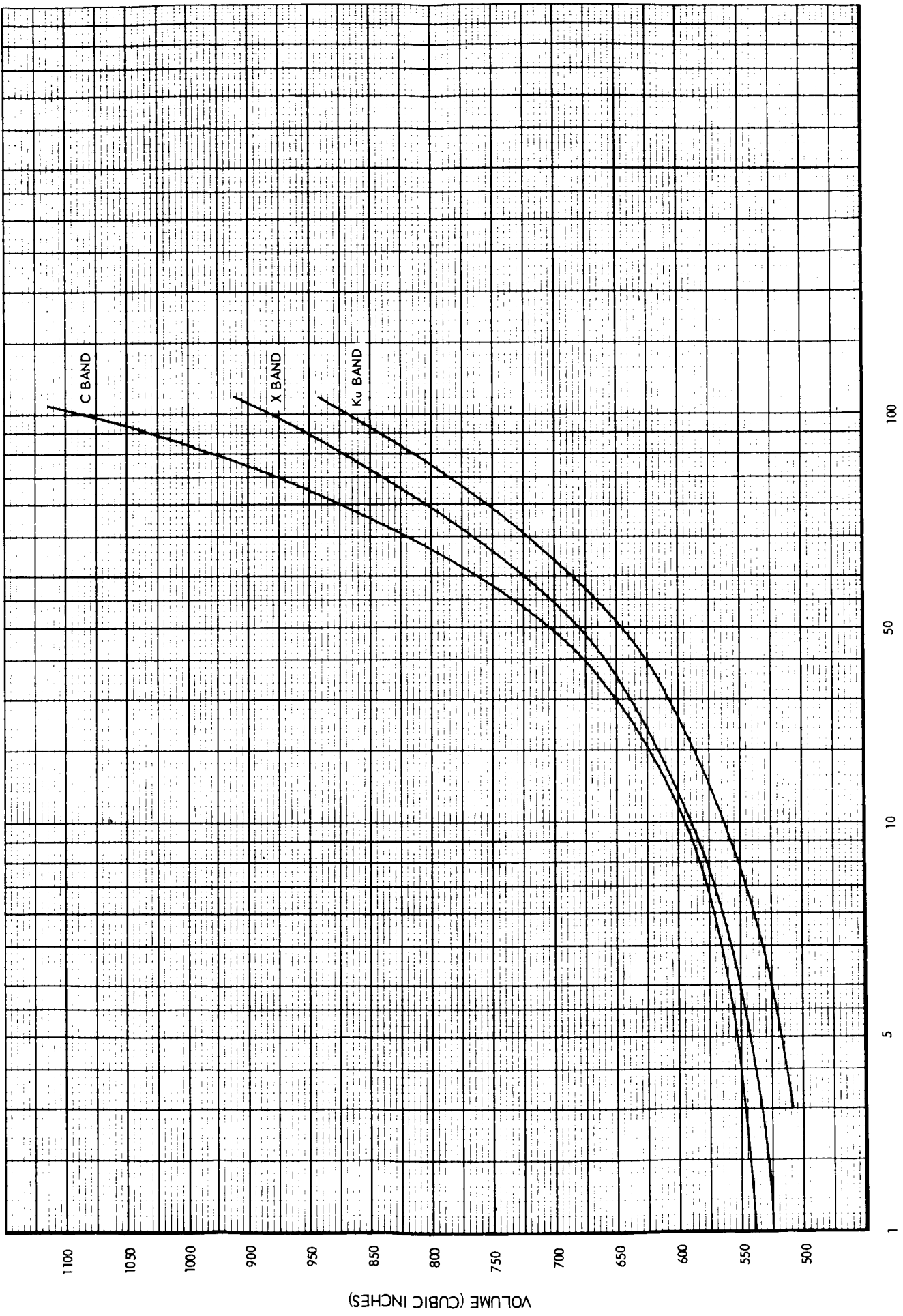


FIGURE 4.3-F-6. SENSOR VOLUME

The antenna weights and volumes are added to these relations in Figures 4.3-F-7 through -9 for the three beamwidths being examined. The slot array antenna weights and volumes are:

<u>Beamwidth</u>	<u>Band</u>	<u>Weights (lbs.)</u>	<u>Volume (in³)</u>
5°	C	27	1550
	X	10	845
	Ku	2	87
3°	C	73	7850
	X	24	2000
	Ku	5	253
1°	C	500	71400
	X	200	22400
	Ku	45	2310

The peak power requirements of Table 4.3-E-1 result in the sensor and antenna weights and volumes listed in Table 4.3-F-2 and 4.3-F-3 respectively.

Beamwidth Frequency Band PRF (pps)	5°			3°			1°		
	<u>C</u>	<u>X</u>	<u>Ku</u>	<u>C</u>	<u>X</u>	<u>Ku</u>	<u>C</u>	<u>X</u>	<u>Ku</u>
4	67.7	53.7	56.4	113.6	66.7	57.9	540	243	106
100	67.5	53.3	55.6	113.0	65.9	55.2	540	242	104
1000	67.4	53.2	55.4	113.0	65.8	55.0	540	242	103

Table 4.3-F-2 SENSOR & ANTENNA WEIGHTS (lbs.)

Beamwidth Frequency Band PRF (pps)	5°			3°			1°		
	<u>C</u>	<u>X</u>	<u>Ku</u>	<u>C</u>	<u>X</u>	<u>Ku</u>	<u>C</u>	<u>X</u>	<u>Ku</u>
4	2120	1480	1060	8420	2620	1140	71970	23010	3490
100	2110	1460	1020	8400	2600	1070	71960	23000	3400
1000	2110	1460	1020	8400	2600	1070	71960	23000	3380

Table 4.3-F-3 SENSOR & ANTENNA VOLUMES (in³)

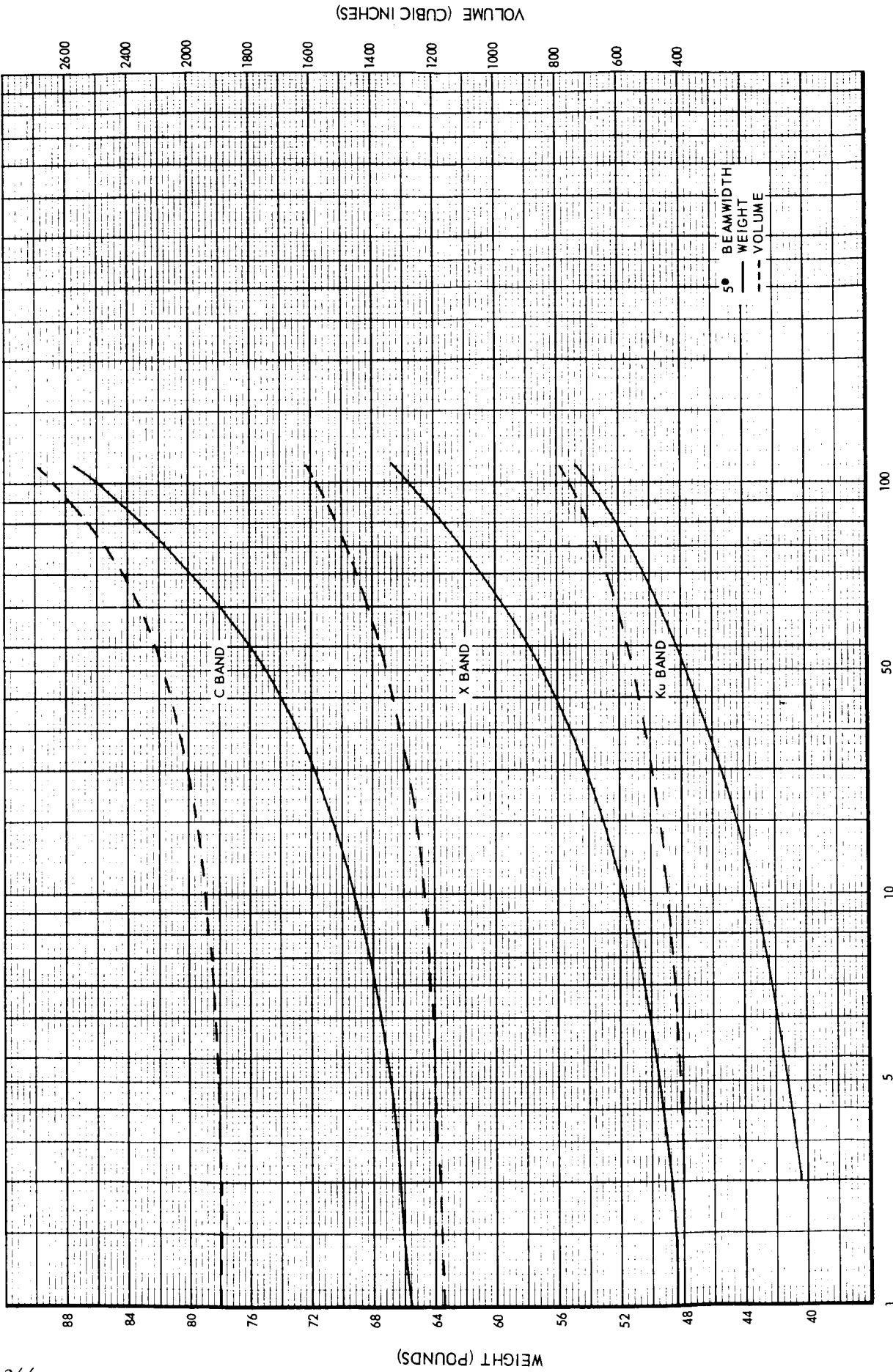


FIGURE 4.3-F-7. SENSOR-ANTENNA WEIGHT-VOLUME

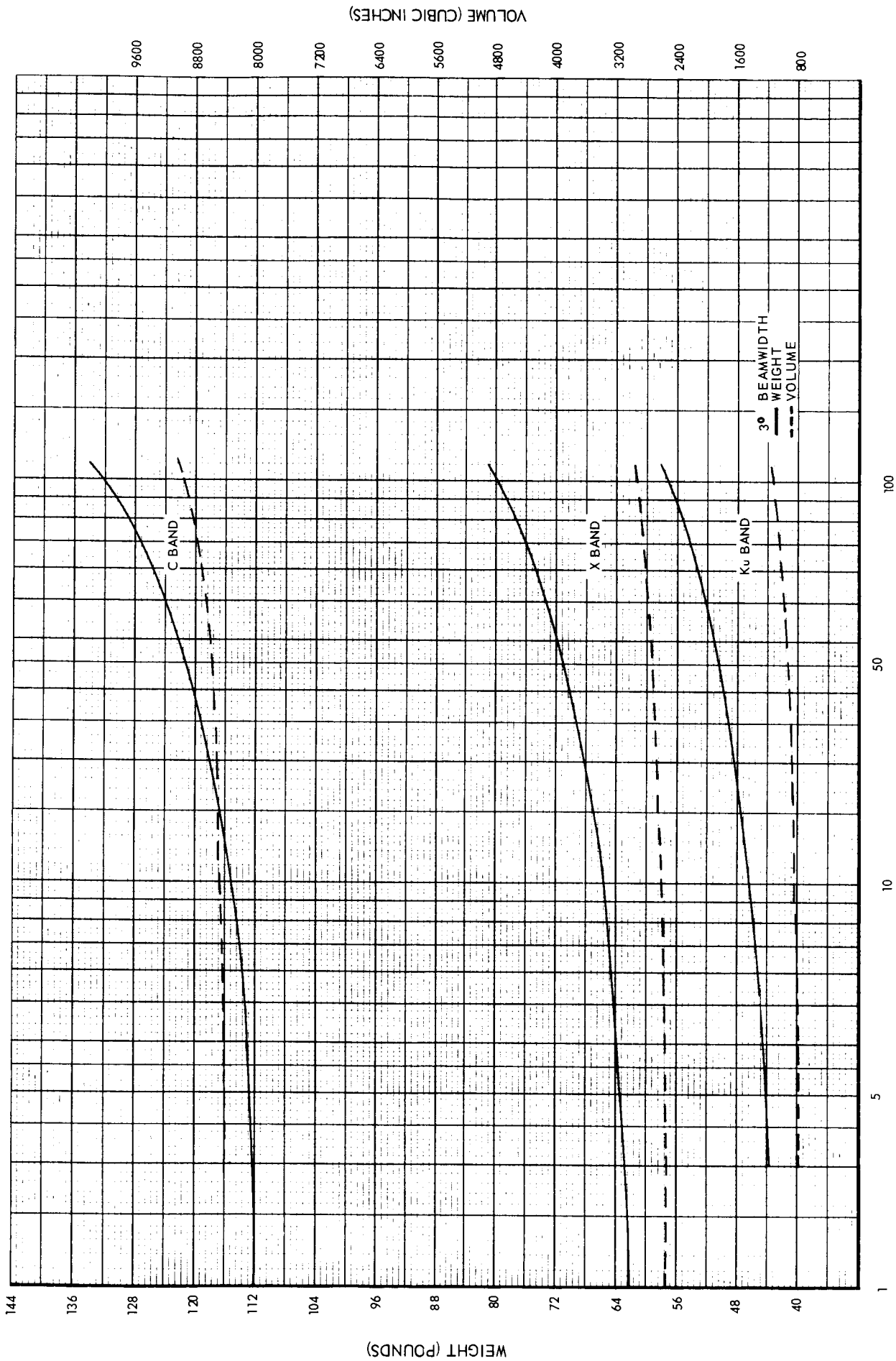


FIGURE 4.3-F-8. SENSOR-ANTENNA WEIGHT - VOLUME

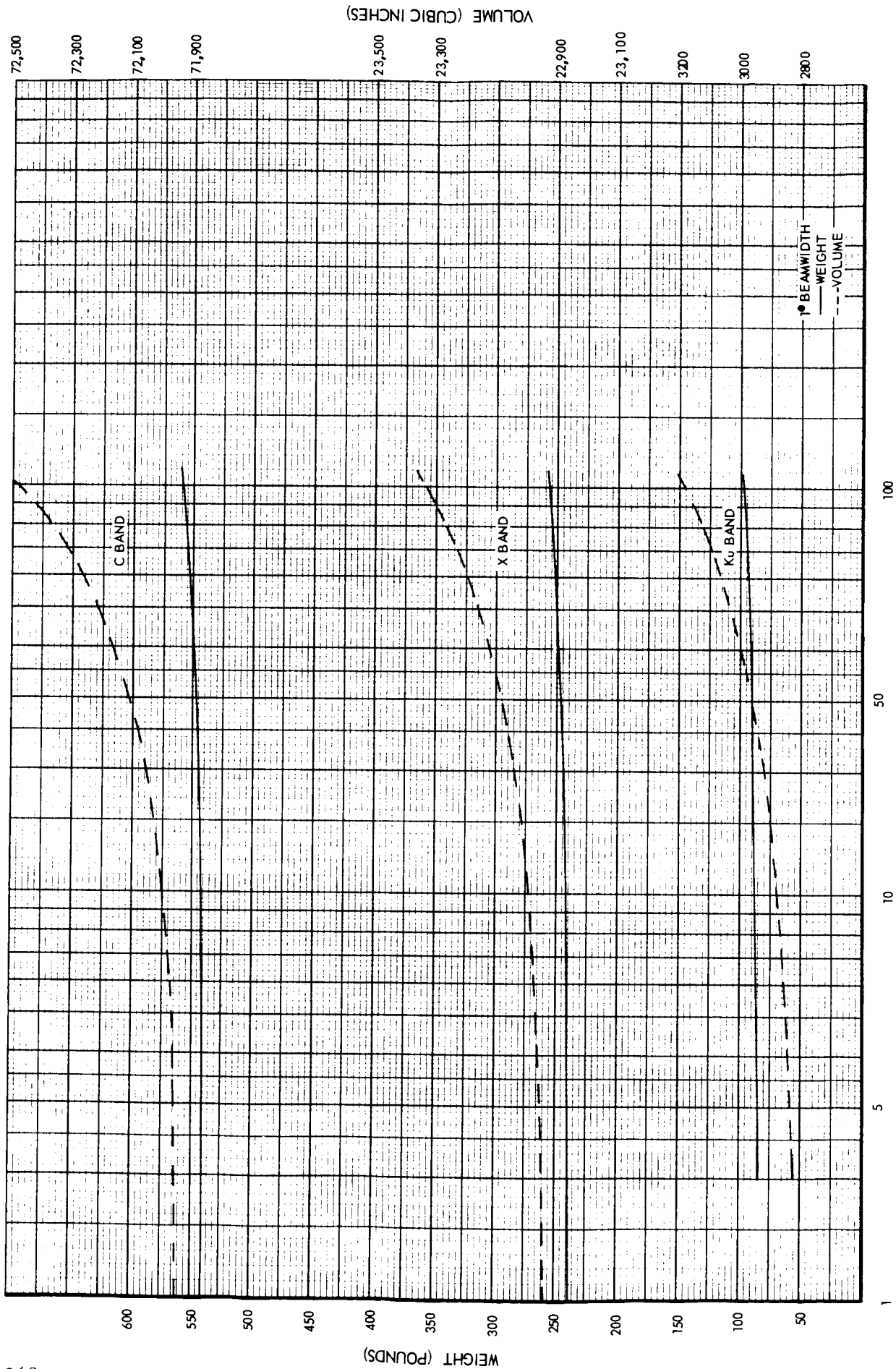


FIGURE 4.3-F-9. SENSOR - ANTENNA WEIGHT - VOLUME

PEAK POWER (KW)

VOLUME (CUBIC INCHES)

72,500

72,300

72,100

71,900

23,500

23,300

22,900

23,100

3,200

3,000

2,800

600

550

500

450

400

350

300

250

200

150

100

50

1

5

10

50

100

--- BEAMWIDTH
—— WEIGHT
--- VOLUME

Only slight dependence on PRF is exhibited; Figure 4.3.3.1-2 in section 4.3.3.1 reflects weight-volume values in bar chart form for a PRF of 100 pps.

PRIME POWER

Appendix 4.3-G

Since the type of prime power source for the LUCOM mission was not known, its weight-volume parameters were not included. Prime power requirements for the cases considered, however, were calculated. The average prime power was calculated from

$$P_p = P_o / P_{av}$$

where P_o = Average sensor prime power independent of peak output power

P_{av} = Prime power necessary to provide required average transmitted power over the pulse-repetition the pulse repetition interval

$$P_{av} = P_t \tau PRF \eta$$

where η = Overall power efficiency

From experience in these type radar sensors, a P_o of 100 watts was used in the study; an efficiency (η) of 10% was also used.

Table 4.3-G-1 reflects the average prime power requirements for the cases considered.

Beamwidth Pulsewidth Frequency Band PRF (pps)	5°			3°			1°		
	1.5 us			1.5 us			1 us		
	<u>C</u>	<u>X</u>	<u>Ku</u>	<u>C</u>	<u>X</u>	<u>Ku</u>	<u>C</u>	<u>X</u>	<u>Ku</u>
4	100	101	108	100	101	106	100	101	109
100	107	124	279	107	117	222	105	113	285
1000	173	334	1879	166	269	1290	144	225	1868

Table 4.3-G-1 PRIME POWER REQUIREMENT (WATTS)

Figure 4.3.3.1-3 in section 4.3.3.1 reflects these values in bar chart form

ERROR ANALYSIS

Appendix 4.3-H

The error sources which are considered in detail in the following sections are:

Return signal variation

Quantization error

Verticality

Threshold detector variation

Clock frequency stability

AGC limitations

Gate jitter

4.3.H-1 Return Signal Variation

The return signal consists of two parts: that due to receiver generated noise and thermal noise attributed to the antenna radiation resistance, and signal reflected from the surface. The statistical make-up of the return was discussed in Appendix 4.3-D. The computer simulation mentioned in that section to determine statistically the rms threshold crossing deviation from a mean is discussed in detail in the following.

A simplified flow diagram for the simulation of the sensor operation is shown in Figure 4.3-H.1-1. The basis for simulation of the signals is generation of values which have an exponential distribution of amplitude. This starts with the choosing of two independent numbers (X and Y) from a Gaussian distribution of mean = 0 and standard deviation = 1. These numbers represent orthogonal components of a Rayleigh distribution ($R = \sqrt{X^2 + Y^2}$) of mean = $\sqrt{2}$. The square of the Rayleigh distribution is an exponential distribution ($W = R^2 = X^2 + Y^2$) which has a mean = 2.

The above process is used, multiplying the Gaussian numbers by a factor XL to generate simulated noise. The simulated return signal is generated in a like manner, except for each succeeding time increment the new Gaussian numbers are added to previous totals, to simulate the buildup of illuminated area on the surface. Time intervals are counted by the factor N. At the beginning of a simulated cycle of operation, N is set to some negative number, representing the opening of the range gate before the return signal is expected. After computing each point N is increased by 1 and as long as N is negative only the noise signal is generated. When N = 0, the simulation of the buildup of the ground return signal is started and added to the noise signal. The time interval represented by unit N must be short enough so that a good representation of the highest frequency involved is obtained. The filter characteristic was chosen because of the ease of implementing on the computer.

The threshold circuit is simulated by a decision circuit which for each time interval determines if the simulated signal exceeds the threshold value of T. The time of threshold crossing is N times the sampling interval measured from the start of the buildup of the ground return. The computer repeats the process M times and computes the average crossing time, TAV, and the root mean square deviation from the average TRMS. Examples of four signal buildup waveforms are shown in Figure 4.3-H.1-2. Also shown as a dash-dot line is the mean signal buildup without the filter, and the dash line the average buildup with the filter. For these examples the noise was set at 0.

The computer simulation program was run for various threshold settings, noise levels, and bandwidths for a total of more than 10,000 threshold crossings to obtain statistics to relate the adjustment of controllable parameters to the altitude error. (A sample bandwidth of 2.5 mc was used in this example). This number of samples is marginal for determining the fine details of variation of the error with very great confidence.

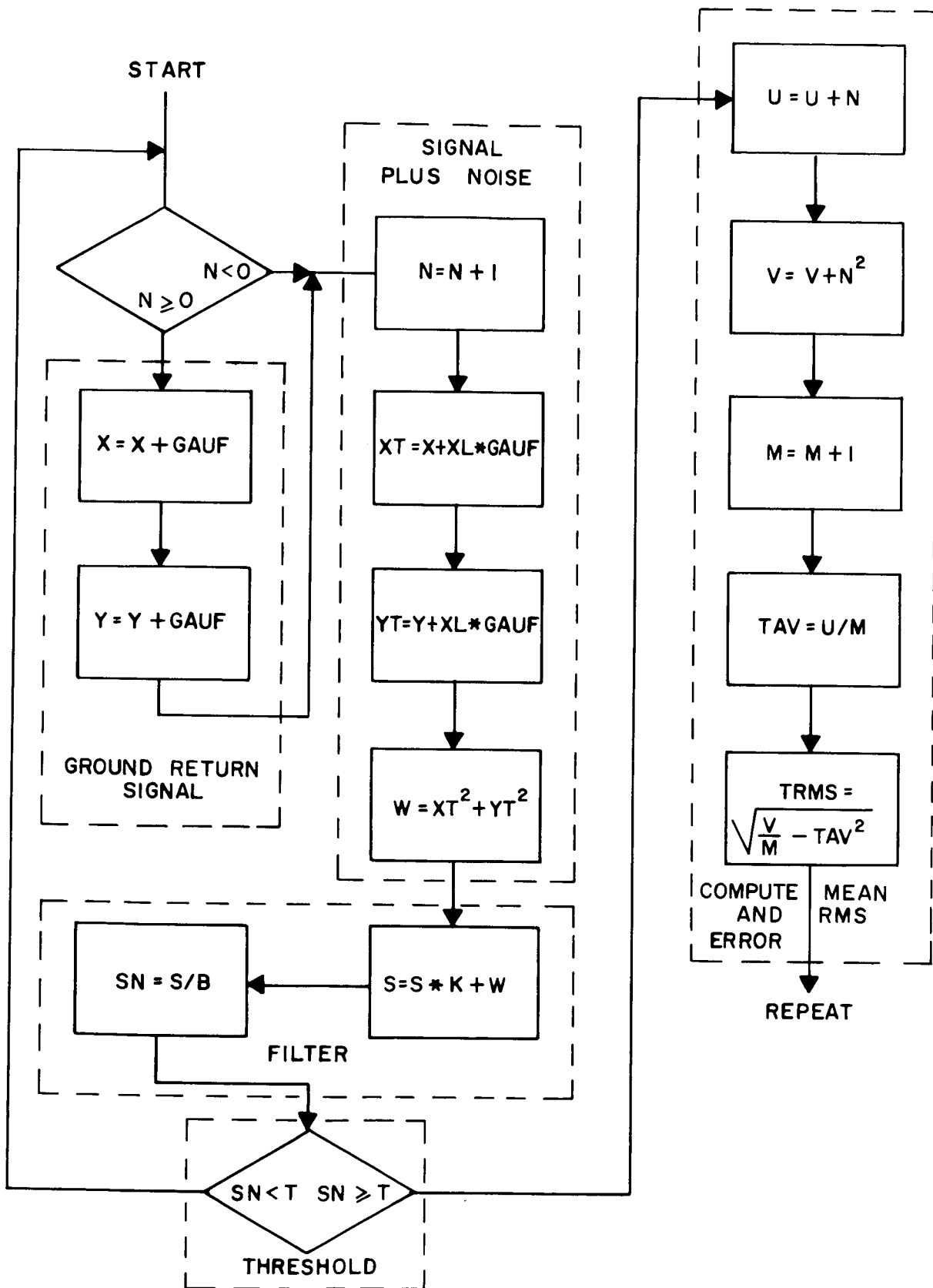


FIGURE 4.3-H.1-1 FLOW DIAGRAM FOR SIGNAL SIMULATION

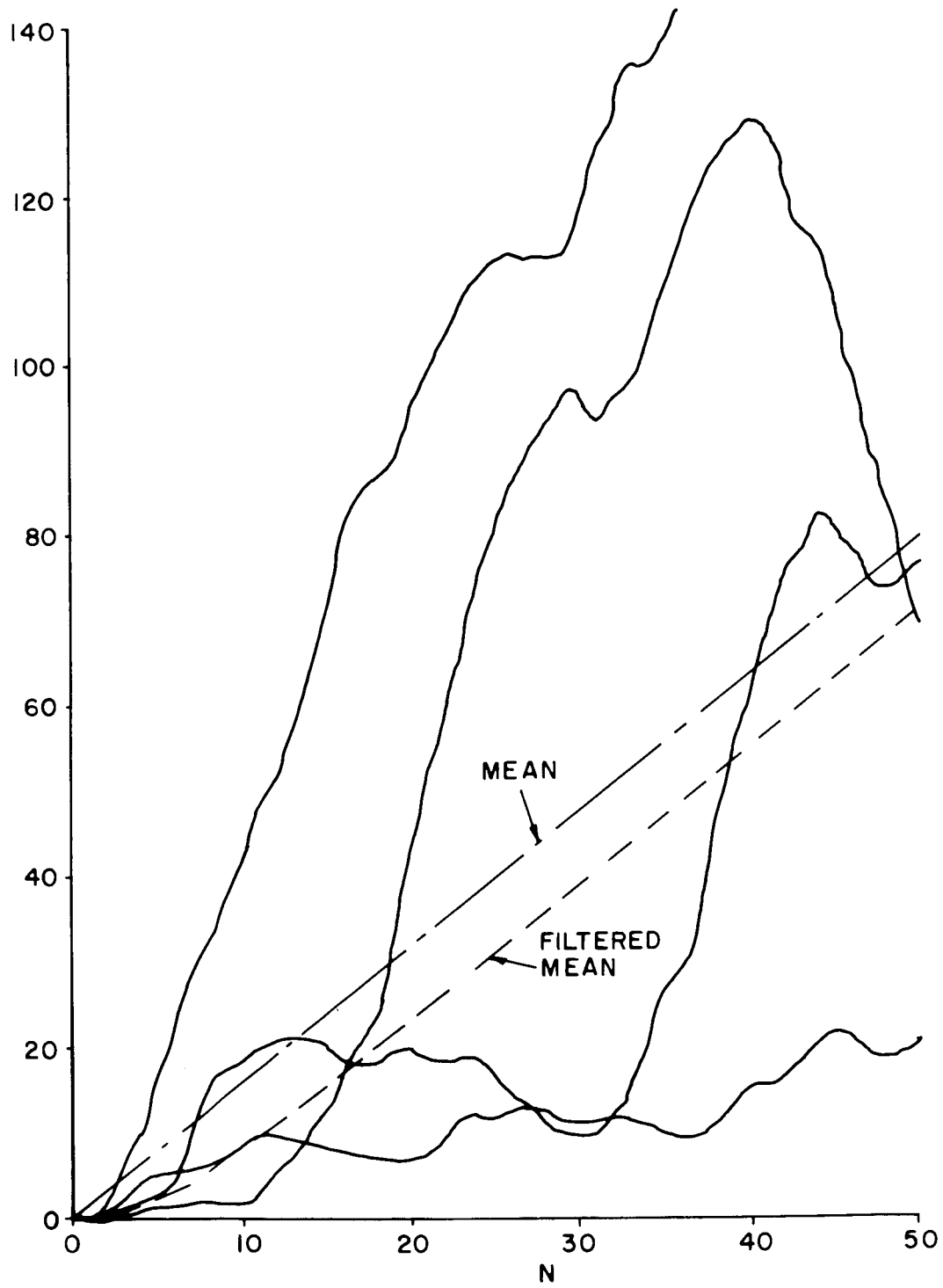


FIGURE 4.3-H.1-2 EXAMPLES OF SIGNAL BUILDUP

Figure 4.3-H. 1-3 and -4 show the effect of signal to noise ratio and threshold setting to the mean delay and rms error about the mean. The following conclusions may be drawn from these figures.

Mean Delay

- a) Mean delay is reduced as the threshold is reduced.
- b) As signal to noise ratio is worsened, the delay becomes shorter.
- c) The effect of reduced signal to noise ratio is more pronounced for lower threshold settings.

RMS Error

- a) The rms error decreases as the threshold is decreased.
- b) As signal to noise is worsened, the rms error increases rapidly.
- c) The signal to noise ratio at which the rms error begins to increase rapidly is related to the threshold setting, lower signal to noise ratios going with lower threshold settings.

Poor signal to noise ratio produces its effect by causing threshold crossings before the ground return signal, and thus reduces the mean delay time and increases RMS error. Noise at this level is also undesirable because it would make acquisition of the signal long because of false alarms.

The effects of receiver bandwidth are shown in Figures 4.3-H. 1-5 and -6. Increasing the bandwidth reduces both the mean delay and the rms error. A 10 to 1 increase in bandwidth produces about the same improvement in rms error as a 2 1/2 to 1 increase in signal to threshold ratio $(S/N)/T$. This reduction in mean delay with increased bandwidth is due to shorter delay time in broader band circuits as well as reduced filter smoothing allowing more frequent, higher noise peaks and thus a greater probability of earlier threshold crossing. The second effect is also responsible for the reduced rms error.

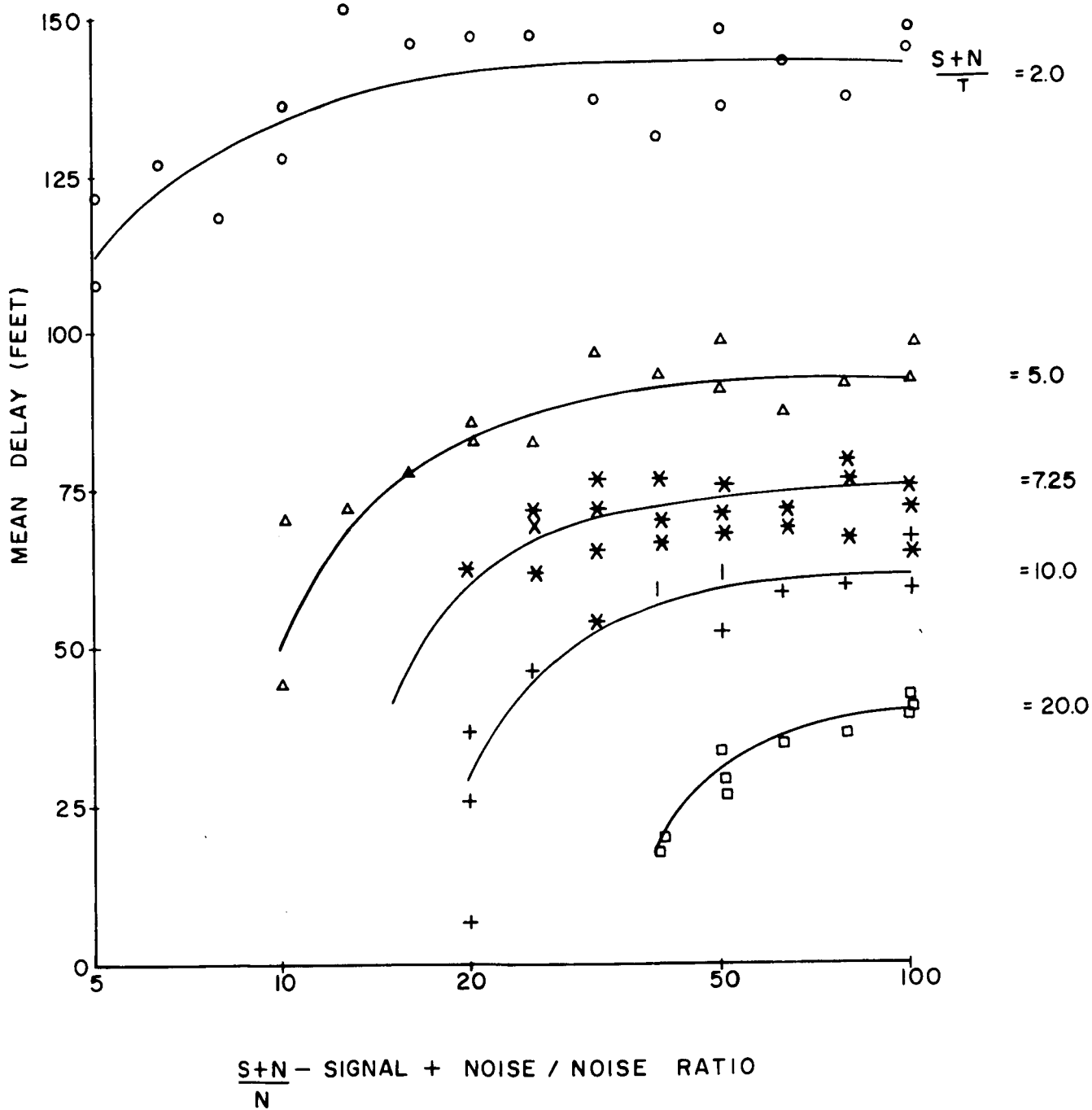


FIGURE 4.3-H.1-3 MEAN DELAY VS NOISE AND THRESHOLD

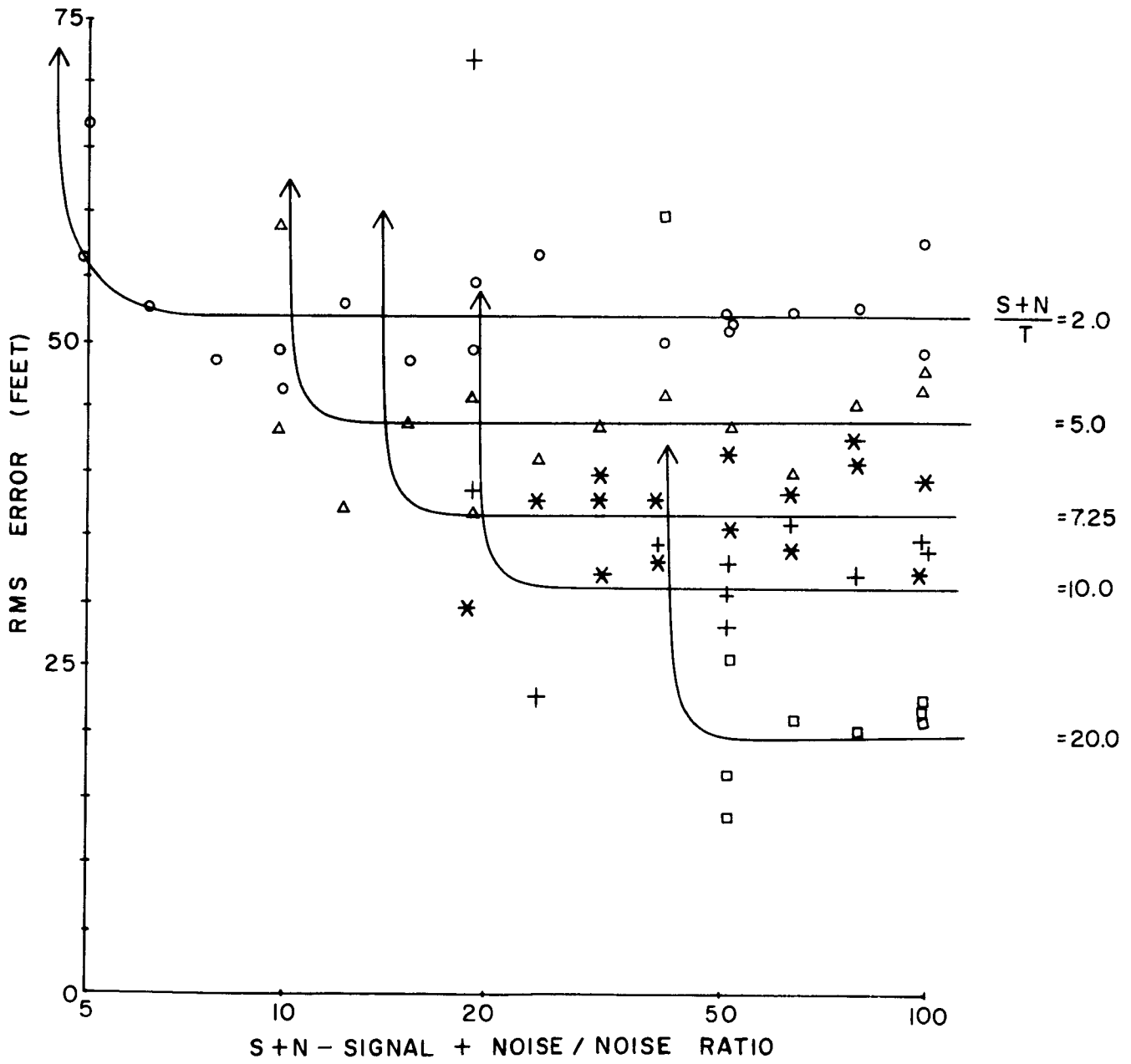


FIGURE 4.3-H.1-4 RMS ERROR VS NOISE AND THRESHOLD

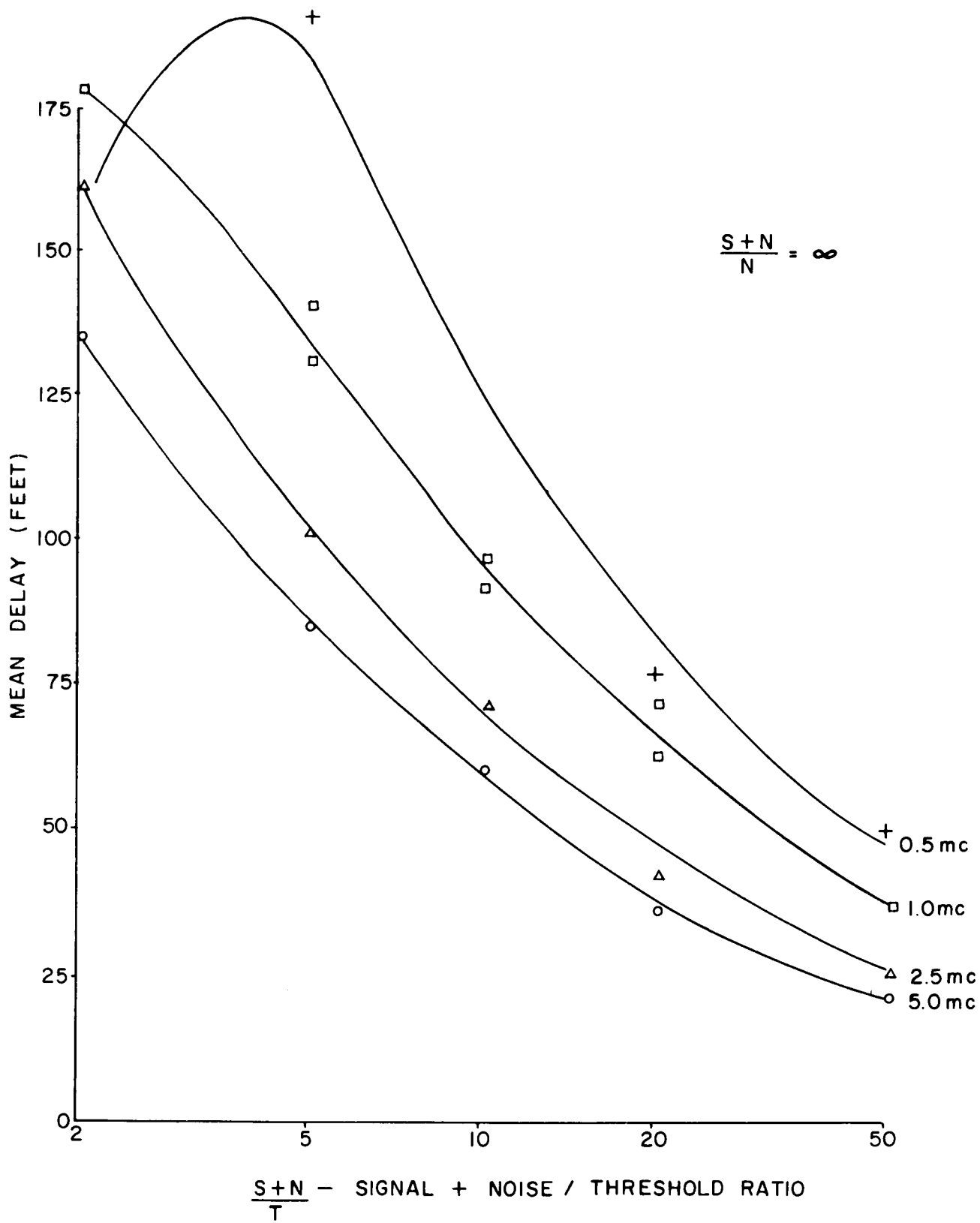


FIGURE 4.3-H.I-5 MEAN DELAY VS BANDWIDTH

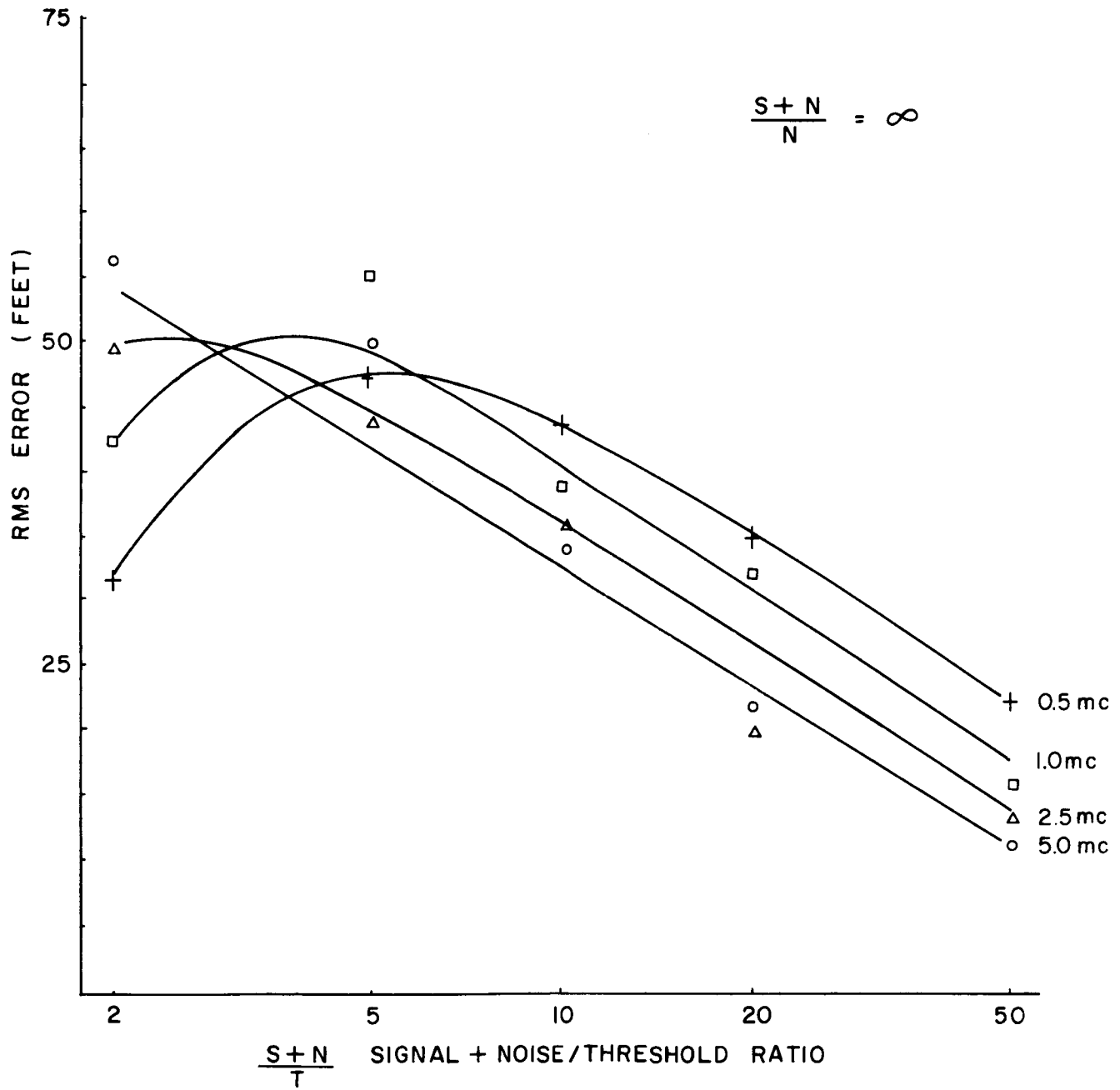


FIGURE 4.3-H.1-6 RMS ERROR VS BANDWIDTH

As indicated earlier, this routine was used in determining like errors for the cases considered in this study. The results are rms values of single sampling distributions and should be used only to indicate orders of magnitudes and trends. This error is frequency independent and insignificantly dependent on PRF. The results of the simulation were

<u>Beamwidth</u>	<u>S/N/N</u>	<u>RMS Error</u>
5°	13.6 db	94 ft.
3°	13.6 db	30.6 ft.
1°	14.0 db	3.3 ft.

To examine this error source as a function of $\frac{S}{N}$, the $\frac{S}{N}$ values were increased for a 100 pps PRF, X band system to values whose corresponding peak power requirements caused a 10% increase in weight for the 5° and 3° cases; in the 1° case the maximum available peak power was reached (200 KW for X band) before the weight increased 10%. The errors were reduced, thusly,

<u>Beamwidth</u>	<u>S/N/N</u>	<u>RMS Error</u>
5°	18.2 db	60 ft.
3°	19.5 db	15.9 ft.
1°	25.9 db	1.6 ft.

4.3-H.2 Quantization Error

Quantization error in the data processor is a result of the clock sinusoidal signal being quantized digitally. For a 50 mc clock the maximum quantization interval is 20 nanoseconds (or 9.8 feet); the distribution of the quantization interval is uniformly random. The mean square of a uniform distribution interval of $-d/2$ to $d/2$ and magnitude $1/d$ is

$$\sigma^2 = \frac{1}{d} \int_{-d/2}^{d/2} x^2 dx = \frac{d^2}{12}$$

The rms of the distribution is then

$$\sigma = \frac{d}{\sqrt{12}}$$

The rms quantization error thus associated with a 50 mc clock is

$$\sigma = \frac{9.8}{\sqrt{12}} = 2.8 \text{ feet}$$

4.3-H.3 Verticality

When there is a verticality error, i. e., altitude deviation moves radiation beam off true vertical, the beam angle at which beamwidth limiting occurs is reduced from that of the antenna beamwidth (θ) for true vertical (Figure 4.3-H.3-1), where the solid beams are vertical case and dashed beams are non-vertical). The power buildup will remain the same until the new beam angle (α) is reached. From Figure 4.3-H.3-2

$$\alpha = \theta - 2\phi$$

where ϕ = verticality error angle. Since the received power is proportional to the area (or beam angle squared), the power buildups are the same until

$$P_1 = \frac{\alpha^2}{\theta^2} P_{\max}$$

where P_{\max} = maximum received power for vertical case

or
$$P_1 = \left[1 - \frac{2\phi}{\theta}\right]^2 P_{\max}$$

If the threshold is set below P_1 , or

$$\frac{A_t}{A_{\max}} \leq \frac{P_1}{P_{\max}} = \left[1 - \frac{2\phi}{\theta}\right]^2 \quad (4.3-H.3-1)$$

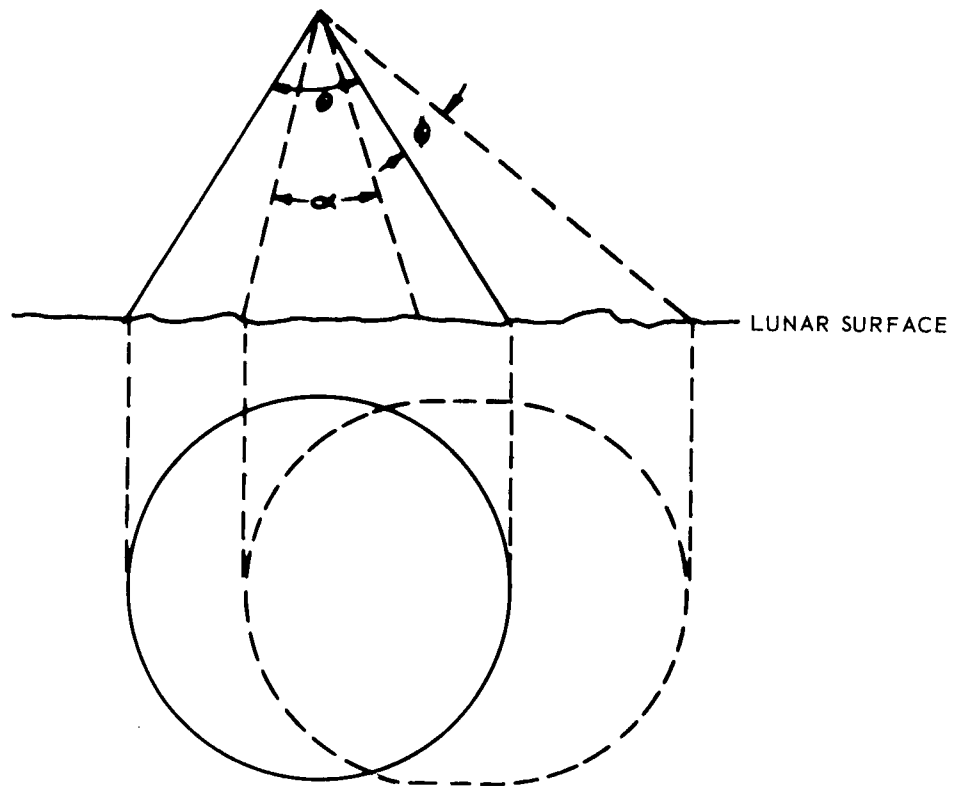


FIGURE 4.3-H.3-1. VERTICALITY ANGLE ERROR

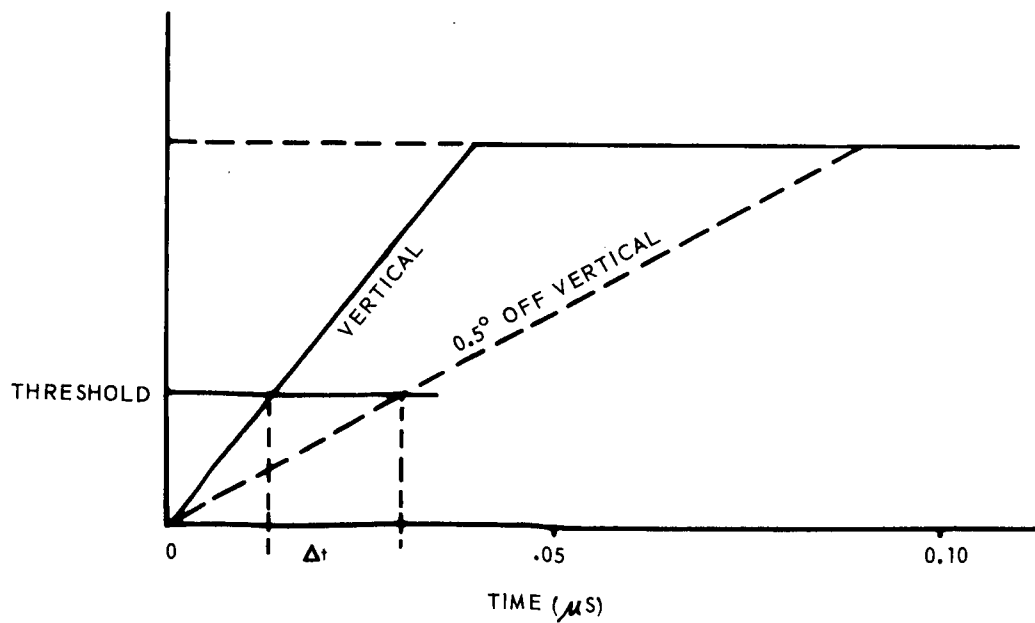


FIGURE 4.3-H.3-2. VERTICALITY THRESHOLD ERROR

where A_{\max} = maximum illuminated area

A_t = threshold area

then non-verticality of θ introduces no timing error at the threshold. For the cases considered and using a maximum error of 0.5° , equation 4.3-H.3-1 shows

θ	A_t/A_{\max}	$\left[1 - \frac{2\phi}{\theta}\right]^2$
5°	0.42	0.64
3°	0.30	0.45
1°	0.34	0

An error at the threshold is exhibited in only the 1° beamwidth case as illustrated in Figure 4.3-H.3-2 where solid buildup is the vertical case and the dashed buildup is non-vertical. With a maximum 0.5° error, a timing error of 0.017 us (or 8.3 ft.) occurs at the threshold. If the verticality error exhibits a random distribution, then as discussed in the previous error section, the rms verticality error is

$$\sigma = \frac{8.3}{\sqrt{12}} = 2.4 \text{ feet}$$

If the increased S/N values of section 4.3-H.1 are used, this error at 1° beamwidth becomes 0.2 feet.

4.3-H.4 Threshold Detector Variation

A variance in the level of threshold detection about some mean would be present and is assumed to be Gaussian distributed. For this analysis, a conservative maximum (3σ) detection level variation of 10% was assumed. This results in rms altitude errors of

<u>Beamwidth</u>	<u>RMS Error</u>
5°	6.9 ft.
3°	1.6 ft.
1°	0.2 ft.

If the increased S/N values of section 4.3-A are used, these errors become:

<u>Beamwidth</u>	<u>RMS Error</u>
5°	2.4 ft.
3°	.4 ft.
1°	0 ft.

4.3-H.5 Clock Frequency Stability

An error is introduced in the sensor measurement by any instability in the clock oscillator frequency. A clock stability of one part in 10^6 , which was assumed for study purposes, results in an error equal to the altitude divided by 10^6 . For the 80 nautical mile orbit (490,000 ft.), an rms error of 0.5 feet results.

4.3-H.6 AGC Limitations

A receiver with AGC automatically compensates for any variation in receiver gain, setting all pulses to a constant power level. The AGC should be capable of reducing gain change to below 5%. The rms timing error (Δt) at the threshold due to a 5% change in gain is

$$\Delta t = t_o P_1 \left[\frac{.05 P_{\max}}{.95 P_{\max}} \right]$$

where $P_1 =$ threshold

or normalizing to P_{\max}

$$\Delta t = .0527 t_o \frac{P_1}{P_{\max}}$$

or $\Delta t = .0527 t_o \frac{A_t}{A_{\max}}$

Thus for the cases considered

<u>θ</u>	<u>t_o</u>	<u>Δt</u>	<u>Δh</u>
5°	1 us	.022	10.8 ft.
3°	.3 us	.0038	2.4 ft.
1°	.04 us	.0007 us	.3 ft.

If the increased S/N values of section 4.3-H.1 are used, these errors become

<u>Beamwidth</u>	<u>RMS Error</u>
5°	3.8 ft.
3°	.6 ft.
1°	0

4.3-H.7 Gate Jitter

The variations in switching times of the many switching points in the data processor would also introduce errors in the altitude measurements. Tests on an LTV MED data processor similar to that proposed for LUCOM show that no error as large as the smallest altitude increment (10 ft.) occurred, so using 10 feet as a maximum (3σ) error and assuming Gaussian distribution, the rms value of this error would be 3.3 feet.

4.3-H.8 Error Summation

The errors previously discussed are statistically independent; thus, an overall rms error statement can be obtained by determining the root of the sum of their mean squares (RSS). Table 4.3-H.8-1 reflects this summation for the cases considered.

Source	RMS Error (ft.)			Mean Square Error (ft. ²)		
	5°	3°	1°	5°	3°	1°
Return Variation	94.0	30.6	3.3	8840	937	10.9
Quantization	2.8	2.8	2.8	7.8	7.8	7.8
Verticality	0	0	2.4	0	0	5.8
Threshold Detector	6.9	1.6	0.2	47.6	2.6	0
Clock Stability	0.5	0.5	0.5	.3	.3	.3
AGC	10.8	2.4	.3	116.8	5.8	.1
Gate Jitter	3.3	3.3	3.3	10.9	10.9	10.9
Total				9023.4	964.4	35.8
RSS (feet)				94.0	31.1	6.0

Table 4.3-H.8-1 ERROR STATEMENT

If the increased S/N values of section 4.3-H.1 are used, the RSS errors become

<u>Beamwidth</u>	<u>RSS Error</u>
5°	60.3 ft.
3°	16.5 ft.
1°	4.7 ft.

Another method to reduce errors in altitude measurements is that of averaging over a number of returns for a single measurement. The mean square values of error sources that yield errors that are independent on a pulse-to-pulse basis can be reduced by a factor equal to the number of pulses averaged. The error sources of this study that meet this criterion are the return signal variation and the quantization error. Where N is the number of returns averaged, the error statement for the lower S/N values become

<u>N</u>	RSS Error (feet)		
	5°	3°	1°
	$\sqrt{\frac{8847.8}{N}} \pm 175.6$	$\sqrt{\frac{944.8}{N}} \pm 19.6$	$\sqrt{\frac{18.7}{N}} \pm 17.1$
1	95.0	31.1	6.0
2	67.8	22.2	5.1
4	48.9	16.0	4.8
16	27.0	8.9	4.3
256	14.5	4.8	4.1

For the increased S/N/N values, these averaged errors become

<u>N</u>	RSS Error (feet)		
	5°	3°	1°
	$\sqrt{\frac{3607.8}{N}} \pm 31.4$	$\sqrt{\frac{260.8}{N}} \pm 11.8$	$\sqrt{\frac{10.4}{N}} \pm 11.6$
1	60.3	16.4	4.7
2	41.6	11.9	4.1
4	30.6	8.8	3.8
16	16.0	5.3	3.5
256	6.8	3.6	3.4

These sets of error values are plotted in Figure 4.3.3.2-1 of section 4.3.3.2 against system weights and volumes for the two ranges of S/N/N. The uppermost points on the solid lines represent the RSS errors for the low set of S/N/N values for the respective beamwidth cases. The lowermost points on the solid lines represent the RSS errors for high set of S/N/N values.

All error sources but quantization, clock stability, and gate jitter are dependent on the threshold level -- the lower the setting, the lower the error. A lower threshold indicates detection at a lower threshold area, thus a trade-off between system errors and profile reproduction remains and should be performed before a final system is generated.

APPENDIX 5-A

TABLES I through XV

TABLE 5-AI

Switching Sequence of Sequence Control Unit (See Block Diagram Figure 5.1.3.1-1). Assumptions:

- A. Transmit commands are initiated by astronaut 600 seconds prior to line-of-sight-to-earth conditions for each orbit and turned off at the end of line-of-sight.
- B. Real time data is transmitted when tape recorders are in rewind mode.
- C. Each recorder alternately records one orbit of data and plays back the data two times during the following half orbit.
- D. Real time bit rate is 10240 bits per second. Recorder playback is 81920 bits per second.
- E. Line-of-sight-to-earth exists at time T_o (Radar Sensor Operate).

<u>Event No.</u>	<u>Time</u>	<u>SCU Command From Astronaut</u>	<u>SCU Switching Function</u>
1	1st orbit prior to T_o	POWER ON TRANSMIT ON	a. Recorder no. 1 RECORD mode b. Transmitter ON with input at Real Time Data
2	T_o (Radar Sensor OPERATE)	None	None (T_o event resets time code generator and flags a bit-level event into the multiplexer-encoder)
3	1st orbit - end line-of- sight	TRANSMIT OFF	a. Transmitter OFF, Recorder No. 1 con- tinues to record

<u>Event No.</u>	<u>Time</u>	<u>SCU Command From Astronaut</u>	<u>SCU Switching Function</u>
4	2nd orbit - 600 seconds prior line- of-sight	TRANSMIT ON	<ul style="list-style-type: none"> a. Recorder No. 2 RECORD mode b. 30 seconds elapsed time to allow data overlap c. Transmitter ON with Real Time Data Input d. Recorder No. 1 REWIND mode to beginning-of-tape sensor. e. Transmitter input to RECORDER No. 1 Data f. Recorder No. 1 PLAYBACK mode to end-of-tape sensor g. Transmitter input to Real Time Data h. Recorder No. 1 REWIND mode to beginning-of-tape sensor i. Transmitter input to RECORDER No. 1 Data j. Recorder No. 1 PLAYBACK mode to end-of-tape sensor k. Transmitter input to Real Time Data. l. Recorder No. 1 REWIND-ERASE to beginning-of-tape sensor m. Recorder No. 1 OFF
5	2nd orbit - end line-of- sight	TRANSMIT OFF	<ul style="list-style-type: none"> a. Transmitter OFF; Recorder No. 2 continues to record
6	3rd orbit - 600 seconds prior line- of-sight	TRANSMIT ON	Same sequence as event No. 4 except interchange functions of Recorders No. 1 and No. 2
7	3rd orbit - end line-of- sight	TRANSMIT OFF	Same as event No. 5 except Recorder No. 1 continues to record.

Table 5-AI (page 2)

<u>Event No.</u>	<u>Time</u>	<u>SCU Command From Astronaut</u>	<u>SCU Switching Function</u>
8	Successive orbits	TRANSMIT ON- OFF	Same as events 4 through 7.
9	Last orbit - end line-of- sight	POWER OFF	a. Recorders OFF b. Transmitter OFF

Table 5-AI (page 3)

TABLE 5-AII
Sample PCM Format

Row	Column				Word Number
	1	2	3	4	
1	Analog Word 1	Altitude Word 1	Altitude Word 2	Event Word 1	1 - 4
2	Analog Word 2	Time Code Word 1	Time Code Word 2	Time Code Word 3	5 - 8
3	Analog Word 3	Altitude Word 1	Altitude Word 2	Event Word 1	9 - 12
4	Analog Word 4	Analog Word 5	Analog Word 6	Analog Word 7	13 - 16
5	Analog Word 8	Altitude Word 1	Altitude Word 2	Event Word 1	17 - 20
6	Analog Word 9	Analog Word 10	Bi-Level Word 1	Bi-Level Word 2	21 - 24
7	Bi-Level Word 3	Altitude Word 1	Altitude Word 2	Event Word 1	25 - 28
8	Analog Word 11	Frame Sync Word 1	Frame Sync Word 2	Frame Ident.	29 - 32

Word Length 8 bits

Frame Length 32 words or 256 bits

Frame Rate 40 frames/second

Word Rate 1280 words/second

Bit Rate 10240 bits/second

Sample Rate - Time Code, Analog and Bi-Level = 40 sps

Sample Rate - Altitude, Events = 160 readings per second

Table 5-AII (page 2)

TABLE 5-AIII
Alternate PCM Format

Row	Column			Word Number
	1	2	3	
1	Altitude Word 1	Altitude Word 2	Event Word 1	1 - 3
2	Time Code Word 1	Time Code Word 2	Time Code Word 3	4 - 6
3	Altitude Word 1	Altitude Word 2	Event Word 1	7 - 9
4	Analog Word 1	Analog Word 2	Analog Word 3	10 - 12
5	Altitude Word 1	Altitude Word 2	Event Word 1	13 - 15
6	Analog Word 4	Analog Word 5	Analog Word 6	16 - 18
7	Altitude Word 1	Altitude Word 2	Event Word 1	19 - 21
8	Analog Word 7	Analog Word 8	Analog Word 9	22 - 24
9	Altitude Word 1	Altitude Word 2	Event Word 1	25 - 27
10	Analog Word 10	Analog Word 11	Bi-Level Word 1	28 - 30
11	Altitude Word 1	Altitude Word 2	Event Word 1	31 - 33
12	Frame Sync Word 1	Frame Sync Word 2	Frame Sync Word 3	34 - 36

Word Length	8 bits
Frame Length	36 words or 288 bits
Frame Rate	35 frames/second
Word Rate	1260 words/second
Bit Rate	10080 bits/second
Sample Rate - Time Code, Analog and Bi-Level = 35 sps	
Sample Rate - Altitude and Events = 210 readings per second	

Table 5-AIII (page 2)

TABLE 5-AIV

<u>RF DATA LINK ANALYSIS</u> <u>Parameters</u>	<u>VHF LINK</u> <u>Assumed Value</u>	<u>LSM-TO-CSM</u> <u>Decibels</u>
Frequency (mc)	260	-
Transmitter Power (dbw)	5 watts	+7
Transmit Antenna Gain (db)	Cross Polarized Stubs	00
Range (nautical miles)	100	-
Free Space Loss (db)	-	-126
*Predicted Losses (db)	-	-3
Received Antenna Gain (db)	-	0
Received Signal Power (dbw)	-	-122

* Predicted losses include atmosphere, polarization and hardware losses. If an existing set of antennas on the Apollo modules are used, add -3 db to predicted losses to cover two multicouplers, and modify the transmit and receive antenna gains.

<u>RF DATA LINK ANALYSIS</u> <u>Parameters</u>	<u>VHF LINK</u> <u>Assumed Value</u>	<u>LSM-TO-CSM</u> <u>Decibels</u>
Overall Receiver Noise Temperature (° K)	300	-
**Receiver Noise Power in 1 cps (dbw)	-	-191
Modulation Bandwidth, Fm (kc)	25	+44
RF Bandwidth (kc)	125	-
Required Input SNR in Fm (db)	-	+15
Receiver Threshold (dbw)	-	-132
<hr/>		
Circuit Margin	-	+10

** Includes 12.8 db receiver noise figure.

TABLE 5-AV

<u>RF DATA LINK ANALYSIS</u> <u>Parameters</u>	<u>S-BAND LINK</u> <u>Assumed Value</u>	<u>CSM-TO-EARTH</u> <u>Decibels</u>
Frequency (mc)	2300	-
Transmitter Power (dbw)	5 watts	+7
Transmitter Antenna Gain (db)	D = 4 ft.	+26.5
Range (nautical miles)	215,000	-
Free Space Loss (db)	-	-212
*Predicted Losses (db)	-	-3
Receiver Antenna Gain (db)	D = 85 ft.	+53
Received Signal Power (db)	-	-128.5
Overall Receiver Noise Temperature (° K)	220	0
Receiver Noise Power in 1 cps (dbw)	-	-206
Modulation Beamwidth, Fm (kc)	200	+53
Required Input SNR in Fm (db)	-	+15
Receiver Threshold	-	-138
Circuit Margin	-	+9.5

* Predicted losses include atmosphere, polarization and hardware losses.

TABLE 5-AVI-1

FUNCTIONAL CHARACTERISTICS - SIGNAL CONDITIONER

Channel Capacity:	<ul style="list-style-type: none">a. Up to eleven analog channels utilizing typical modules as described on following pages.b. Up to twenty-four bi-level events utilizing typical modules as described on following pages.c. Up to twenty-four digital bits.
Power Supply:	<p>An internal power supply shall be utilized to provide the voltages required by the signal conditioning modules. The primary to secondary isolation and grounding philosophy shall satisfy the requirements of MIL-I-26600.</p> <p>The efficiency of the power supply including all necessary regulators, transient suppressors, rfi filtering, etc. shall be 50 percent or greater when loaded with a full module complement.</p>
RFI:	Electro interference shall conform to the requirements of MIL-I-26600.
Power:	28 volts dc \pm 4 volts.

TABLE 5-AVI-2

ANALOG SIGNAL CONDITIONER - DC AMPLIFIER

Input Signal Range:	0 \pm 10 millivolts to 0 \pm 5 volts full scale
Input Impedance:	500,000 ohms minimum
Output Signal :	0 to \pm 5 volts at 0.4 milliampere maximum
Output Impedance:	250 ohms maximum
Accuracy:	\pm 1.2 percent
Zero and Gain Stability:	\pm 0.7 percent
Resolution:	\pm 0.3 percent
Repeatability:	\pm 0.1 percent
Linearity and Hysteresis:	\pm 0.2 percent
Frequency Response:	12 db/octave at 100 cps, 18 db/octave at 400 cps
Ripple:	5 millivolts peak-to-peak

TABLE 5-AVI-3

ANALOG SIGNAL CONDITIONER - ANALOG BUFFER

Input Signal:	0 to 5 volts DC full scale
Input Impedance:	500,000 ohms minimum
Output Signal:	0 to \pm 5 volts at 0.4 milliampere maximum
Output Impedance:	100 ohms maximum
Accuracy:	\pm 0.4 percent
Zero and Gain Stability:	\pm 0.2 percent
Repeatability:	\pm 0.02 percent
Linearity and Hysteresis:	\pm 0.1 percent
Frequency Response:	12 db/octave at 400 cps
Ripple:	5 millivolts peak-to-peak

TABLE 5-AVI-4

ANALOG SIGNAL CONDITIONING - RF POWER DETECTOR

Signal Input:	5 to 50 millivolts peak, 1 microsecond pulse width
Input Impedance:	50 ohms
Signal Output:	0 to ± 5 volts dc
Output Impedance:	250 ohms minimum
Accuracy:	± 2 percent
Zero and Gain Stability:	± 1.2 percent
Repeatability:	± 1 percent
Linearity and Hysteresis:	± 0.1 percent
PRF Variations:	Stable to ± 1.0 percent with variations in PRF from 100 to 1000 pps
Ripple:	50 millivolts peak-to-peak with 100 pps PRF

TABLE 5-AVI-5

ANALOG SIGNAL CONDITIONER - TEMPERATURE CONVERTER

Input Signal (4 channels):	100 ohms to 2500 ohms full scale at 1 milliampere maximum
Output Signal (4 channels):	0 to 5 volts at 0.4 milliampere maximum
Output Impedance :	250 ohms maximum
Accuracy:	\pm 1.0 percent
Zero and Range Stability:	\pm 0.7 percent
Repeatability:	\pm 0.1 percent
Hysteresis and Tracking:	\pm 0.1 percent
Frequency Response:	18 db/octave at 50 cps
Ripple:	\pm 0.1 percent of full scale

TABLE 5-AVI-6

ANALOG SIGNAL CONDITIONER - ACTIVE ATTENUATOR

Input Signal:	± 6 VDC to ± 35 VDC full scale
Input Impedance:	100,000 ohms minimum
Output Signal:	0 to ± 5 volts DC
Output Impedance:	100 ohms maximum
Accuracy:	± 0.5 percent
Zero and Gain Stability:	± 0.5 percent
Resolution:	± 0.1 percent
Repeatability:	± 0.1 percent
Linearity and Hysteresis:	± 0.1 percent
Frequency Response:	12 db/octave at 800 cps
Ripple:	5 millivolts peak-to-peak

TABLE 5-AVI-7

BI-LEVEL SIGNAL CONDITIONER - BUFFER

Input Signal (8 channels):	Closure or 28 VDC ground
Input Impedance :	10,000 ohms minimum
Output Signal (8 channels):	+0.5 to +6 volts -0 +4
Rise and Fall Time:	1 millisecond maximum
Ripple :	50 millivolts peak-to-peak

TABLE 5-AVII

FUNCTIONAL CHARACTERISTICS - MULTIPLEXER - ENCODER

Analog Input Voltage :	0 to \pm 5 volts
Number of Analog Inputs:	11 Channels
Analog Input Impedance :	500000 ohms minimum
Leakage Current Into Source :	2 microamperes maximum
Overvoltage Fault Protection:	\pm 30 volts
Analog-to-Digital Converter Output :	8-bit parallel binary code
Analog Accuracy :	\pm 0.5 percent overall multiplexer-encoder accuracy. Zero volts or less is represented by the binary number 00000010, and 5 volts or greater is represented by the binary number 11111100.
Crosstalk :	Within 0.2 percent of full scale
Bi-level and Digital Input Voltage:	-0.5 to \pm 1.0 volts for "zero" \pm 3.0 to \pm 6.0 volts for "one"
Number of Bi-level Inputs:	24 Channels
Number of Digital Inputs :	24 Bits
Interlock:	An internal 24-bit storage register shall be provided to accept digital data. Parallel read-in shall be accomplished at equal time increments dictated by the frame format. An inhibit signal occurring coincident with altitude data changes will be supplied by the sensor/signal conditioner to inhibit data read-in at this time.

Time Code:	24-bit parallel binary, 1 millisecond per increment. Accuracy 1×10^5 , stability 1×10^6 .
Time Correlation:	A 24-bit storage register shall be provided to accept time code data. Parallel read-in shall be accomplished coincident with read-in of the altitude data. Internal inhibit functions shall be provided to prevent read-in during changes in the time code increments.
Time Code Reset Command:	± 4 to ± 6 volts pulse, 1 microsecond pulse width. Time code resets to zero on pulse leading edge.
Bit Clock:	An internal clock shall generate the bit rate. The stability and accuracy shall conform to IRIG 106-60.
Bit Rate:	10240 bits per second
Word Rate:	1280 words per second
Frame Rate:	40 frames per second
Frame Sync:	24-bits located at the last three words in the frame format
Frame Format:	See following page
Output Code form:	Split Phase (bi-phase)
RFI:	Electro-Interference shall conform to the requirements of MIL-I-26600
Power:	28 volts dc ± 4 volts

Table 5-AVII (Page 2)

TABLE 5-AVII

FRAME FORMAT

Row	Column				Word Number
	1	2	3	4	
1	A1	H1	H2	H3	1 - 4
2	A2	T1	T2	T3	5 - 8
3	A3	H1	H2	H3	9 - 12
4	A4	A5	A6	A7	13 - 15
5	A8	H1	H2	H3	17 - 20
6	A9	A10	B1	B2	21 - 24
7	B3	H1	H2	H3	25 - 28
8	All	Frame Sync	Frame Sync	Frame Sync	29 - 32

Analog Input Channels 1 through 11 are designated A1 through A11, respectively. Bi-level input words are designated Bn-j, where "n" of 1 or 2 designates the word and "j" of 1 through 8 designates the bit location within the word. The 24-bit time code is separated into three 8-bit words designated T1 through T3. The most significant bit is T1-1 and the least significant bit is T3-8. The altitude data and time correlation events are designated H1 through H3. The most significant altitude bit is H1-1.

Table 5-AII (Page 3)

TABLE 5-AVIII

FUNCTIONAL CHARACTERISTICS - VHF TRANSMITTER

Modulation:	True FM.
Modulation Input:	± 0.7 volts peak centered about zero split phase PCM at 10,200 bits per second.
Input Impedance:	10,000 ohms minimum shunted by 200 picofarads maximum.
Frequency Deviation:	10.2 KC ± 5 percent when modulated with the above input signal. The deviation stability shall be within ± 5 percent for all environmental conditions.
Modulation Frequency Response:	± 1 db from 300 cps to 30 KC.
Modulation Distortion:	Less than 3 percent for peak deviation of 125 KC and modulating frequency from 300 cps to 30 KC.
Incidental FM:	± 2 KC maximum.
Output Frequency:	Selectable within the range of 225 to 260 MC.
Frequency Stability:	± 0.005 percent for all environmental conditions.
Output Impedance:	50 ohms.
Output Power:	5 watts minimum for all environmental conditions when operating into a 50 ohm load with a VSWR of 1.5 to 1 or less.
Warm-Up Time:	60 seconds to meet all electrical and environmental requirements.
Power Input:	28 volts dc ± 4 volts.

TABLE 5-AIX

FUNCTIONAL CHARACTERISTICS - VHF RECEIVER

Modulation:	True FM.
Input Impedance:	50 ohms.
RF Frequency:	Selectable within the range of 225 to 260 MC.
Frequency Stability:	± 0.005 percent for all environmental conditions.
IF Bandwidth:	25 KC
Sensitivity:	Less than 1.0 microvolt for 25 KC IF bandwidth gives 10 db minimum signal-to-noise ratio at output.
AGC Dynamic Range:	The output shall be ± 2 volts peak ± 20 percent over an input range from 2 microvolts to 2 millivolts.
Load Impedance:	Operate into a 2,000 ohm load impedance.
Power Input:	28 volts dc ± 4 volts.

TABLE 5-AX

FUNCTIONAL CHARACTERISTICS - BIT SYNCHRONIZER AND DATA REGENERATOR

Signal Input:	± 2 volts peak ± 20 percent split phase PCM code at 10,240 bits per second ± 1 percent.
Input Impedance:	2000 ohms.
Signal Output:	Noise-free regenerated split phase PCM code at 10,240 bits per second, synchronized with input.
Output Levels:	Zero and ± 4 volts peak ± 5 percent.
Output Impedance:	100 ohms maximum.
Output Rise and Fall Time:	The rise time or fall time shall not exceed 1 microsecond into a 3 K ohm load shunted by 500 picofarads.
Output Jitter:	Pulse-to-pulse jitter of the regenerated data shall not exceed 0.05 percent of the average bit period.
Synchronization Acquisition:	Bit synchronization shall be acquired with a peak signal-to-rms noise ratio of ± 3 db or greater.
Bit Errors:	Curve II of Figure 1 shall be the design goal. The limit of Curve I shall not be exceeded. The noise of Figure 1 is measured after a 36 db octave Gaussian filter with cutoff of 1.5 times the bit rate.
Synchronization Errors:	The bit error rate of Figure 1, Curve I shall not be exceeded whether the errors are caused by synchronization slippage or errors in detection. Bit synchronization shall be maintained with a peak signal-to-rms noise ratio of -3 db.
Power:	28 volts dc ± 4 volts.

TABLE 5-AXI

FUNCTIONAL CHARACTERISTICS - MAGNETIC TAPE RECORDER

Signal Input:	4 volts \pm 5 percent split phase PCM code at 10,240 bits per second \pm 1 percent.
Input Impedance:	10,000 ohms minimum shunted by 100 picofarads maximum.
Packing Density:	2,730 bits per inch with less than 1 bit error in 10^5 bits.
Bit Rate Stability:	Long term bit rate variation less than \pm 2 percent. Bit rate deviation less than 0.1 percent/second/second over the average of 1,000 consecutive bits. Pulse-to-pulse jitter less than 0.1 percent of the average period.
Number of Data Tracks:	One.
Signal Output:	4 volts \pm 5 percent split phase PCM.
Output Impedance:	100 ohms maximum.
Tape Capacity:	2,300 feet of 1/4 inch wide, 1 mil instrumentation tape.
Start Time:	At 3.75 inches per second, less than 2 seconds. At 45 inches per second, less than 3 seconds.
Reversal and Mode Switch Time:	Less than 2 seconds.
Tape Speed:	Record, 3.75 inches per second. Rewind, playback, erase, 45 inches per second.
Power:	28 volts dc \pm 4 volts.

TABLE 5-AXII

PRELIMINARY FUNCTIONAL CHARACTERISTICS - SEQUENCE CONTROL UNIT

Signal Inputs:	<ol style="list-style-type: none"> 1. Real Time Data (RTD). 2. Recorder No. 1 Data (RC1D). 3. Recorder No. 2 Data (RC2D).
Power Input:	28 volts dc \pm 4 volts.
Command Inputs:	<ol style="list-style-type: none"> 1. Transmit (TX). 2. Recorder No. 1 Beginning-of-Tape Sense (RC1BT). 3. Recorder No. 1 End-of-Tape Sense (RC1ET). 4. Recorder No. 2 Beginning-of-Tape Sense (RC2BT). 5. Recorder No. 2 End-of-Tape Sense (RC2ET).
Command Outputs:	<ol style="list-style-type: none"> 1. Transmitter ON (TX). 2. Recorder No. 1 Record (RC1RC). 3. Recorder No. 1 Rewind (RC1RW). 4. Recorder No. 1 Playback (RC1PB). 5. Recorder No. 1 Erase (RC1ER). 6. Recorder No. 2 Record (RC2RC). 7. Recorder No. 2 Rewind (RC2RW). 8. Recorder No. 2 Playback (RC2PB). 9. Recorder No. 2 Erase (RC2ER).
Command Voltages:	28 volts dc \pm 4 volts.
Signal Outputs:	<ol style="list-style-type: none"> 1. Real Time Data (RTD). 2. Recorder No. 1 Data (RC1D). 3. Recorder No. 2 Data (RC2D).
Command Sequence:	The sequence of output commands shall conform to the state diagram, Figure 5-BI-1.

TABLE 5-AXIII

FUNCTIONAL CHARACTERISTICS - S-BAND TRANSMITTER

Modulation:	True FM.
Modulation Input:	Zero and 4 volts peak split phase PCM signal at 82,000 bits per second.
Input Impedance:	10,000 ohms minimum shunted by 200 picofarads maximum.
Frequency Deviation:	100 KC \pm 5 percent when modulated with the above input signal. The deviation stability shall be within \pm 5 percent for all environmental conditions.
Modulation Frequency Response:	\pm 1 db from 300 cps to 300 KC.
Modulation Distortion:	Less than 3 percent for peak deviation of 300 KC and modulating frequency of 300 cps to 300 KC.
Incidental FM:	\pm 6 KC maximum.
Output Frequency:	Selectable within the range 2,200 to 2,300 MC.
Frequency Stability:	\pm 0.005 percent for all environmental conditions.
Output Impedance:	50 ohms.
Output Power:	5 watts minimum for all environmental conditions when operating into a 50 ohm load with a VSWR of 1.5 to 1 or less.
Warm-Up Time:	600 seconds to meet all electrical and environmental requirements.
Power Input:	28 volts dv \pm 4 volts.

TABLE 5-AXIV

DATA LINK VOLUME, WEIGHT, POWER USING CONVENTIONAL CIRCUITS

Model No. 1 Concept

<u>Module</u>	<u>Subassembly</u>	<u>Vol. (in. ³)</u>	<u>Wt. (lbs.)</u>	<u>Power (watts)</u>
LSM	Signal Conditioner	172.3	7.3	11.2
	Multiplexer-Encoder	294.0	11.0	11.2
	VHF Transmitter	<u>67.5</u>	<u>1.5</u>	<u>56.0</u>
	Data Link Vol., Wt., Pwr.	533.8	19.8	78.4
CSM	VHF Receiver	42.0	1.0	2.8
	Bit Sync. and Data Regen.	172.3	5.0	21.0
	Tape Recorder No. 1	400.0	12.0	14.0
	Tape Recorder No. 2	400.0	12.0	14.0
	Seq. Contr. Unit	288.0	10.0	25.0
	S-band Transmitter	<u>110.0</u>	<u>8.0</u>	<u>53.2</u>
	Data Link Vol., Wt., Pwr.	1412.3	48.0	130.0

Model No. 2 Concept

<u>Subassembly</u>	<u>Vol. (in. ³)</u>	<u>Wt. (lbs.)</u>	<u>Power (watts)</u>
Signal Conditioner	172.3	7.3	11.2
Multiplexer-Encoder	294.0	11.0	11.2
Tape Recorder No. 1	400.0	12.0	14.0
Tape Recorder No. 2	400.0	12.0	14.0
Seq. Contr. Unit	288.0	10.0	25.0
S-band Transmitter	<u>110.0</u>	<u>8.0</u>	<u>53.2</u>
Data Link Total	1664.3	60.3	128.6

TABLE 5-AXV

DATA LINK, VOLUME, WEIGHT, POWER USING INTEGRATED CIRCUITS

Model No. 1 Concept

<u>Module</u>	<u>Subassembly</u>	<u>Vol. (in. ³)</u>	<u>Wt. (lbs.)</u>	<u>Power (watts)</u>
LSM	Signal Conditioner	172.3	7.3	7.5
	Multiplexer-Encoder	147.0	5.5	6.5
	VHF Transmitter	<u>20.6</u>	<u>1.3</u>	<u>30.3</u>
	Data Link Vol., Wt., Pwr.	339.9	14.1	44.3
CSM	VHF Receiver	42.0	1.0	2.8
	Bit Sync. and Data Regen.	169.0	7.4	10.0
	Tape Recorder No. 1	300.0	8.0	10.0
	Tape Recorder No. 2	300.0	8.0	10.0
	Seq. Contr. Unit	36.0	2.0	5.0
	S-band Transmitter	<u>110.0</u>	<u>8.0</u>	<u>53.2</u>
	Data Link Vol., Wt., Pwr.	957.0	34.4	91.0

Model No. 2 Concept

<u>Subassembly</u>	<u>Vol. (in. ³)</u>	<u>Wt. (lbs.)</u>	<u>Power (watts)</u>	
Signal Conditioner	172.3	7.3	7.5	
Multiplexer-Encoder	147.0	5.5	6.5	
Tape Recorder No. 1	300.0	8.0	10.0	
Tape Recorder No. 2	300.0	8.0	10.0	
Seq. Contr. Unit	36.0	2.0	5.0	
S-band Transmitter	<u>110.0</u>	<u>8.0</u>	<u>53.2</u>	
	Data Link Vol., Wt., Pwr.	1065.3	38.8	92.2

APPENDIX 5-BI

SEQUENCE CONTROL UNIT - STATE DIAGRAM DEFINITIONS

The logic signals as used in the state diagram and logic diagram are defined as follows:

- A. Recorder 1 Beginning-of-tape (RC1BT) is an output signal that is true when recorder 1 is at the beginning of its tape (RC2BT is identical except for recorder 2).
- B. Recorder 1 End-of-tape (RC1ET) is an output signal that is true when recorder 1 reaches the end of its tape (RC2ET is identical except that it applies to recorder 2).
- C. Recorder 1 Record (RC1RC) is a true signal that initiates the record mode of recorder 1 (RC2RC applies similarly to recorder 2).
- D. Recorder 1 Rewind (RC1RW) is a time signal that initiates the re-winding of the tape on recorder 1 (RC2RW applies similarly to recorder 2).
- E. Recorder 1 Playback (RC1PB) is a true signal that causes recorder 1 to begin the playback of data previously recorded (RC2PB applies similarly to recorder 2).
- F. Recorder 1 Erase (RC1ER) is a true signal that initiates the erase current to recorder 1 to remove any data previously recorded (RC2ER applies similarly to recorder 2).
- G. Recorder 1 Data (RC1D) is a time controls signal used to indicate the transmission of data from recorder 1 via the transmitter (RC2D applies similarly to recorder 2).
- H. Real Time Data (RTD) is a true control signal used to indicate the transmission of real-time-data via the transmitter.
- I. Transmitter On (TX) is a time signal indicating that the transmitter is in the transmit mode.

- J. Time Delay (TD) is a true signal generated by the TX signal and a 30 second delay element.
- K. Clock Pulse (CP) is a clock signal supplied to the SCU and is used to gate all flip-flops and generally to synchronize the various switching functions.
- L. Transmitter On (X) - Off (\bar{X}) are the transmitter on (off) synchronization pulses and are generated in the SCU by using TX (TX) and CP.
- M. Clear (CL) is a signal used to clear all flip-flops when power is initially turned on.

STATE DIAGRAM DESCRIPTION

The State Diagram is shown in Figure 5-BI-1 and contains 19 states representing the various output conditions. Each state is designated by a 6-bit binary number and Pxy number; where x = decimal equivalent of first two binary bits, and y = decimal equivalent of 4-stage Johnson counter output. The lone exception is the STOP state which is designated by STOP only.

- A. POO; Standby - POO is designated by a state control of 000000. Standby is reached by turning the power on, and in this condition the SCU is waiting for a command to begin the sequencing of its various outputs. The SCU always begins operation in this state.
- B. P10; RC1RC, RTD - P10 is designated by state control of 010000 and is entered from POO only when a TX signal occurs. In the P10 state the outputs present are RC1RC and RTD.
- C. P30; RC1RC - P30 is designated by a state control of 110000 and is entered when a TX signal occurs. P30 may be entered from the P10 or P27 state. In the P30 state, RC1RC is the output.
- D. P31; RC1RC, RTD, RC2RC - P31 is designated by a state control of 111000 and is entered from P30 only when a TX signal occurs. In the P31 state the outputs are RC1RC, RTD and RC2RC.
- E. P32; RC1RW, RTD, RC2RC - P32 is designated by a state control of 111100 and is entered from P31 when a TD signal occurs. The outputs present in P32 are RC1RW, RTD and RC2RC.

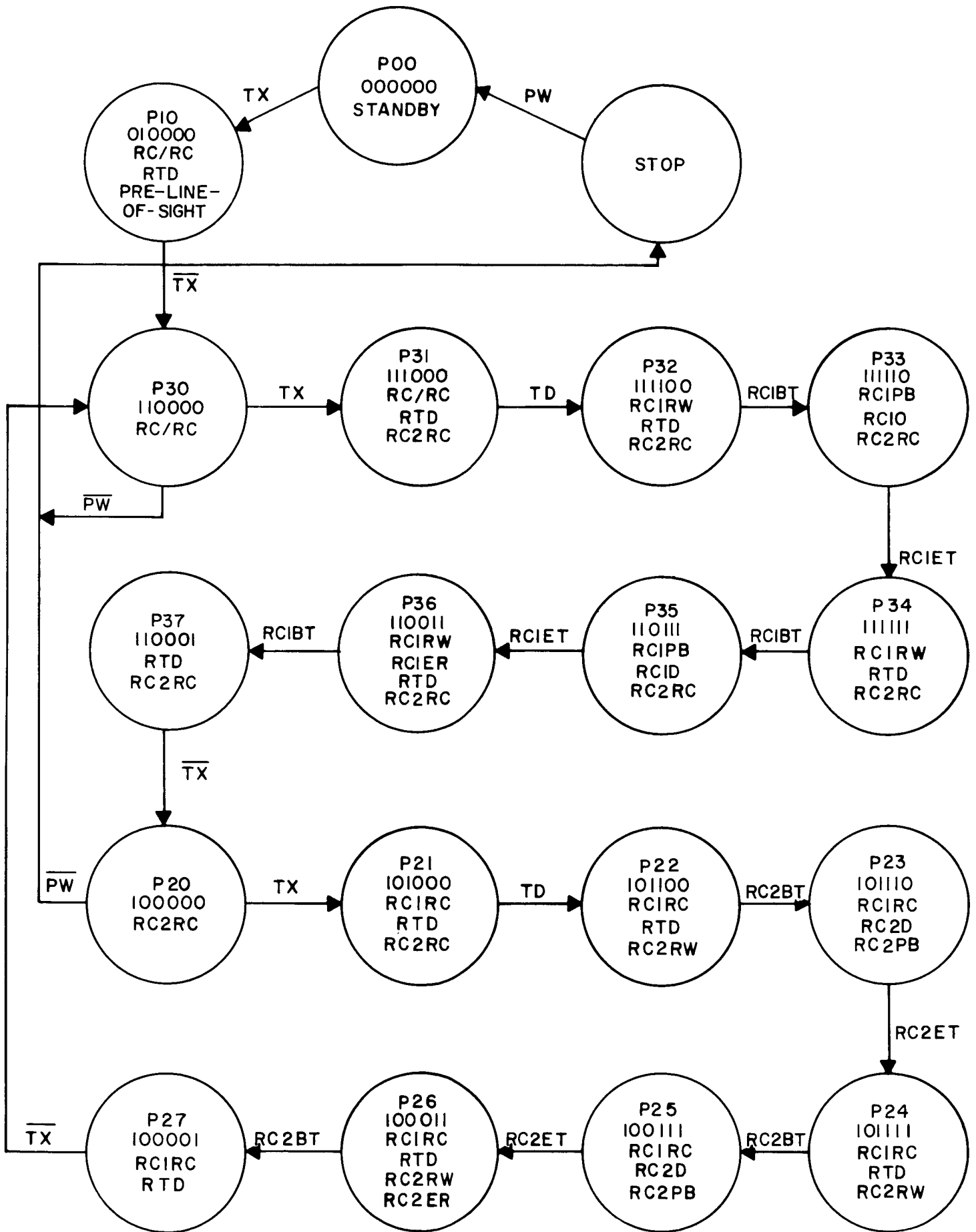


FIGURE 5-BI-1 SEQUENCE CONTROL UNIT STATE DIAGRAM

- F. P33; RC1PB, RC1D, RC2RC - P33 is designated by a state control of 111110 and is entered from P32 when an RC1BT signal occurs. The outputs present in P33 are RC1PB, RC1D, RC2RC.
- G. P34; RC1RW, RTD, RC2RC - P34 is designated by a state control of 111111 and is entered from P33 when an RC1ET signal occurs. The outputs present in 34 are RC1RW, RTD, and RC2RC.
- H. P35; RC1PB, RC1D, RC2RC - P35 is designated by a state control of 110111 and is entered from P34 when an RC1BT signal occurs. The outputs present during P35 are RC1PB, RC1D, and RC2RC.
- I. P36; RC1RW, RC1ER, RTD, RC2RC - P36 is designated by a state control of 110011 and is entered from P35 when an RC1ET signal occurs. The outputs present during P36 are RC1RW, RC1ER, and RTD, and RC2RC.
- J. P37; RTD, RC2RC - P37 is designated by a state control of 110001 and is entered from P36 when an RC1BT occurs. The outputs present during P37 are RTD and RC2RC.
- K. P20 through P27 - P20 through P27 states are the same as P30 through P37 with the RC1 and RC2 functions reversed.
- L. STOP - STOP is not designated and is entered from P30 or P30 when a \overline{PW} signal occurs.

APPENDIX 5-BII

LOGIC EQUATIONS FOR SEQUENCE CONTROL UNIT

- A. State flip-flop input (set - reset) equations.

$$\begin{array}{ll}
 R_A = 0 & R_B = AB\overline{X} \\
 S_A = \overline{ABX} & S_B = \overline{ABX} + \overline{ABX} \\
 R_C = F & R_D = \overline{C}
 \end{array}$$

$$\begin{array}{ll}
 S_C = \overline{F} & S_D = C \\
 R_E = \overline{D} & R_F = \overline{E} \\
 R_E = D & S_F = E
 \end{array}$$

B. Logic equations of clock pulse for state flip-flops:

$$\begin{aligned}
 CP_{AB} &= CP \\
 CP_{CDEF} &+ A \cdot CF \cdot TX + \overline{CD} \cdot TD + \overline{DE} (RC1BT + RC2BT) \\
 &+ \overline{EF} (RC1ET + RC2ET) + CF (RC1ET + RC2BT) \\
 &+ \overline{CD} (RC1ET + RC2ET) + \overline{DE} (RC1BT + RC2BT) \\
 &+ \overline{EF} \cdot \overline{TX} \cdot CP
 \end{aligned}$$

C. Logic equations for X, \overline{X} , and TD:

$$\begin{aligned}
 X &= M\overline{N} \\
 \overline{X} &= \overline{M}N \\
 TD &= P\overline{Q}
 \end{aligned}$$

D. Output Logic Equations

1. $RC1RC = \overline{AB} + AB (\overline{DF}) + \overline{AB} (C + F)$
2. $RC2RC = \overline{AB} (\overline{DF}) + AB (C + F)$
3. $RC1RW = AB (\overline{DE} + CD + \overline{DE})$
4. $RC2RW = \overline{AB} (\overline{DE} + CE + \overline{DE})$
5. $RC1PB = AB (\overline{EF} + \overline{CD})$
6. $RC2PB = \overline{AB} (\overline{EF} + \overline{CD})$
7. $RC1ER = AB (\overline{DE})$
8. $RC2ER = \overline{AB} (\overline{DE})$
9. $RTD = \overline{AB} + A(\overline{CE} + CF + \overline{DF})$

APPENDIX 5-C

DERIVATION OF THE BIT ERROR PROBABILITY
 VS.
 PEAK SIGNAL TO RMS NOISE CURVES OF
 FIGURE 5.1.6-1

Based upon the assumptions made by Dr. Crow in reference 1, the statistical function that describes the probability of incorrectly detecting a bit in a PCM wavetrain is expressed as follows

$$P(y) = \int_y^{\infty} \frac{e^{-\frac{x^2}{2}}}{\sqrt{2\pi}} dx$$

Where P(y) is the probability that the instantaneous noise voltage exceeds the signal and has opposite polarity, and y is the ratio of the peak signal output of the detector to the standard deviation, or rms noise out of the detector.

The probability function can be evaluated using standard probability tables² for different signal to noise ratios if it is manipulated into the following form:

$$P(y) = 1/2 \left[1 - \int_{-y}^y \frac{e^{-\frac{x^2}{2}}}{\sqrt{2\pi}} dx \right]$$

In arriving at curve I of Figure 5.1.6-1, a PCM detector having a 36 db/octave Gaussian filter with cut-off at 1/2 the bit rate is fed a signal that has been premodulation filtered by a 36 db/octave Gaussian filter with cut-off at 3/4 the bit rate. The polarity of the detector output at the midpoint of the bit period represents the bit decision. Since the normalized output of the detector is a function of bit pattern, and filtering affects each pattern differently, the overall probability of an incorrect bit decision can be expressed:¹

$$P_o(S/N) = 1/2 P\left(\frac{.86 S}{N\sqrt{1.05}}\right) + 1/4 P\left(\frac{.80 S}{N\sqrt{1.05}}\right) + 1/4 P\left(\frac{S}{N\sqrt{1.05}}\right)$$

Substituting values, the results for plotting curve I of Figure 5.1.6-1 are tabulated below:

S/N (db)	S/N	$P\left(\frac{.86 S}{N\sqrt{1.05}}\right)$	$\left(P\frac{.80 S}{N\sqrt{1.05}}\right)$	$P\left(\frac{S}{N\sqrt{1.05}}\right)$	$P_o (S/N)$
2	1.259	1.45×10^{-1}	1.63×10^{-1}	1.10×10^{-1}	1.46×10^{-1}
4	1.585	9.18×10^{-2}	1.08×10^{-1}	6.10×10^{-2}	8.82×10^{-2}
6	1.995	4.71×10^{-2}	5.97×10^{-2}	2.58×10^{-2}	4.50×10^{-2}
8	2.512	1.75×10^{-2}	2.50×10^{-2}	7.10×10^{-3}	1.79×10^{-2}
10	3.162	3.99×10^{-3}	6.80×10^{-3}	1.02×10^{-3}	3.96×10^{-3}
12	3.981	4.19×10^{-4}	9.44×10^{-4}	5.10×10^{-4}	4.58×10^{-4}
14	5.012	1.31×10^{-5}	4.58×10^{-5}	5.05×10^{-7}	1.81×10^{-5}
16	6.310	5.98×10^{-8}	4.22×10^{-7}	3.73×10^{-10}	1.35×10^{-7}

A slicer can be inserted in the detector which amplifies a slice of the signal at the zero crossing and prior to making the bit decision. The slicer limits the positive and negative peaks of the signal plus noise, but preserves the intelligence at the zero crossing. The expression for the bit error probability becomes:

$$P_o (S/N) = P\left(\frac{S}{N\sqrt{1.05}}\right)$$

The results are tabulated above, and plotted in curve II of Figure 5.1.6-1. It should be noted that a 1.5 db improvement results due to slicing prior to detection.

LIST OF REFERENCES

REFERENCES FOR SECTION 3.0

1. Anderson, John D., "Theory of Orbit Determination - Part I Classical Methods", JPL Technical Report No. 32-497, October 1, 1963.
2. Anderson, John D., "Theory of Orbit Determination - Part II Estimation Formulas", JPL Technical Report No. 32-498, October 1, 1963.
3. Barabashov, N. P., et.al, "The Moon", ASTIA AD 261784, May 23, 1963.
4. Hertzberger, M., "The Normal Equations of the Method of Least Squares and Their Solution", Quart, Appl. Math. 7,217 (1949).
5. Kalensher, B. E., "Selenographic Coordinates", JPL Technical Report No. 32-41, February 24, 1961.
6. Linnik, Y. V., "Method of Least Squares and Principles of Theory of Observations", Pergamon Press, New York, 1961.
7. Morrison, D. D., "Tracking Programs and Orbit Determination", JPL (1960).
8. Whittaker and Robinson, "The Calculus of Observations", Blackie and Son, London, Fourth Ed., 1958.
9. Gauss, K. F., "Theory of Motion of Heavenly Bodies", Dover, New York, 1963.

10. Goudas, C. L., "Development of the Lunar Topography into Spherical Harmonics, II", Air Force Cambridge Research Laboratories, 64-428, February 1964.

REFERENCES FOR SECTION 4.1

1. Meisenholder, G. W., Planet Illuminance, Technical Report No. 23-361, Jet Propulsion Laboratory, Pasadena, November 10, 1962.
2. Beckmann, P. and Spizzichino, A.; The Scattering of Electromagnetic Waves from Rough Surface; The MacMillan Company, New York, 1963.
3. Kruse, P. L. McGlauchlin and R. McQuistan, Infrared Technology, John Wiley & Sons, New York (1962).
4. M. L. Stitch, E. J. Woodbury, C. V. Smith, F. J. Myers, et al, "Application of the Laser to Active Ranging: The Colidor, "Notes for Summer Course on Optical Masers - LB-29 June 1962 at the Massachusetts Institute of Technology.
5. M. Hunter, "Comparison of Ruby and Neodymium Laser Ranging Systems for Visibility Limited Applications, General Electric Company, Defense Electronics Division, Light Military Electronics Department, unpublished report.
6. Yariu and Cordon, "The Laser", Proc. IEEE, Vol. 51, pp. 4-29; January, 1963.
7. R. Reiffen and H. Sherman, "An Optimum Demodulator for Poisson Processes: Photon Source Detectors", Proc. of the IEEE, October 1963.
8. Tables of the Individual and Cumulative Terms of Poisson Distribution, D. Van Nostrand Company, Inc., New York, 1962.
9. C. R. Smith, et al, "Optical Radar Design Using Lasers", Aerospace Group, Hughes Aircraft Co., Culver City, California.
10. G. Biernson, R. F. Lucy, "Requirements of a Coherent Laser Pulse-Doppler Radar", Proc. IEEE, January 1963.

11. P. M. Woodward, Probability Theory with Applications to Radar, Pergamon Press, London, 1953.
12. S. A. Collins, Jr., "Lasers: Principles and Uses", *Electro-Technology*, March, 1963.
13. Skolnik, M. I., Introduction to Radar Systems, McGraw-Hill, 1962.

REFERENCES FOR SECTION 4.3.5

1. Gilden, M. and L. Gould, "Handbook on High Power Capabilities of Waveguide Systems", 1963, Microwave Associates.
2. Kraus, J. D., "Antenna", McGraw-Hill, 1950.
3. Lawson, J. L. and G. E. Uhlenback (eds), "Threshold Signals", MIT Radiation Laboratory Series, Vol. 24, McGraw-Hill, 1950.
4. Marcum, J. I. and P. Swerling, "Studies of Target Detection by Pulsed Radar", *IRE Transactions on Information Theory*, Vol. IT-6, April, 1960.
5. Povejsil, D. J., R. S. Raven, and P. Waterman, "Airborne Radar", D. Van Nostrand, 1961.
6. Silver, S., "Microwave Antenna Theory and Design", McGraw-Hill, 1949.
7. Skolnik, M. I., "Introduction to Radar Systems", McGraw-Hill, 1962.

REFERENCES FOR SECTION 5.0

1. Crow, J. H., PCM Signal-to-Noise Performance, Proceedings of the 1962 National Telemetry Conference, Volume 1, 5-1.
2. U.S. Department of Standards Applied Math. Series 23, Tables of Normal Probabilities Functions, June 5, 1953.